Complex structure of Piton de la Fournaise and its underlying lithosphere revealed by MT 3D inversion.

Lydie-Sarah Gailler[1], Anna Marti[2], Jean-François Lénat[1]

[1] Université Clermont Auvergne, Laboratoire Magmas et Volcans - CNRS, UMR 6524, IRD, R 163, 6 Avenue Blaise Pascal TSA 60026 – CS 60026, 63178 AUBIERE Cedex, FRANCE

[2] Departament de Geodinàmica i Geofísica, Universitat de Barcelona, Spain

Corresponding author: lydiegailler@hotmail.fr

Abstract

La Réunion is a large volcanic construction resting on Paleocene oceanic crust. Through the 3D inversion of a large set of magnetotelluric (MT) soundings, our results reveal the general resistivity structure of the western part of Piton de la Fournaise volcano down to its base and the first ten kilometers or so of the underlying lithosphere. The upper resistive layer is associated to a superimposition of unsaturated and probably water-saturated lava flows with an averaged thickness of 1.5 km overlying more or less continuous highly conductive patches which imply the presence of highly conductive fluids and/or minerals. In the summit area and Enclos, this conductor is unambiguously attributed to the presently active hydrothermal system. In the Plaine des Sables, it is tentatively associated with the hydrothermal alteration beneath the ancient volcanic center. A third widespread conductive patch is observed below the NW flank of Piton de la Fournaise resulting more likely from volcanic activity since it coincides with part of the N120 rift zone. In the area beneath the Plaine des Sables where a dense intrusive complex has been inferred from gravity models, the resistivity is not significantly higher. The upper lithosphere is markedly more resistive than the bulk of the

volcanic construction (except for the upper part of this latter) forming a virtual horizon around -4 km in depth. However, one main conductive anomaly is present in the crust beneath the NW flank along the N120 rift zone assumed to be linked with present day seismic and degassing activity. The NW flank therefore appears as a main area of interest in the study of Piton de la Fournaise activity and its evolution as well. We therefore demonstrate the capability of the method to image major shallow structures such as the hydrothermally altered zones, and deeper ones such as possibly the heterogeneity of the crust.

Keywords: Piton de la Fournaise; magnetotelluric data; 3D inversion; hydrothermal system; oceanic lithosphere; plumbing system.

1. Introduction

The architecture of volcanic systems is important to know because: (1) it provides information on the construction and evolution of the volcanic structures; (2) it has an influence on the magma paths (the conduits) and (3) it may generate its own volcano-tectonic activity through, for example, gravitational instabilities. The need of high resolution imagery of the interior of the volcanic systems is therefore obvious and is the main motivation for the application geophysical prospecting methods in volcanology. Several geophysical techniques can be used to image the structures and rocks physical properties at depth. The most common are seismics, gravity and electrical resistivity measurements. The magnetotelluric (MT) method has been used since the early 1980s in volcanic areas for both geothermal exploration and volcanological studies. It is particularly well suited for volcanic studies (Piña et al. 2014 and references therein) since the electrical conductivity is influenced by both temperature and compositional variations. But is has also the capability to probe deep in the crust and the mantle (Jones, 1999)

Electrical resistivity of crustal rocks generally varies over several orders of magnitude (1 10^{-4} to 100 kohm·m), depending on a wide range of petrological and physical parameters, such as bound versus free water, composition of the fluids, temperature, and the content of clay or metallic minerals. Resistivity is usually dominated by the ionic conductivity of the fluids present in the interconnected pores. In general, a basaltic shield consists predominantly of a pile of highly permeable lava flows. If not altered or water saturated, such formations generally have resistivity as high as 10–100 kohm-m. A large resistivity variation usually exists at the transition between the vadose zone, where rocks contain only some moisture, and the zone beneath the water table, where the rocks are fully water saturated. On oceanic islands, the basal water table consists of a lens of fresh water (Ghyben-Herzberg lens; e.g., see Vacher, 1988) floating over the seawater- saturated zone. The top of the freshwater lens generally takes place at an elevation of a few meters to a few tens of meters above the sea level. However, this model, initially derived for the Hawaiian Islands, may not apply when the hydraulic conductivity decreases significantly with depth. In this case, the water table forms a high elevation dome within the edifice. The latter model is preferred in the case of Piton de la Fournaise by Join et al. (2005).The resistivity of a basaltic pile saturated with fresh water is generally a few hundred ohm·m, but drops to a few tens of ohm·m or less when saturated with sea water. In addition to water saturation, the nature of the formation also plays a role in the resistivity distribution. In intrusion zones (central zone, rift zones), swarms of subvertical dikes can create impermeable barriers that impound bodies of water at high elevations (Stearns, 1942; Takasaki, 1981; Jackson and Kauahikaua, 1987). Alteration, particularly hydrothermal alteration, tends to lower the rock resistivity through the formation of highly conductive, hydrated minerals such as clay minerals and zeolites. Similarly, pyroclastic and breccia deposits generally have lower resistivity values than lava flows, because they typically contain hydrated minerals. Magma has a resistivity of only a few ohm·m or less (Rai and Manghnani, 1977; Haak, 1982). The resistivity of the upper oceanic lithosphere underlying a volcanic edifice may be different and more complex than regular oceanic lithosphere. Constable and Cox (1996) indicate that the resistivity of an undisturbed upper oceanic lithosphere is more than 100 ohm·m. Increasing compaction with depth causes a decrease in the effective porosity and hence increases the resistivity. However, it may vary significantly depending on its temperature, and hence often its age: a young, hotter, lithosphere will be less resistive than its older counterpart (Nobes et al., 1992; Unsworth, 1994; MacGregor et al., 1998). The presence of conductive layers (e.g. fluid and/or mineral-filled fractures, magma) will also contribute to lowering the rock resistivity. In the case of hot spot volcanism, magmatic underplating is a common feature, and this has been suggested by Charvis et al. (1999) and Gallart et al. (1999) for La Réunion. Therefore the presence of magma beneath the crust can be investigated with the MT data. At greater depths, as the temperature increases, the mantle becomes more conductive. Laboratory experiments on basaltic and mantle rocks show the very low electrical conductivity of melts. For example, at the scale of the Hawaiian hot spot swell, 2D electrical models have shown a resistive lithosphere underlain by a conductive lower mantle, and a narrow conductive plume connecting the surface of the island to the lower mantle (Constable and Heinson, 2004).

In this work, we focus on La Réunion volcanic edifice, which has been extensively studied since decades, with a special interest given to Piton de la Fournaise volcano (see Lénat et al. (2012a and reference therein)). However, the deep architecture of Piton de la Fournaise and its underlying lithosphere remain poorly known. Previous geoelectrical studies carried out by Lénat et al. (2000) focused on the first kilometer or so of the active part of the volcano. The aim of the current study is to take advantage of a new large set of MT soundings acquired during a geothermal reconnaissance of Piton de la Fournaise in order to image the resistivity structure down to several to tens of kilometers. The good spatial coverage of the sites and the lack of a preferred strike direction obtained from the dimensionality analysis allowed us to invert the data and obtain a 3D geoelectrical model of the volcanic edifice and its surrounding which is discussed it in terms of large scale structures.

2. Geological and geophysical structure of Piton de la Fournaise and its basement

Piton de la Fournaise is located on the southeast of La Réunion Island (Fig. 1a), and is one of the world's most active basaltic shield volcanoes. Its evolution can be reconstructed by means of its deep valleys. The evolution can be divided into two main periods: the Ancient Shield (> 0.15 Ma) and the Recent Shield (< 0.15 Ma). At the base of the deep valleys (Rivière des Remparts, Rivière de l'Est and Rivière Langevin) (Fig. 1a), a differentiated unit called Pintades Unit (Bachèlery, 1981; Bachèlery and Mairine, 1990; Merle et al., 2010) is evidenced. It is dated from at least 530 kyr to 400/450 kyr, and is inferred by Smetiana (2011) to belong to a volcano which predates Piton de la Fournaise called Les Alizés volcano (Rançon et al., 1989; Malengreau et al., 1999; Lénat et al., 2001). The Pintades Unit is observed up to 1000/1200 m in elevation in the Rivière des Remparts, and therefore Piton de La Fournaise, rising at 2632 m, must be a relatively thin edifice (Merle et al., 2010).

Since about 290 kyr, the geological history of Piton de la Fournaise is summarized as a sequence of volcano-tectonic events with alternating episodes of volcanic destruction and reconstruction (Merle et al., 2010). Two calderas have been identified during the Ancient Shield period: the Rivière des Remparts caldera at about 250 kyr and the Morne Langevin caldera at about 150 kyr. During the Ancient Shield period, the volcanic center is inferred to have been located in what is presently the Plaine des Sables (Fig. 1). Bachèlery and Mairine (1990) propose that the eastward displacement of the volcano to its present location (Fig. 1b) could have taken place at about 150 kyr, concurrently with the formation of the Morne

Langevin caldera, although it could be as young as the formation of the Plaine des Sables caldera, which formed at about 65 and/or 40 kyr (Gillot and Nativel, 1989; Bachèlery, P. and Mairine, 1990; Staudacher and Allègre, 1993; Merle et al., 2010). Letourneur et al. (2008) suggest the possibility of an intermediate location before the present one. The formation of the most recent, 8 km-wide caldera, called the Enclos Fouqué caldera (or, simply, Enclos), has been dated at about 4.5 kyr (Bachèlery, 1981; Staudacher and Allègre, 1993; Mohamed-Abchir, 1996), but the recent reappraisal of the existing radiocarbon data and new ages suggest two younger collapse episodes at around 3700, 3100 and 2300 kyr (Morandi et al., 2015). The present eruptive center is located on the Central Cone which has grown inside the Enclos caldera, which is breached to the east (the Grandes Pentes and Grand Brulé areas). The relationships between the Enclos Fouqué, the Grandes Pentes and the Grand Brûlé are still debated (Bachèlery, 1981; Merle and Lénat, 2003; Michon and Saint-Ange, 2008).

The locations of the magma reservoirs and transfer structures have been recently reviewed by Michon et al. (2016). Whereas most of the recent eruptive activity took place within the Enclos, either on the Central Cone or along the NE and SE rift zones, the presence of eruptive fissures and pyroclastic cones in other areas of the edifice indicates that magmas have reached the surface via different paths. In addition to the NE and SW rift zones that radiate from the Central Area of Piton de la Fournaise and extend beyond the Enclos (Fig 1a), a broad, diffuse N120 rift zone occurs between Piton des Neiges and Piton de la Fournaise volcanoes. It is marked by numerous (~160) cinder cones and lava flows. The age of this rift zone is not well defined, but eruptions began at least 29 ky ago (McDougall, 1971) and the last eruption is dated at 0.140 kyr (Morandi et al., 2015). Another concentration of cones is observed at the base of the subaerial south flank of Piton de La Fournaise. Michon et al. (2016) name this area the "South Volcanic Zone". Michon et al. (2016) propose to interpret the deep seismicity observed at La Réunion in connection with the distribution of the volcanic zones at the surface. They use a compilation of the volcano-tectonic (VT) seismicity from 1993 to 2013. Below a depth of 10-11 km (base of the crust, according to (Gallart et al., 1999)), most of the VT events are located beneath the northwestern part of Piton de la Fournaise and beneath the NW flank of Piton de la Fournaise and the Plaine des Cafres areas. They are generally deeper (up to about 30 km) to the NW and become progressively shallower (up to 10-11 km) near the presently active area of Piton de la Fournaise. No seismicity is observed from the base of the crust to a region above 8 km in depth. Michon et al. (2016) suggest that this aseismic zone could correspond to a zone of magma storage (underplating). They also propose that the deep northwestern seismicity is organized along a N30-40 axis at depths greater than 20 km and then rotates and concentrates beneath the N120 NW rift zone. Michon et al. (2016) link the deep seismicity with magma transfer, and suggest a vertical ascent of magma between 30 and 20 km in depth. Earthquakes are observed from about 8 km in depth to the surface before and during volcanic crises with an overall lateral migration of the seismic swarms along 10-11 km, from the Plain des Sables toward the presently active area of Piton de la Fournaise. In addition, a high resolution survey of soil CO_2 emissions carried out on the western flank of Piton de la Fournaise (Boudoire et al., 2017) has evidenced that narrow zones of high fluxes are aligned along a well-defined N135° axis coincident with seismic swarms detected during the reawakening of the volcano (2014–2015). The authors have called this alignment the Songit Lineament (Fig. 1a) which is consistent with the orientation of paleo-spreading axes. They also suggest that this latter could result from the inheritance of the oceanic lithosphere.

Receiver function techniques have also provided information in depth (Fontaine et al., 2015). A joint inversion of receiver function and surface wave dispersion suggests that thin magmatic underplating may be present below La Réunion. Lateral variations of its thickness suggest that this latter could result from an important interaction between the plume and lithosphere. In addition, a low velocity layer interpreted as a zone of partial melt beneath the active volcano is evidenced at a depth of about 33 km.

At Piton de la Fournaise, recent geophysical explorations using electromagnetic surveys have provided new hydrogeological information (Join et al., 2005). Their hydrogeological model suggests the presence of a continuous aquifer which domes at 1800 m asl below the central active part. It deepens to between 1600 to 1400 m asl beneath the Plaine des Sables and is even deeper beneath the Fond de la Rivière de l'Est depression. A recent synthesis of all available data led Lénat et al. (2012 and reference therein) to propose a geological model of the infrastructure of Piton de la Fournaise and its basement (Fig. 1b). We summarize here the main points of this interpretative geological section, starting from the surface: (1) shallow accumulation of dense lava flows in paleo depressions, (2) presence of pervasive hydrothermal alteration, (3) the presumed interface with Les Alizés volcano, (4) presence of hypo-volcanic complexes (gabbros, cumulates) beneath the Plaine des Sables area, (5) possible ancient and recent magma reservoir at the interface between La Réunion and the oceanic crust, (6) no significant flexure of the lithosphere, and (7) possible magma underplating at the base of the crust.

The dense Ancient Shield hypovolcanic complex (ASC) beneath the Plaines des Sables-Enclos area is a major feature inside the edifice that creates a positive gravity anomaly. The location of the complex has been deduced from 2D ¾ and 3D gravity modelling (Gailler et al., 2009). Gabbro and cumulate xenoliths found in lava flows and tephra above this complex (Bachèlery, 1981) probably originated from it. The base of the volcanic edifice on the oceanic crust is inferred to be around -4 km in elevation, which is the level of the oceanic floor around La Réunion. This is a reasonable assumption given that seismic studies (De Voogd et al., 1999; Gallart et al., 1999) suggest that there is no lithospheric flexure beneath La Réunion.

Lastly, we note that the estimated Curie depth, based on analysis of the magnetic anomalies (Gailler et al., 2016), shows a bulge in the Curie surface below the island, with its top shifted offshore to the NE of Piton de la Fournaise. Nevertheless, several features as well as the deep structure, beyond the volcanic edifice sensu stricto remains poorly imaged.

3. Resistivity data

In order to investigate the deep structure of the edifice, we have compiled all available electrical data, especially magnetotelluric (MT) soundings which provide the greatest depth of investigation in the western part of Piton de la Fournaise area.

3.1. Previous studies and new data

Electric and electromagnetic surveys have been carried out on La Réunion Island for hydrogeologic studies (Courteaud, 1996; Schnegg, 1997), structural studies of Piton de la Fournaise (Schnegg, 1997; Lénat et al., 2000) and geothermal prospecting (Benderitter and Gérard, 1984; Benderitter, 1990; Smith, 1996). A compilation of these datasets has been already provided by Gailler and Lénat (2012) to study the island at a larger scale. In this study, we have mostly used new data acquired during a geothermal reconnaissance project between 2001 and 2004. The main datasets (Fig. A1 in Supporting Information A) come from a magnetotelluric (MT) survey carried out by Phoenix Geophysics in 2002 (34 collocated MT soundings, AMT for audiomagnetotellurics and TDEM for Time Domain ElectroMagnetic soundings) and an MT survey by PB Power (53 collocated MT and TDEM soundings). The data were collected in the 10^{-3} to 10^{4} Hz frequency range. We have also used 24 AMT soundings (in the range 1 to 10^{4} Hz) acquired by our group (here designated as UBP) in 2001 (7 collocated with shallow Direct Current (DC) older electrical soundings), 4 MT soundings (in the range 10^{-3} to 10^{3} Hz) acquired in 2001 by University Pierre et Marie Curie (here designated as Paris) and 3 old MT soundings acquired by the Bureau de la Recherche

Géologique et Minière (BRGM). The data of the latter (in the range 10^{-2} to 10^{2} Hz) were digitized from paper copies.

3.2. Data processing and analysis

The MT and AMT data were processed using WinGlink® software package from Geosystem. When multiple sets of data were available for the same location (i.e. HF and LF for AMT and MT data), the data were combined into a single sounding. A first quality inspection based on the error bars and the consistency of the resistivity curves made us reduce the dataset to 108 sites located in figure 2. It can be observed that the density of soundings is much higher in the Plaine des Sables, since this area was the target of the geothermal reconnaissance survey. However, parts of the Fond de la Rivière de l'Est, Plaine des Remparts and even the NW flank of Piton de la Fournaise Central Cone and Enclos are well enough covered by the data to allow us to expand our study to these areas.

3.2.1. Dimensionality analysis

We have carried out a dimensionality analysis using the WALDIM code from Martí et al. (2009), which is based on the WAL invariants (Weaver et al., 2000).We used a threshold value of 0.2 and assumed an error percentage of 5%. As shown in Figure 3, the distribution of dimensionality shows a predominant 1D behavior for shorts periods (< 1s) and a few 2D and mainly 3D as periods increases beyond 1s, which seem to be reasonable. The behavior becomes fully 3D for periods longer than 10 s (Fig. 3), suggesting that a 3D inversion of the data is needed for a consistent interpretation of the overall dataset.

In order to better investigate the quality of the data and to provide a first general view of the resistivity distribution in depth, we provide maps of invariant phases for periods ranging from 10^{-4} to 10^{3} (Fig. 4a) using WINGLINK software. In such analysis, the invariant phase is calculated as the arithmetic mean of the phases elements, provides an image of the variation of resistivity with the period, and presents the strong advantage to be unaffected by static shift. To complete the data analysis, Bostick resistivity inversions are also presented showing the main distribution of resistivity at fixed elevations (Fig. 4b). An overall good coherency is evidenced between both representations (Fig. 4a and b). For the shortest period (10^{-4}s), the shallowest layer (2000 m asl) shows a very low invariant phase as well as high resistivity values for most of the study area. At an intermediate range of periods (between 0.001 and 1s), the invariant phase then progressively increases, especially in the area of Enclos Fouqué, Plaine des Sables and Fond de la Rivière de l'Est. This feature could be correlated with the decrease in resistivity observed from 1000 m to – 2000 m asl. Beyond a period of 100s and a depth of -4000 m, the invariant phase scheme and the resistivity distribution are more complex, with an overall increase in resistivity with depth.

Therefore, this analysis enables to delineate several interesting features: i) a resistive shallow layer above 1000 m asl, ii) an intermediate conductive layer between 1000 and – 2000 m in average, and iii) higher resistivity more in depth with both lateral and vertical heterogeneities at depths greater than -4000 m asl. The 3D model will help depict the details of this general description.

3.2.2. Sea water and topography artifacts

In an oceanic environment such as La Réunion with strong reliefs, it should be stressed that the data artifacts associated to the sea, topography and bathymetry can be important. This is especially the case for coastal soundings where the influence of the sea could be significant and affect the interpretation of AMT and MT data. Pinã-Varas et al. (2014) have identified such effects on the MT data by constructing a 3D conceptual geoelectrical model of Tenerife Island, using known geological and geophysical data. Details on this synthetic test are given in their study, suggesting that the MT responses are strongly distorted by topography and sea effects at frequencies lower than 0.1 Hz. These effects will not be an issue as far as the bathymetry, topography and sea water are included in the model. A 3D approach should be, here again, preferred to provide reliable modeling of our dataset. 2D inversions have been also performed using Winglink software to investigate several profiles of interest. However, the structures are not fully reliable given the strong assumption of strike direction and TE and TM mode.

4. 3D inversion

4.1. Initial model

We have computed a 3D electrical resistivity model of Piton de la Fournaise area using the ModEm code (Egbert and Kelbert, 2012; Kelbert et al., 2014). The starting 3D mesh model was build using WINGLINK described by Mackie and Madden (1993) subsequently developed and implemented by Geosystem. The initial model was discretized onto a 79 (NS) x 70 (EW) x 78 (vertical) grid, where topography and bathymetry were defined and fixed using a digital elevation model. The resistivity value of the seawater was set to 0.33 ohm·m, and a thin layer of conductive sediments underwater was added in the initial model fixed at 200 ohm.m. The mesh was more refined in the first km (from 2600 m asl to -5000 m bsl) with the aim of obtaining a clear image of the area of hydrothermal alteration and eventually the presence of a magmatic reservoir more in depth. The inversions were undertaken using both the off-diagonal (Zxy, Zyx) and diagonal when available (Zxx, Zyy) components of the impedance tensor for a maximum of 15 periods in the period range between 0,0001 s to 1000 s, depending on the stations. A 5 % error floor in the impedance components was imposed during the inversion process. A smoothing of 0.2 was applied in all directions and an initial lambda value of 10 was chosen. The starting RMS was 9.45, while the final RMS is 1.50 after 63 iterations. Fig. B1 in the supplementary material B shows the comparison between the raw data and model responses as apparent resistivity and phases curves for each site used in inversion. Figure 5 shows an example for one site showing that the fits of the diagonals are not perfect but acceptable. Several tests have been also done inverting either the full tensor or only the off-diagonals. The resulting models are very similar, which confirms the overall good consistency of the final 3D model described hereafter.

4.2. The 3D final model

In order to better visualize the 3D model, we present here two multi-segments sections crossing the main areas of interest, i.e. Plaine des Sables, Enflos Fouqué, Fond de la Rivière de l'Est and NW flank of Piton de la Fournaise (Fig. 6a and b). The geological studies described above and in figure 1b constitute a good reference model to start interpreting our 3D resistivity model. To the first order, the general structure can be described as follows:

(1) In the shallow resistive layer, the interface between the highly and moderately resistive values more or less mimics the topography.
(2) A very conductive layer, not continuous in the model is more superficial and thinner below the Plaines des Sables, western of the dense hypovolcanic complex modeled from gravity data (Gailler, 2010), and below the Enclos.
(3) In the deeper part of the edifice, the hypovolcanic complex is not individualized by a resistivity contrast.
(4) The lithosphere is globally moderately resistive but not fully homogeneous.

4.2.1. The shallow resistive layer

In detail, the shallow resistive layer can be separated into a highly resistive layer (~1000 to 10000 ohm·m) with a thickness of 1 km – 1.5 km, overlying a thinner and less resistive one (~100 to 1000 ohm·m). The shallower resistive layer is easily identified to piles of unsaturated lava flows. The underlying layer has resistivity values compatible with that of water-saturated lava flows, although it is observed at a relatively high elevation, slightly higher than that of the regional water-table calculated by Join et al. (2005).

4.2.2. The intermediate conductive layer

A very conductive layer (~ 4 ohm·m or less to about 30 ohm·m) is observed below, with an average thickness of about 1 km. In the model, it does not form a continuous layer but appears as elongated patches. It is not possible to assume whether this discontinuous appearance is real or an artefact of the model due to the distribution and quality of the data. This very conductive layer is present in two different zones. The first one is at high elevation below the Enclos (we have to keep in mind that the Central Cone is less resolved because it is not covered by MT soundings), the Plaine des Sables, the Plaine des Remparts and the Fond de la Rivière de l'Est. The second one is just above the inferred oceanic floor on the NW flank of Piton de la Fournaise.

This conductor has been found in all the previous resistivity surveys (e.g. (Benderitter and Gérard, 1984; Courteaud et al., 1997; Schnegg, 1997; Lénat et al., 2000)), in the different areas of Piton de la Fournaise. Various interpretations have been proposed to explain the presence of this conductor. Benderitter and Gérard (1984) attribute the very low resistivity to hydrothermal alteration whereas Courteaud et al. (1997) explain it by the presence of clay-rich brecciated material resulting from volcano-tectonic processes (caldera and flank collapses). For Lénat et al. (2000), the conductor, rising to a depth of about 300 m beneath the summit, is caused by the central hydrothermal activity within the Enclos. They suggest that in the Plaine des Sables it could also be associated with the hydrothermal activity of Piton de la Fournaise's old active center until the volcano center shifted to its present location in the Enclos (Bachèlery and Mairine, 1990). In the other zones, the geological nature of the conductor has not been identified.

Since the conductor is well above the expected level of sea water, the presence of which could explain low resistivity values, such low resistivity values suggest the presence of hydrated minerals, which could be found in landslide breccias, in hydrothermally altered zones, or in thick pyroclastic layers. Therefore, the nature of the conductor may be different in each zone.
Below the NW flank of Piton de la Fournaise, the conductor above the preexisting sea floor coincides with the N120 rift zone (Michon et al., 2016; Chevallier and Bachèlery, 1981; Villeneuve and Bachèlery, 2006) characterized by a high density of large cinder cones. These are fed by primitive magmas through deeply rooted intrusions (Michon et al., 2016). The hydrothermal alteration caused by the swarm of the dikes in the rift zone is a possible explanation of this resistivity anomaly.

4.2.3. The base of the edifice and the transition with the crust

As indicated above, the base of the volcanic edifice on the oceanic crust is inferred to lie at around -4 km in elevation and the lithosphere does not show any significant flexure. A -4 km resistivity transition is clear in two areas only. The first one is beneath La Plaine des Sables-Fond de la Rivière de l'Est where the oceanic crust is more resistive (> 150 ohm.m) than the base of the volcanic construction (< 100 ohm.m). The second one is at the NW, where, as indicated above, a very conductive layer is present at the base of the volcanic construction. A third transition is suggested beneath the Rivière des Remparts, but in this area the model is poorly constrained by MT soundings.
The hypovolcanic dense complex of the Ancient Shield (ASC) of Piton de la Fournaise revealed by gravity in the interior of the edifice (Fig. 6 a and b) would be expected to show a higher resistivity that its surrounding, as it is the case for another intrusive complex beneath Piton des Neiges volcano (Gailler and Lénat, 2012). Here, the dense complex does not show a resistivity contrast with the rest of the lower part of the edifice. This lack of correlation between the resistivity distribution and the gravity model may be explained by two types of

reasons. The geometry and density distribution of gravity model may be biased by the fact that constant density is assumed for both the intrusive complex and its surrounding. This could be a too large simplification of the reality and the geometry of the dense body could be significantly different if large density variations exist within the dense body and within its surrounding. A second type of explanation would be to consider that parts of the dense body are fractured and/or hydrothermally altered, and therefore less resistive. As a whole, the deep part of the edifice seems rather homogeneous in resistivity and no structural features, such as the transition with Les Alizés, is observed.

4.2.4. The oceanic lithosphere

The upper oceanic lithosphere beneath La Réunion is globally resistive with values up to several thousand ohm·m (Fig. 6a and b). The boundary between the crust and the upper mantle, estimated to be around –12 km (Gallart et al., 1999), is not marked in the model. At this range of depth, resistivity contrasts are suggested only below Plaine des Sables and Enclos area on the Bostick analysis (Fig. 4b). Beneath the NW flank, a pronounced conductive anomaly of the crust extends at large depth. It starts at the NW of the Plaines des Sables-Fond de la Rivière de l'Est area and deepens down to about 8 km at the border of the model. It seems to more or less follow the N120 rift zone comprising a very conductive (< 5 ohm.m) zone in the upper 2 km that is distinct from a similar feature observed above in the volcanic construction.

High resistivity values (>1000 ohm.m) below the W flank and the Rivière des Remparts from about -8 to -16 km in depth, are not reliable, because this area is only covered by a few number of soundings and lies at the edge of the model. The highly conductive area at a depth of -16 km covering a large area below the Plaine des Sables-Fond de la Rivière de l’Est and even part of the Enclos and the NW flank of Piton de la Fournaise on the Bostick analysis

(Fig. 4b) is also not reliable, because our study area is relatively narrow and may be not adequate to resolve the resistivity distribution in this range of depths (Bhattacharya and Shalivahan, 2002).

5. Discussion and conclusion

The interior of Piton de la Fournaise has been investigated by numerous geophysical and geological studies. However, the information for all the methods become less precise with depth and therefore the deep part of the volcanic construction and its interaction with the lithosphere are poorly known. Our MT study offers the advantages of being able to probe both the volcanic construction and the upper lithosphere and to use a different physical parameter than those of the previous seismic, gravity and magnetic studies. An interpretative scheme is presented in figure 6c, based on our 3D resistivity model and results from other studies.

The upper part of the edifice is very typical of basaltic shield volcanoes predominantly built by highly permeable lava flows. Accordingly, the first layer of water unsaturated lava flows is highly resistive. The fact that it evolves at depth to a more conductive layer (water saturated lava flows) supports the hydrogeological model of Join et al. (2005) that postulates the presence of a continuous high water table at Piton de la Fournaise. This contrasts with the classical Hawaiian hydrogeological model where high elevation groundwater bodies are disconnected and impounded by dike swarms or impervious layers.

At depth, within the edifice, the presence of more or less continuous highly conductive (< 5 ohm.m) patches is a special feature. Such low resistivity values imply the presence of highly conductive fluids and/or minerals. High conductivity fluids should be hot and/or mineralized ones. High conductivity minerals in this context are hydrated minerals commonly resulting from hydrothermal alteration. The high conductivity layer is described in greater detail by Lénat et al. (2000) beneath the Central Cone where it can be unambiguously linked to the presently active hydrothermal system of the volcano. Beneath the Plaine des Sables-Fond de la Rivière de l'Est, an hydrothermal origin of the conductor can only be presumed. Gravity studies have shown that this area is underlain by a dense structure interpreted as a hypovolcanic intrusive system (Gailler, 2010), source of heat and fluids for hydrothermal activity. This complex would have formed during the Ancient Shield stage and, therefore, the conductor beneath the Plaine des Sables would have developed during this period. The third notable patch of high conductor in the study area is the one observed in the lower part of the volcanic construction below the NW flank of Piton de la Fournaise (Fig. 6b). The fact that this conductor is not a widespread but a localized structure suggests that it is not due to an invasion of seawater but more likely to volcanic activity. Its location coincides with that of a part of the N120 rift zone with numerous cinder cones. In this framework, it can be tentatively explained by hydrothermalized and /or hot volume of rocks developing around a dense swarm of cooling intrusions at the base of the edifice and, possibly in the upper part of the crust where a similar conductor is observed. This system may be still active because a deep seismic activity (between about 10 and 20 km) and CO_2 emanations are observed in this area (Liuzzo et al., 2015; Michon et al.; 2016; Boudoire et al., 2017).

The dense hypovolcanic intrusive system found beneath the Plaine des Sable and the western part of the Enclos by Gailler (2010) is not characterized by a resistivity contrast with the rest of the edifice. Only overlying highly conductive layer may attest of its presence. Similarly, the interface between Les Alizés and Piton de la Fournaise volcanoes inferred by Lénat et al. (2012b) does not correspond to any obvious resistivity contrast in our model.

The upper lithosphere is markedly more resistive than the bulk of the volcanic construction (except for the upper part of this latter). However, one main resistivity anomaly is present in the crust, located beneath the NW flank. It spatially coincides, as indicated above, with the N120 rift zone assumed to be linked with present day seismic and degassing activity. It is therefore appealing to suggest that the lowering of the resistivity of the crust in this area may be due to the magmatic activity (magma intrusion, hydrothermal activity, presence of hot fluids …). The NW flank therefore appears as a main area of interest in the study of Piton de la Fournaise activity and its evolution as well. Also note that, at the base of the crust, the underplating is not imaged in our 3D resistivity model. For further investigations in depth, the study should be extended to the whole island to study the structures beneath Piton des Neiges and the whole of the Piton de la Fournaise area.

Aknowledgments

We are very grateful to the 'Conseil Régional de la Réunion' for its financial support for the acquisition of gravity and electromagnetic data in the framework of a geothermal exploration project and for its encouragement to use the data for academic research purposes. All the Geothermal Project participants are also thanked for their various contributions (E. Delcher, B. Robineau, P. Andrieu, F. Ranvier, T. Souriot, X. Pierre, B. Lapierre, D. Runavot, L. Fornot, O. Odon). The dataset will be available from the authors of this manuscript. We thank the staffs of the Observatoire Volcanologique du Piton de la Fournaise (Aline Peltier, Valérie Ferrazini, Nicolas Villeneuve), of Université de la Réunion (Laurent Michon, Anthony Finizola), and of University of Barcelona (Pilar Queralt, Juanjo Ledo and Alejandro Marcuello) for their contribution and discussions about this study. We also thank Naser Meqbel for its help around 3D Grid software. Last we acknowledge Michael Walter, Volker Rath and an anonymous reviewer tor for very insightful comments and suggestions.

Figure captions

Figure 1: a) 3D view of Piton de la Fournaise showing the main structural features and the location of the main places discussed in the text. The study area is framed in red; **b)** Interpretive W–E geological section of Piton de la Fournaise by Lénat et al. (2012a). Coordinates in kilometers (WGS84, UTM40S).

Figure 2: Location of the resistivity soundings used in this study. The area of interest is framed in red. Coordinates in kilometers (WGS84, UTM40S). More details are given in Supporting Information (Fig. S1).

Figure 3: Map of dimensionality for six different period bands, using WALDIM code (Martı´ et al., 2009).

Figure 4: a) Map of invariant phases for periods ranging from 10^{-4} to 10^{3}, using WINGLING software. **b)** Bostick resistivity inversions are also presented showing the main distribution of resistivity at fixed elevation, using WINGLING software.

Figure 5: Comparison of the apparent resistivity and phases between the model responses and the raw data for the G10 sounding a) off-diagonal components; b) all components.

Figure 6: a) 3D model represented as a multi-segments section crossing the main area of interest, i.e. Plaine des Sables, Enflos Fouqué, Fond de la Rivière de l'Est and NW flank of Piton de la Fournaise. b) Interpretative scheme of the 3D model. ASC for Ancient Shield Complex.

References

Bachèlery, P. (1981), Le Piton de la Fournaise (Ile de la Réunion): étude volcanologique, structurale et pétrologique, 255 pp., Univ. Blaise Pascal, Clermont-Ferrand.

Bachèlery, P., and P. Mairine (1990), Evolution volcano–structurale du Piton de la Fournaise depuis 0.53 Ma, in Le volcanisme de la Réunion, Monographie, edited by J.-F. Lénat, pp. 213–242, Centre de Recherches Volcanologiques, Clermont-Ferrand.

Bachèlery, P. and P. Mairine (1990), Evolution volcano–structurale du Piton de la Fournaise depuis 0.53 Ma, in Le volcanisme de la Réunion, Monographie, edited by J.-F. Lénat, pp. 213–242, Centre de Recherches Volcanologiques, Clermont-Ferrand.

Battaglia, J., V. Ferrazzini, T. Staudacher, K. Aki, and J. L. Cheminée (2005), Pre-eruptive migration of earthquakes at the Piton de la Fournaise volcano (Réunion island), Geophys. J. Int., 161, 549–558.

Benderitter, Y. (1990), Études géoélectrique et électromagnétiques à la Réunion, in Le volcanisme de la Réunion, monographie, edited by J. F. Lénat, pp. 29–42 , Centre de Recherches Volcanologiques, Clermont-Ferrand.

Benderitter, Y., and A. Gérard (1984), Geothermal study of Réunion Island: audiomagnetotelluric survey, J. Volcanol. Geotherm. Res., 20, 311–332.

Bhattacharya B.B, Shalivahan (2002), The electric moho underneath Eastern Indian Craton, Geophysi al Research Letters, Vol. 29, NO. 10, 1376, 10.1029/2001GL014062.

Boudoire G., Liuzzo M., Di Muro A, Ferrazzini V., Michon L., et al.. Investigating the deepest part of a volcano plumbing system: Evidence for an active magma path below the western flank of Piton de la Fournaise (La Réunion Island). Journal of Volcanology and Geothermal Research, Elsevier, 2017, 341, pp.193-207.<10.1016/j.jvolgeores.2017.05.026>.

Charvis, P., A. Laesanpura, J. Gallart, A. Hirn, J. C. Lepine, B. de Voogd, T. A. Minshull, Y. Hello, and B. Pontoise (1999), Spatial distribution of hotspot material added to the lithosphere under La Réunion, from wide-angle seismic data, J. Geophys. Res., B104,(2), 2875–2893.

Chevallier, L., and P. Bachèlery (1981), Evolution structurale du volcan actif du Piton de la Fournaise. Ile de la Réunion, Océan Indien, Bull. Volc., 44 (4), 723–741.

Constable, S., and G. Heinson (2004), Hawaiian hot-spot swell structure from seafloor MT sounding, Tectonophysics, 389, 111–124.

Constable, S. C., and C. S. Cox (1996), Marine controlled source electromagnetic sounding: 2. The PEGASUS experiment, J. Geophys. Res., 101, 5519–5530.

Courteaud, M. (1996), Etude des structures géologiques et hydrogéologiques du Massif de la Fournaise par la méthode audiomagnétotellurique, 212 pp., Thèse d’Université, Univ. de la Réunion.

Courteaud, M., P. Bachèlery, B. Robineau, and J. L. Join (1997), Les brèches de Saint-Gilles. Note technique géologique, Laboratoire des Sciences de la Terre, Univ. de La Réunion. .

Egbert, G. D. and A. Kelbert, (2012), Computational recipes for electromagnetic inverse problems, Geophysical Journal International, 189, 251-267.

Kelbert, A., N.M. Meqbel, G. D. Egbert & K. Tandon, 2014.ModEM: A modular system for inversion of electromagnetic geophysical data,/Comp. Geosci./, 66, 40-53, ISSN 0098-3004, http://dx.doi.org/10.1016/j.cageo.2014.01.010.

Fontaine, F.R., G. Barruol, H. Tkalčić, I. Wölbern, G. Rümpker, T. Bodin, M. Haugmard (2015), Crustal and uppermost mantle structure variation beneath La Réunion hotspot track, Geophysical Journal International, 203, Issue 1, 1, 107–126.

Gailler, L., J.F. Lénat, M. Lambert, G. Levieux, N. Villeneuve, and J. L. Froger (2009), Gravity structure of Piton de la Fournaise volcano and inferred mass transfer during the 2007 crisis, J. Volcanol. Geotherm. Res., 184, 31–48, doi:doi:10.1016/j.jvolgeores.2009.01.024.

Gailler, L., J.F. Lénat, and R.J. Blakely (2016), Depth to Curie temperature or magnetic sources bottom in the volcanic zone of La Réunion hot spot, Earth Planet. Sci. Lett.

Gailler, L.S. (2010), Structure interne d'un système océanique volcanique, La Réunion (Océan Indien) – Approches géophysiques, 471 pp., Université Blaise Pascal-Laboratoire Magmas et Volcans, Clermont-Ferrand.

Gailler, L.S., and J.F. Lénat (2012), Internal architecture of La Réunion (Indian Ocean) inferred from geophysical data, J. Volcanol. Geotherm. Res., 221-222, 83–98.

Gallart, J., L. Driad, P. Charvis, M. Sapin, A. Hirn, J. Diaz, B. de Voogd, and M. Sachpazi (1999), Perturbation to the lithosphere along the hotspot track of La Réunion from an offshore-onshore seismic transect, J. Geophys. Res., B, Solid Earth Planets, 104(2), 2895–2908.

Gillot, P. Y., and P. Nativel (1989), Eruptive history of the Piton de la Fournaise volcano, Réunion Island, Indian Ocean, J. Volcanol. Geotherm. Res., 36, 53–65.

Haak, V. (1982), Electrical Conductivity of Minerals and Rocks at Temperatures and Pressures, in Zahlenwerte und Funktionen aus Naturwissenschaften und Technik /Landolt-Brrnstein, vol. V/1b, edited by G. Angenheister, pp. 291–307, Springer, Berlin.

Jackson, D.B., and J. Kauahikaua (1987), The high-level water table beneath Kilauea Volcano, Hawaii. How Volcanoes Work, Hilo, Hawaii, January 19–25, 120.

Join, J.L., J. L.Folio, and B. Robineau (2005), Aquifers and groundwater within active shield volcanoes. Evolution of conceptual models in the Piton de la Fournaise volcano, J. Volcanol. Geotherm. Res., 147, 187–201.

Jones, A.G. (1999), Imaging the continental upper mantle using electromagnetic methods. Lithos 48, 57– 80.

Lénat, J.F., P. Bachèlery, and O. Merle (2012a), Anatomy of Piton de la Fournaise volcano (La Réunion, Indian Ocean), Bull. Volcanol, 74:1945–1961. doi:10.1007/ s00445-012-0640-y.

Lénat, J.F., D. Fitterman, and D.B. Jackson (2000), Geoelectrical structure of the central zone of Piton de la Fournaise volcano (Réunion), Bull. Volc., 62 (2), 75–89.

Lénat, J.F., B. Gibert-Malengreau, and A. Galdéano (2001), A new model for the evolution of the volcanic island of Reunion (Indian Ocean), J. Geophys. Res., B, 106,(5), 8645–8663.

Lénat, J.F., P. Bachèlery, and A. Peltier (2012b), The interplay between collapse structures, hydrothermal systems and magma intrusions: the case of the central area of Piton de la Fournaise volcano, Bull. Volcanol., 74, 407–421, doi:10.1007/s00445-011-0535-3.

Letourneur, L., A. Peltier, T. Staudacher, and A. Gudmundsson (2008), The effects of rock heterogeneities on dyke paths and asymmetric ground deformation: the example of Piton de la Fournaise volcano, J. Volcanol. Geotherm. Res., 173, 289–302.

Liuzzo, M., A. Di Muro, G. Giudice, L. Michon, V. Ferrazzini, S. Gurrieri (2005), New evidence of CO2 soil degassing anomalies on Piton de la Fournaise volcano and the link with volcano tectonic structures, Geochem. Geophys. Geosyst., 16, 10.1002/2015GC006032

MacGregor, L.M., S.C. Constable, and M. C.Sinha (1998), The RAMESSES experiment—III. Controlled-source electromagnetic sounding of the Reykjanes Ridge at 57°45'N, Geophys. J. Int., 135, 772–789.

Malengreau, B., J.F. Lénat, and J.L. Froger (1999), Structure of Reunion Island (Indian Ocean) inferred from the interpretation of gravity anomalies, J. Volcanol. Geotherm. Res., 88(3), 131–146.

Martı´ A, P. Queralt, J. Ledo (2009), WALDIM: a code for the dimensionality analysis of magnetotelluric data using the rotational invariants of the magnetotelluric tensor. Comput. Geosci. 35(12):2295–2303.

McDougall, I. (1971), The geochronology and evolution of the young volcanic island of Réunion (Indian Ocean), Geochem. Cosmochim. Acta., 35(3), 261–288.

Merle, O., and J.F. Lénat (2003), Hybrid collapse mechanism at Piton de la Fournaise volcano, Reunion Island, Indian Ocean, J. Geophys. Res., 108 (B3), 2166, doi:doi:10.1029/2002JB002014.

Merle, O., P. Mairine, L. Michon, P. Bachèlery, and M. Smietana (2010), Calderas, landslides and paleo-canyons on Piton de la Fournaise volcano (La Réunion Island, Indian Ocean), J. Volcanol. Geotherm. Res., in press.

Michon, L., and F. Saint-Ange (2008), Morphology of Piton de la Fournaise basaltic shield volcano (La Réunion Island): Characterization and implication in the volcano evolution, J. Volcanol. Geotherm. Res., 113(B03203), 1–19, doi:doi:10.1029/2005JB004118.

Michon, L., V. Ferrazzini, A. Di Muro (2016), Magma intrusions paths of Piton de la Fournaise. In: Bachèlery, P., Lénat, J.F., Di Muro, A., Michon, L. (Editor), Active Volcanoes of the Southwest Indian Ocean: Piton de la Fournaise and Karthala. Active Volcanoes of the World. Springer-Verlag Berlin and Heidelberg. pp. 91-106.

Mohamed-Abchir, A. (1996), Les Cendres de Bellecombe: un événement majeur dans le passé récent du Piton de la Fournaise, Ile de la Réunion, 248 pp., Université de Paris VII.

Morandi, A., A. Di Muro, C. Principe, L. Michon, G. Leroi, F. Norelli, and P. Bachèlery (2015), Pre-historic explosive activity at Piton de la Fournaise volcano, in Active Volcanoes of the Southwest Indian Ocean: Piton de la Fournaise and Karthala. Active Volcanoes of the World., edited by P. Bachèlery, J.F. Lénat, A. Di Muro, and L. Michon.

Nobes, D.C., L.K. Law, and R.N. Edwards (1992), Results of a sea-floor electromagnetic survey over a sedimented hydrothermal area on the Juan de Fuca Ridge, Geophys. J. Int., 110, 333–346.

Pinã-Varas P., L. Ledo, P. Queralt, A. Marcuello, F. Bellmunt, R. Hidalgo, M. Messeiller (2014), 3-D Magnetotelluric Exploration of Tenerife Geothermal System (Canary Islands, Spain), Surv. Geophys. 35:1045–1064, doi 10.1007/s10712-014-9280-4.

Rai, M.P., and M.H. Manghnani (1977), Electrical conductivity of basalts to 1550°C. Chapman conference on partial melting in the earth's upper mantle proceedings. Oregon Department of Geology and Mineralogy Bull. 96:219–232 ,

Rançon, J.P., P. Lerebour, and T. Augé (1989), The Grand Brûlé exploration drilling; new data on the deep framework of the Piton de la Fournaise Volcano; Part 1, Lithostratigraphic units and volcanostructural implications, J. Volcanol. Geotherm. Res., 36(1-3), 113–127.

Schnegg, P.A. (1997), Electrical structure of Plaine des Sables caldera, Piton de la Fournaise volcano (Réunion Island), Ann. Geofis., 40, 305–317.

Smith, D.K. (1996), Comparison of the shapes and sizes of seafloor volcanoes on Earth and "pancake" domes on Venus, J. Volcanol. Geotherm. Res., 73(1-2), 47–64.

Staudacher, T., and C.J. Allègre (1993), Ages of the second caldera of Piton de la Fournaise volcano (Réunion) determined by cosmic ray produced 3He and 21Ne, Earth Planet Sci Lett, 119, 395–404.

Stearns, H.T. (1942), Hydrology of volcanic terranes, in Physics of the earth, vol IX. Hydrology. Dover, New York, pp. 678–703.

Takasaki, K.J. (1981), Evaluation of major dike-impounded groundwater reservoirs, Island of Oahu, US Geol. Surv. Open-File Rep. 81-1119146.

Unsworth, M.J. (1994), Exploration of a mid-ocean ridge with a frequency-domain EM system, Geophys. J. Int., 116, 447–467.

Vacher, H.L. (1988), Dupuit-Ghyben-Herzberg analysis of strip-island lenses, Bull. Geol. Soc. Am., 100, 580–591.

Villeneuve, N., and P. Bachèlery (2006), Revue de la typologie des éruptions au Piton de la Fournaise, processus et risques volcaniques associés: Cybergeo: European Journal of Geography (http://cybergeo.revues.org/2536).,

De Voogd, B., S. Pou Palomé, A. Hirn, P. Charvis, J. Gallart, D. Rousset, J. Danobeitia, and H. Perroud (1999), Vertical movements and material transport during hotspot activity; seismic reflection profiling offshore La Réunion, J. Geophys. Res. B, Solid Earth Planets, 104,(2), 2855–2874.

Weaver, J.T., A.K. Agarwal, F.E.M. Lilley (2000), Characterization of the magnetotelluric tensor in terms of its invariants. Geophys. J. Int. 141(2):321–336. http://dx.doi.org/10.1046/j.1365-246x.2000.00089.x.

Figure 1

(a)

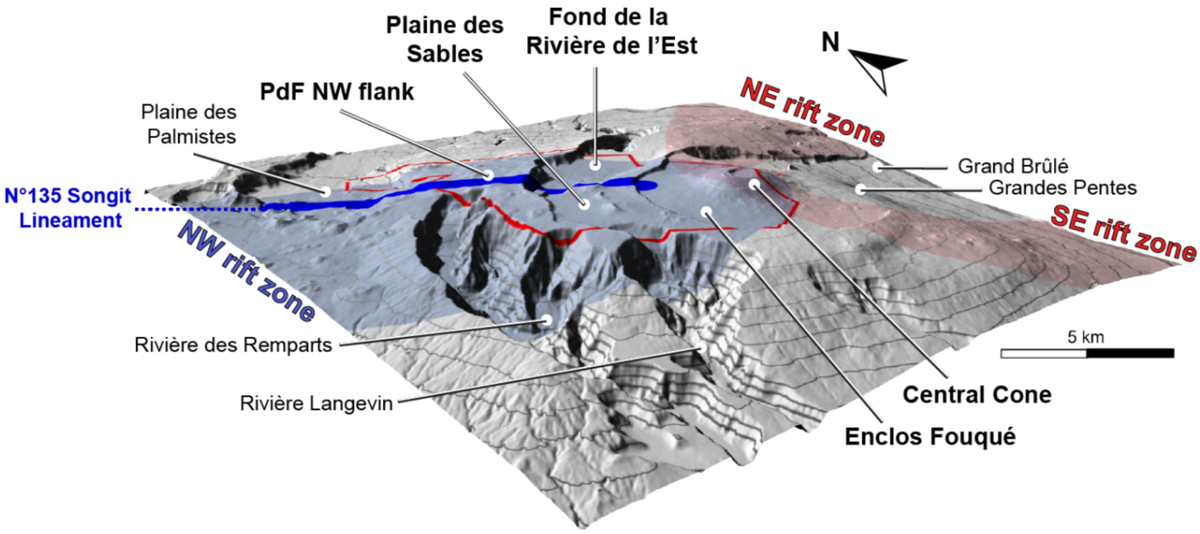

Plaine des Sables
Fond de la Rivière de l'Est
N
PdF NW flank
Plaine des Palmistes
NE rift zone
Grand Brûlé
Grandes Pentes
N°135 Songit Lineament
NW rift zone
SE rift zone
5 km
Rivière des Remparts
Rivière Langevin
Central Cone
Enclos Fouqué

(b)

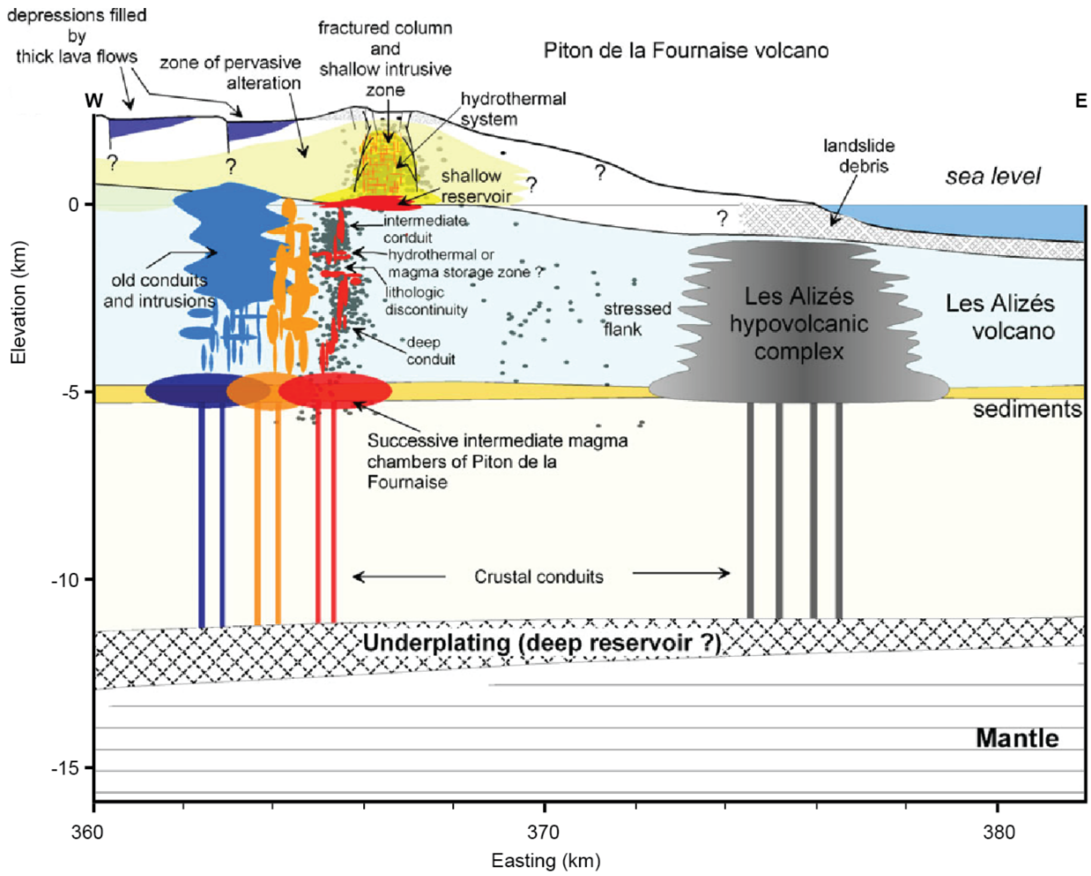

depressions filled by thick lava flows
zone of pervasive alteration
fractured column and shallow intrusive zone
Piton de la Fournaise volcano
hydrothermal system
W
E
shallow reservoir
landslide debris
sea level
intermediate conduit
hydrothermal or magma storage zone ?
lithologic discontinuity
deep conduit
old conduits and intrusions
stressed flank
Les Alizés hypovolcanic complex
Les Alizés volcano
sediments
Successive intermediate magma chambers of Piton de la Fournaise
Crustal conduits
Underplating (deep reservoir ?)
Mantle
Elevation (km)
0
-5
-10
-15
360
370
380
Easting (km)

Figure 2

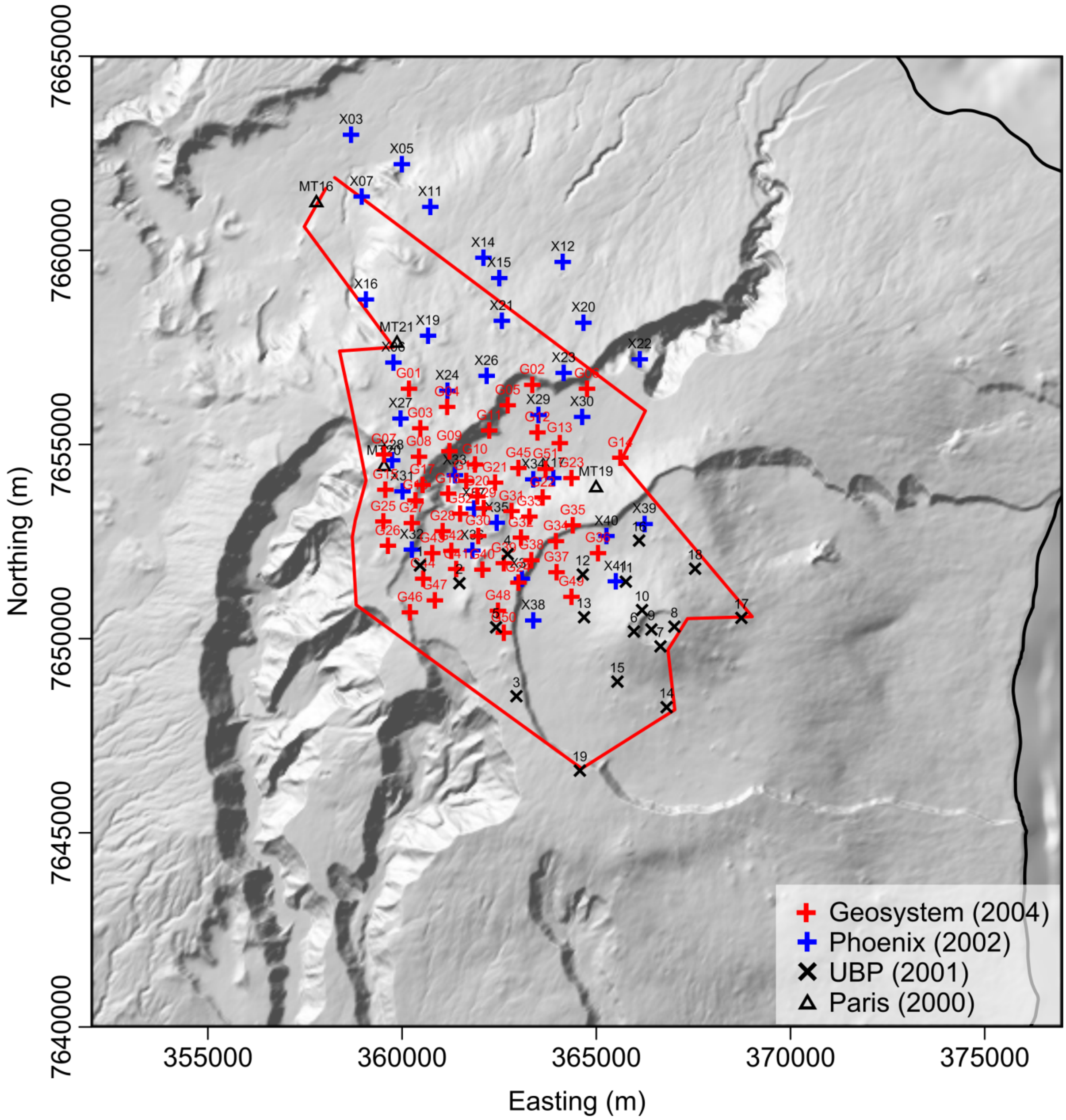

7665000
7660000
7655000
7650000
7645000
7640000
Northing (m)
355000
360000
365000
370000
375000
Easting (m)
Geosystem (2004)
Phoenix (2002)
UBP (2001)
Paris (2000)

Figure 3

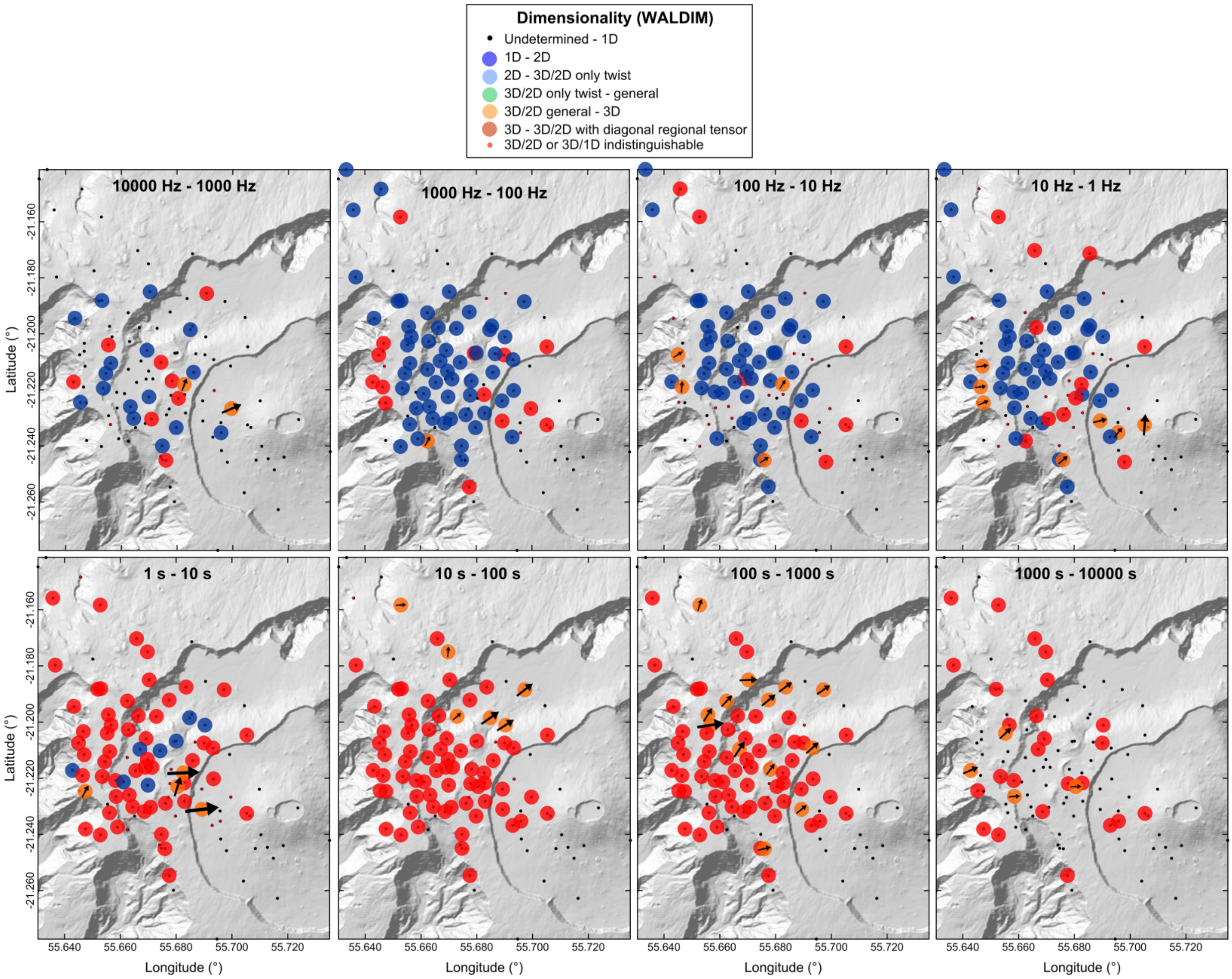

Dimensionality (WALDIM)
Undetermined - 1D
1D - 2D
2D - 3D/2D only twist
3D/2D only twist - general
3D/2D general - 3D
3D - 3D/2D with diagonal regional tensor
3D/2D or 3D/1D indistinguishable
10000 Hz - 1000 Hz
1000 Hz - 100 Hz
100 Hz - 10 Hz
10 Hz - 1 Hz
1 s - 10 s
10 s - 100 s
100 s - 1000 s
1000 s - 10000 s
Latitude (°)
-21.160
-21.180
-21.200
-21.220
-21.240
-21.260
Longitude (°)
55.640
55.660
55.680
55.700
55.720

Figure 4

(a)

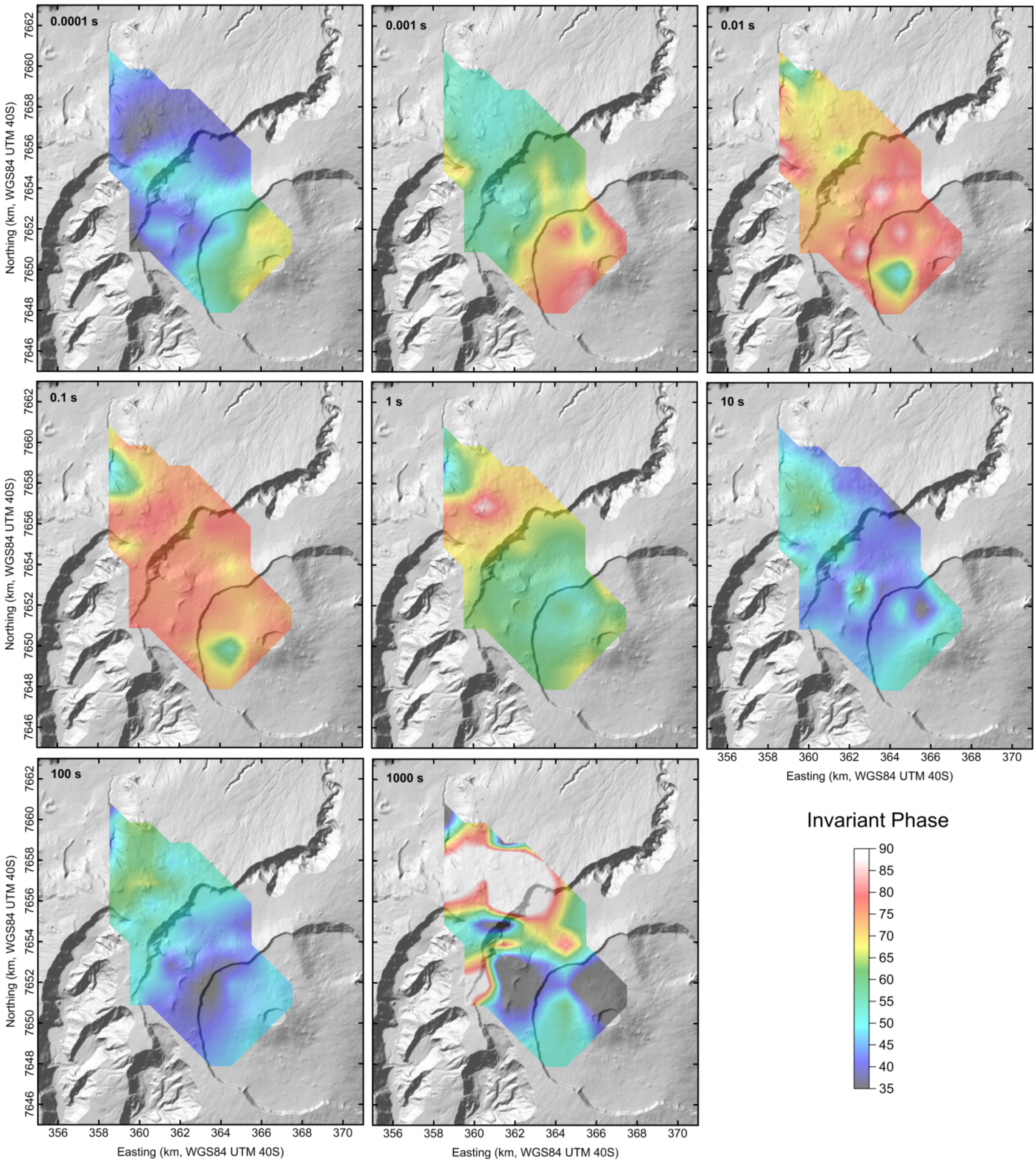

0.0001 s
0.001 s
0.01 s
0.1 s
1 s
10 s
100 s
1000 s
Northing (km, WGS84 UTM 40S)
7662
7660
7658
7656
7654
7652
7650
7648
7646
Easting (km, WGS84 UTM 40S)
356
358
360
362
364
366
368
370
Invariant Phase
90
85
80
75
70
65
60
55
50
45
40
35

(b)

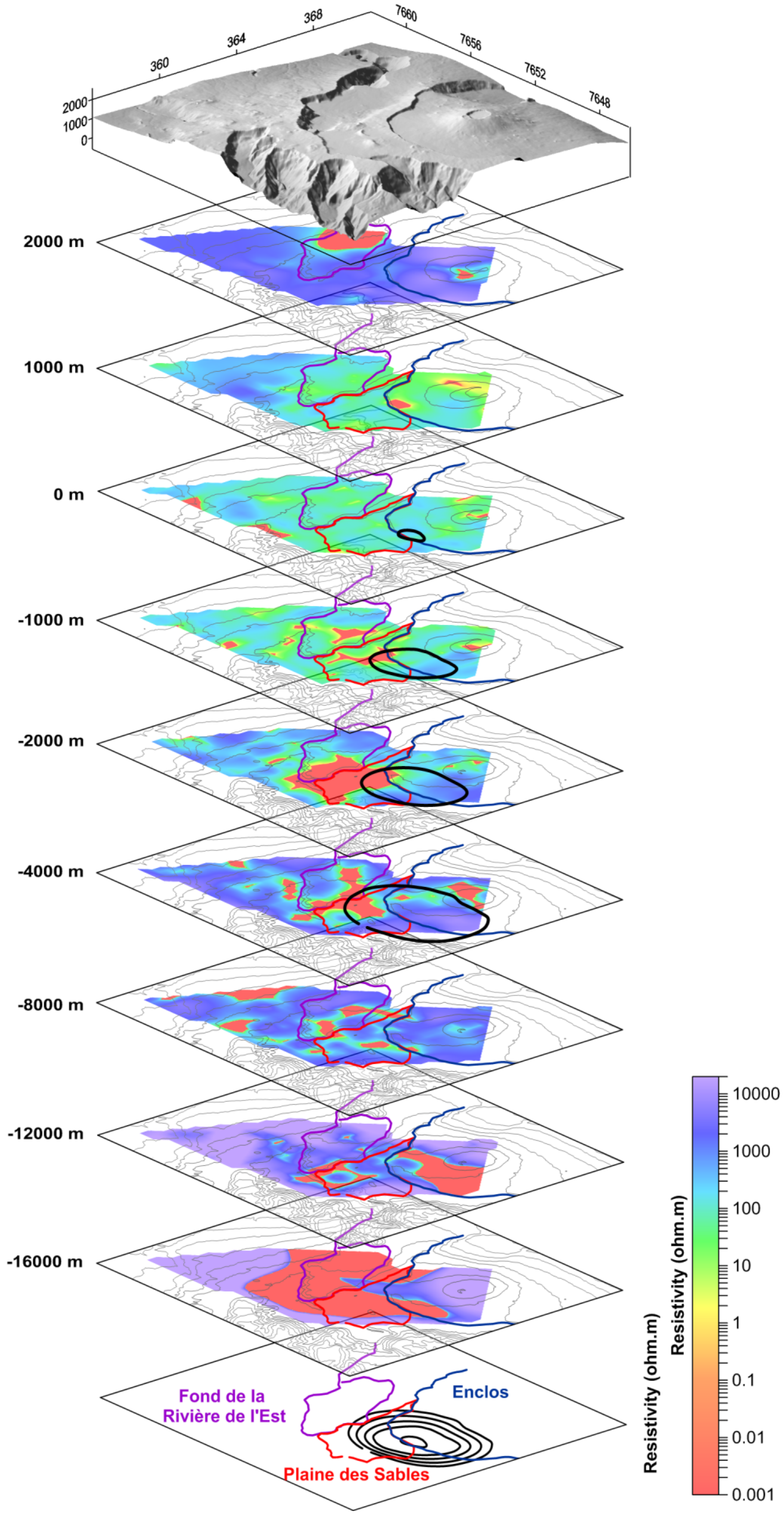
360
364
368
7660
7656
7652
7648
2000
1000
0
2000 m
1000 m
0 m
-1000 m
-2000 m
-4000 m
-8000 m
-12000 m
-16000 m
Fond de la Rivière de l'Est
Enclos
Plaine des Sables
10000
1000
100
10
1
0.1
0.01
0.001
Resistivity (ohm.m)

Figure 5

(a)

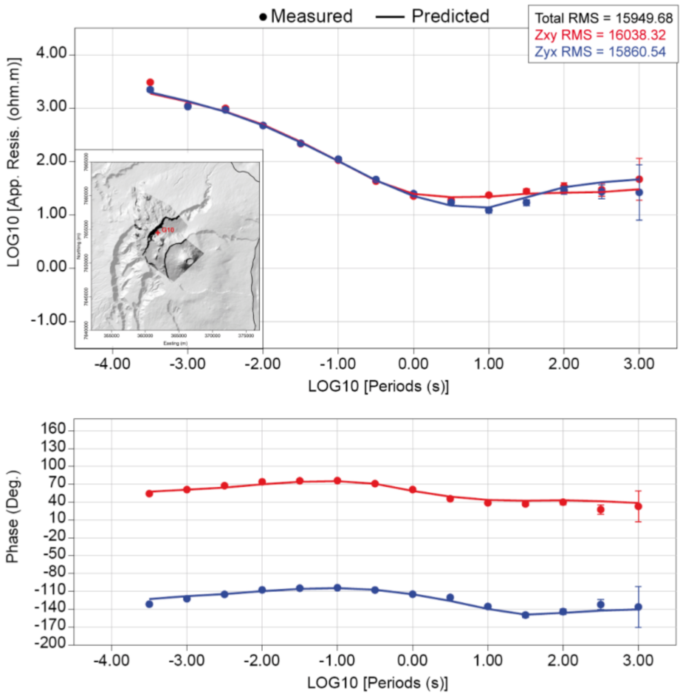

Measured
Predicted
Total RMS = 15949.68
Zxy RMS = 16038.32
Zyx RMS = 15860.54
LOG10 [App. Resis. (ohm.m)]
LOG10 [Periods (s)]
Phase (Deg.)
LOG10 [Periods (s)]

(b)

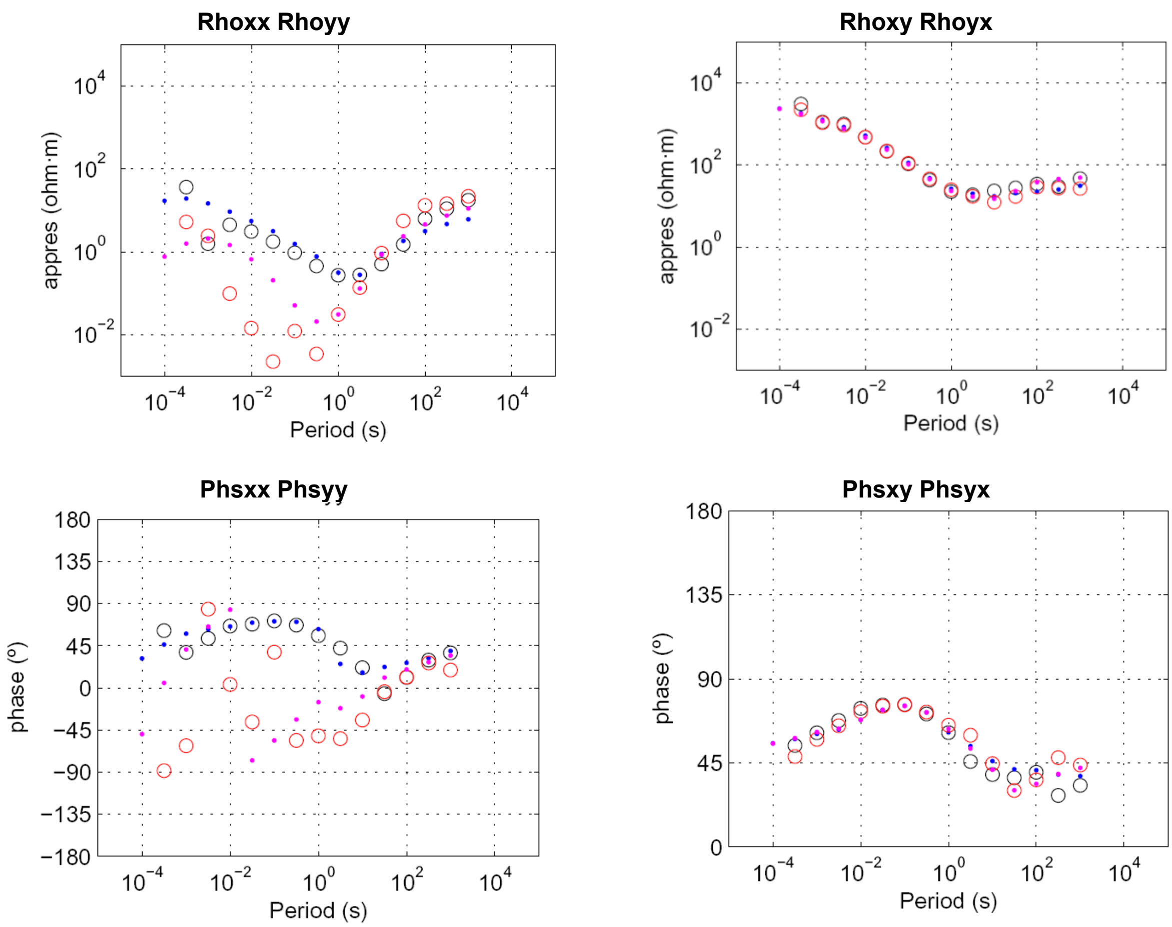

Rhoxx Rhoyy
appres (ohm·m)
Period (s)
Rhoxy Rhoyx
appres (ohm·m)
Period (s)
Phsxx Phsyy
phase (°)
Period (s)
Phsxy Phsyx
phase (°)
Period (s)

Figure 6

(a)

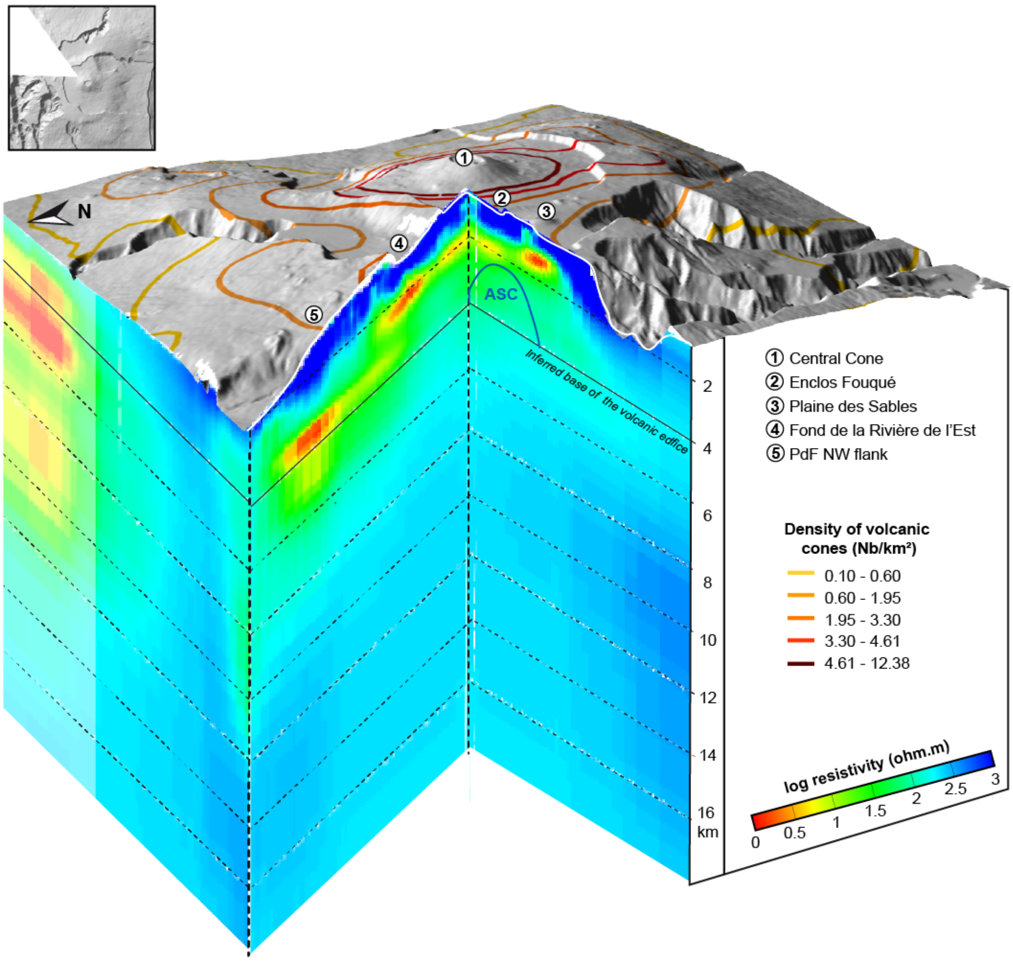
N
① Central Cone
② Enclos Fouqué
③ Plaine des Sables
④ Fond de la Rivière de l'Est
⑤ PdF NW flank
ASC
Inferred base of the volcanic edifice
2
4
6
8
10
12
14
16
km
Density of volcanic cones (Nb/km²)
0.10 - 0.60
0.60 - 1.95
1.95 - 3.30
3.30 - 4.61
4.61 - 12.38
log resistivity (ohm.m)
0
0.5
1
1.5
2
2.5
3

(b)

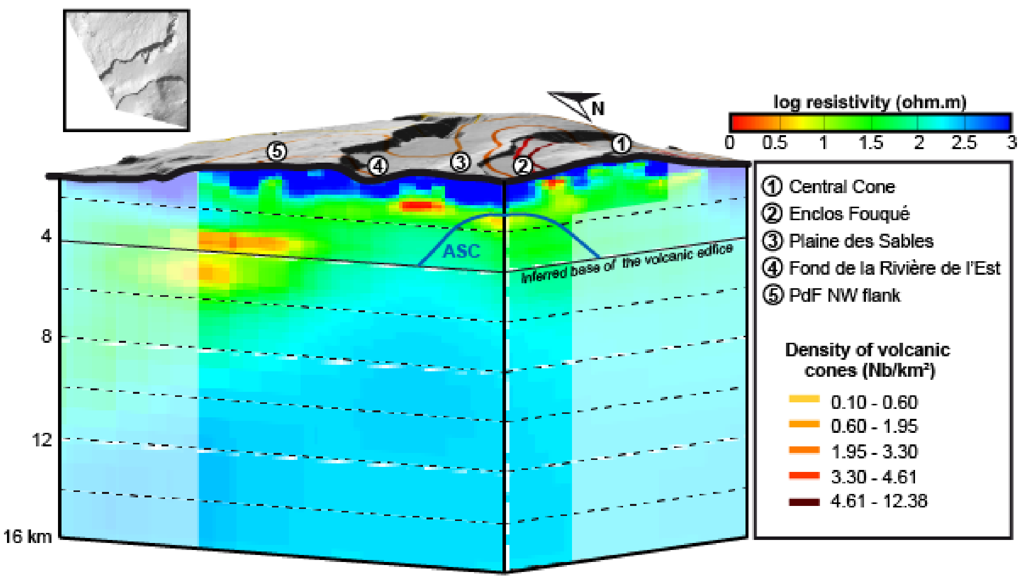
N
log resistivity (ohm.m)
0
0.5
1
1.5
2
2.5
3
ASC
Inferred base of the volcanic edifice
4
8
12
16 km
① Central Cone
② Enclos Fouqué
③ Plaine des Sables
④ Fond de la Rivière de l'Est
⑤ PdF NW flank
Density of volcanic cones (Nb/km²)
0.10 - 0.60
0.60 - 1.95
1.95 - 3.30
3.30 - 4.61
4.61 - 12.38

(c)

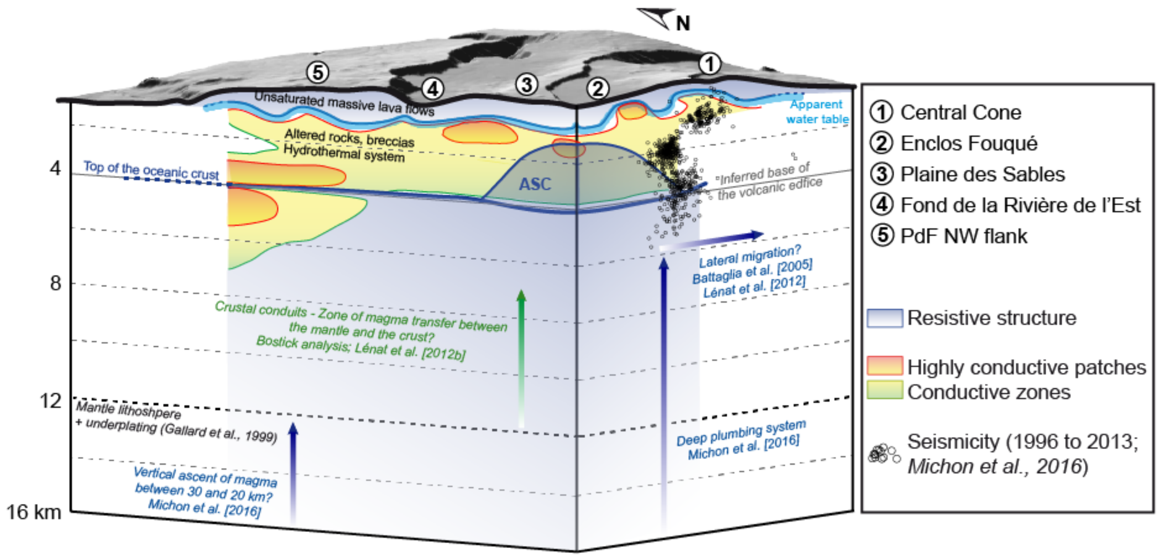
N
1
2
3
4
5
Unsaturated massive lava flows
Altered rocks, breccias
Hydrothermal system
Apparent water table
Top of the oceanic crust
ASC
Inferred base of the volcanic edifice
Lateral migration?
Battaglia et al. [2005]
Lénat et al. [2012]
Crustal conduits - Zone of magma transfer between the mantle and the crust?
Bostick analysis; Lénat et al. [2012b]
Mantle lithoshpere
+ underplating (Gallard et al., 1999)
Deep plumbing system
Michon et al. [2016]
Vertical ascent of magma between 30 and 20 km?
Michon et al. [2016]
4
8
12
16 km
1 Central Cone
2 Enclos Fouqué
3 Plaine des Sables
4 Fond de la Rivière de l'Est
5 PdF NW flank
Resistive structure
Highly conductive patches
Conductive zones
Seismicity (1996 to 2013; Michon et al., 2016)

Supplementary Online material A

Details on MT-AMT data location

At the scale of the study area, the final dataset includes 118 MT and AMT soundings, and 17 electrical soundings from various organizations (Fig. A.1).

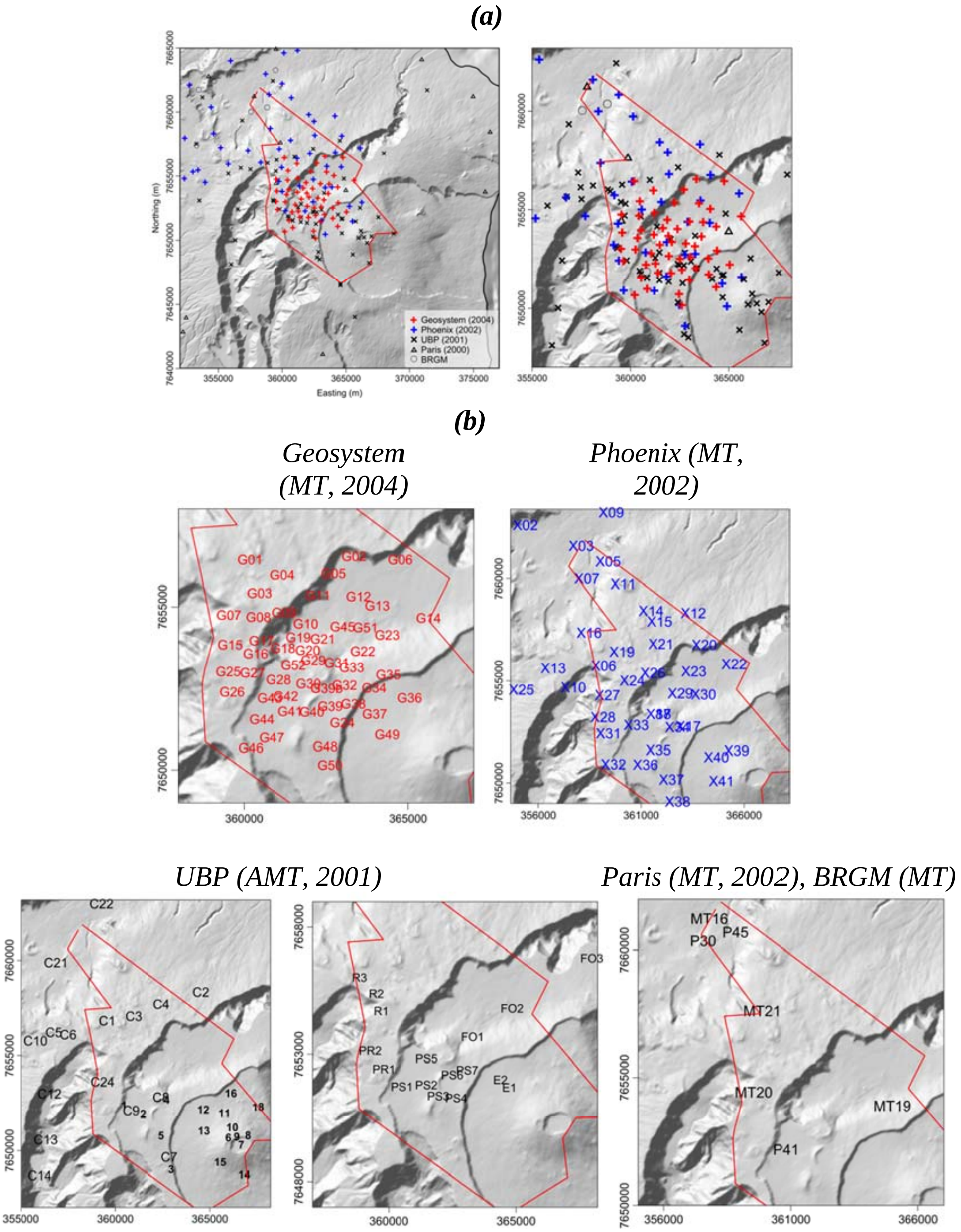

Figure A.1: a) *Location of the resistivity soundings used in this study at the scale of Piton de la Fournaise.* ***b)*** *Zoom on each set of soundings from various organizations. The study area is framed in red.*

The soundings have a typical spacing of 700 m in the center of the survey area (2 by km²), increasing to 1000 m towards the periphery.

The data, available as EDI files, were processed using WinGLink ™ Version 2.6.02 provided by Geosystem society. In addition to treatment and modelling options, this software also provides features of a geo-referenced database for all geophysical measurements. When multiple sets of data were available for a sounding (i.e. HF and LF for AMT and MT data), the combination of the data was also performed with this software.

Supplementary Online material B

Raw data versus model responses

Fig. B.1: Comparison between the raw data and model responses as apparent resistivity and phases curves for each site used in inversion.

Site: 2

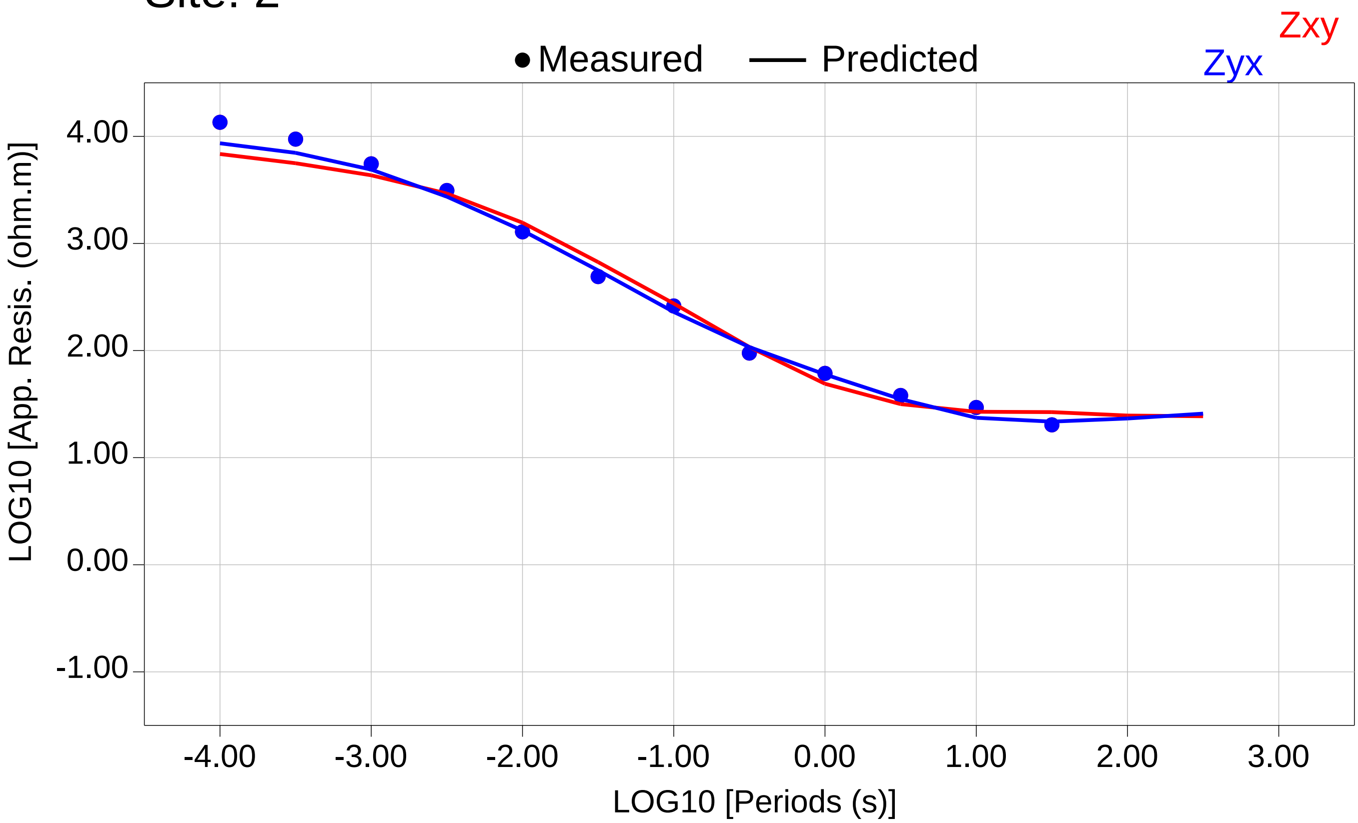

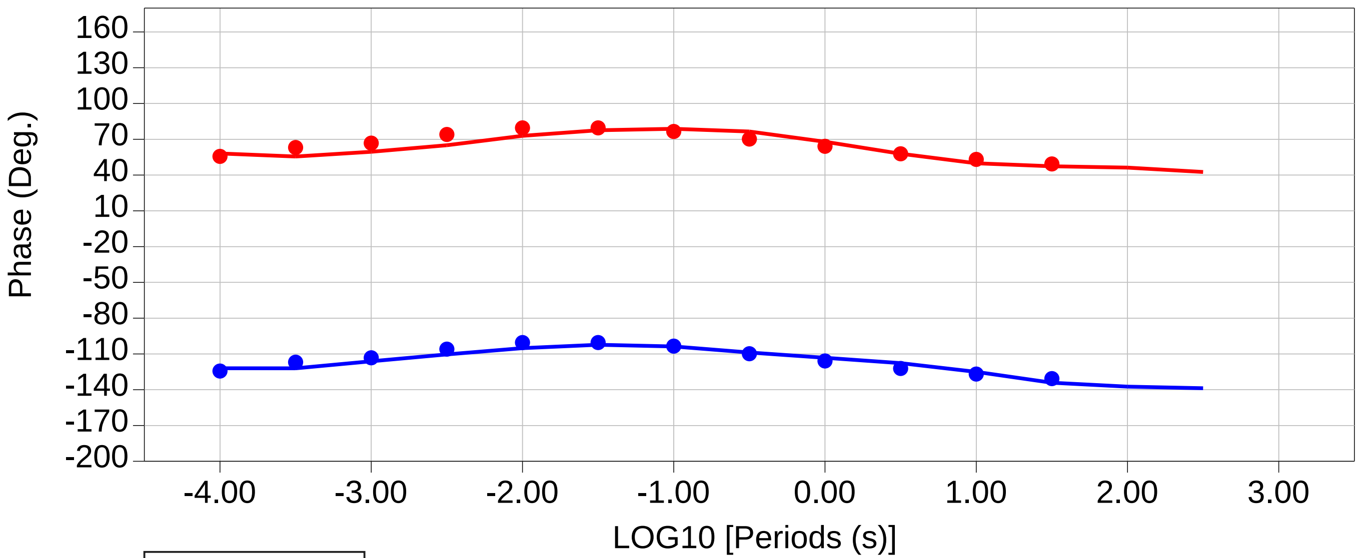

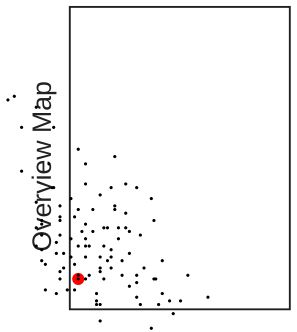

Total RMS = 20196.14

Zxy RMS = 20404.41
Zyx RMS = 19985.71

Site: 3

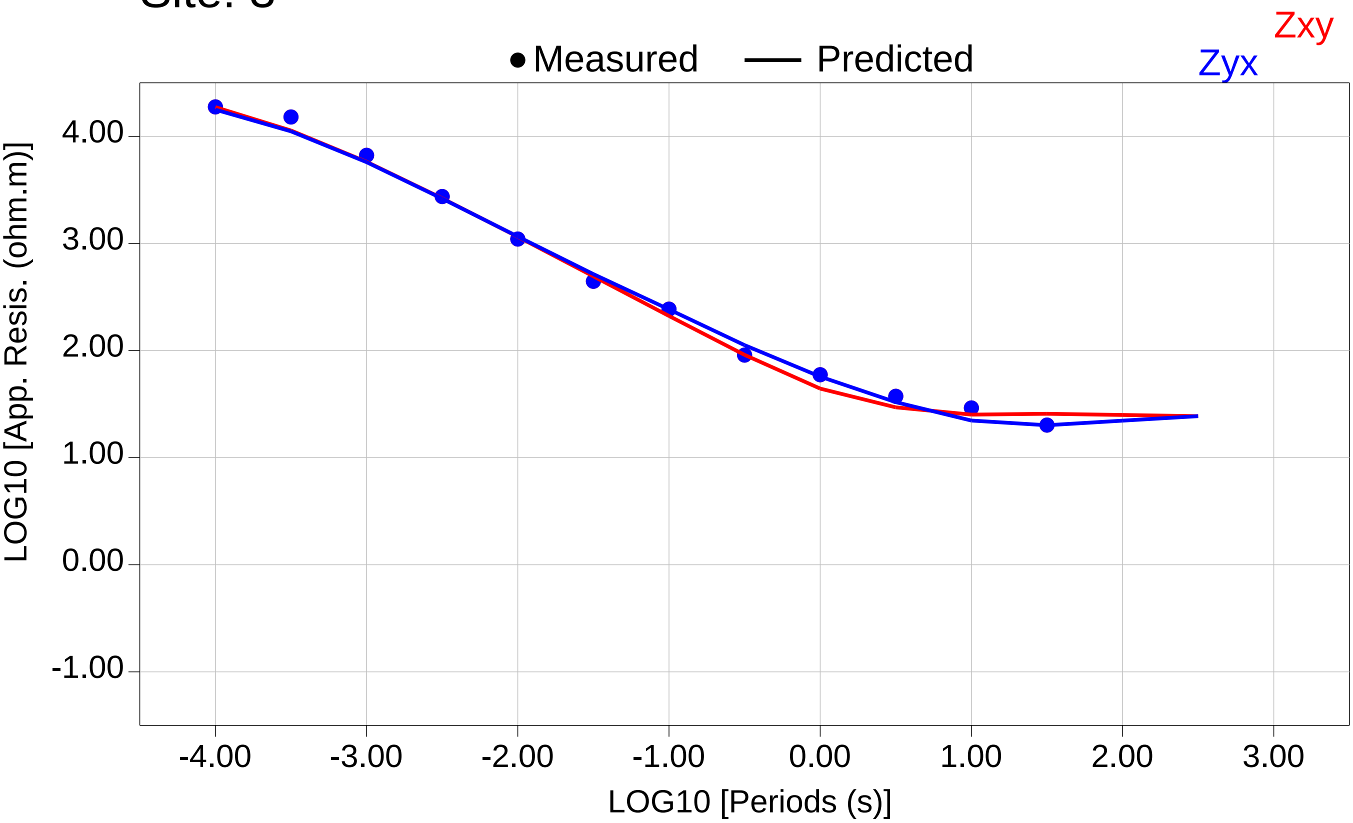

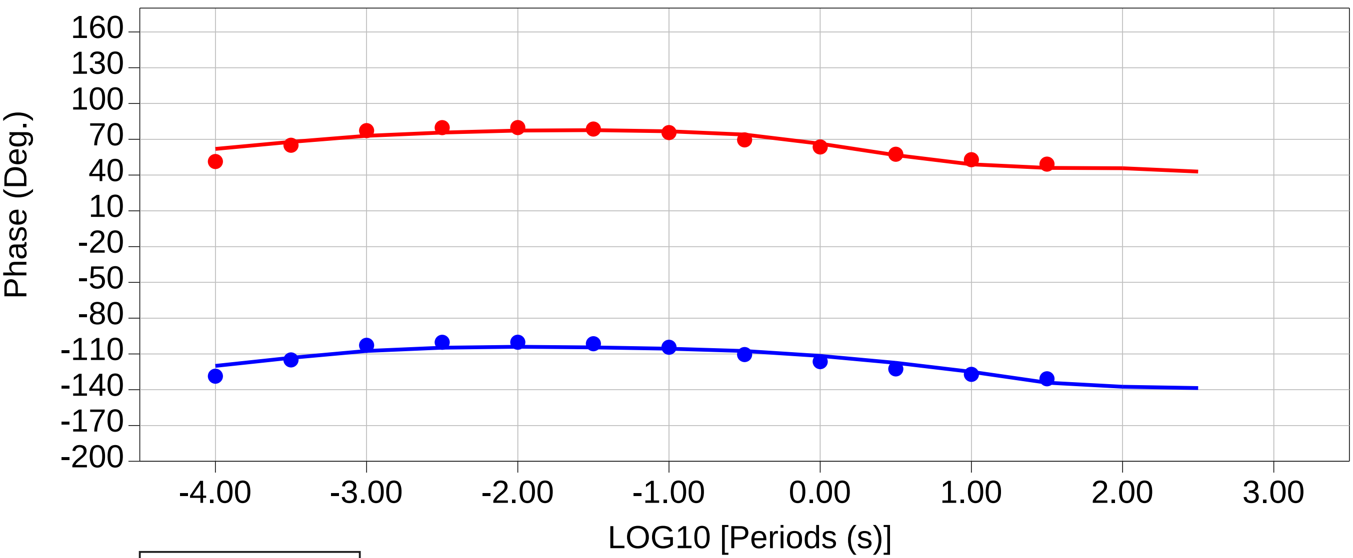

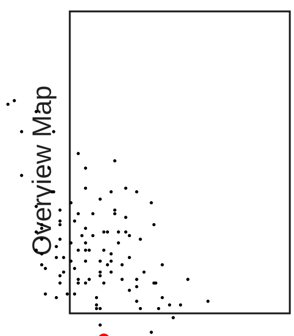

Total RMS = 20560.45

Zxy RMS = 20339.08

Zyx RMS = 20779.46

Site: 18

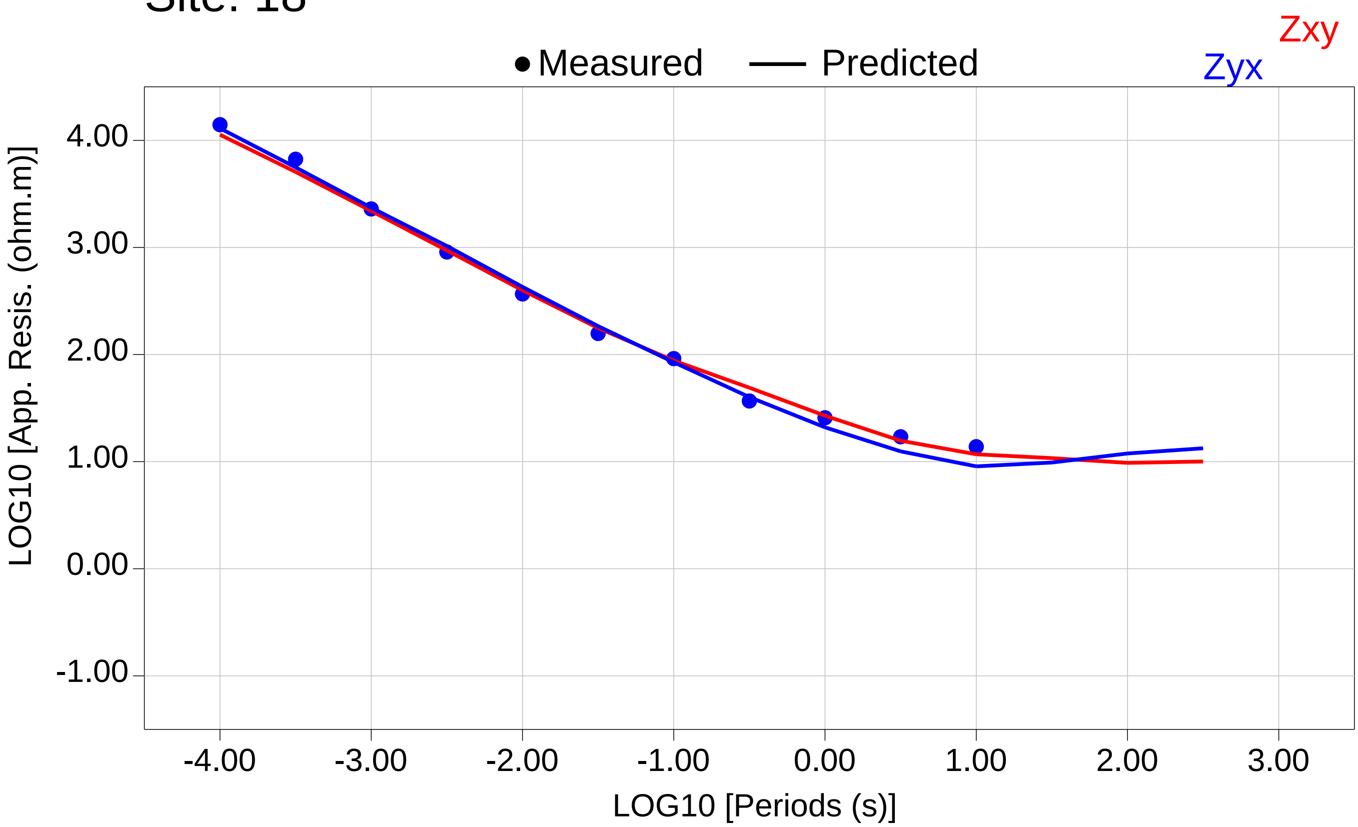

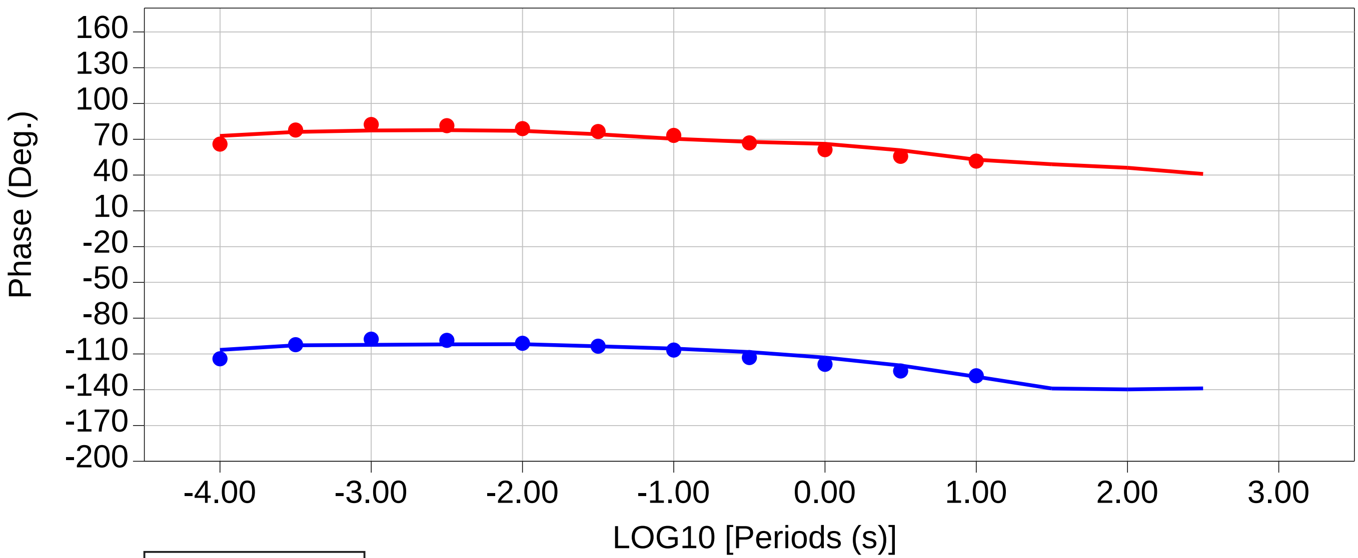

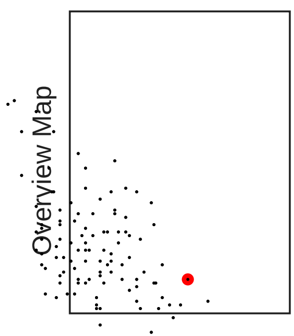

Total RMS = 21298.52

Zxy RMS = 21243.25
Zyx RMS = 21353.66

Site: G02

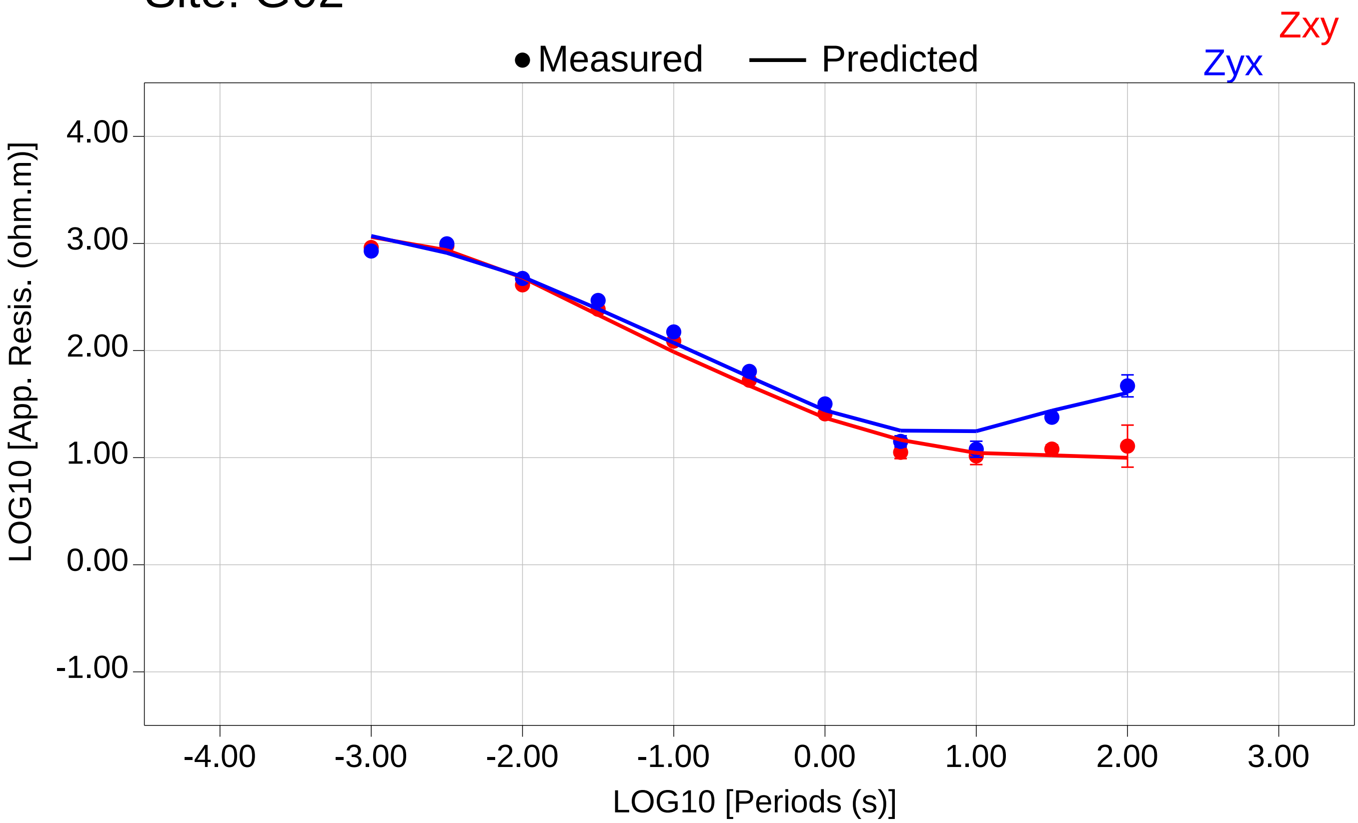

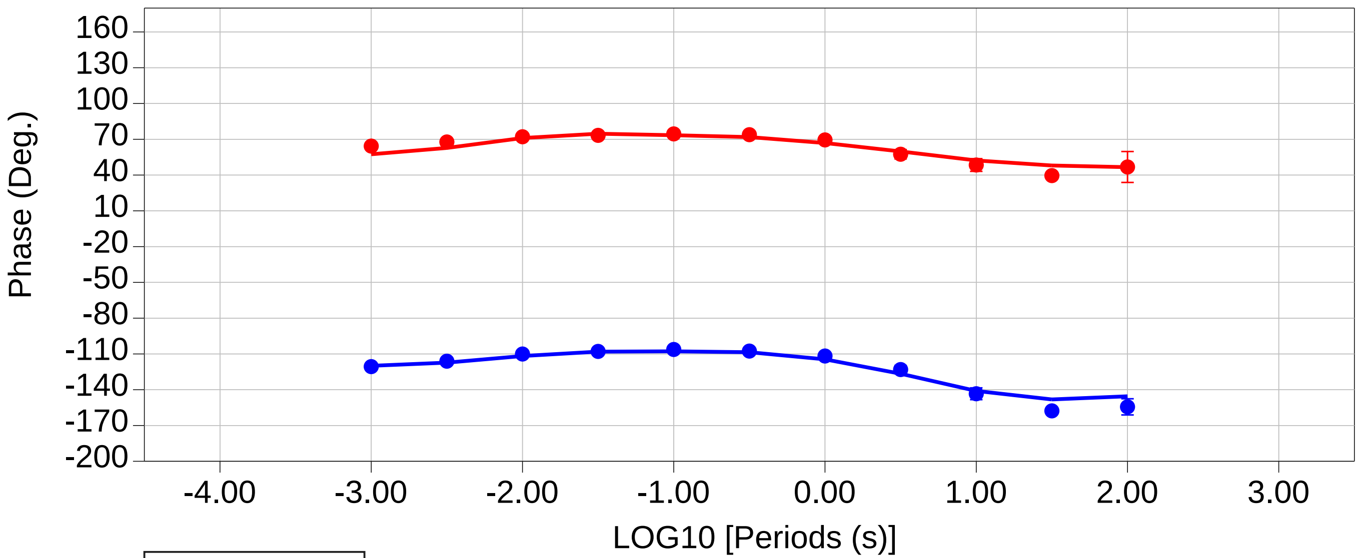

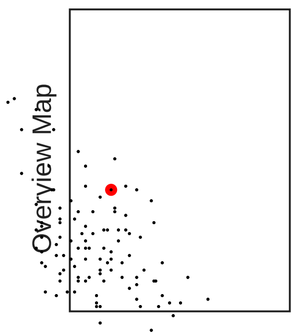

Total RMS = 16595.32

Zxy RMS = 16033.28
Zyx RMS = 17138.94

Site: G03

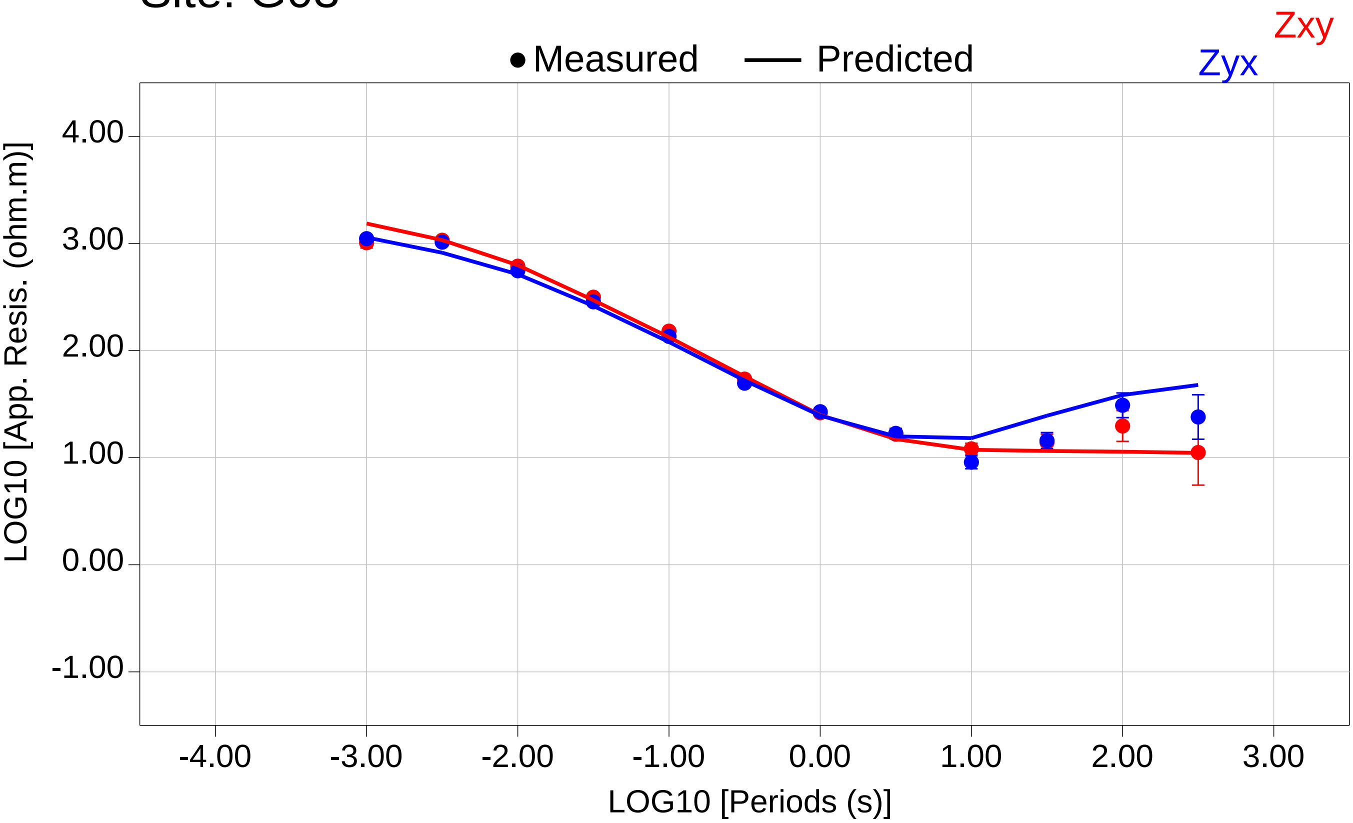

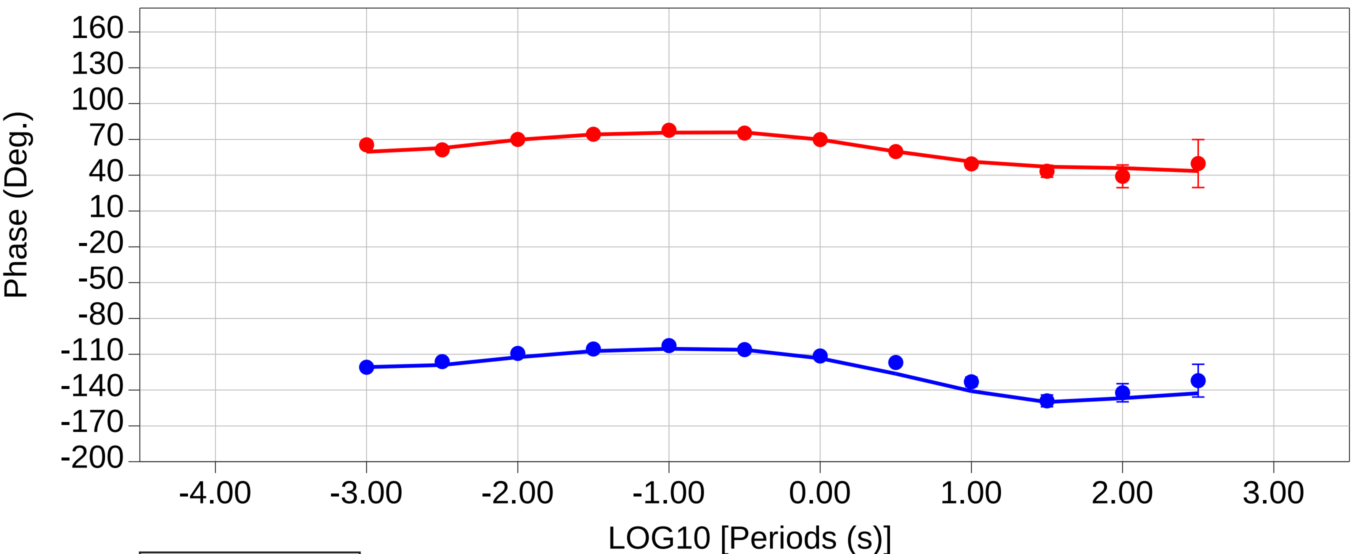

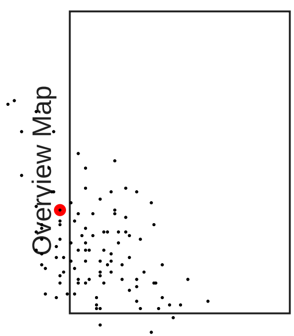

Total RMS = 16040.16

Zxy RMS = 16495.12
Zyx RMS = 15571.92

Site: G05

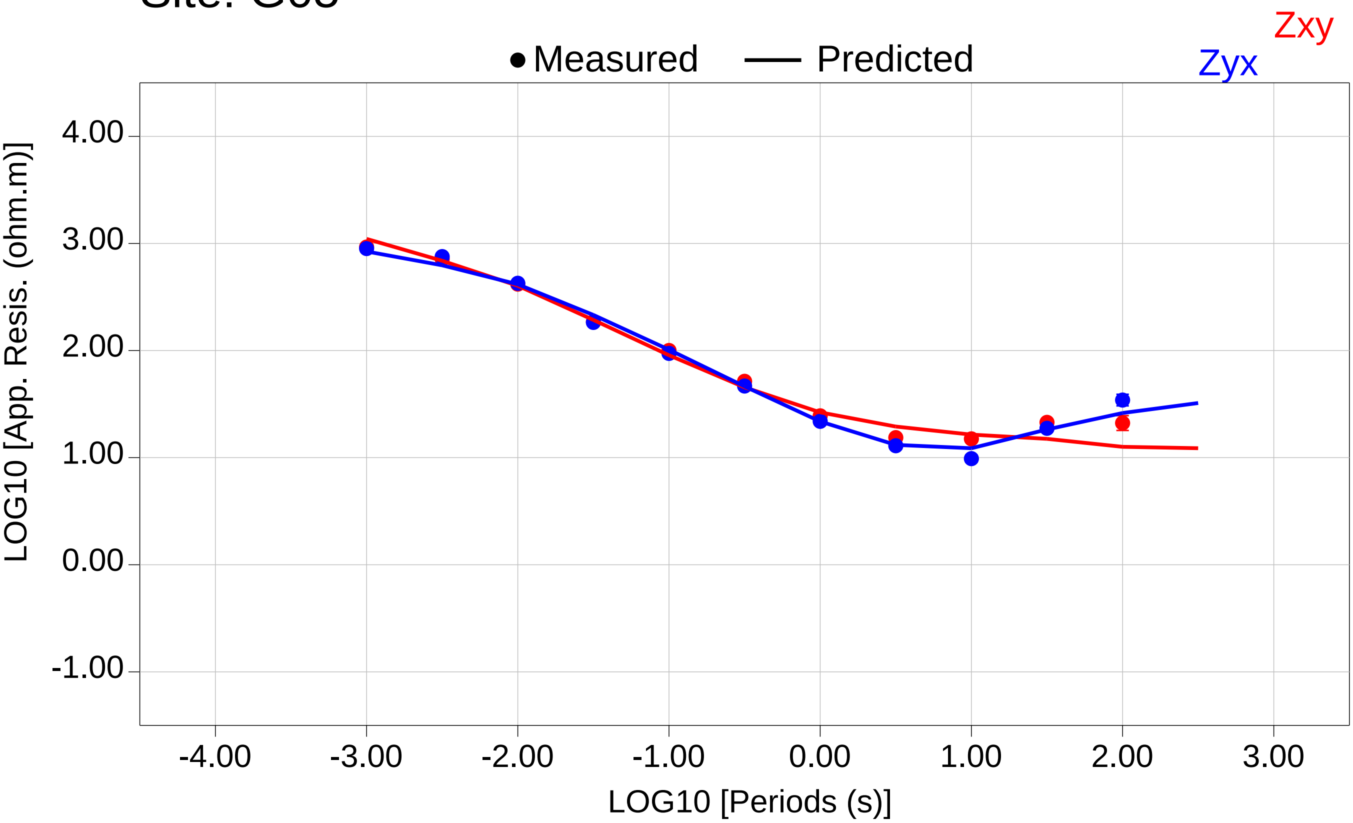

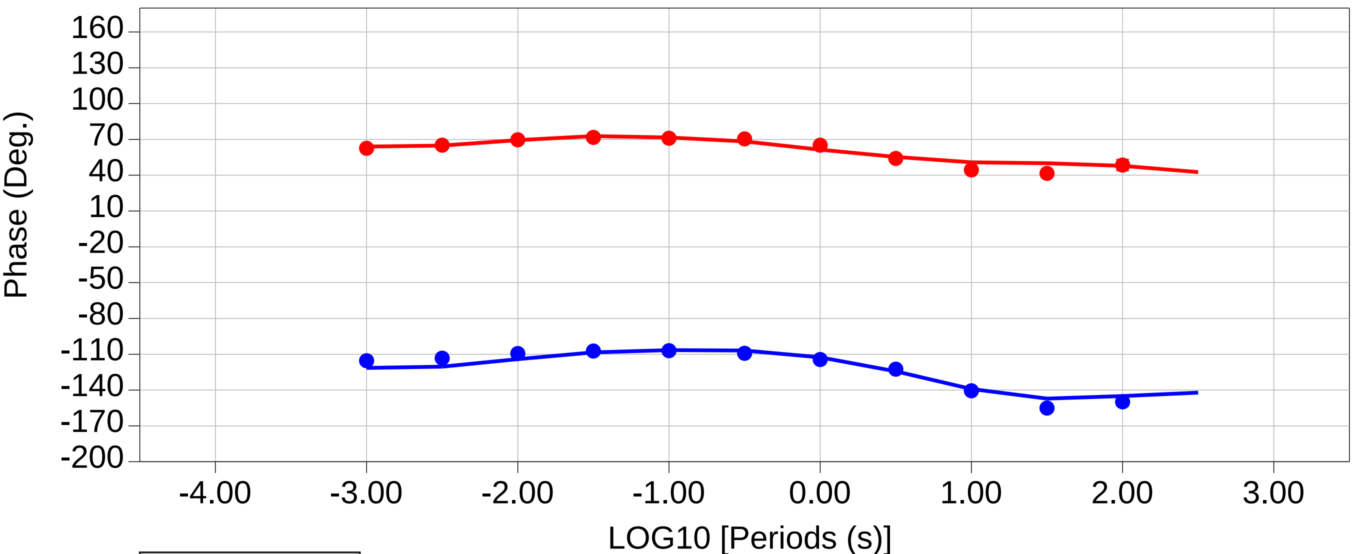

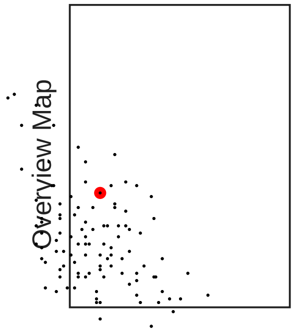

Total RMS = 18732.56

Zxy RMS = 19105.57
Zyx RMS = 18351.98

Site: G06

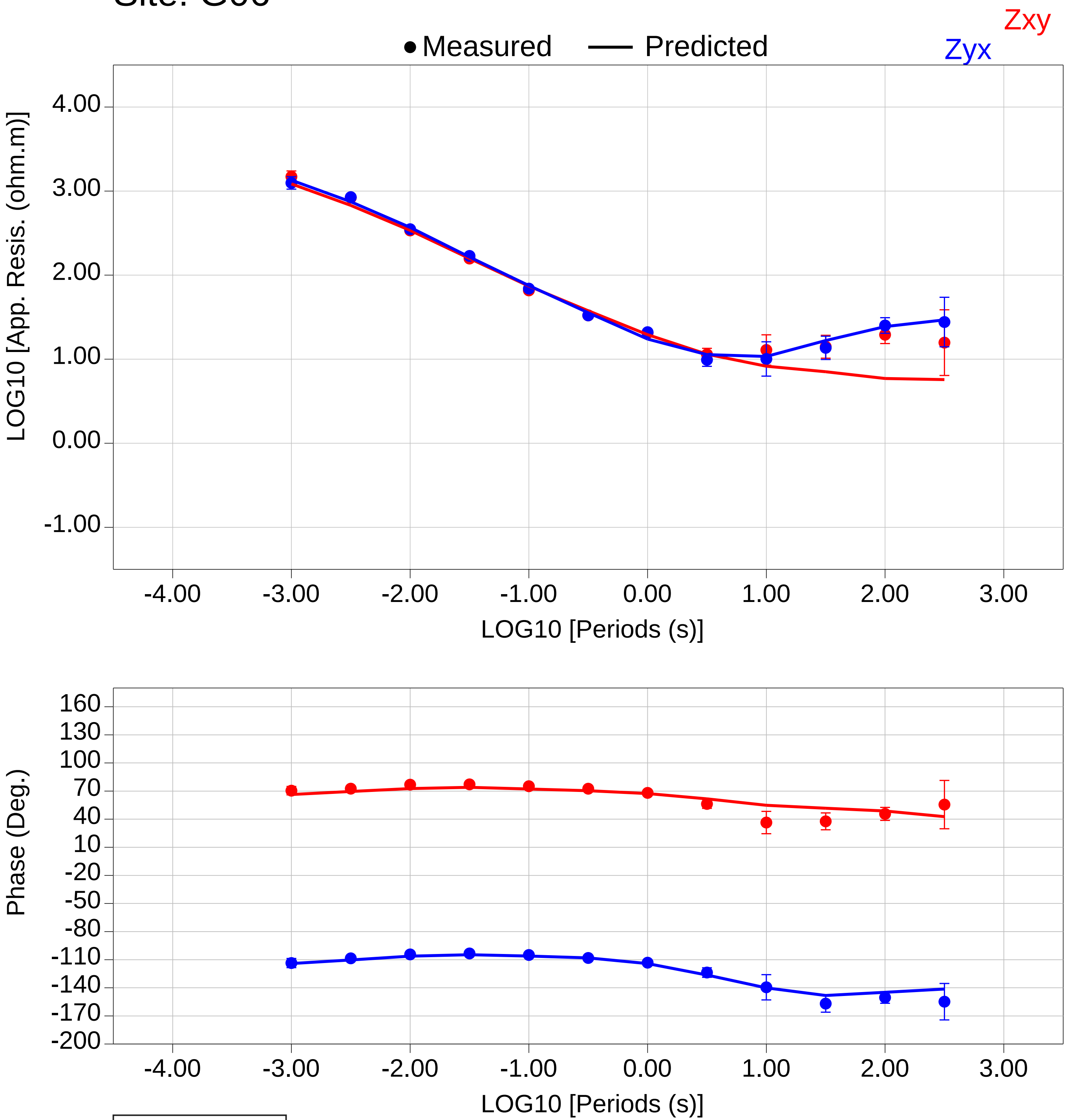

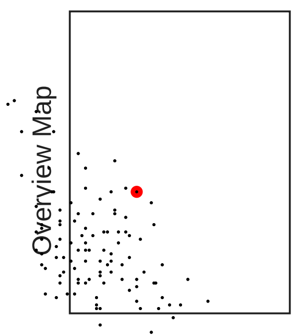

Total RMS = 15633.57

Zxy RMS = 15428.56

Zyx RMS = 15835.92

Site: G08

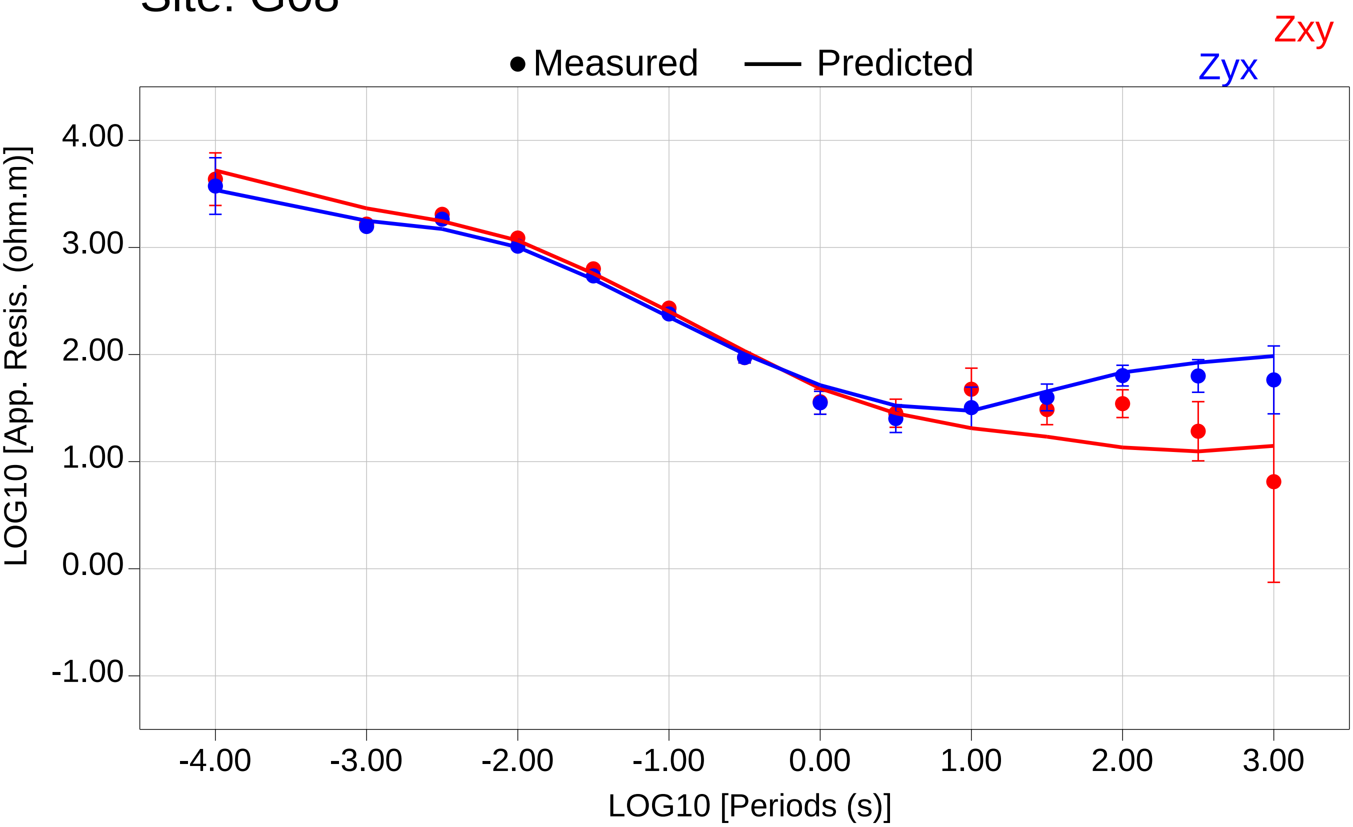

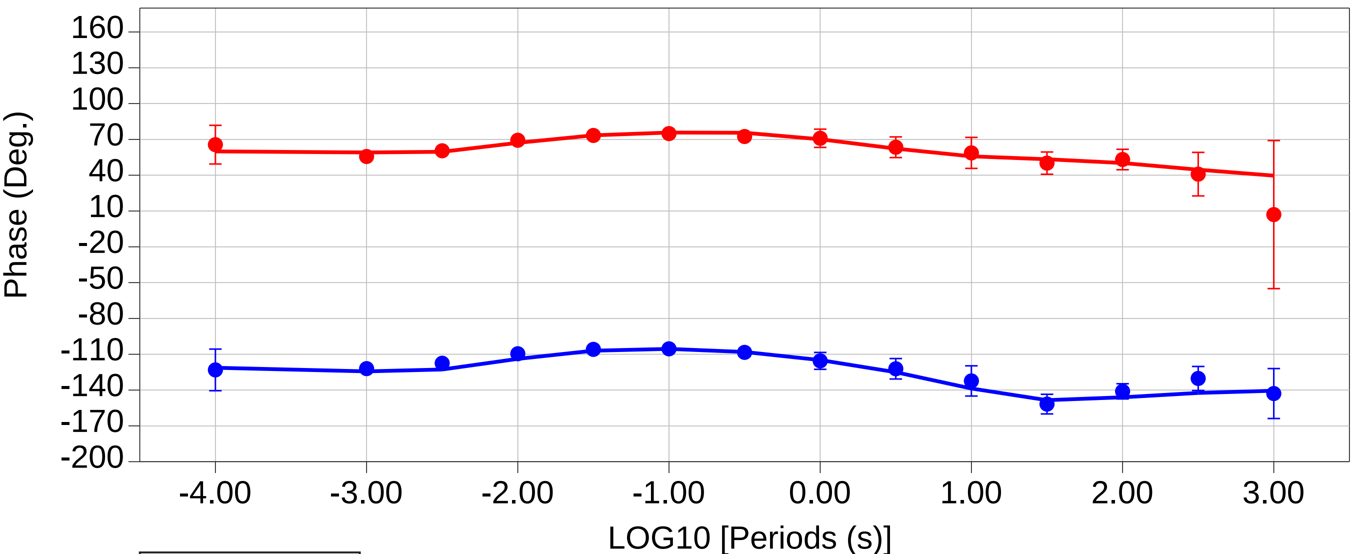

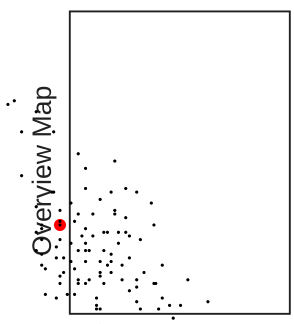

Total RMS = 12092.52

Zxy RMS = 12525.79
Zyx RMS = 11643.14

Site: G09

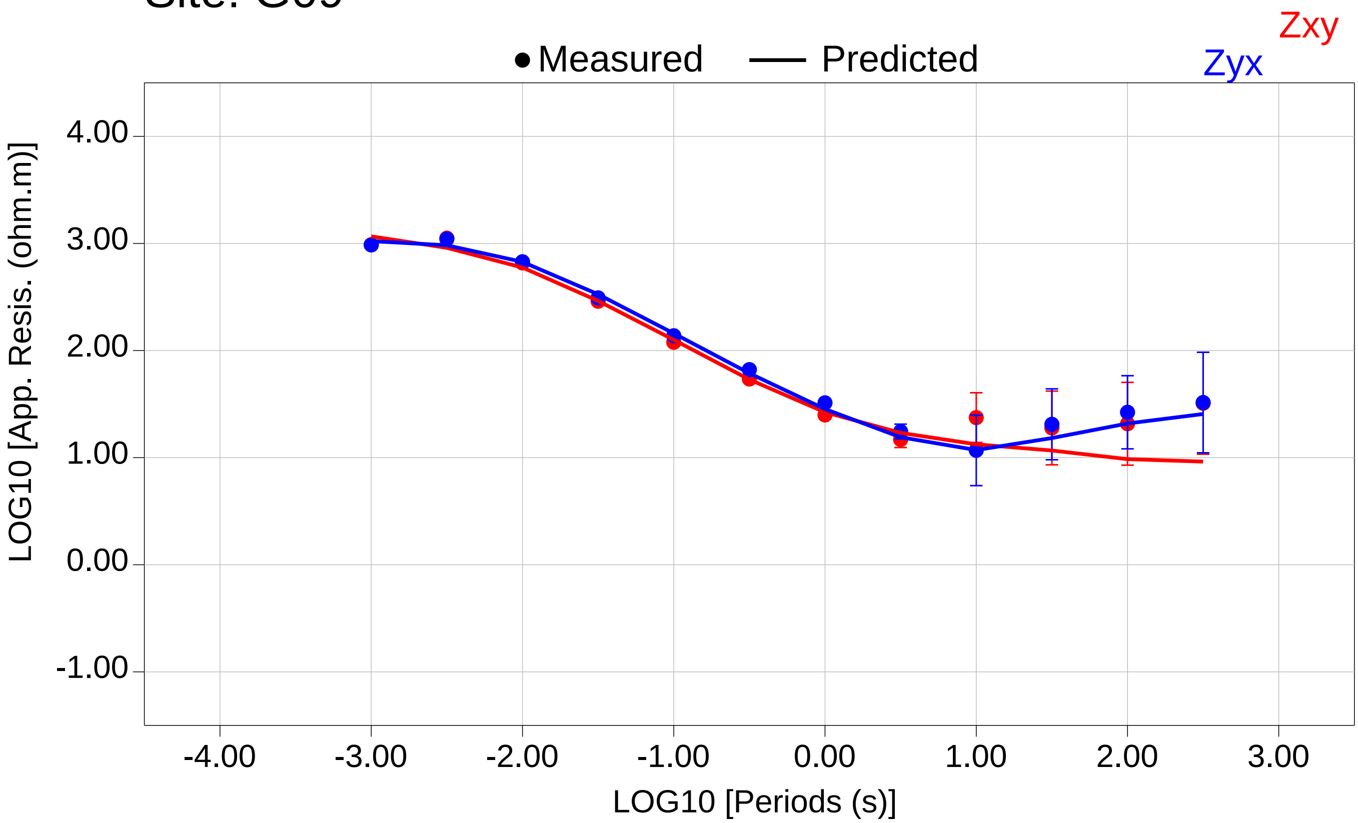

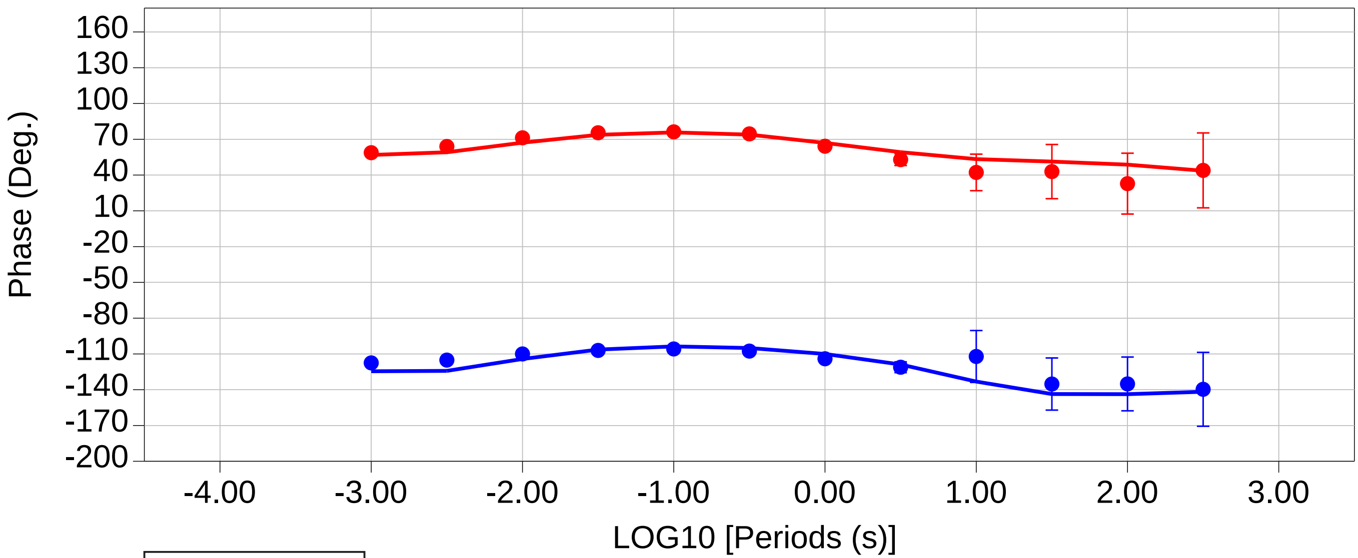

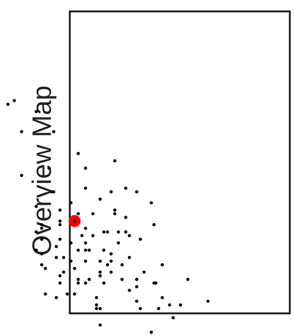

Total RMS = 15210.51

Zxy RMS = 14903.62
Zyx RMS = 15511.34

Site: G10

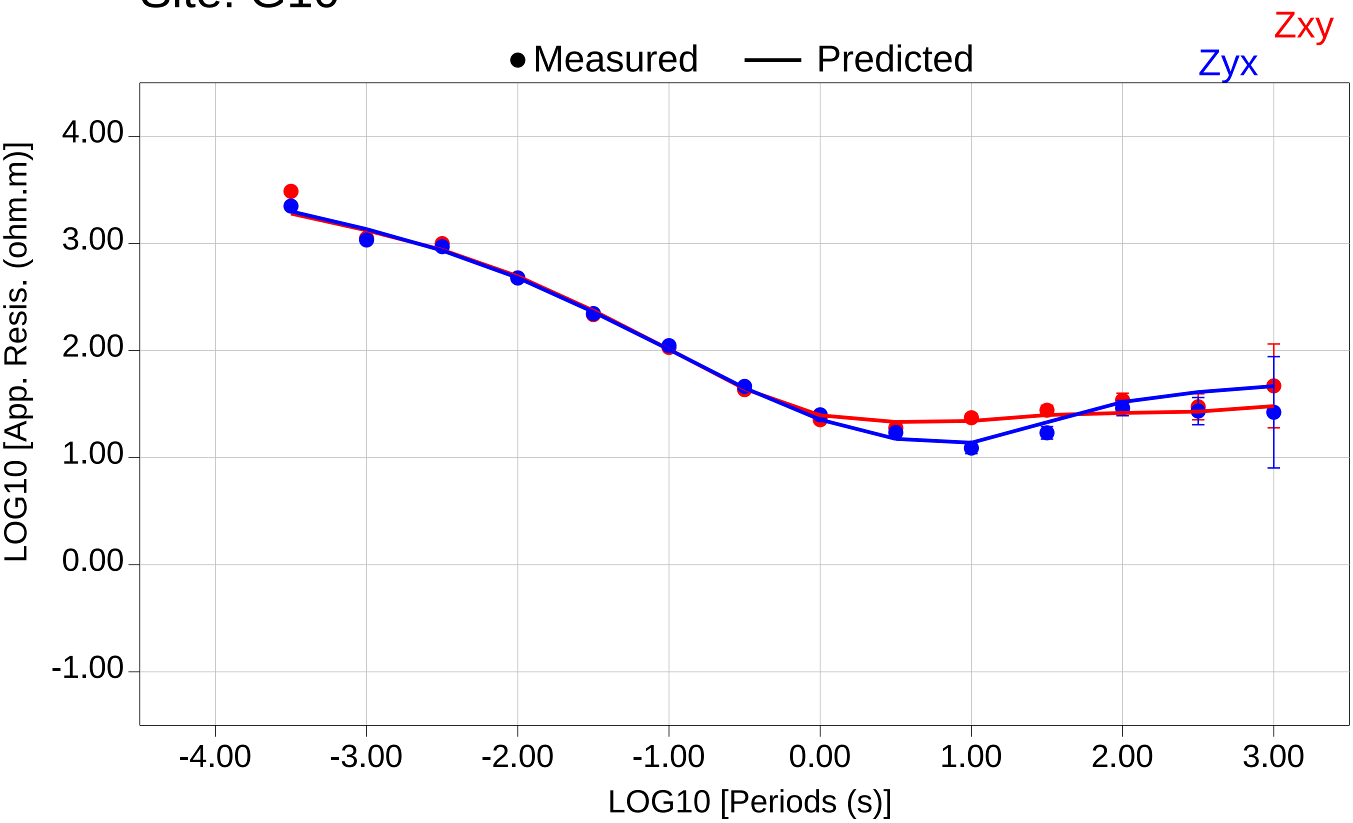

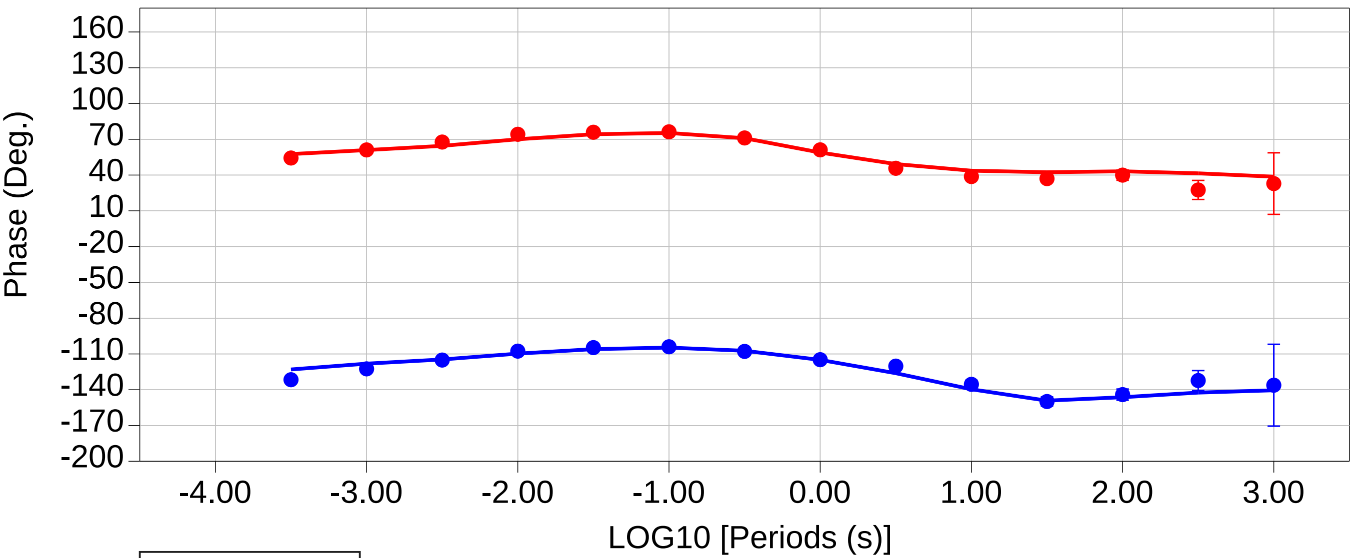

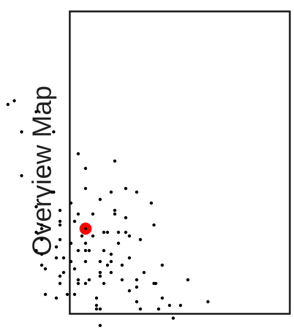

Total RMS = 15949.68

Zxy RMS = 16038.32

Zyx RMS = 15860.54

Site: G25

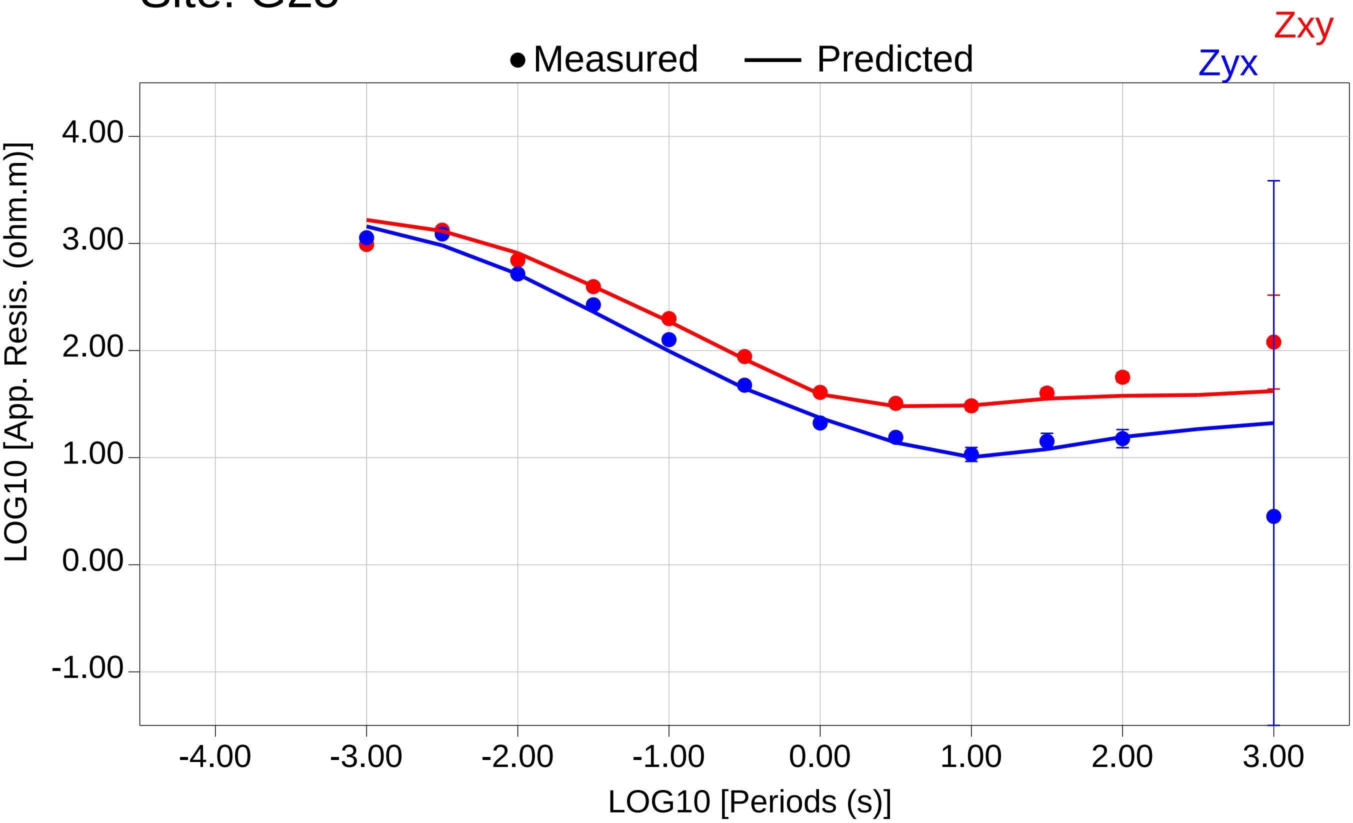

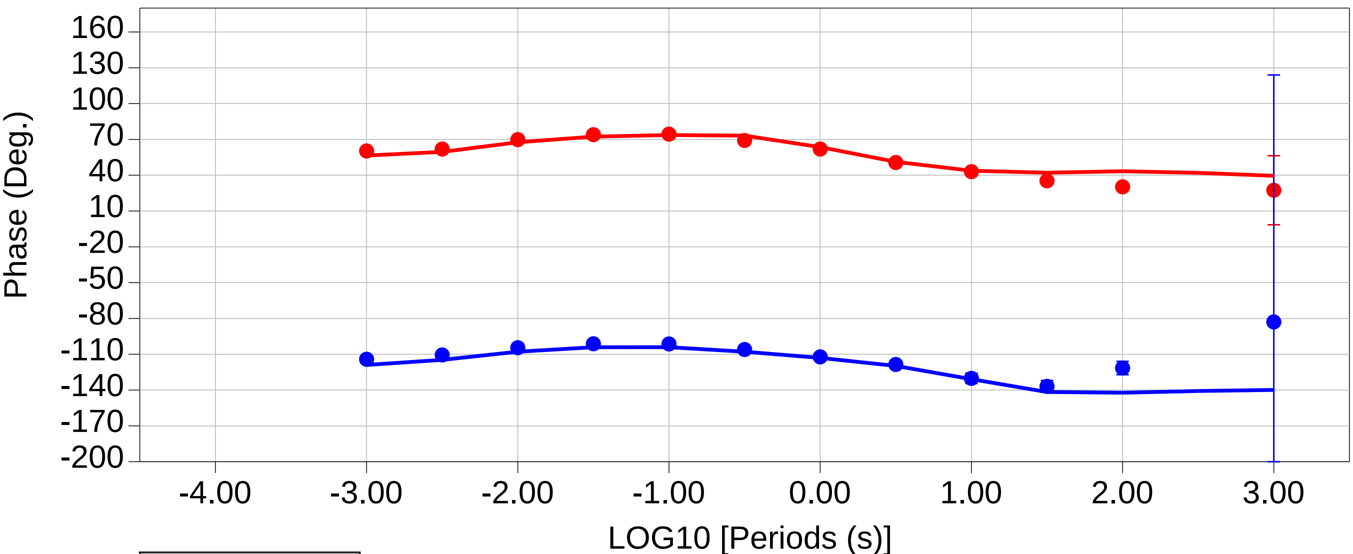

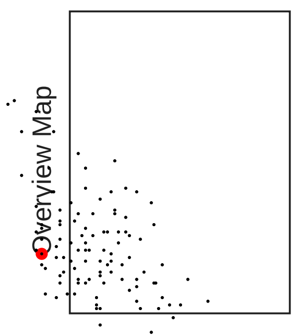

Total RMS = 16749.41

Zxy RMS = 18478.39
Zyx RMS = 14820.07

Site: G26

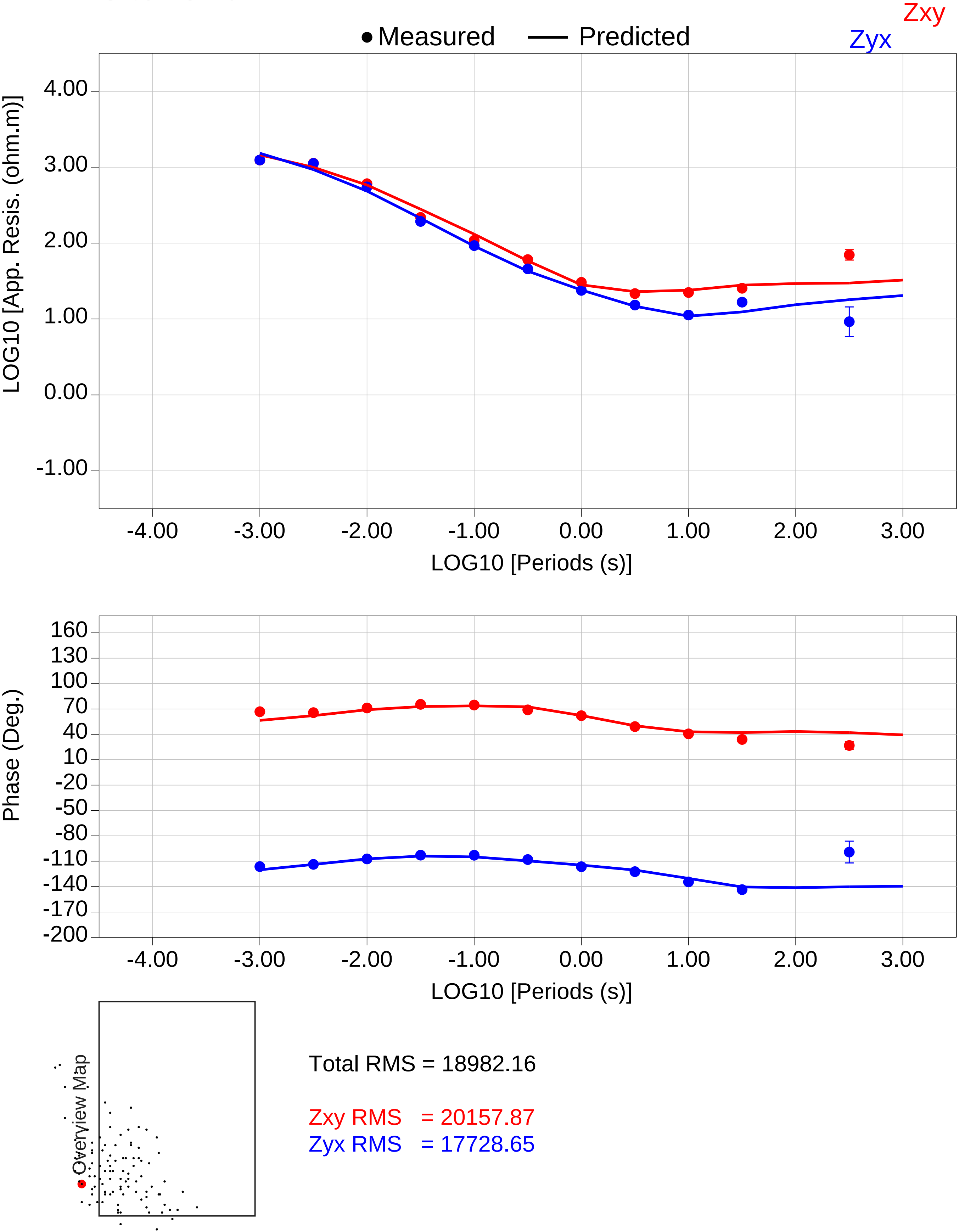

Total RMS = 18982.16

Zxy RMS = 20157.87
Zyx RMS = 17728.65

Site: G27

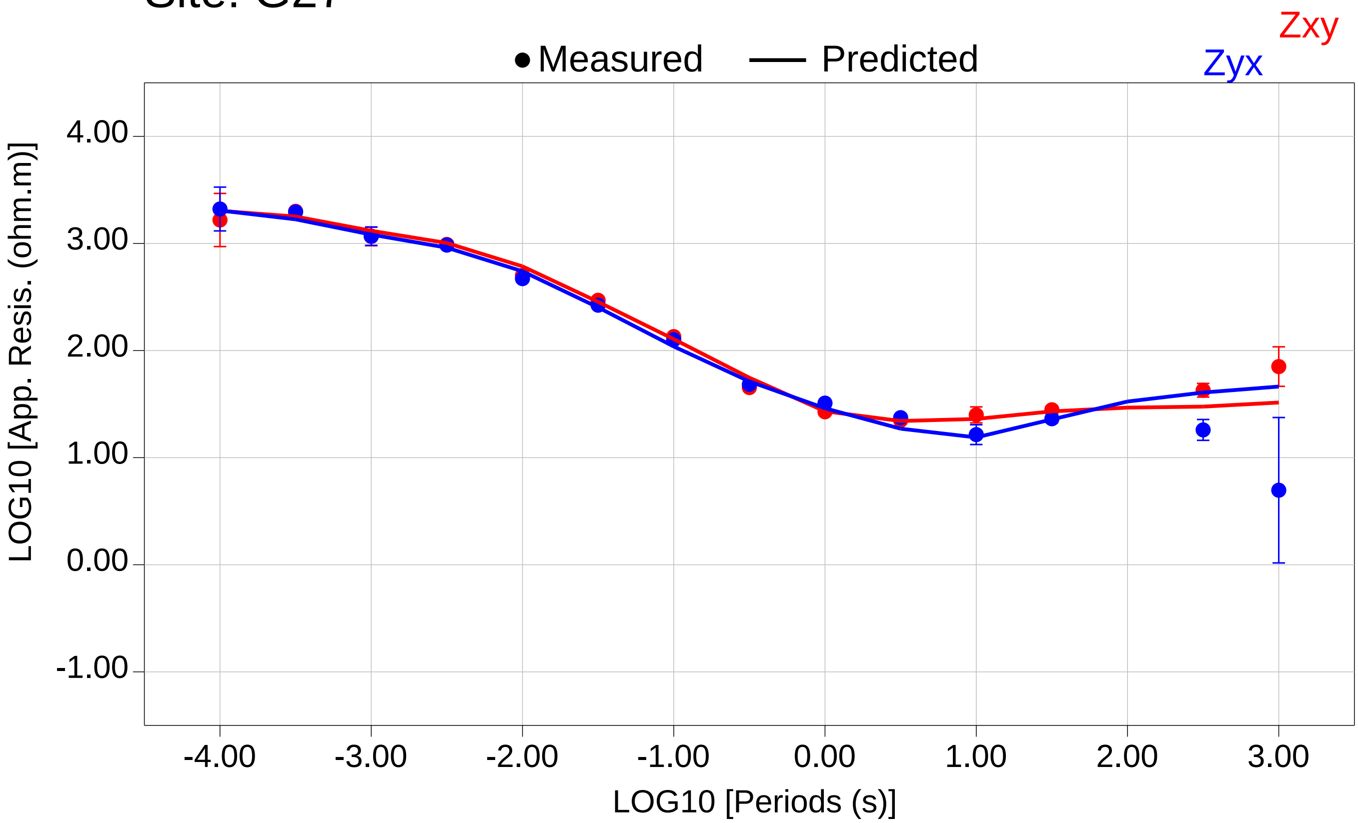

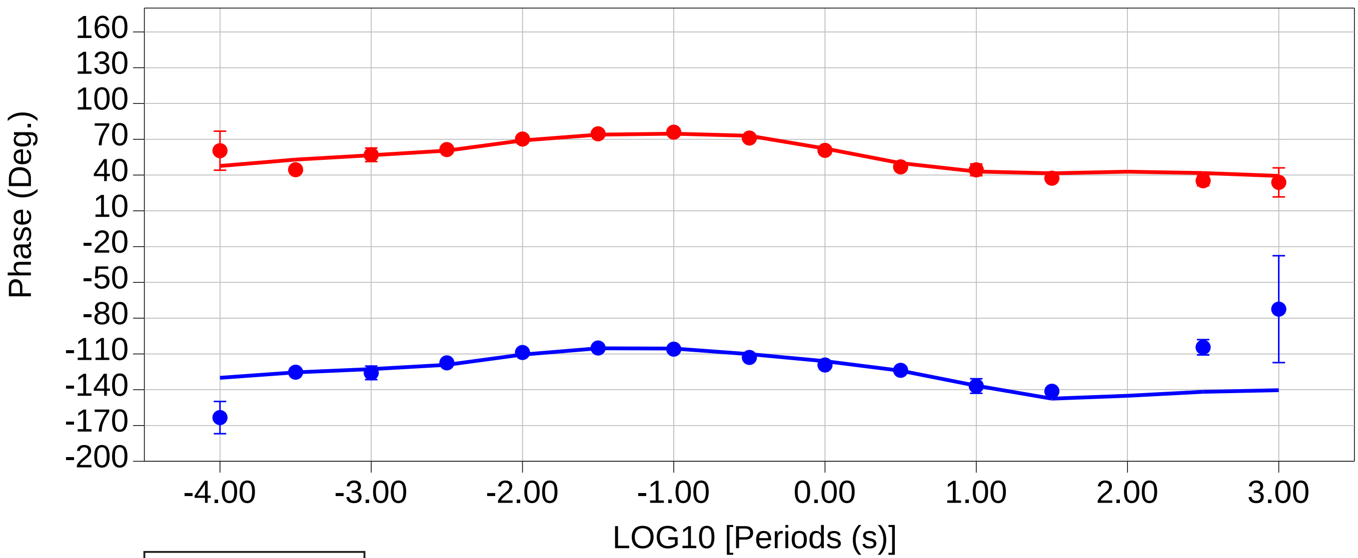

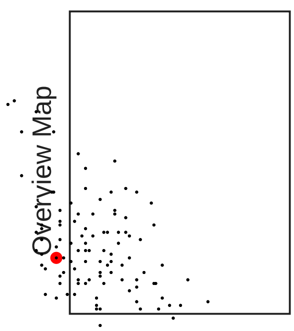

Total RMS = 16839.70

Zxy RMS = 17219.77
Zyx RMS = 16450.85

Site: G28

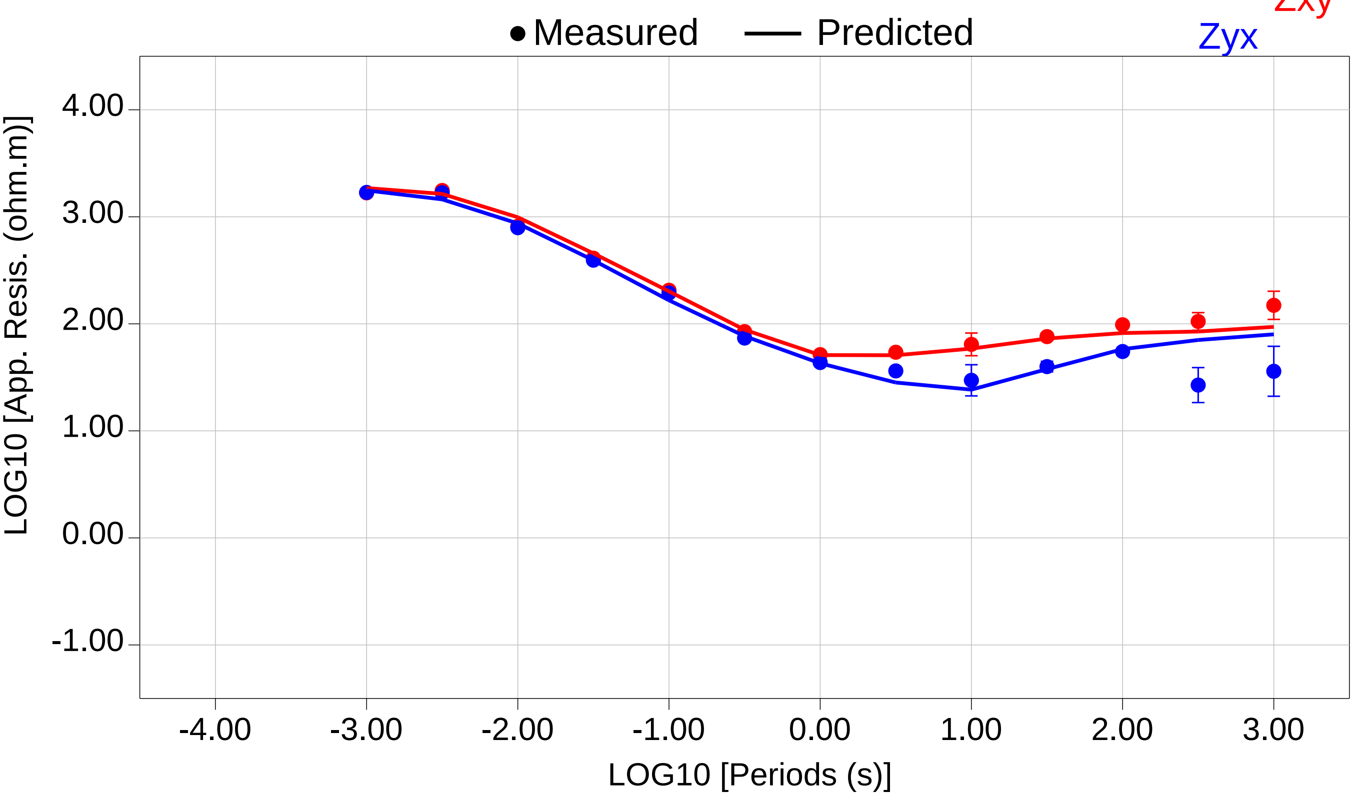

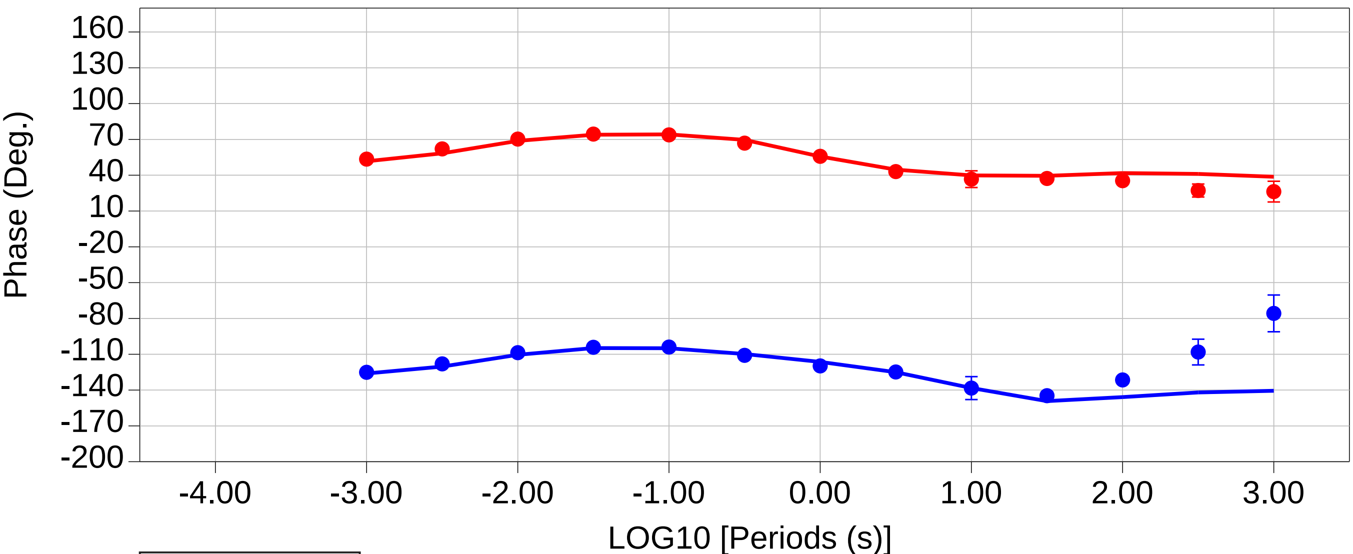

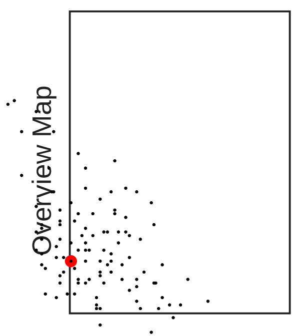

Total RMS = 16537.34

Zxy RMS = 17289.55
Zyx RMS = 15749.23

Site: G29

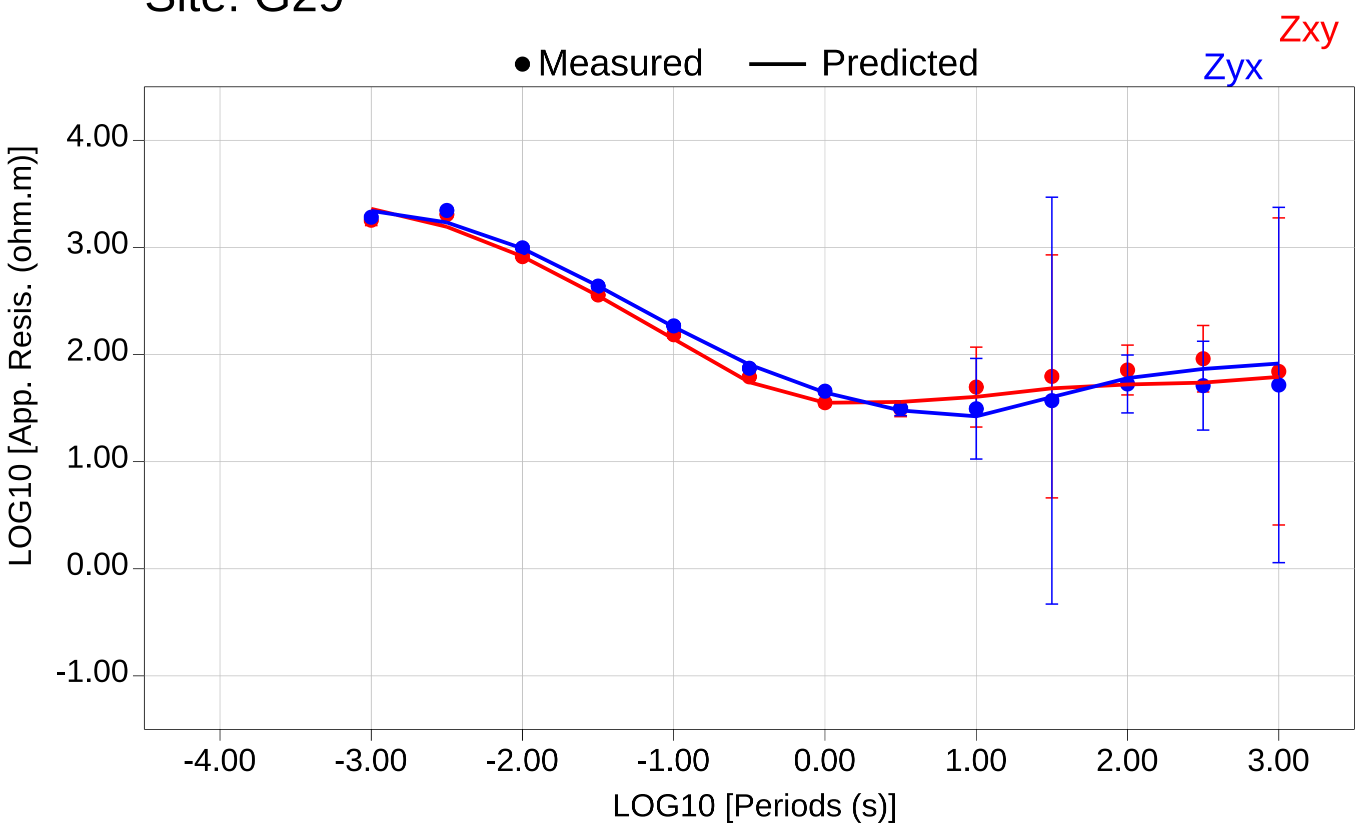

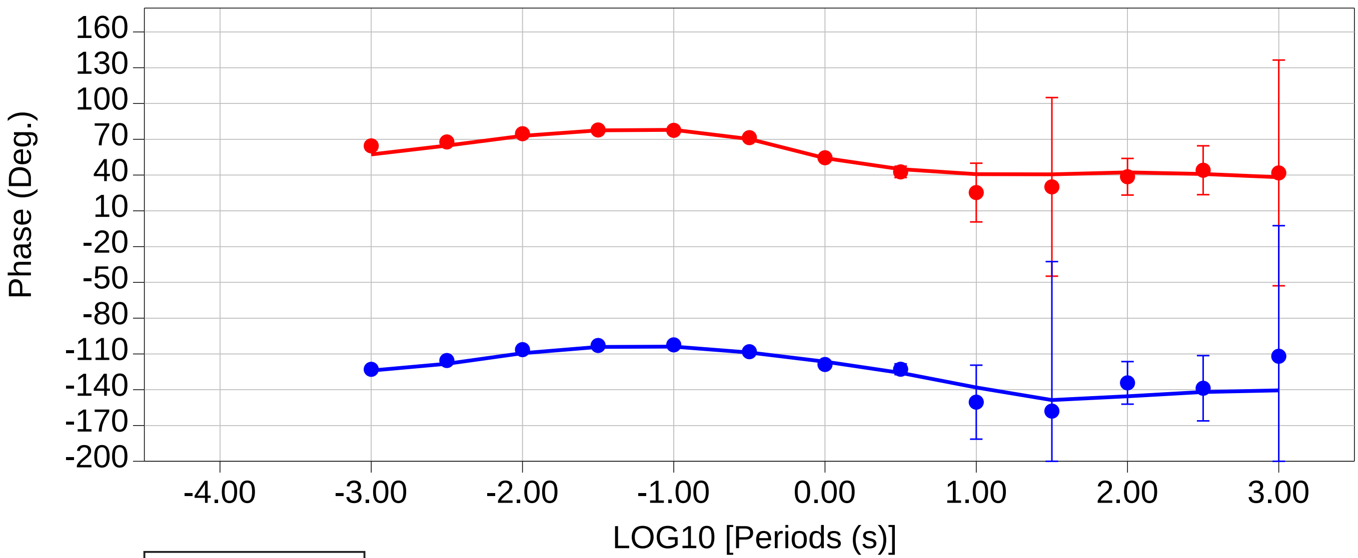

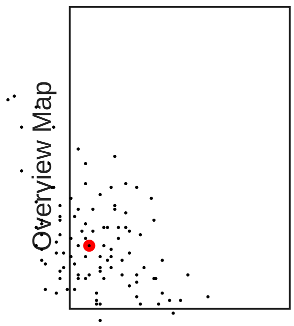

Total RMS = 14708.17

Zxy RMS = 13939.03
Zyx RMS = 15439.04

Site: G30

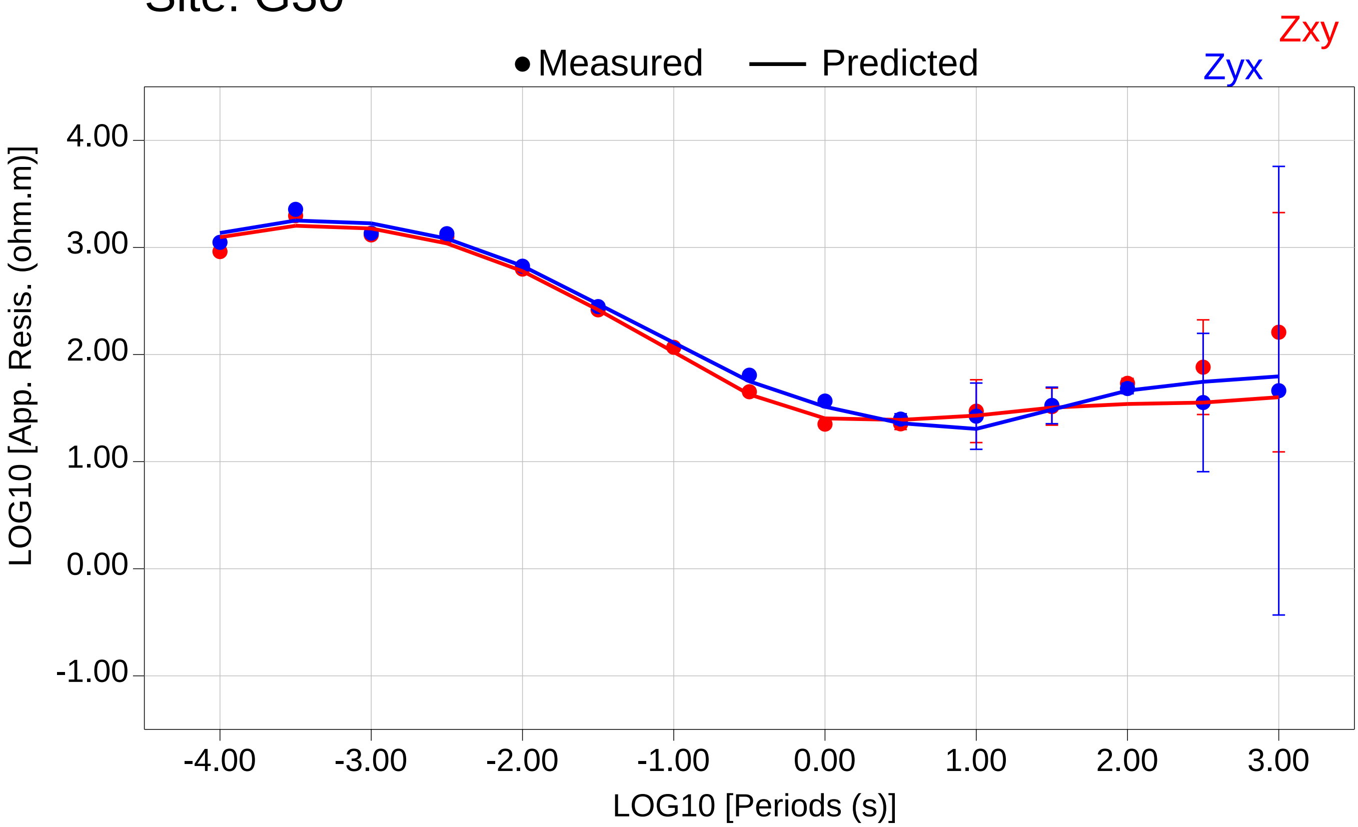

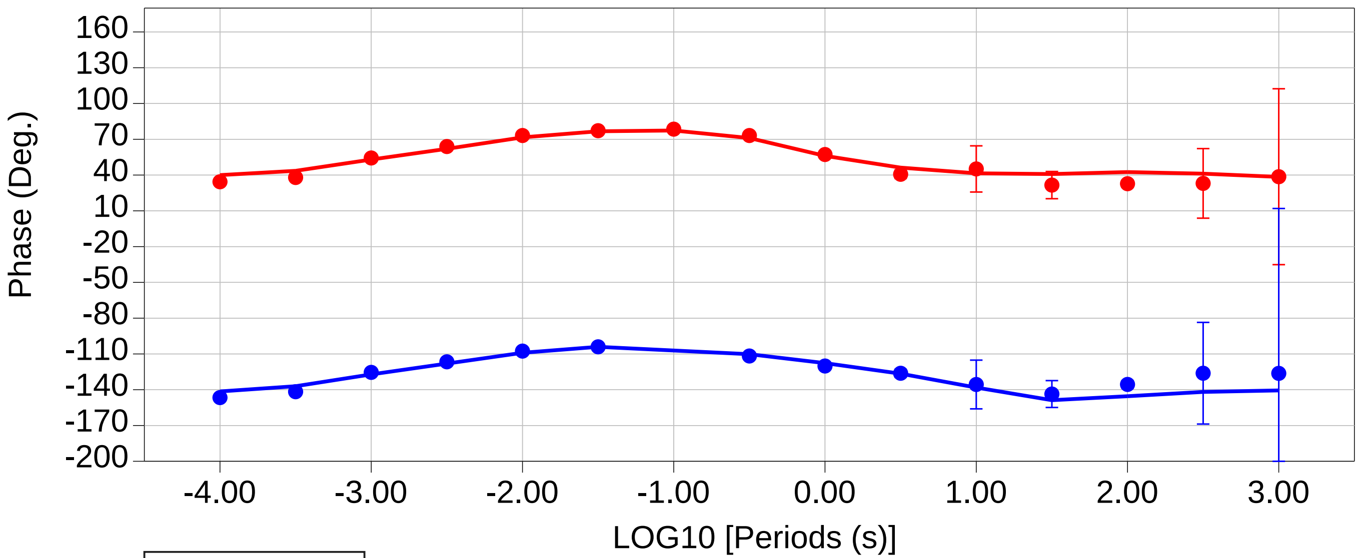

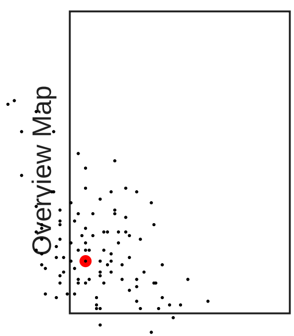

Total RMS = 14179.85

Zxy RMS = 14620.19
Zyx RMS = 13692.35

Site: G31

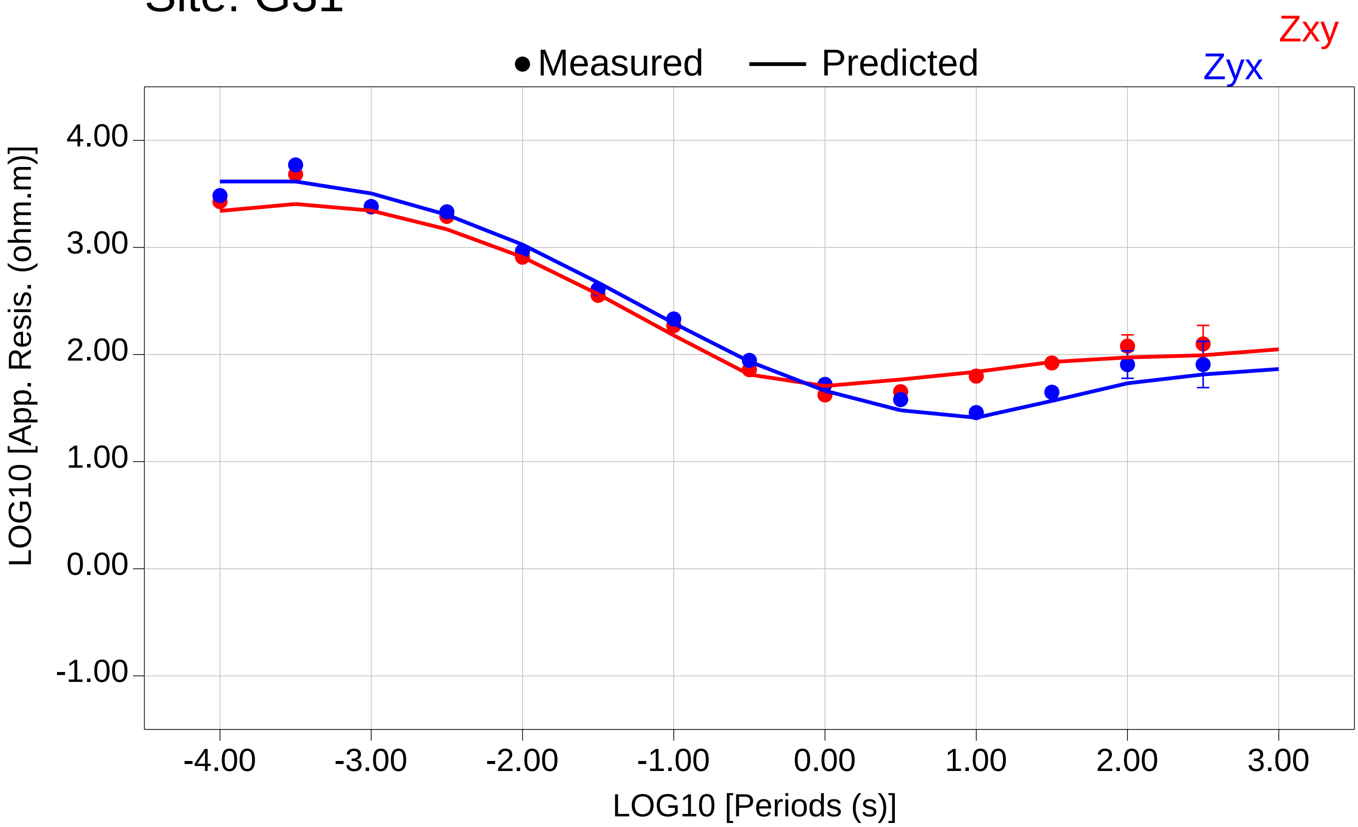

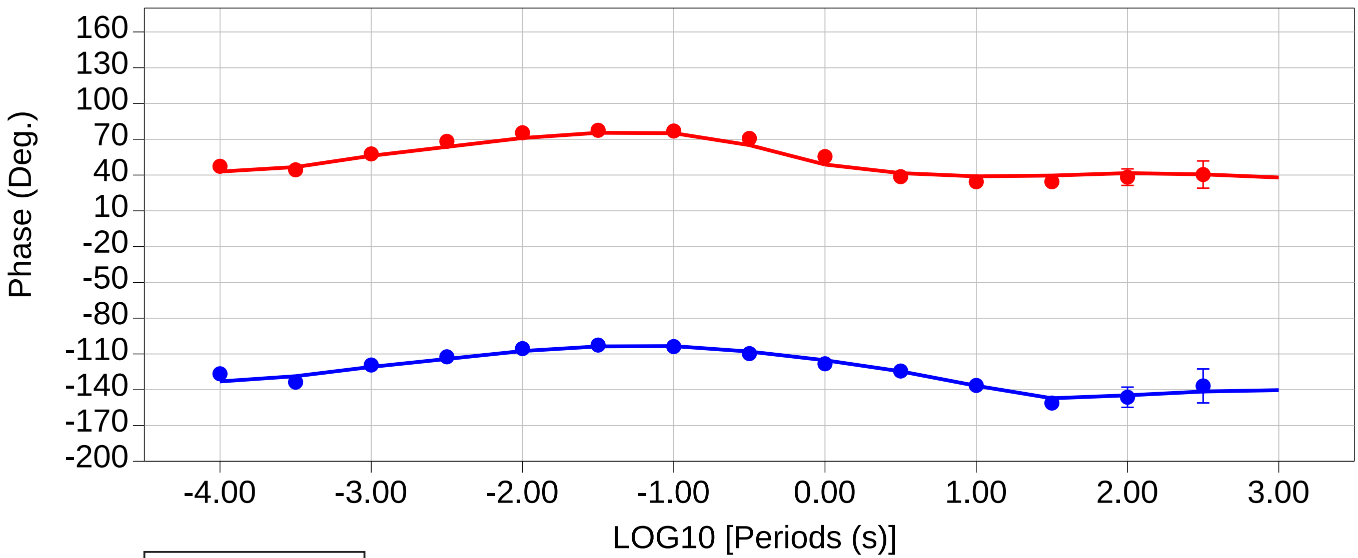

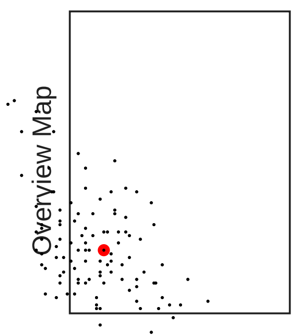

Total RMS = 17140.71

Zxy RMS = 16530.46
Zyx RMS = 17729.97

Site: G32

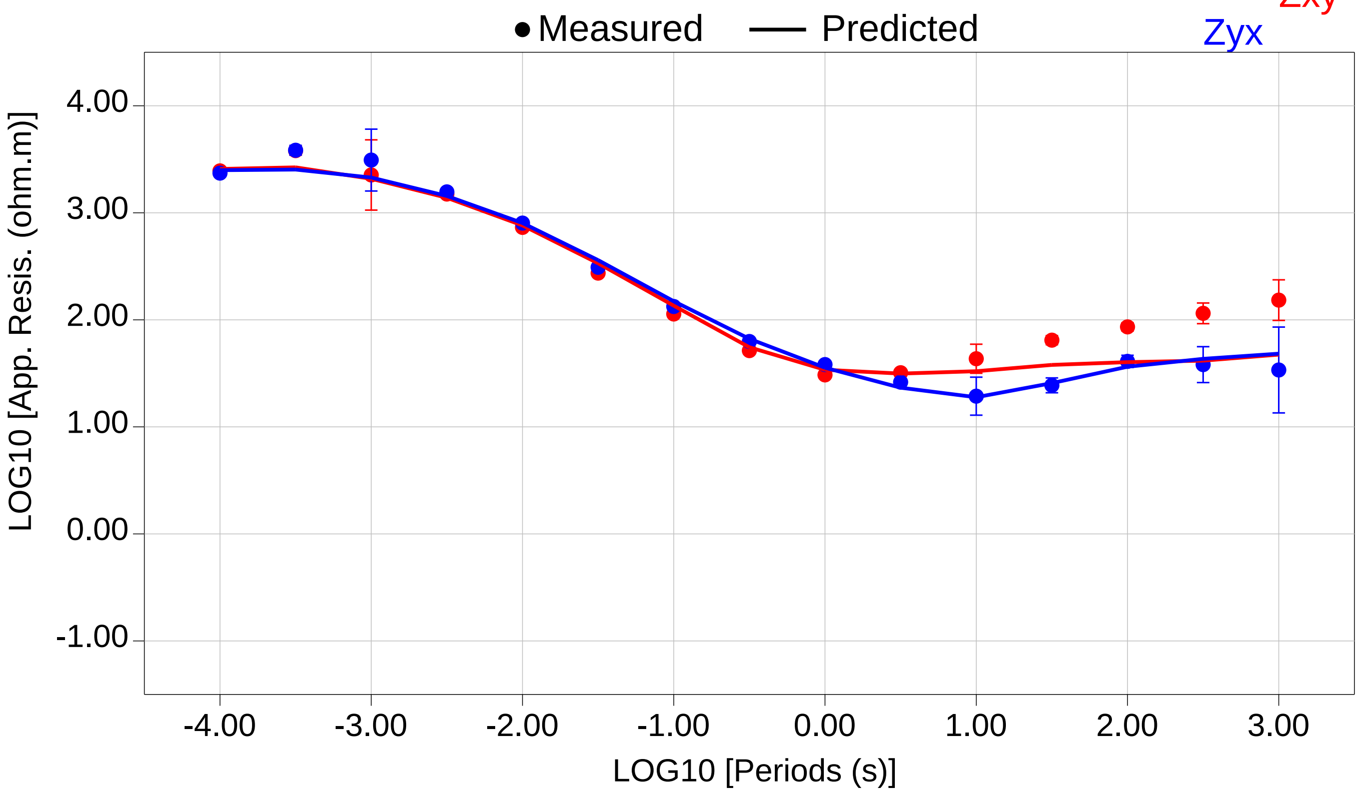

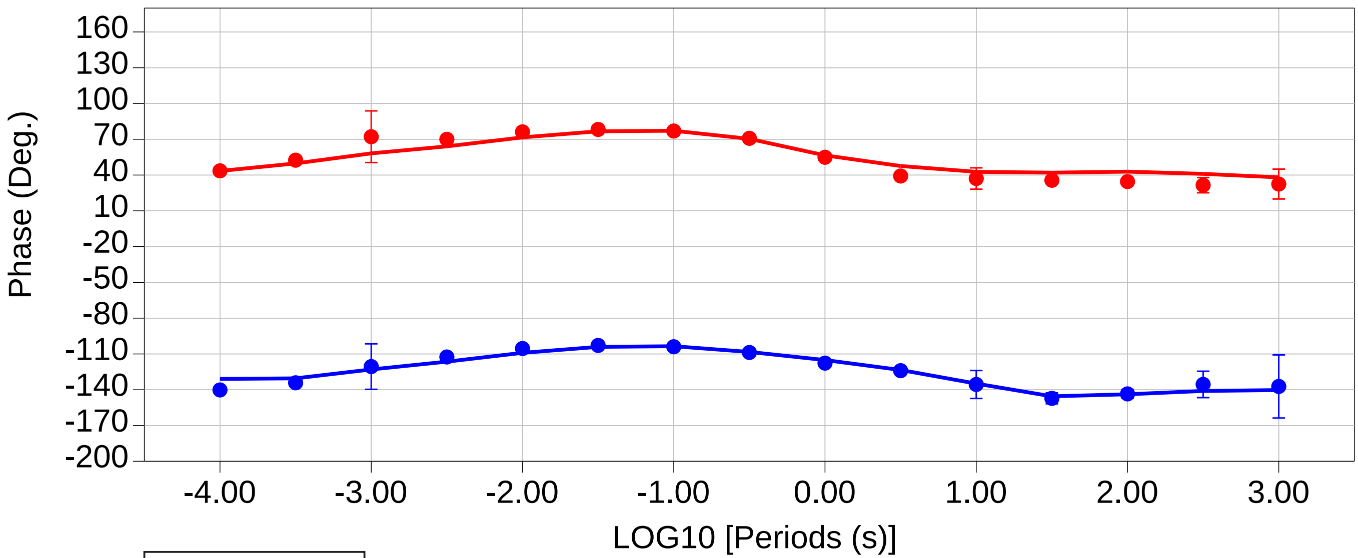

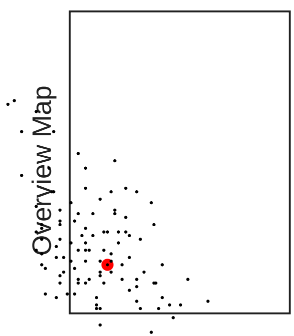

Total RMS = 16158.40

Zxy RMS = 16013.28

Zyx RMS = 16302.23

Site: G33

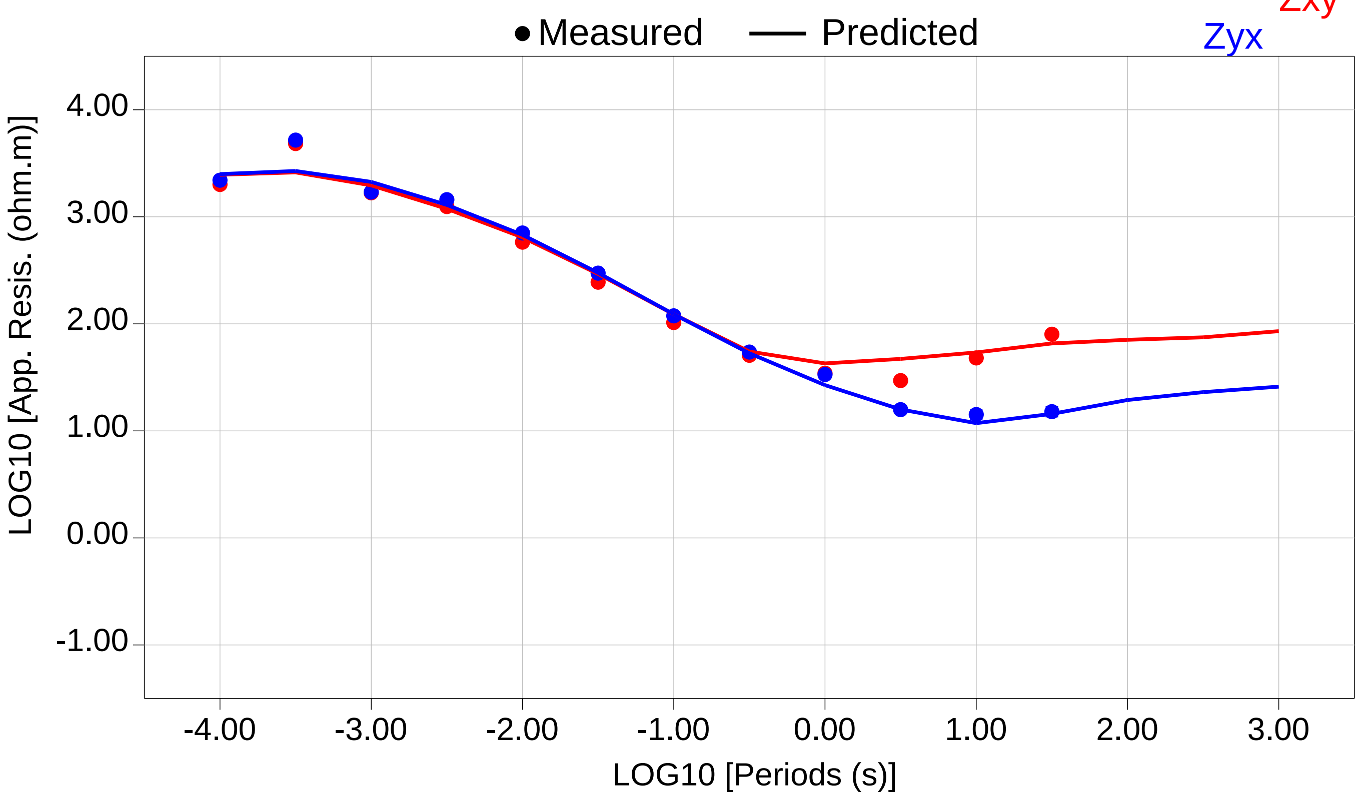

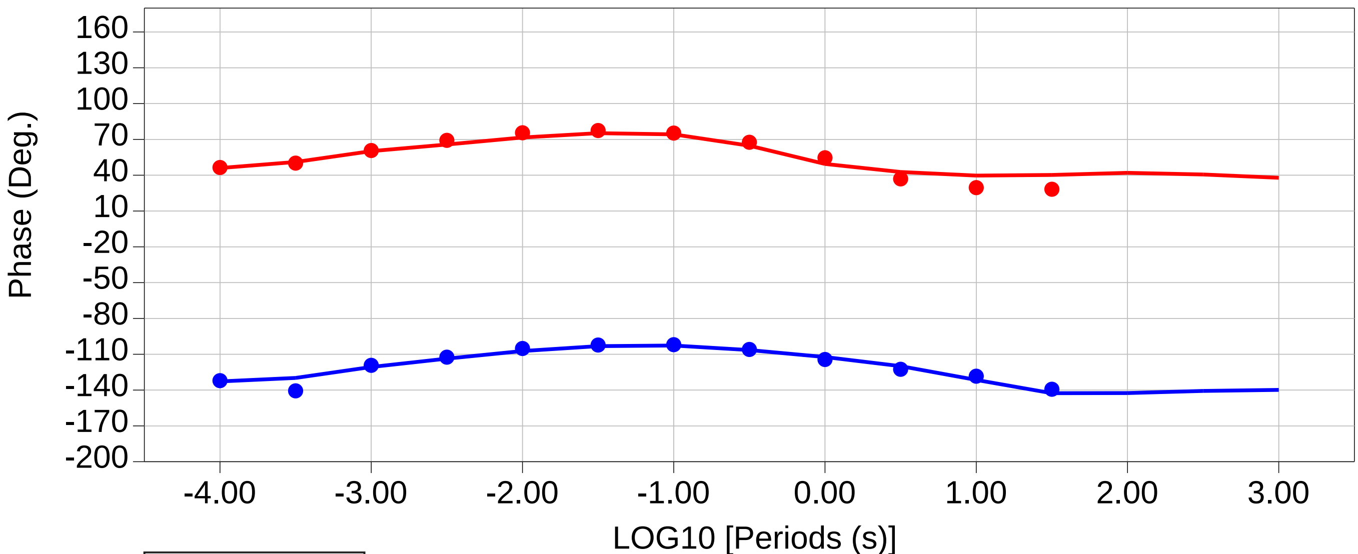

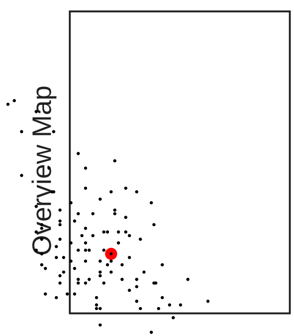

Total RMS = 19592.65

Zxy RMS = 20550.51
Zyx RMS = 18585.49

Site: G34

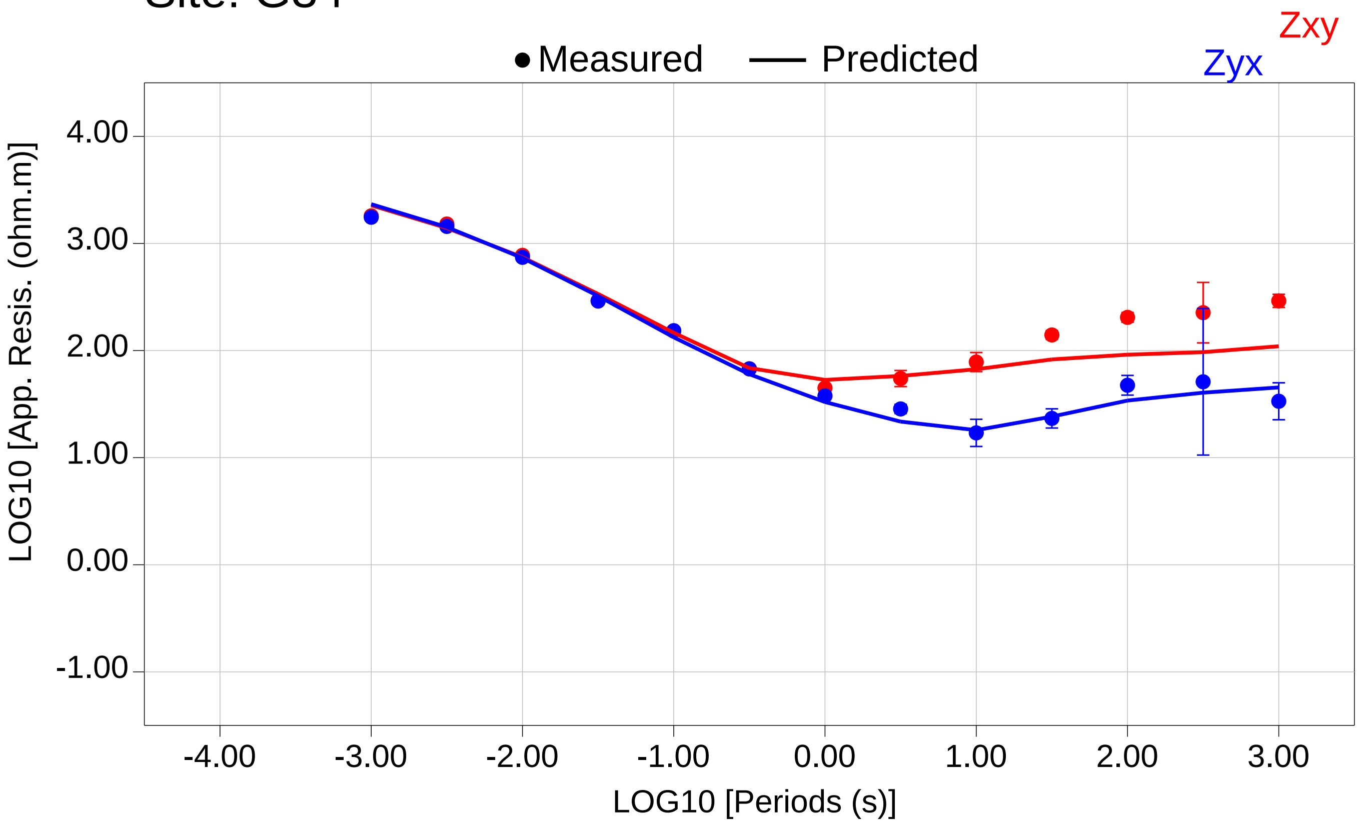

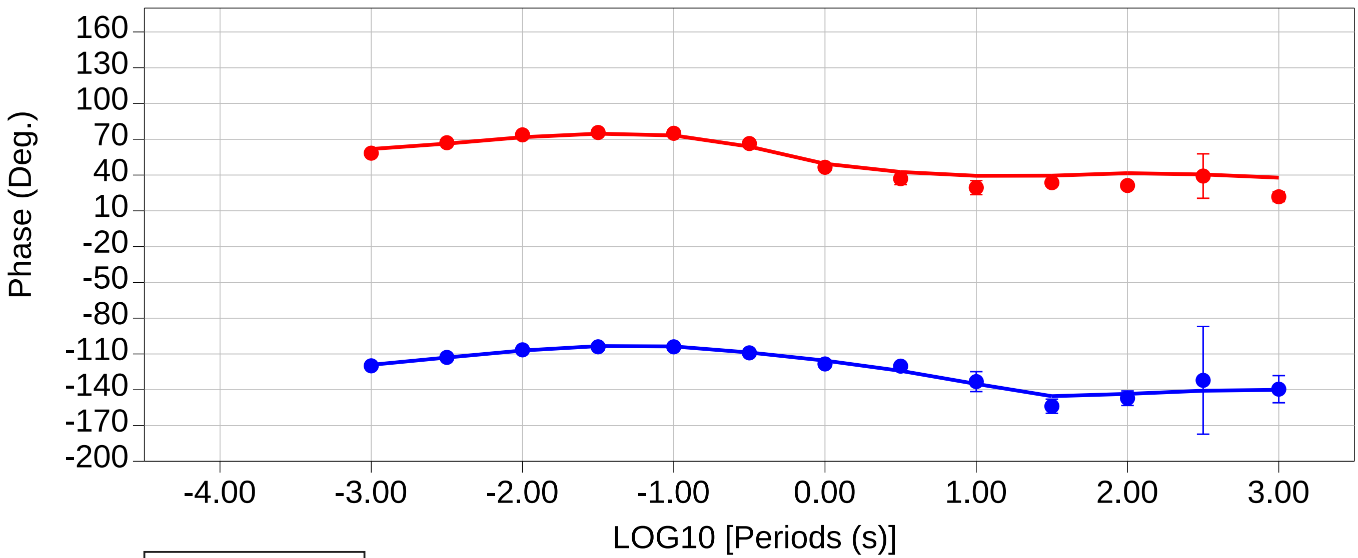

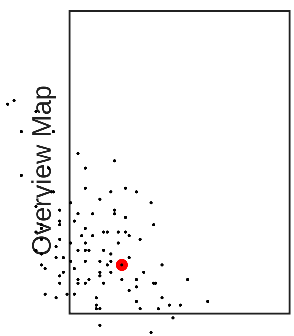

Total RMS = 15834.54

Zxy RMS = 15926.74

Zyx RMS = 15741.81

Site: G35

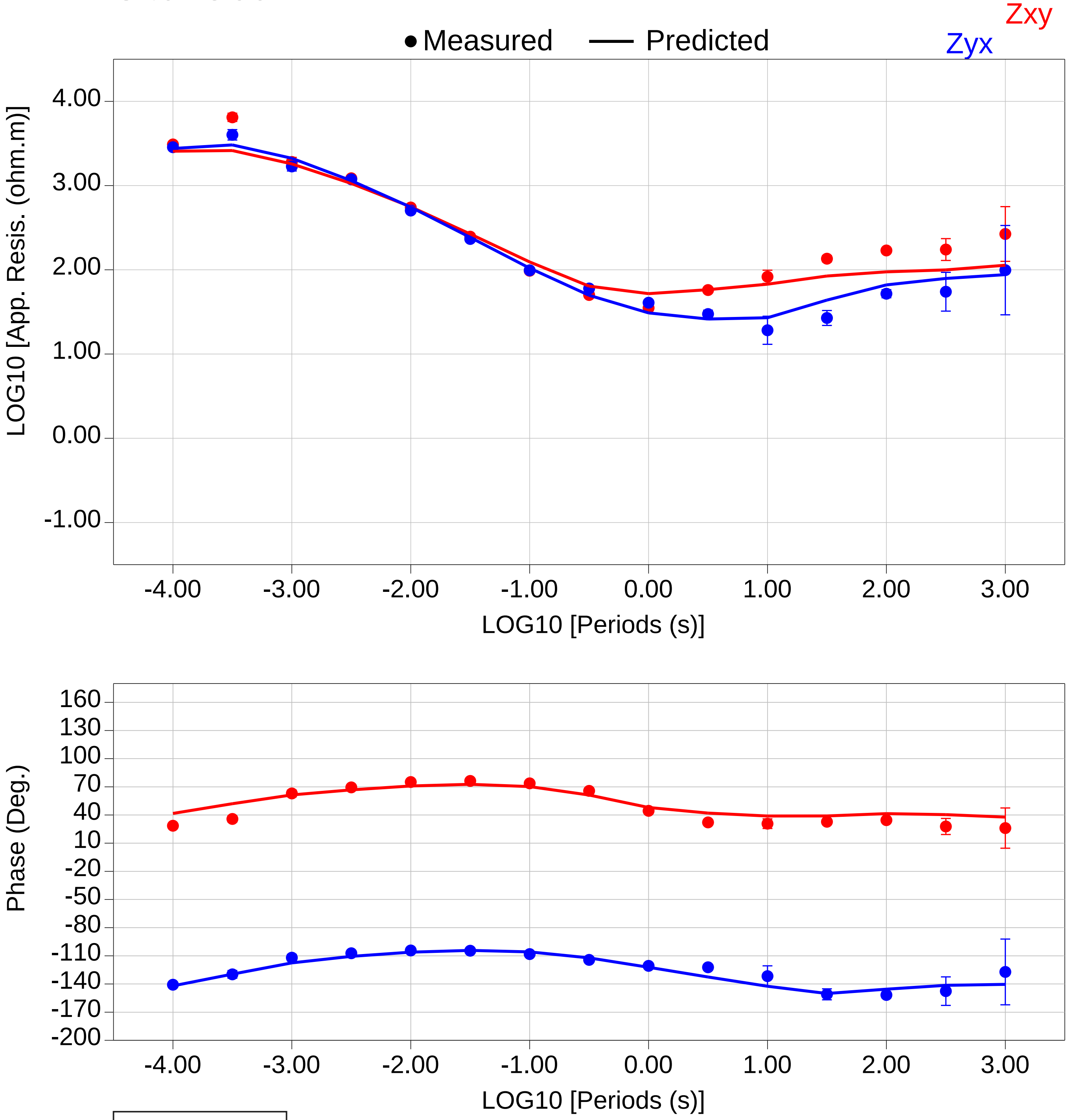

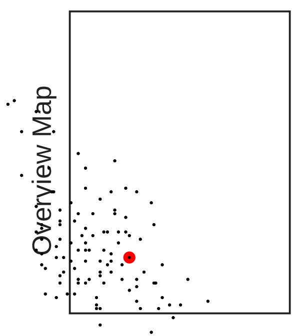

Total RMS = 15338.90

Zxy RMS = 15802.70
Zyx RMS = 14860.64

Site: G36

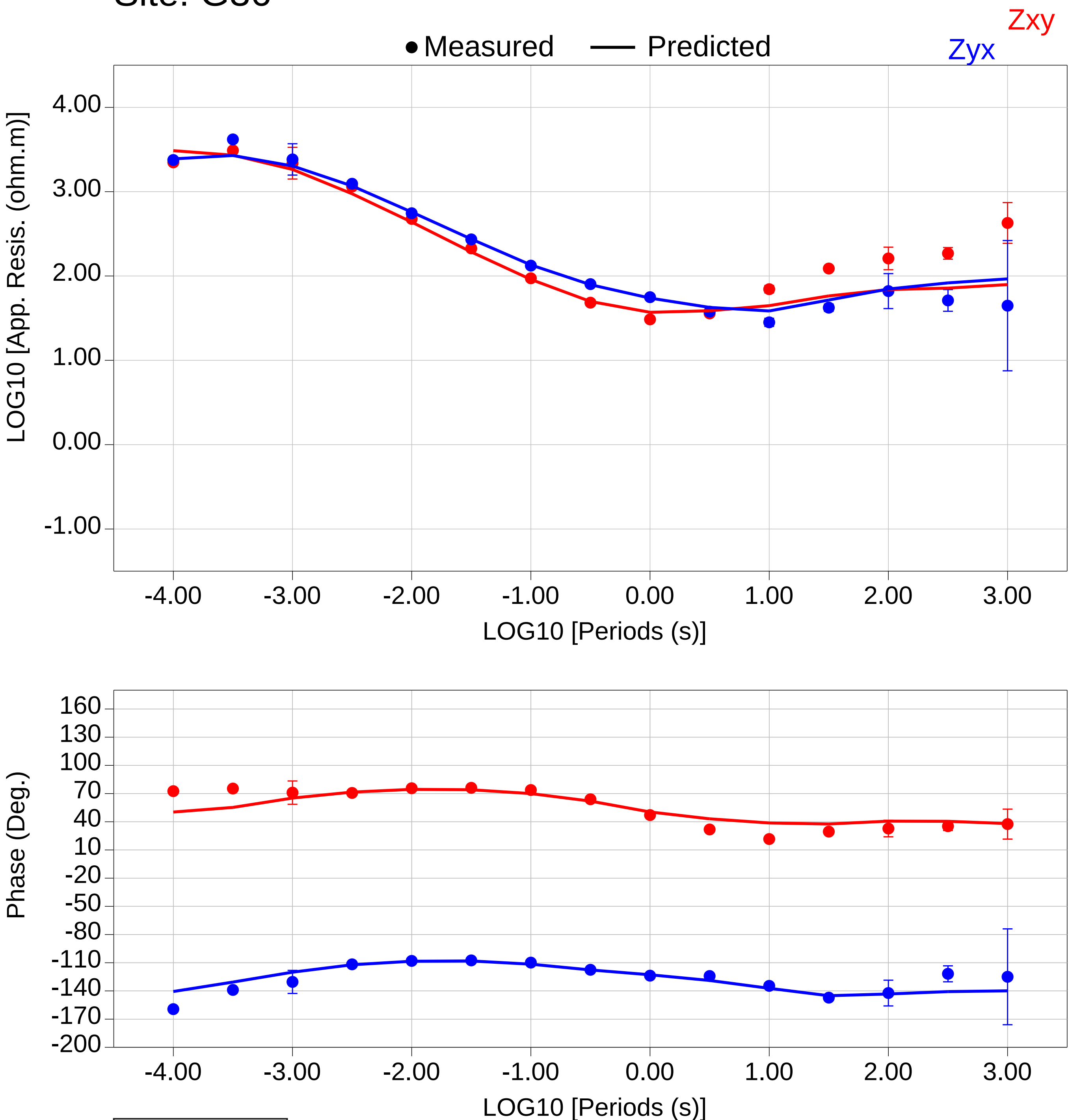

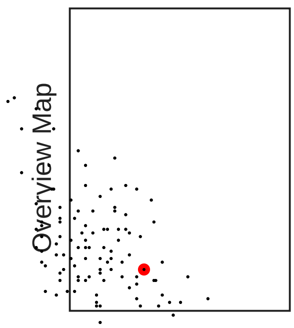

Total RMS = 15956.09

Zxy RMS = 15017.94
Zyx RMS = 16842.07

Site: G37

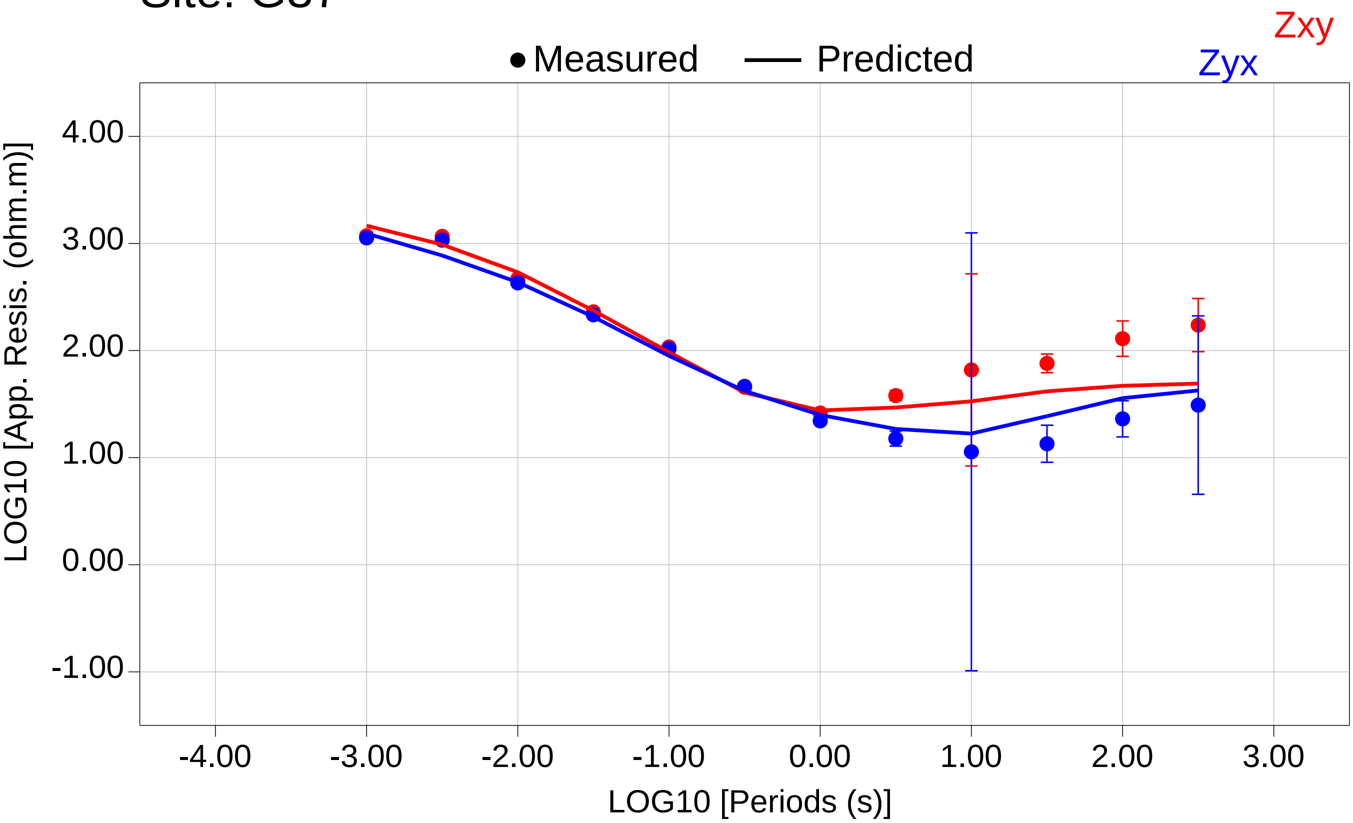

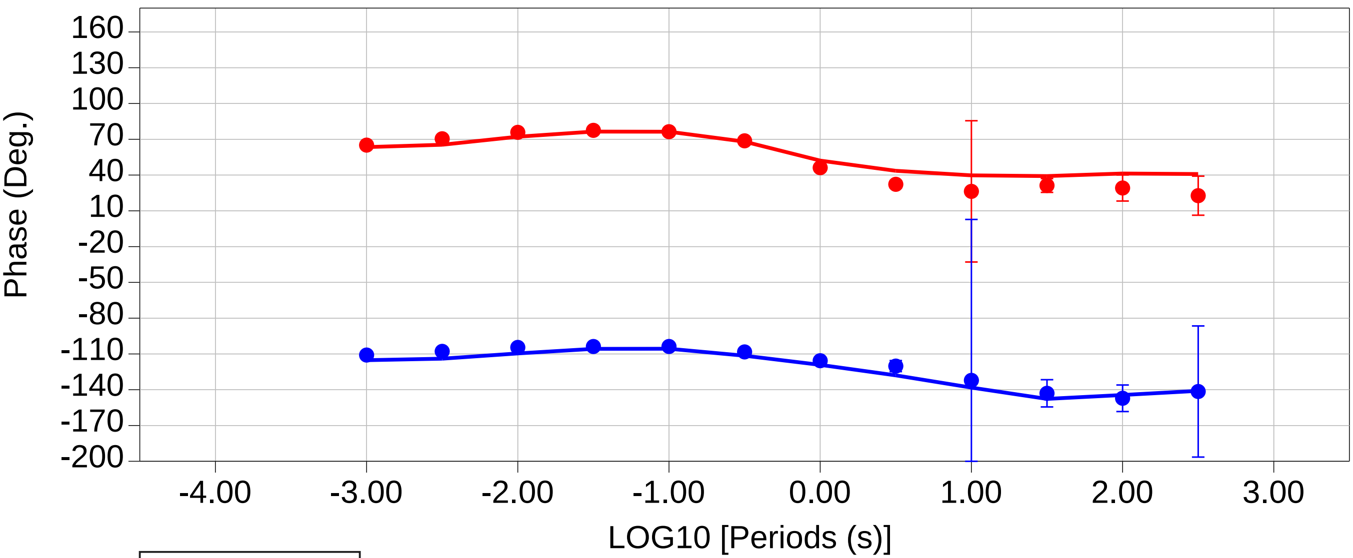

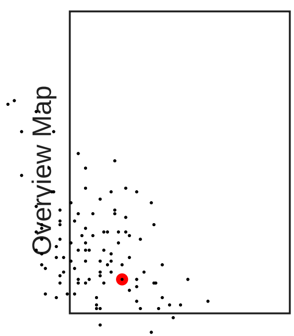

Total RMS = 15411.35

Zxy RMS = 15950.64

Zyx RMS = 14852.48

Site: G38

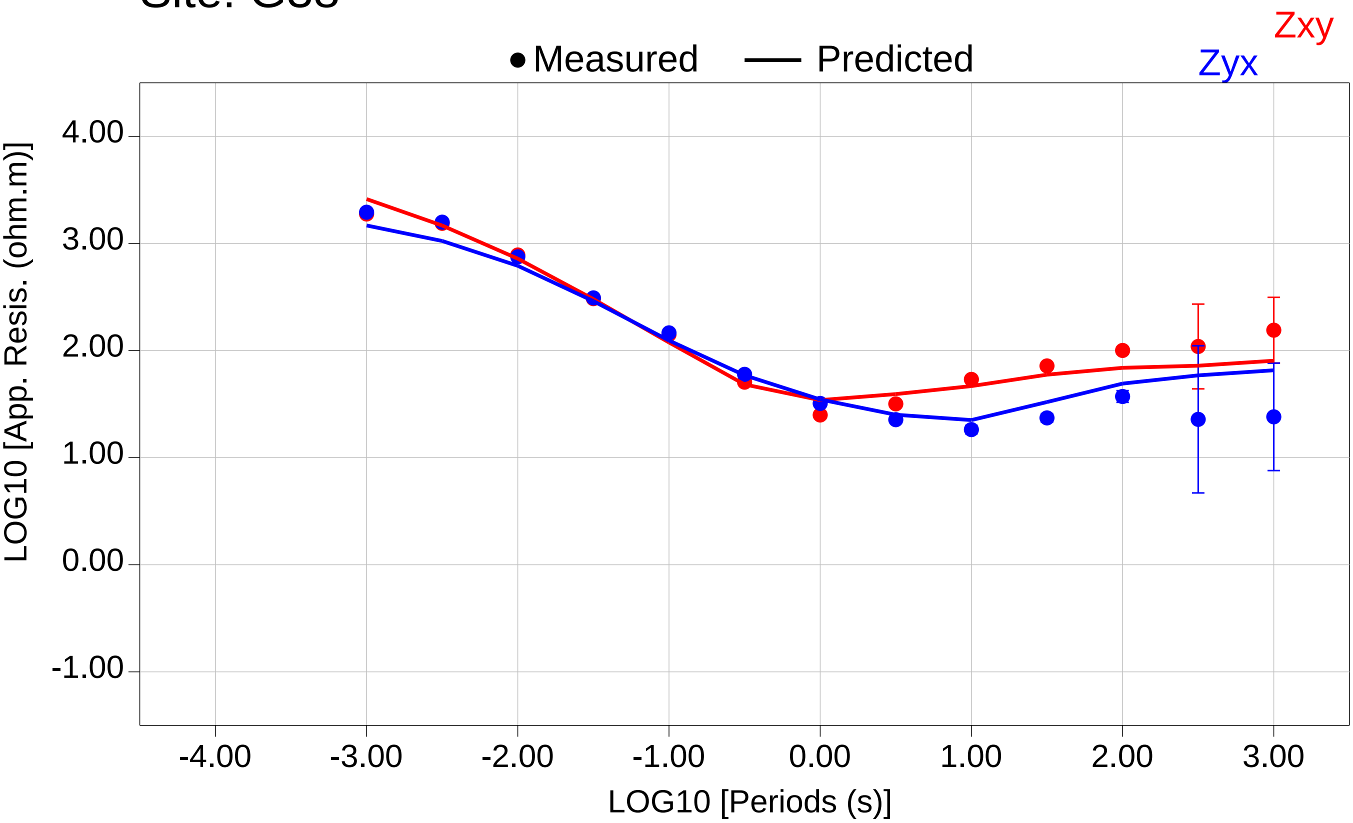

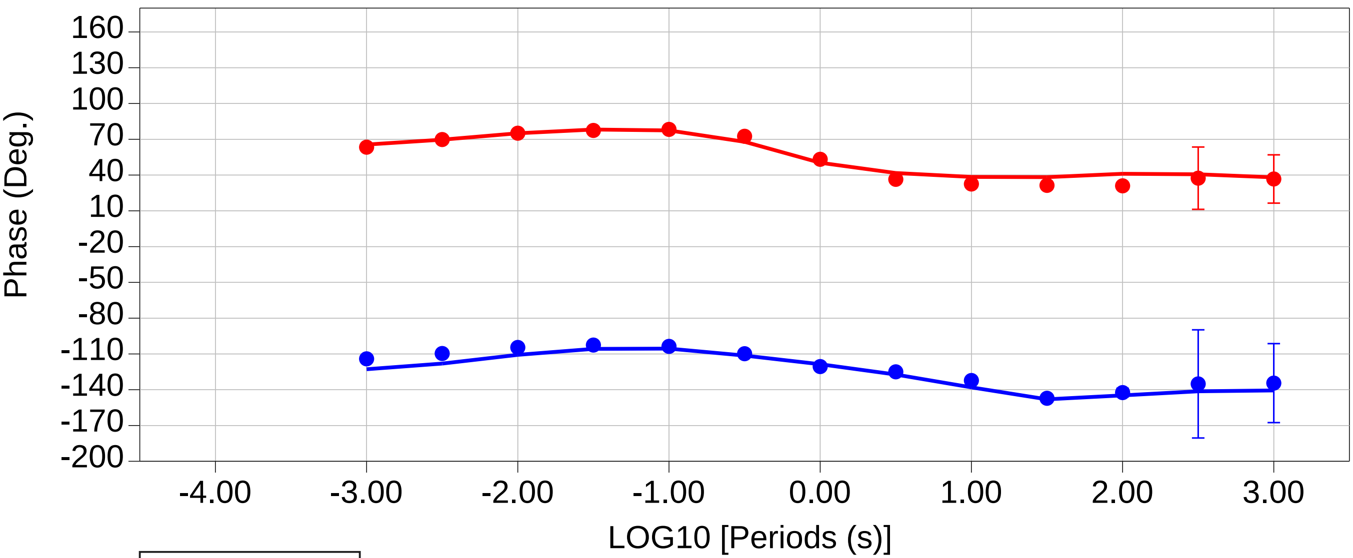

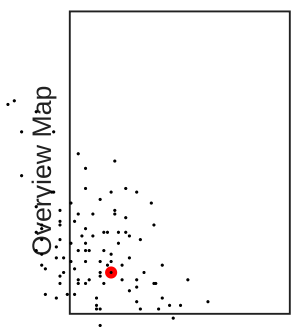

Total RMS = 17188.67

Zxy RMS = 18076.96
Zyx RMS = 16251.89

Site: G39

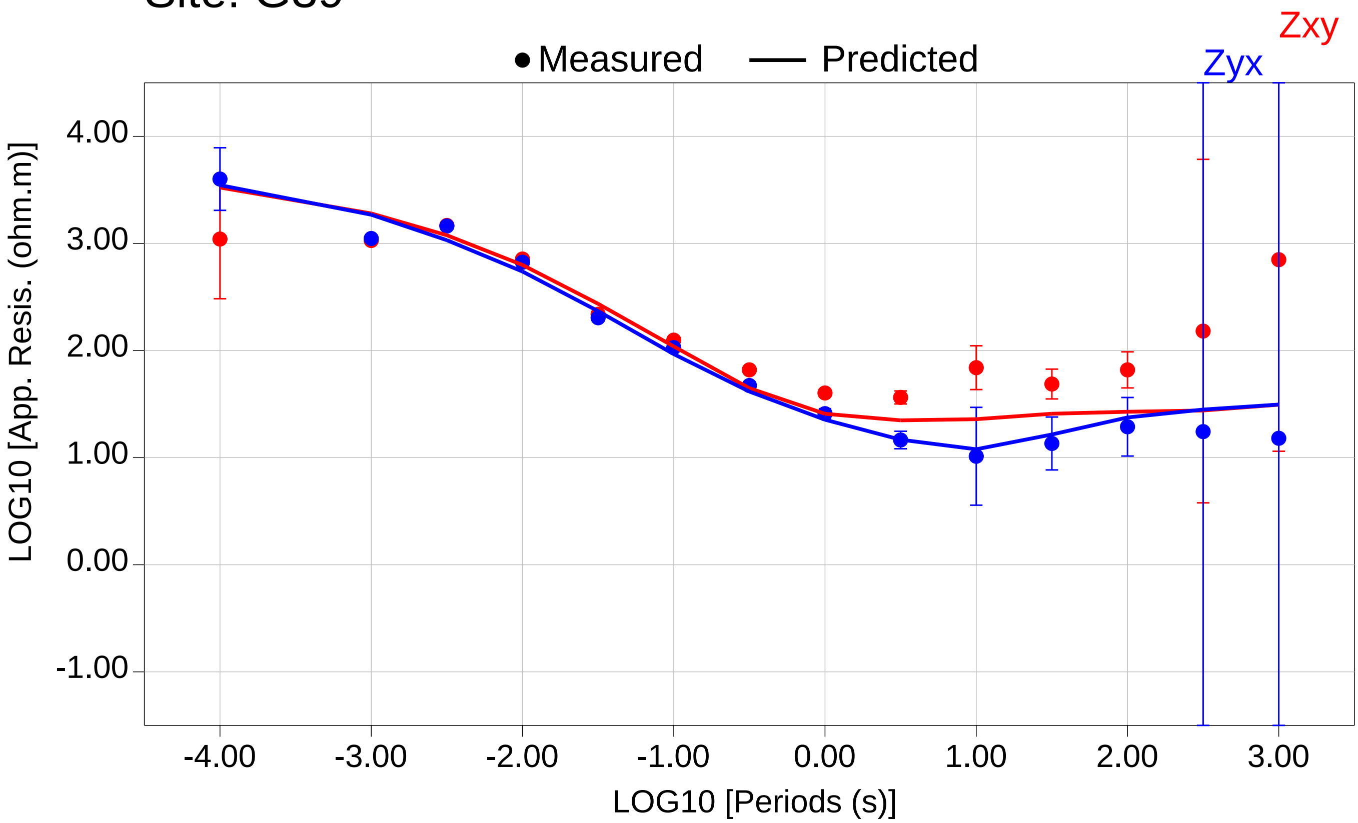

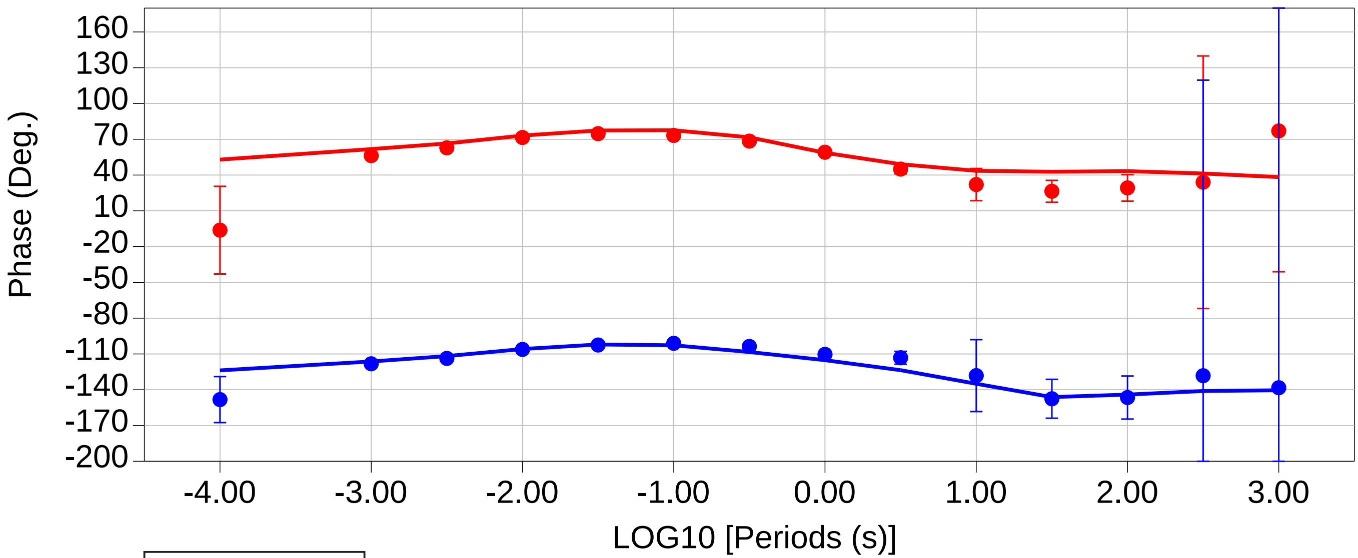

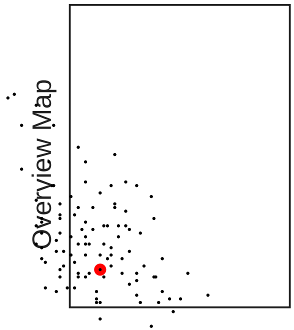

Total RMS = 14490.77

Zxy RMS = 14886.06
Zyx RMS = 14084.39

Site: G40

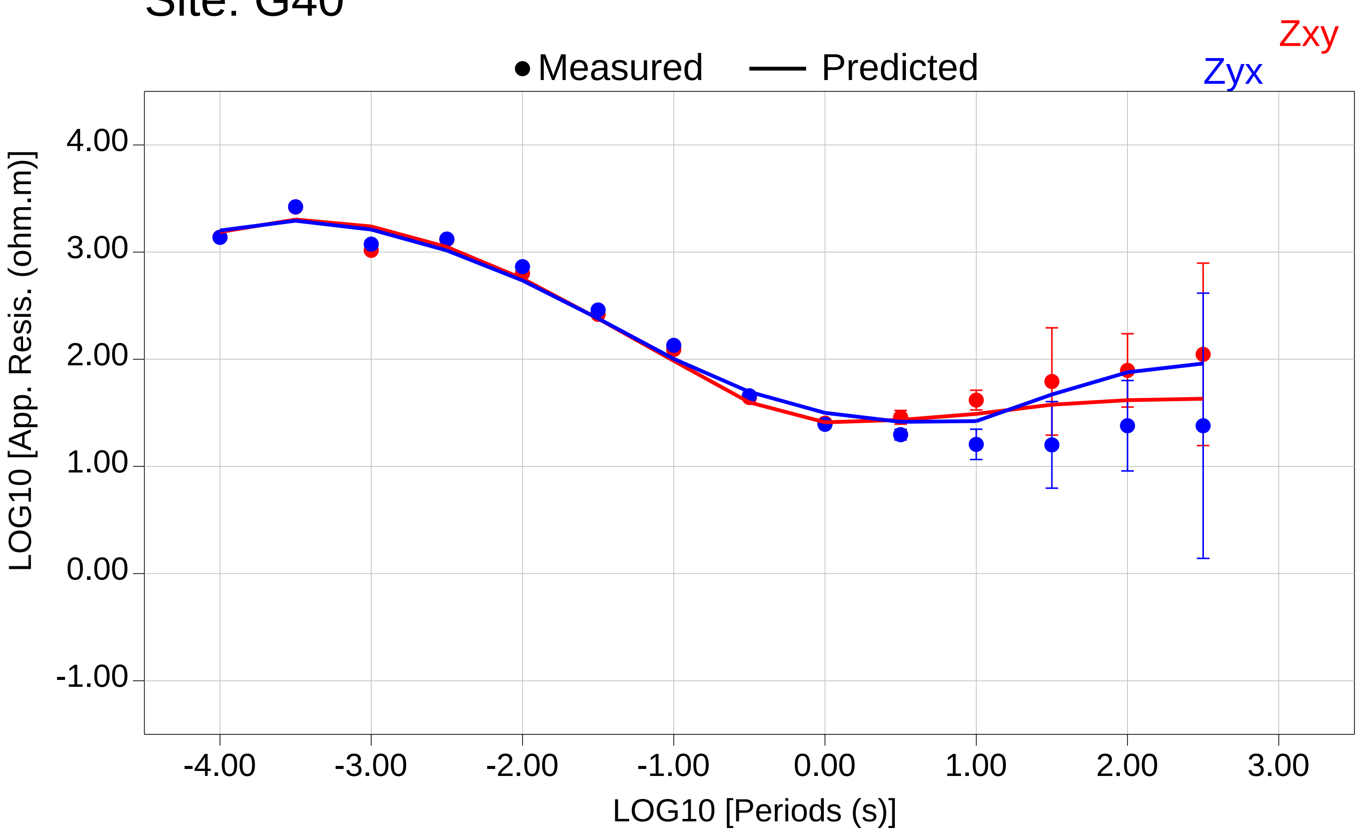

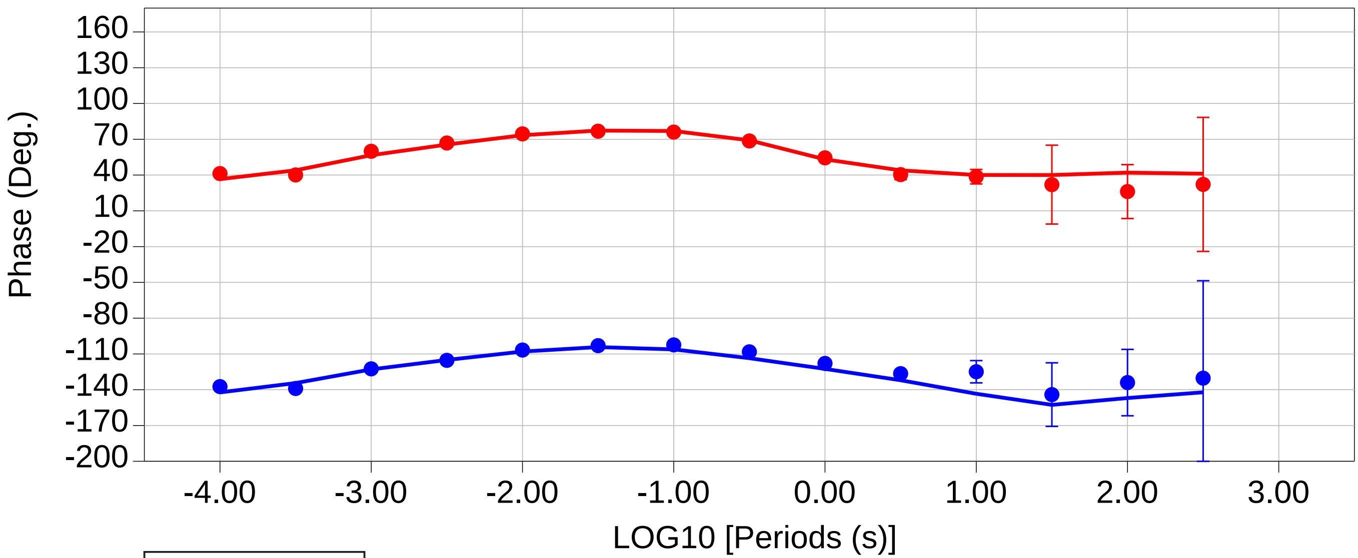

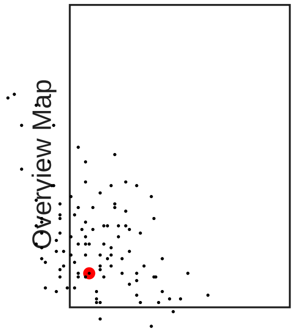

Total RMS = 15332.18

Zxy RMS = 15116.79

Zyx RMS = 15544.59

Site: G41

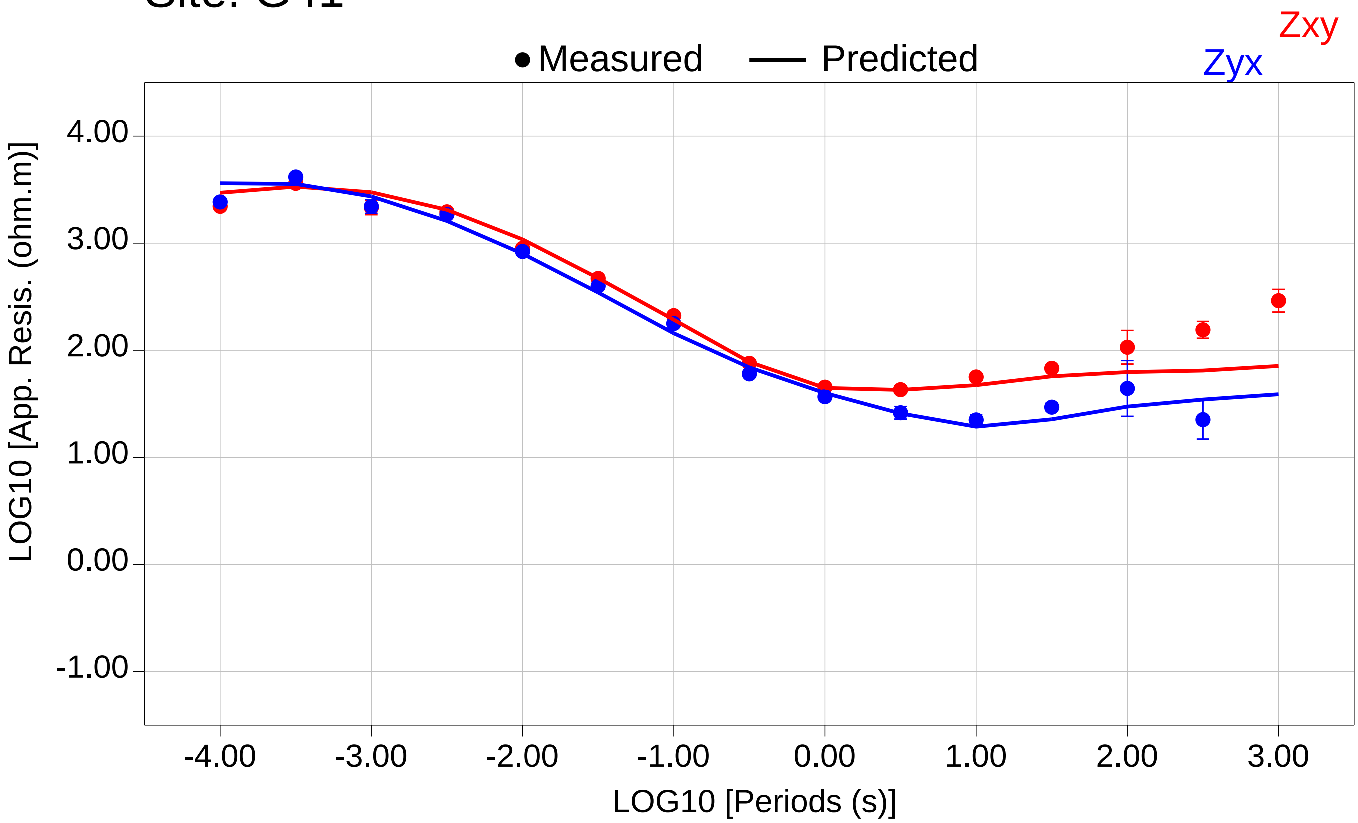

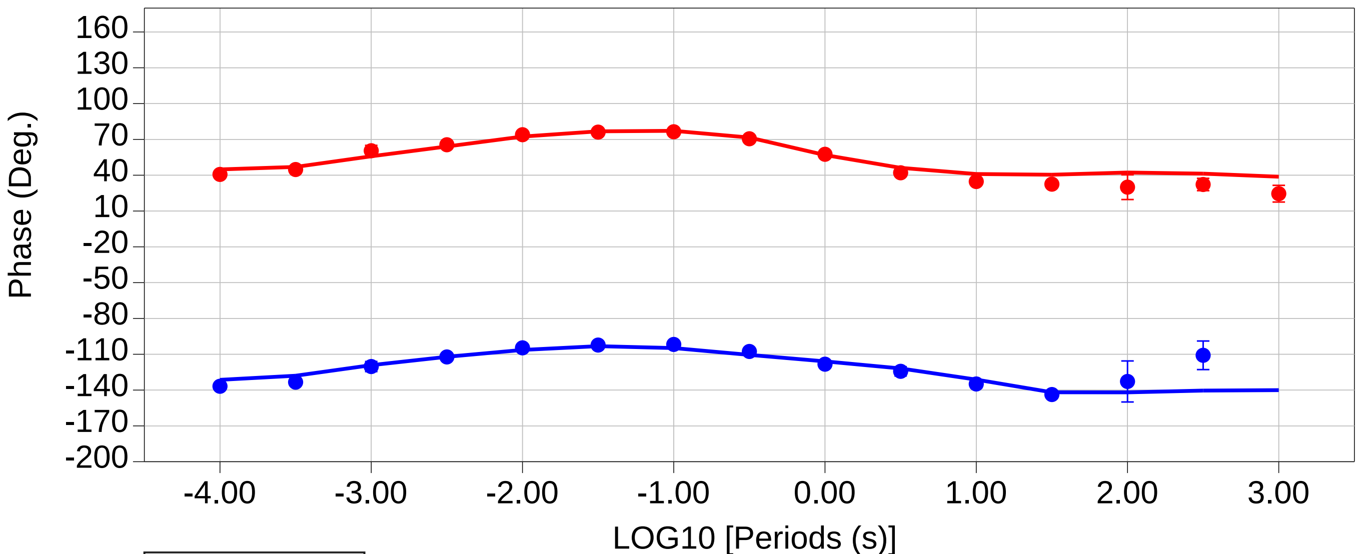

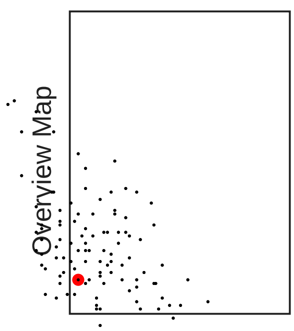

Total RMS = 16716.44

Zxy RMS = 17499.59
Zyx RMS = 15834.42

Site: G42

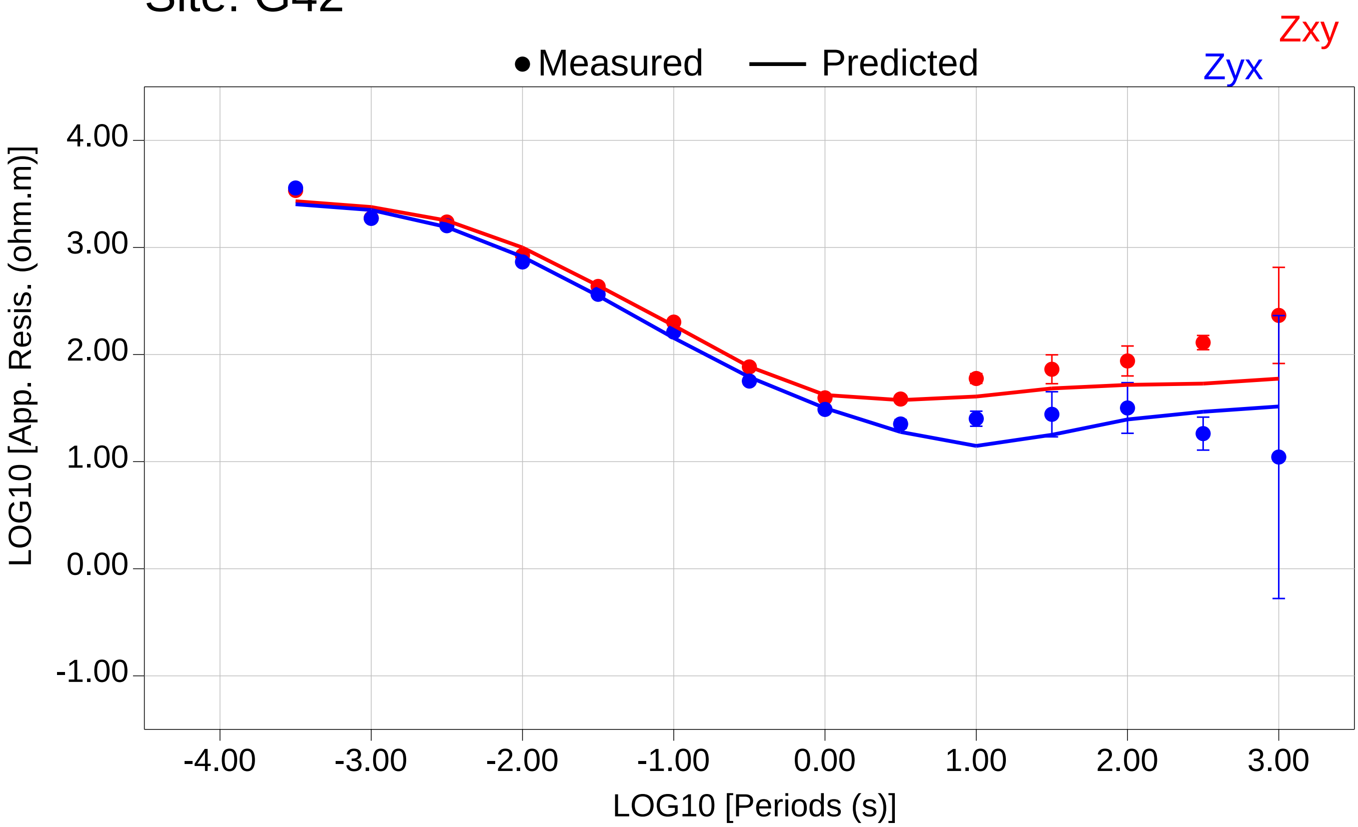

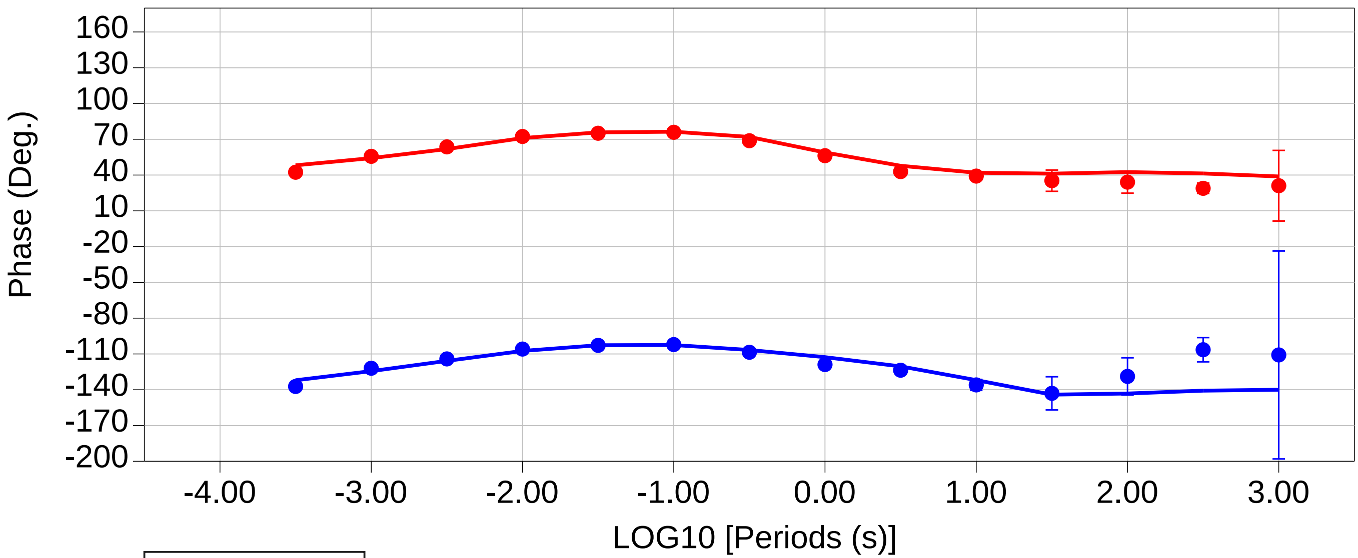

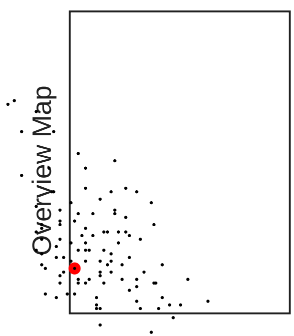

Total RMS = 15693.14

Zxy RMS = 16494.77
Zyx RMS = 14848.29

Site: G43

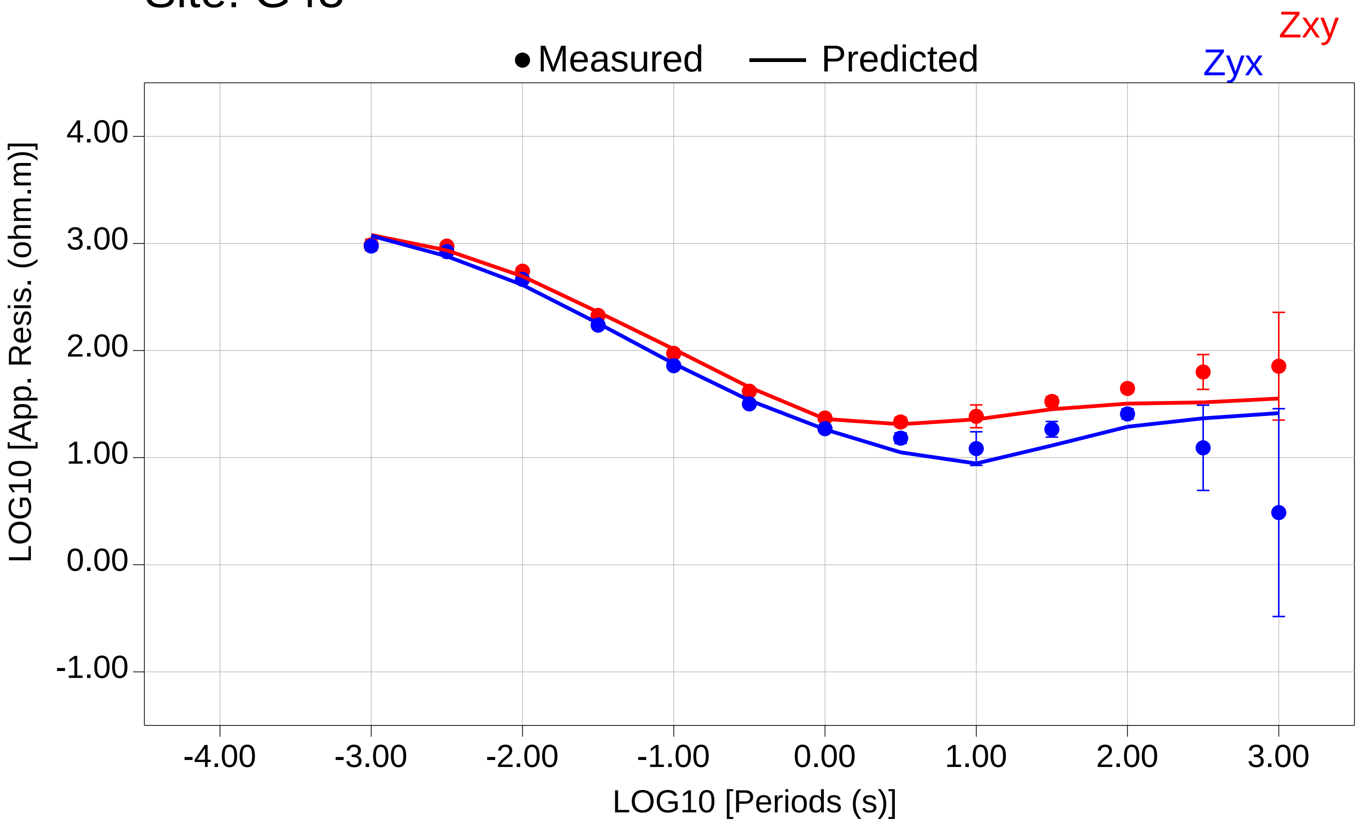

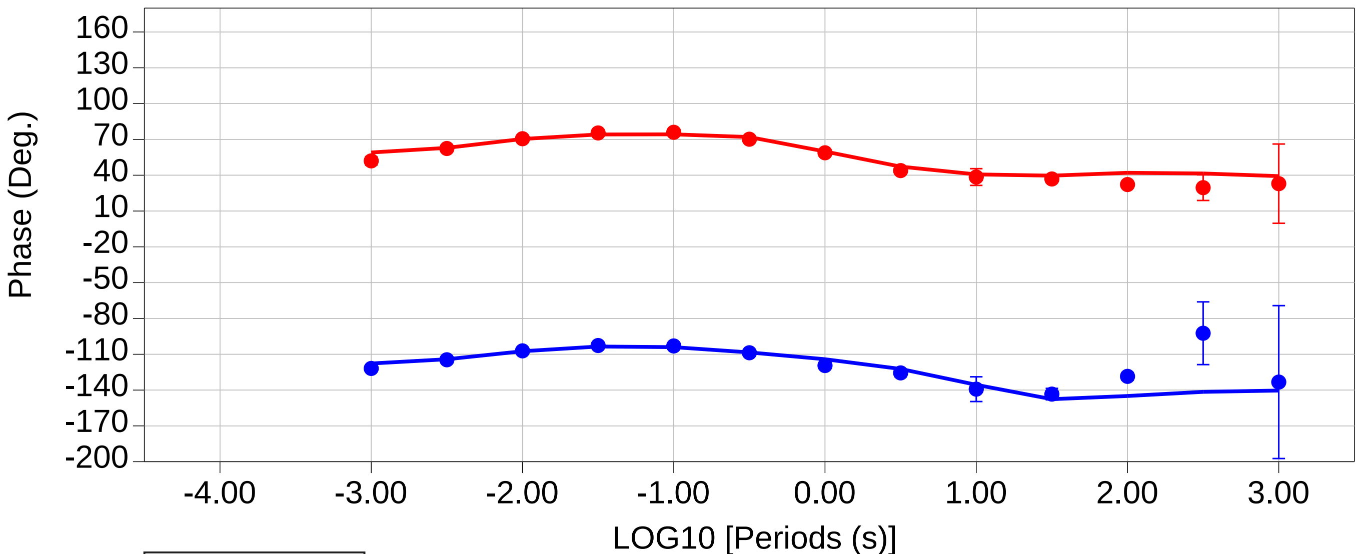

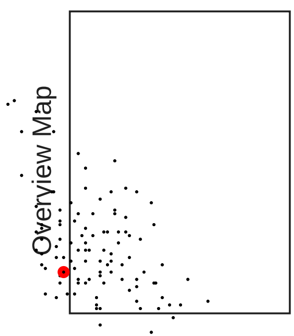

Total RMS = 15880.53

Zxy RMS = 16607.10
Zyx RMS = 15119.09

Site: G44

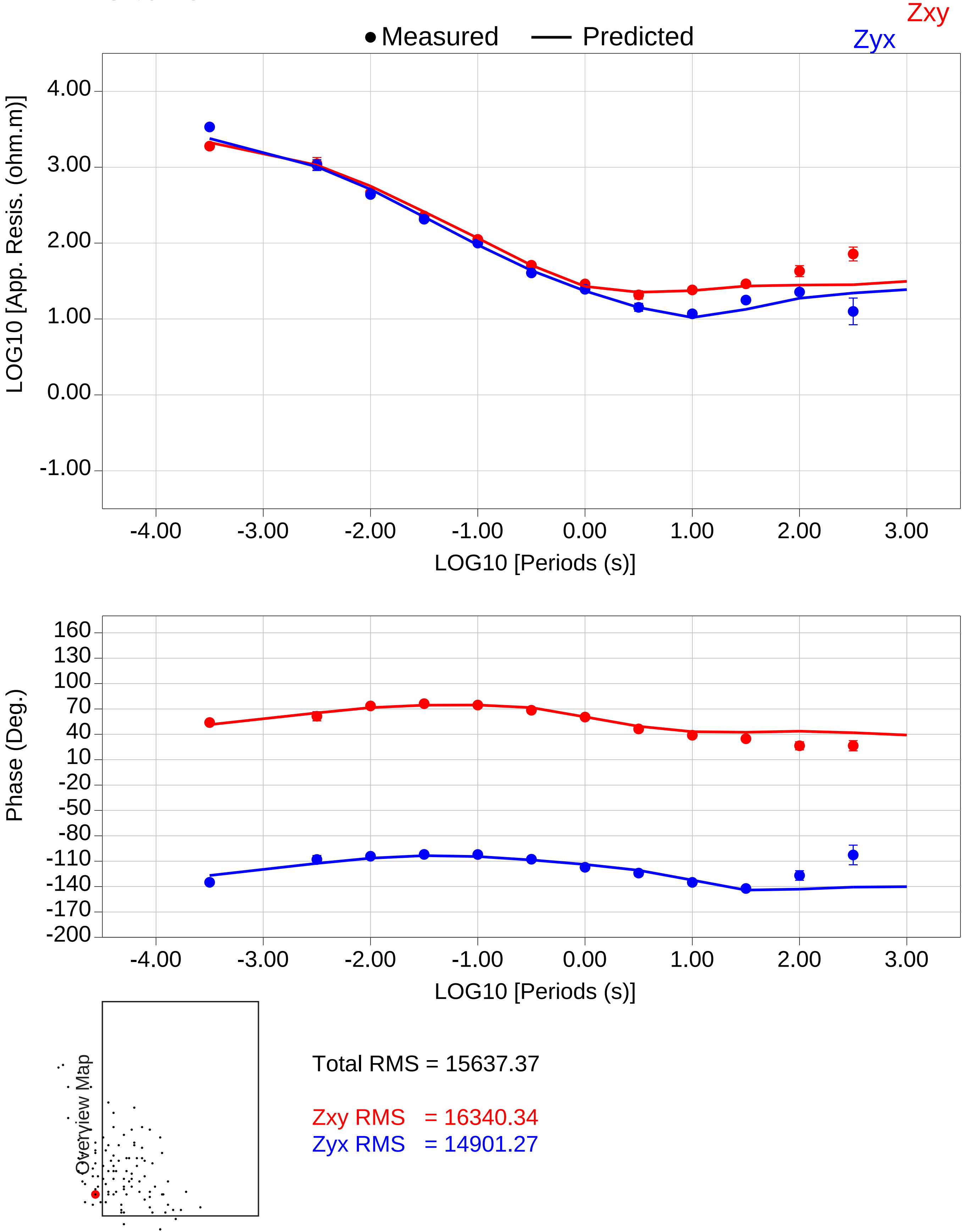

Total RMS = 15637.37

Zxy RMS = 16340.34
Zyx RMS = 14901.27

Site: G45

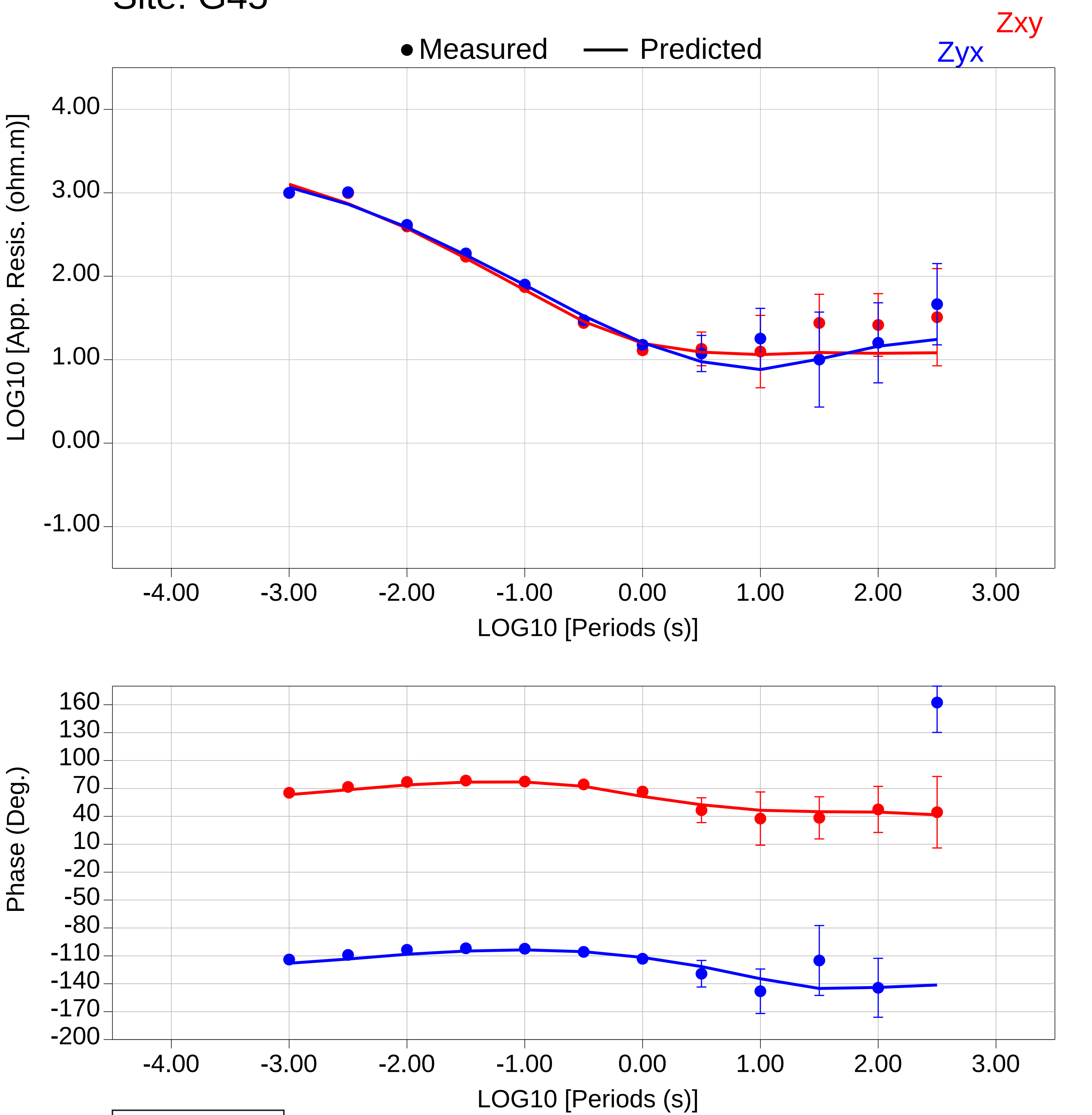

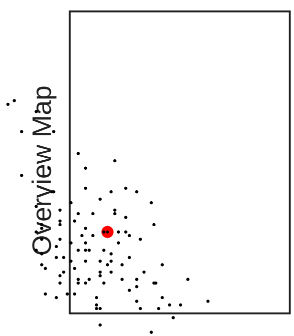

Total RMS = 15393.25

Zxy RMS = 15206.71

Zyx RMS = 15577.55

Site: G46

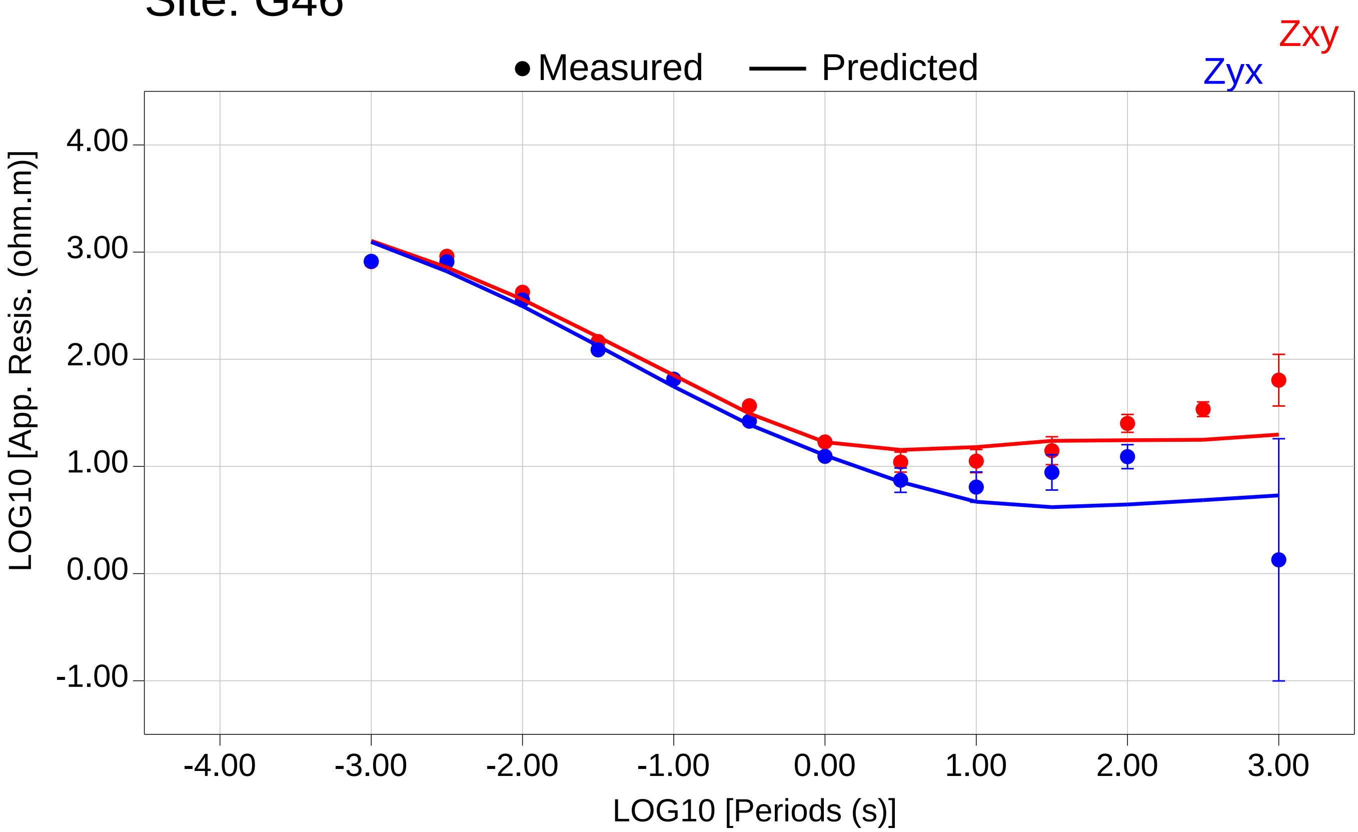

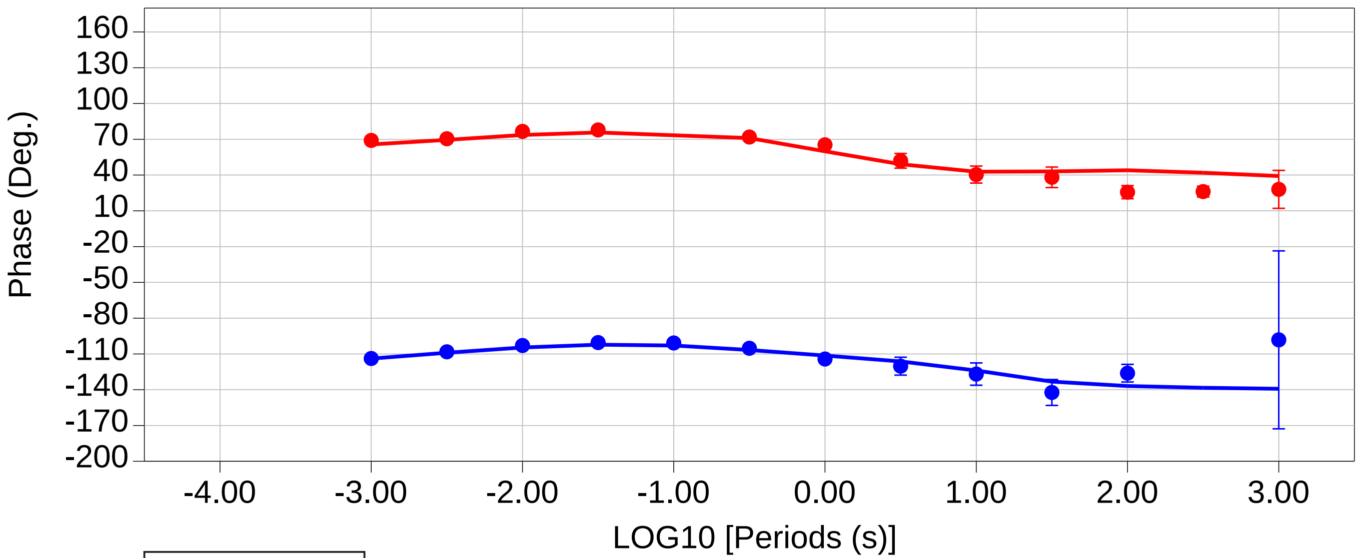

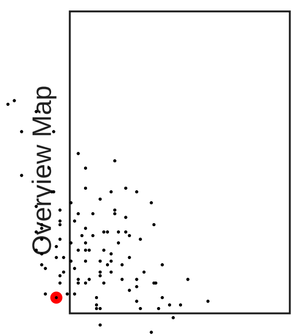

Total RMS = 14380.60

Zxy RMS = 13629.48
Zyx RMS = 15094.40

Site: G47

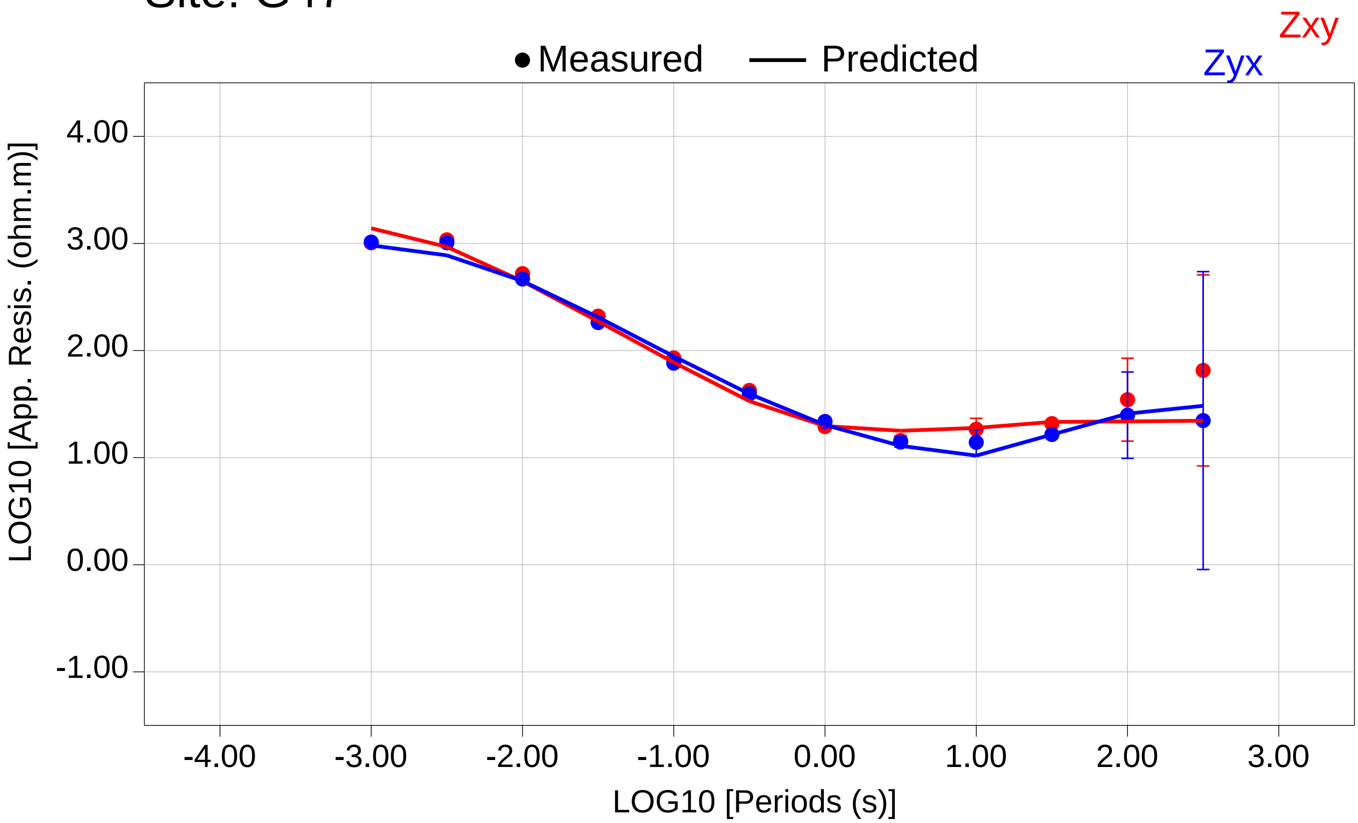

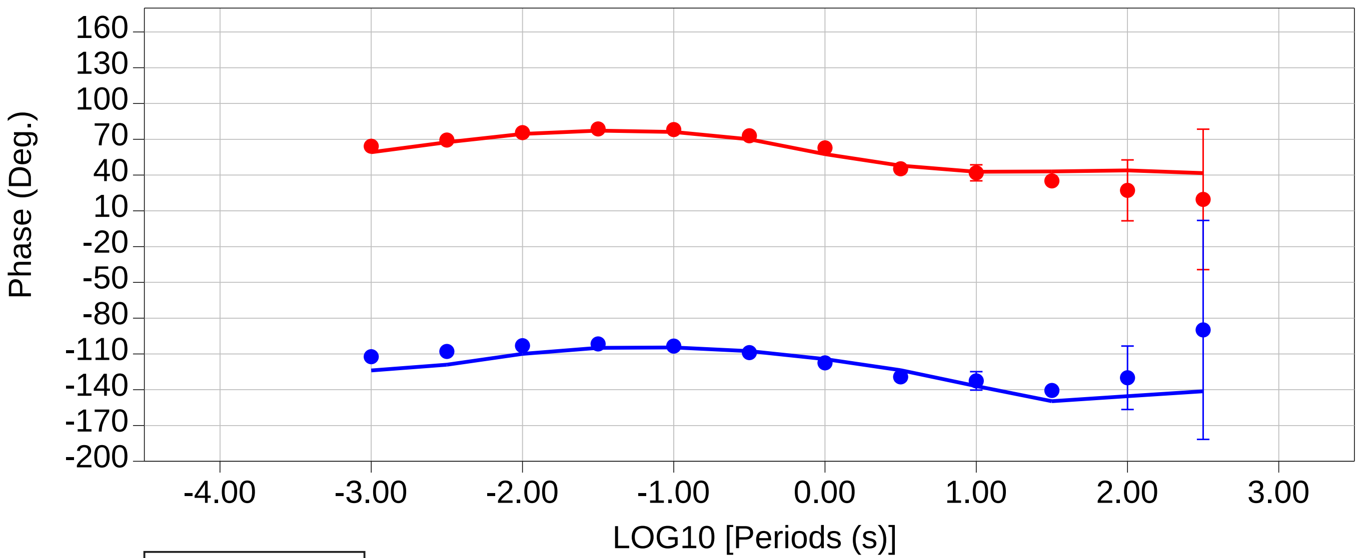

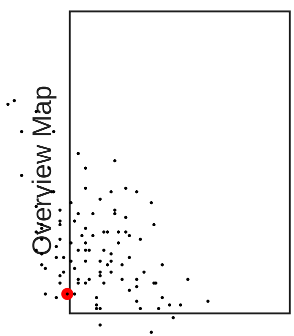

Total RMS = 16398.34

Zxy RMS = 16715.07

Zyx RMS = 16075.38

Site: G48

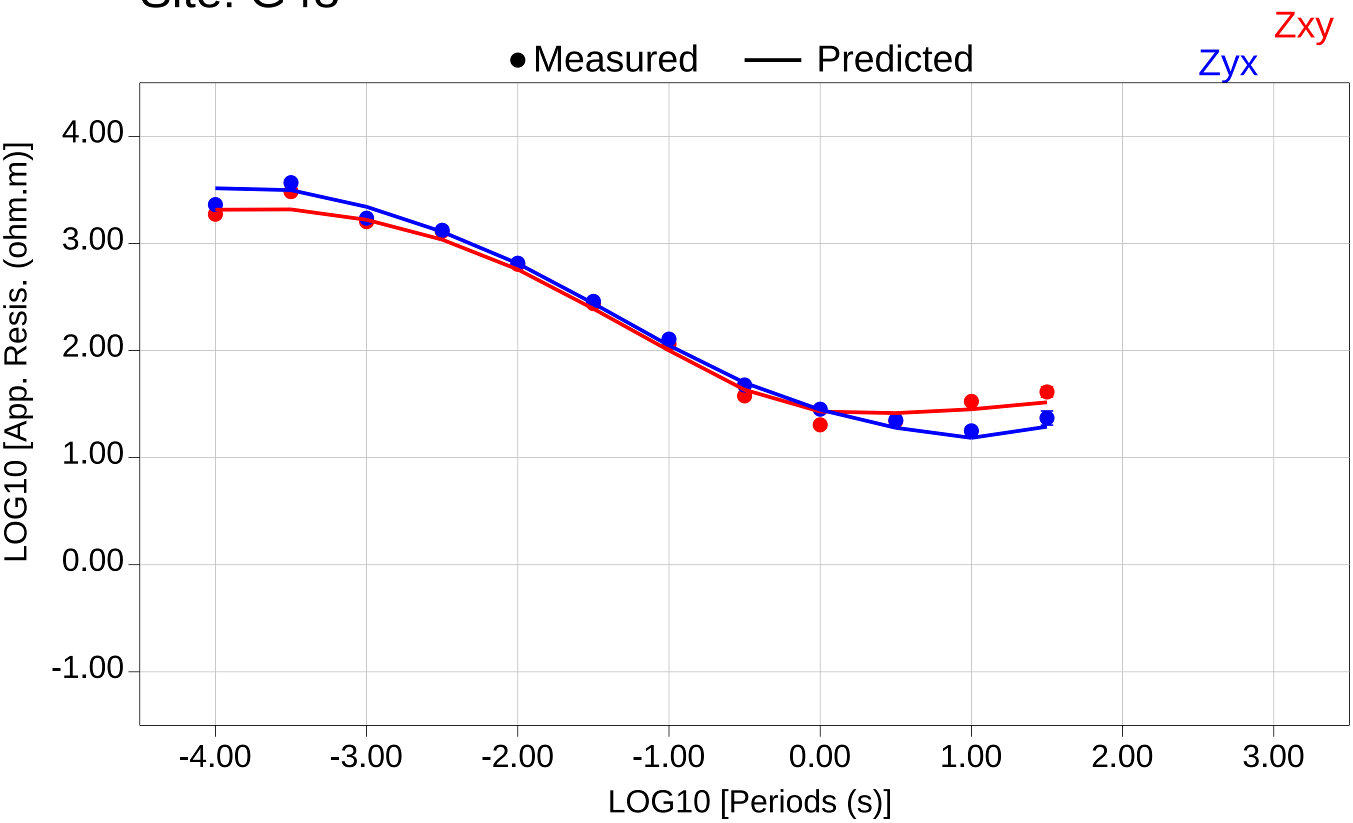

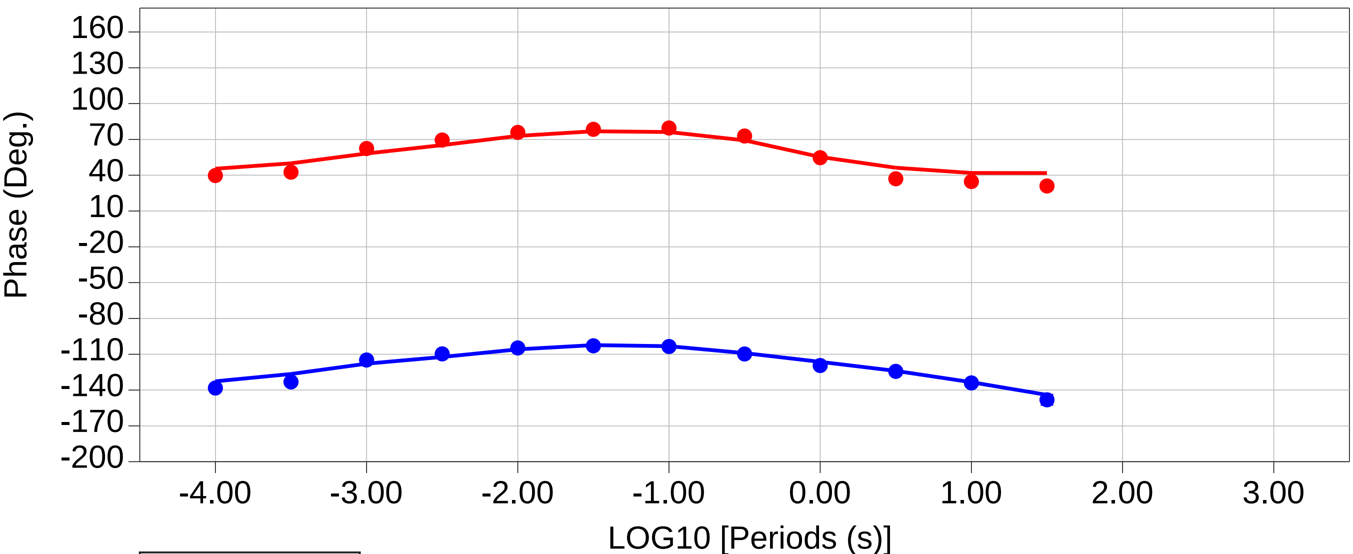

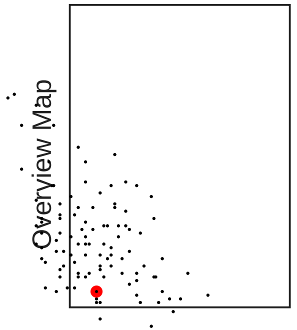

Total RMS = 18339.42

Zxy RMS = 17670.07

Zyx RMS = 18985.18

Site: G49

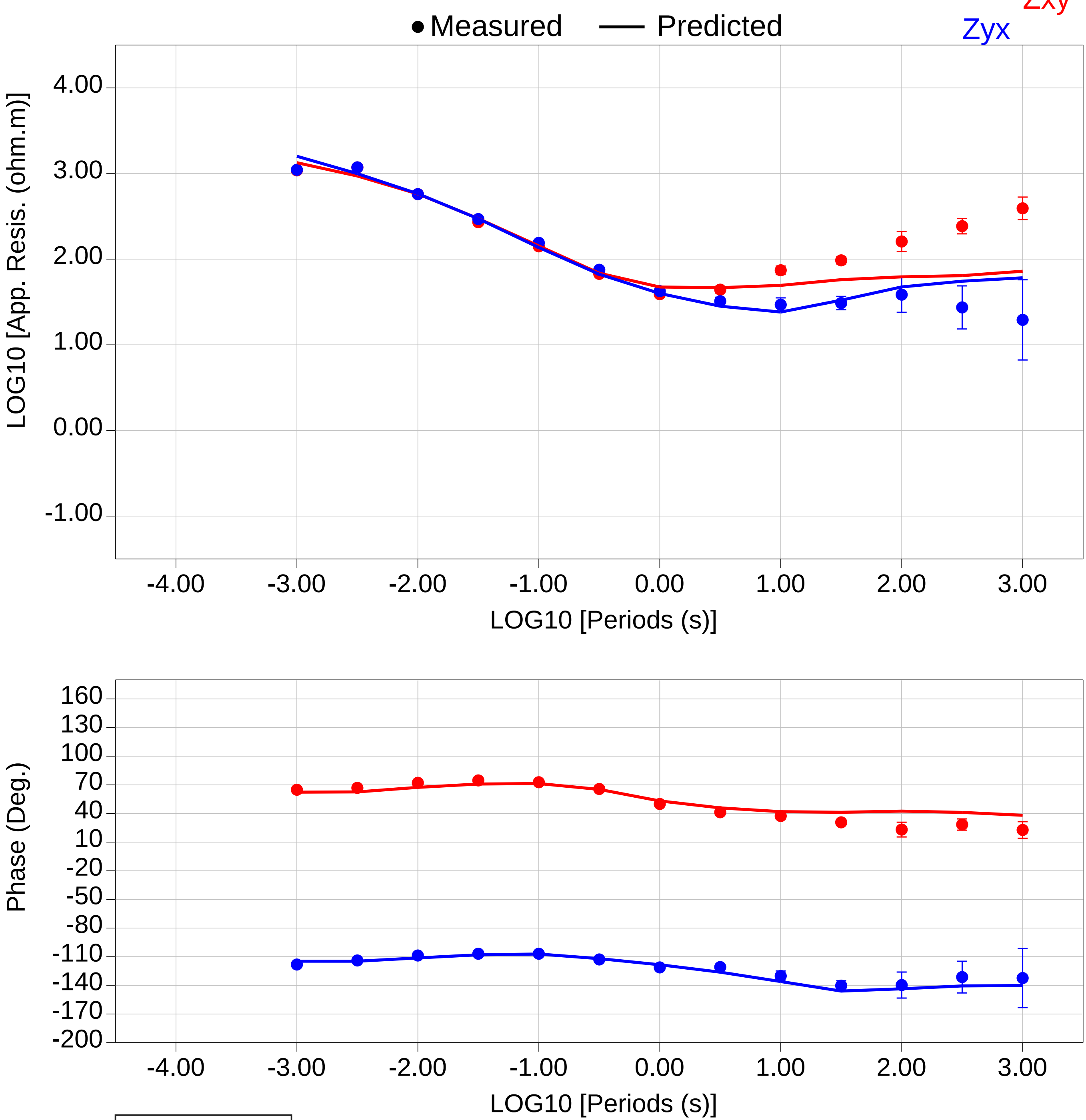

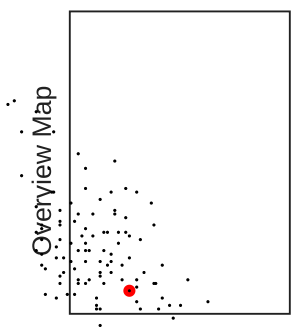

Total RMS = 15208.89

Zxy RMS = 15280.30
Zyx RMS = 15137.14

Site: G50

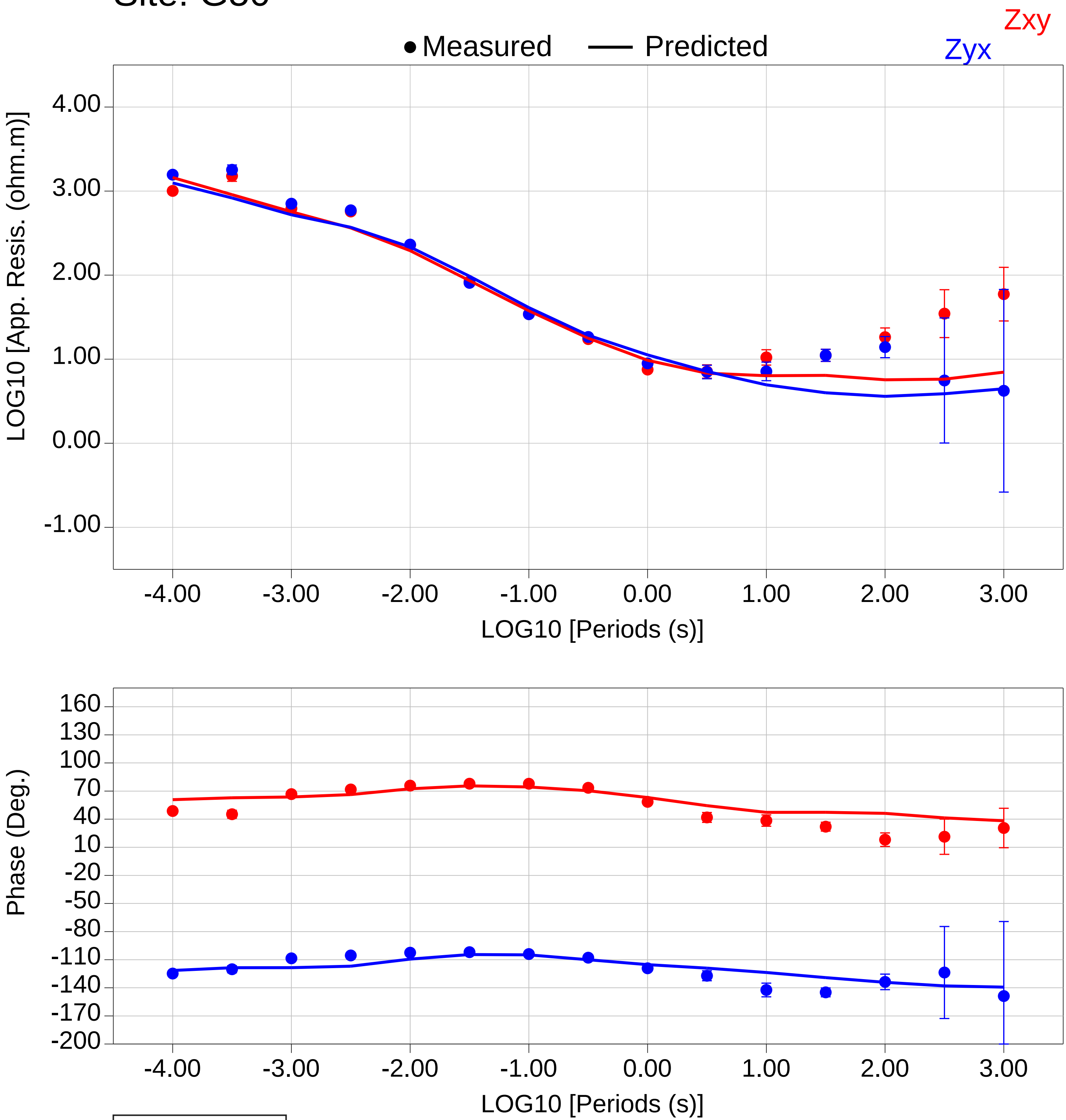

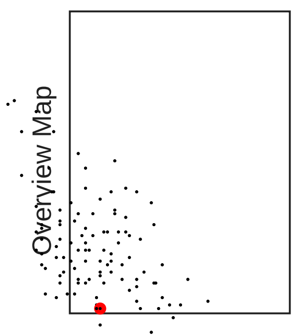

Total RMS = 14461.07

Zxy RMS = 14280.00

Zyx RMS = 14639.91

Site: G51

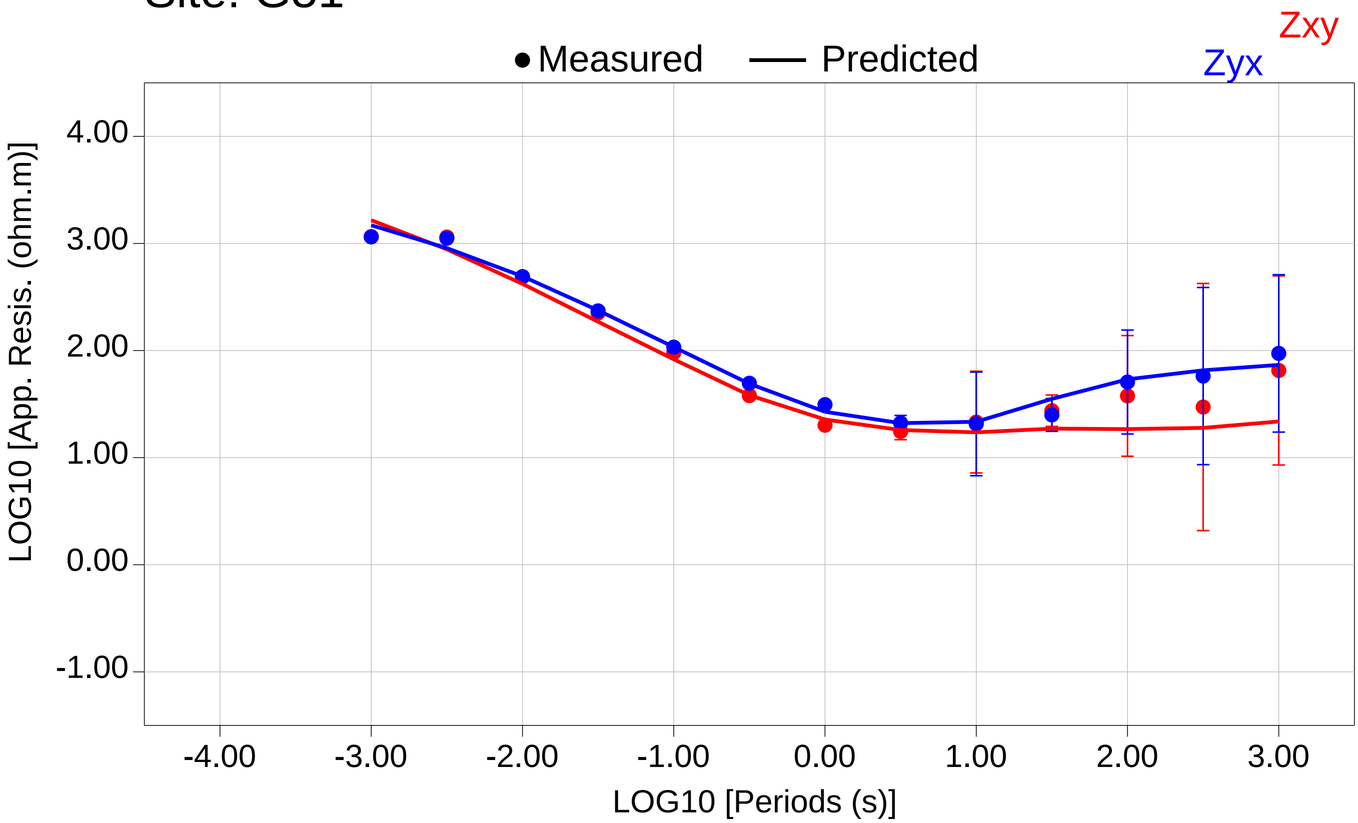

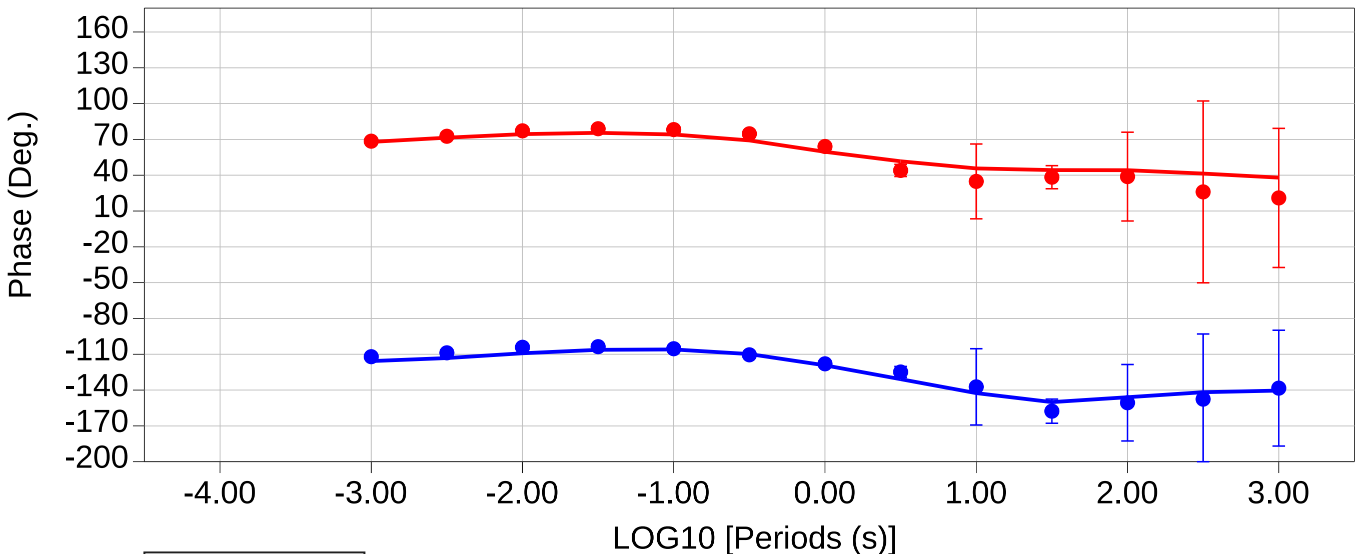

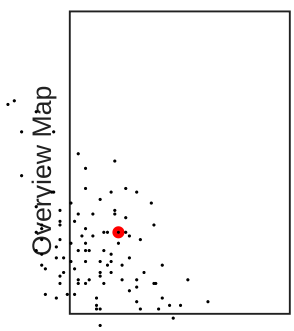

Total RMS = 14848.28

Zxy RMS = 14359.02

Zyx RMS = 15321.93

Site: G52

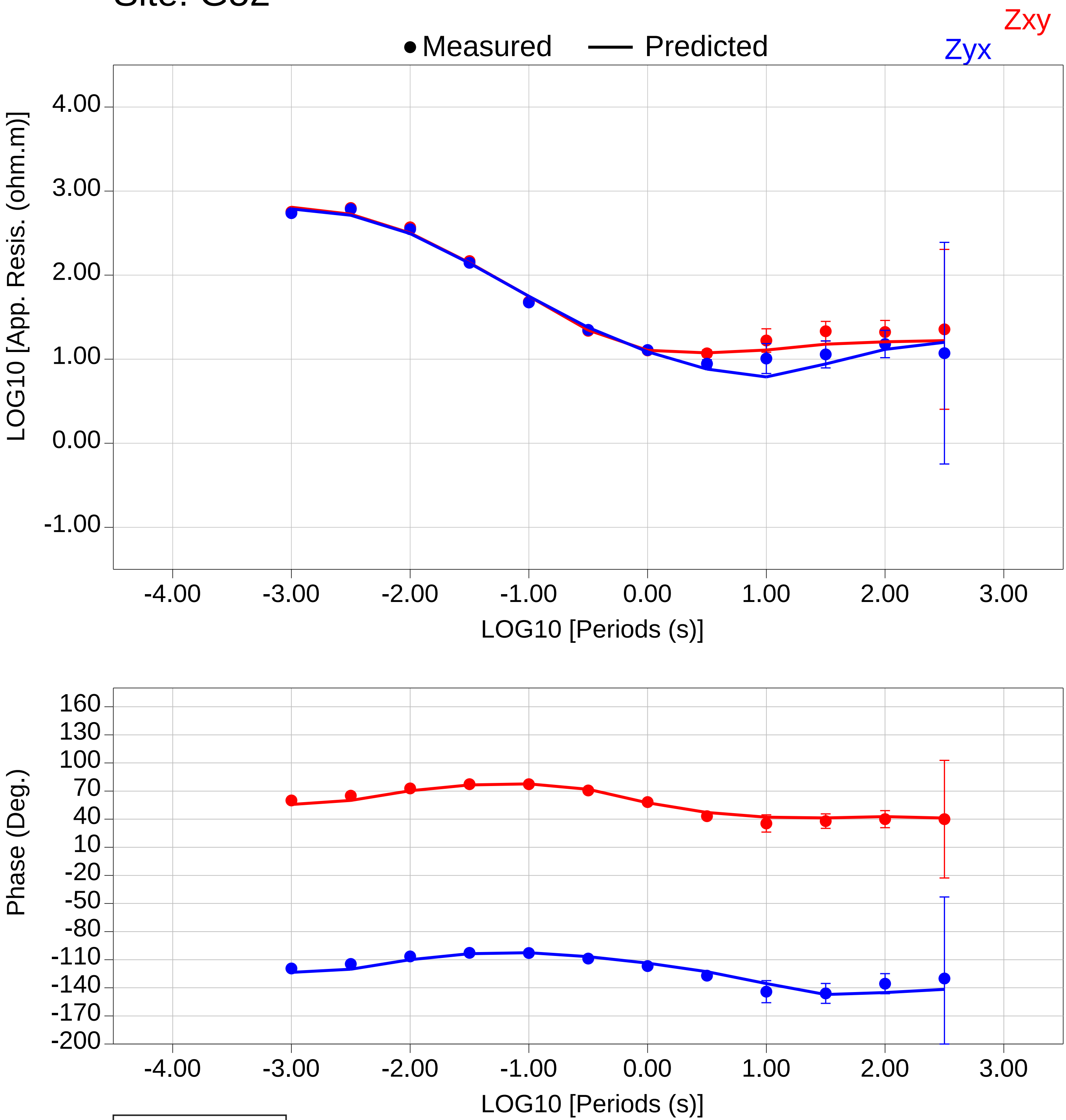

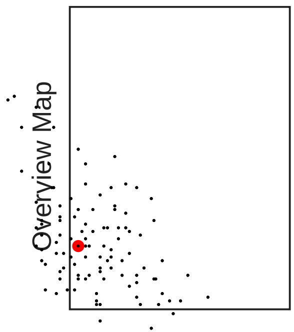

Total RMS = 16028.94

Zxy RMS = 16114.83
Zyx RMS = 15942.59

Site: MT16

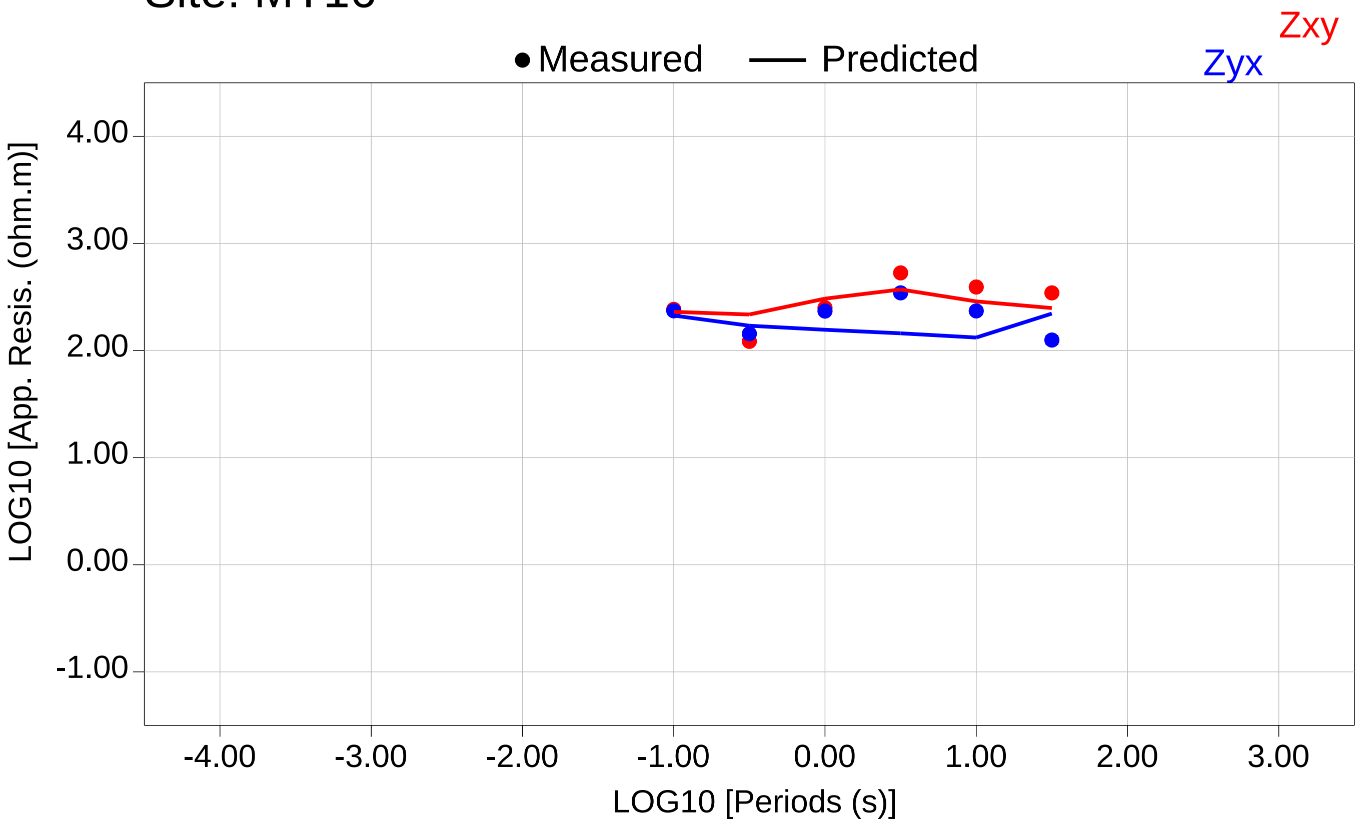

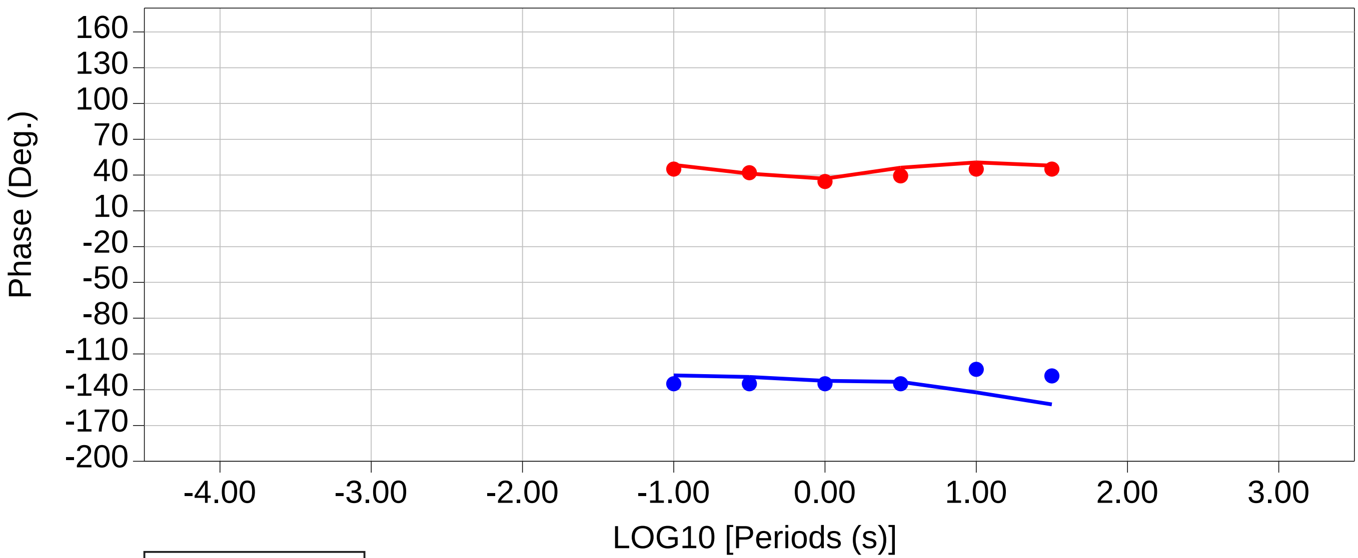

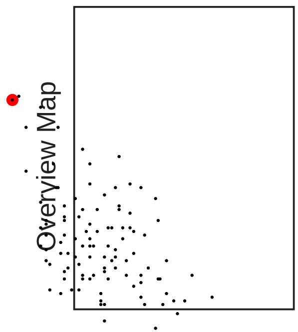

Total RMS = 16398.04

Zxy RMS = 17957.32
Zyx RMS = 14673.99

Site: MT19

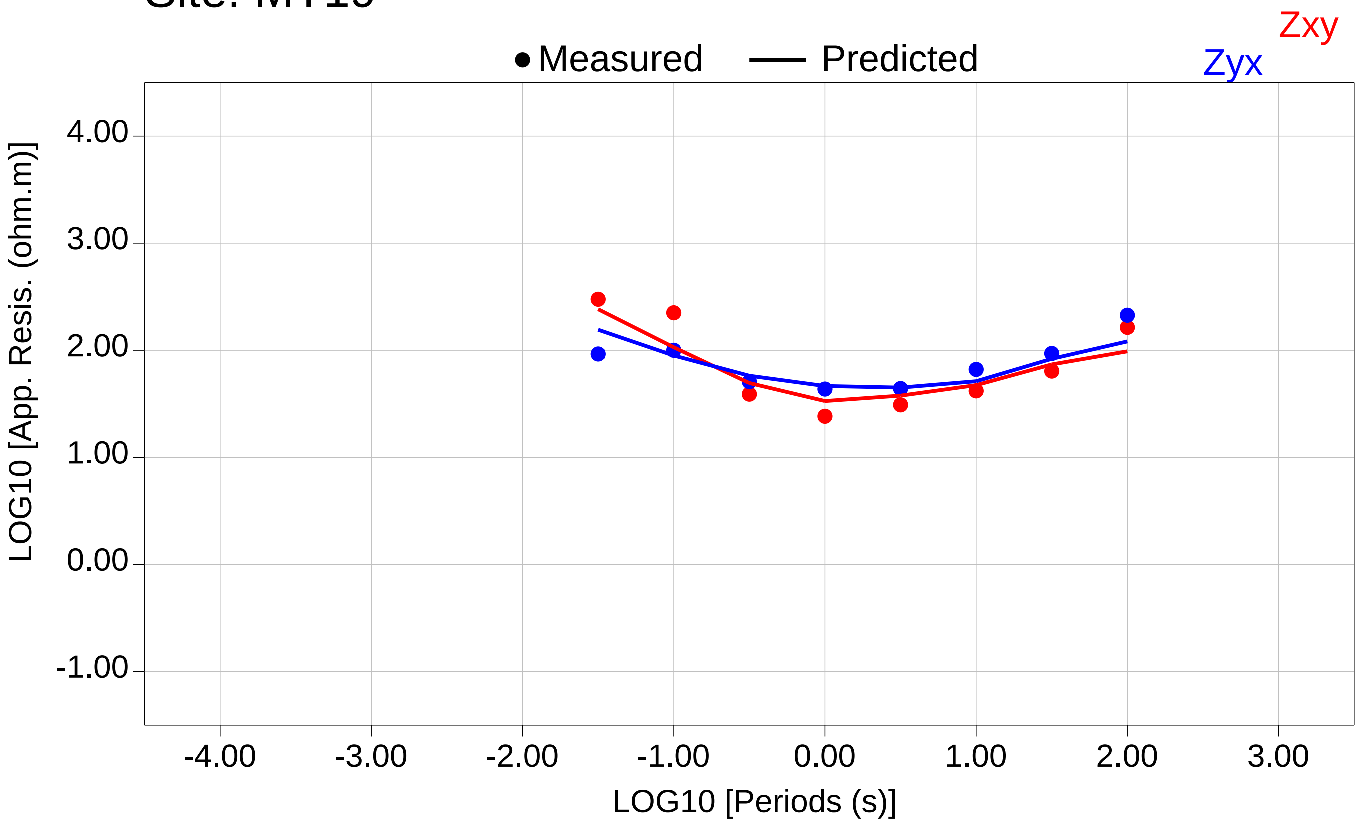

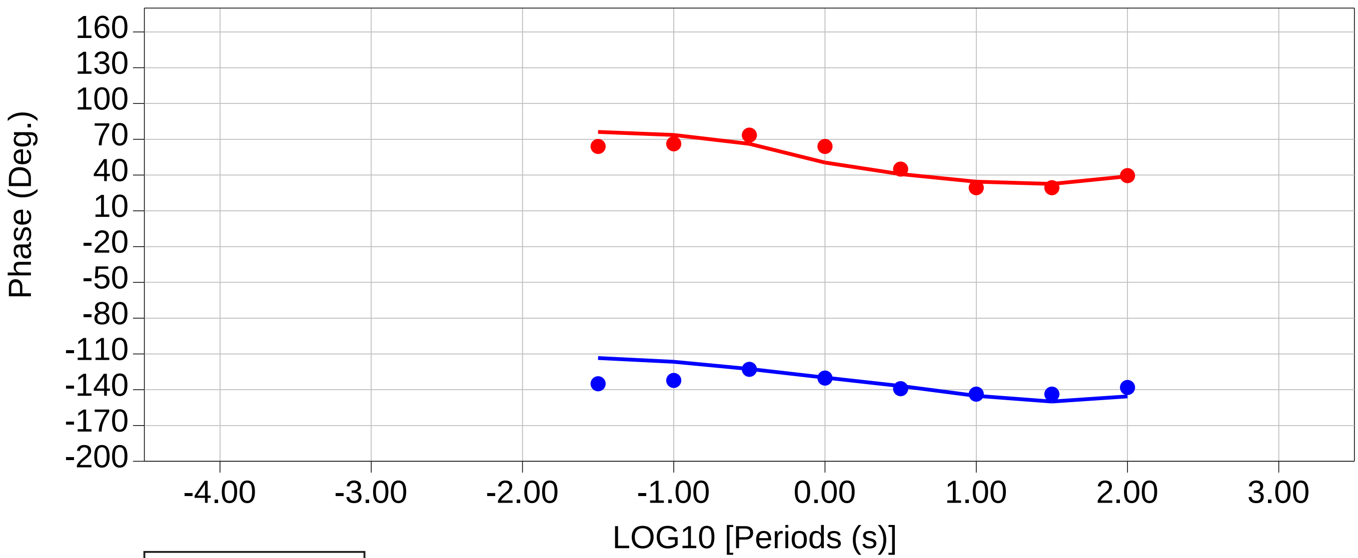

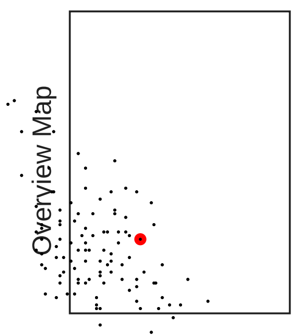

Total RMS = 15821.50

Zxy RMS = 15692.19

Zyx RMS = 15949.77

Site: MT20

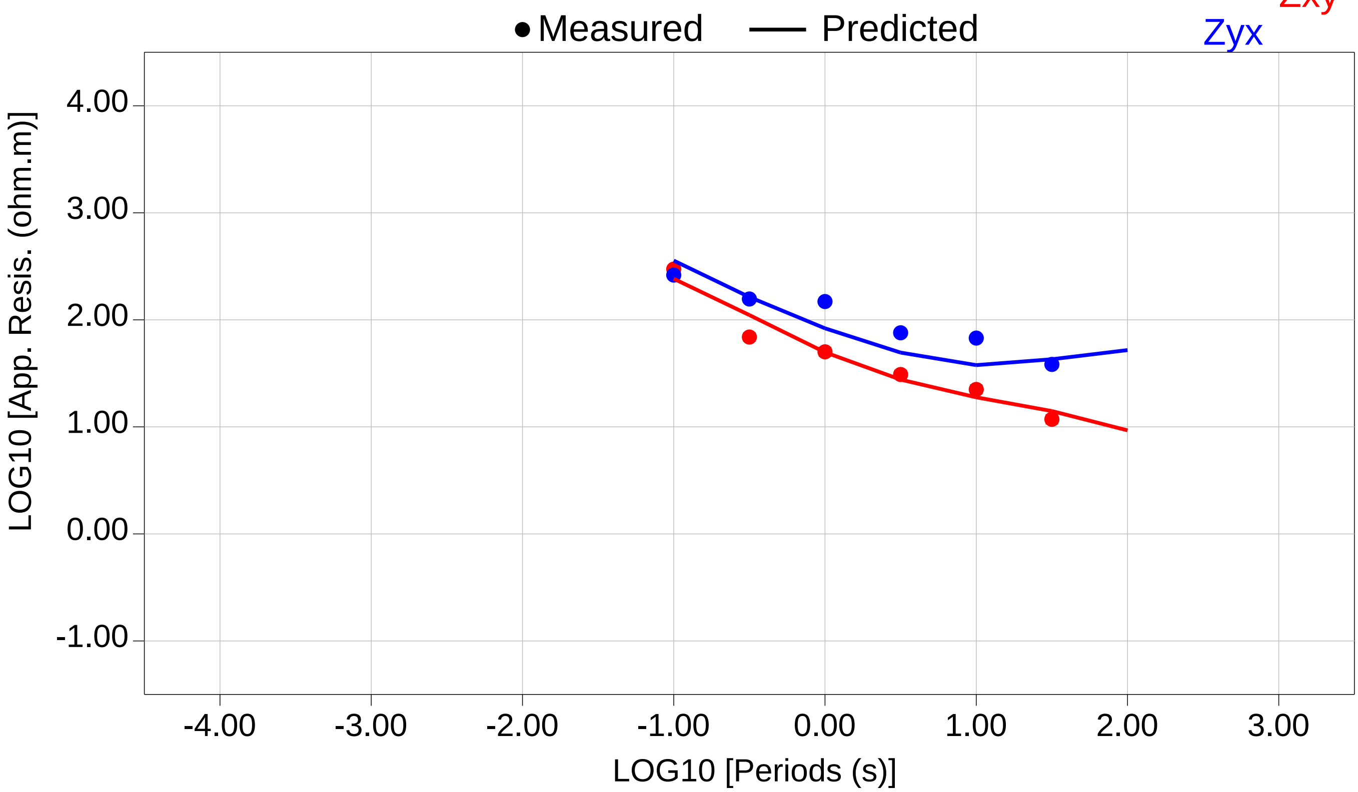

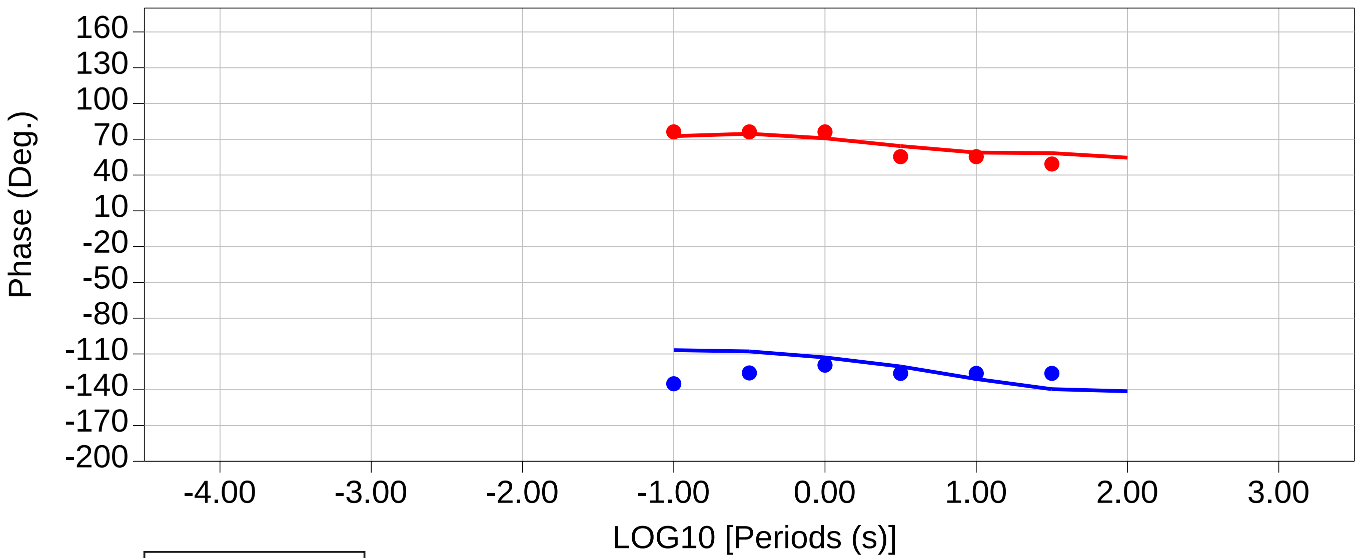

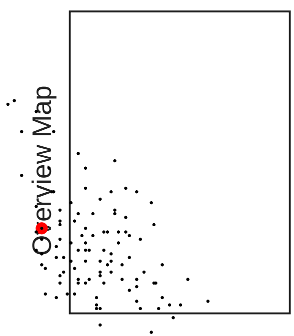

Total RMS = 20672.62

Zxy RMS = 17998.55

Zyx RMS = 23038.36

Site: MT21

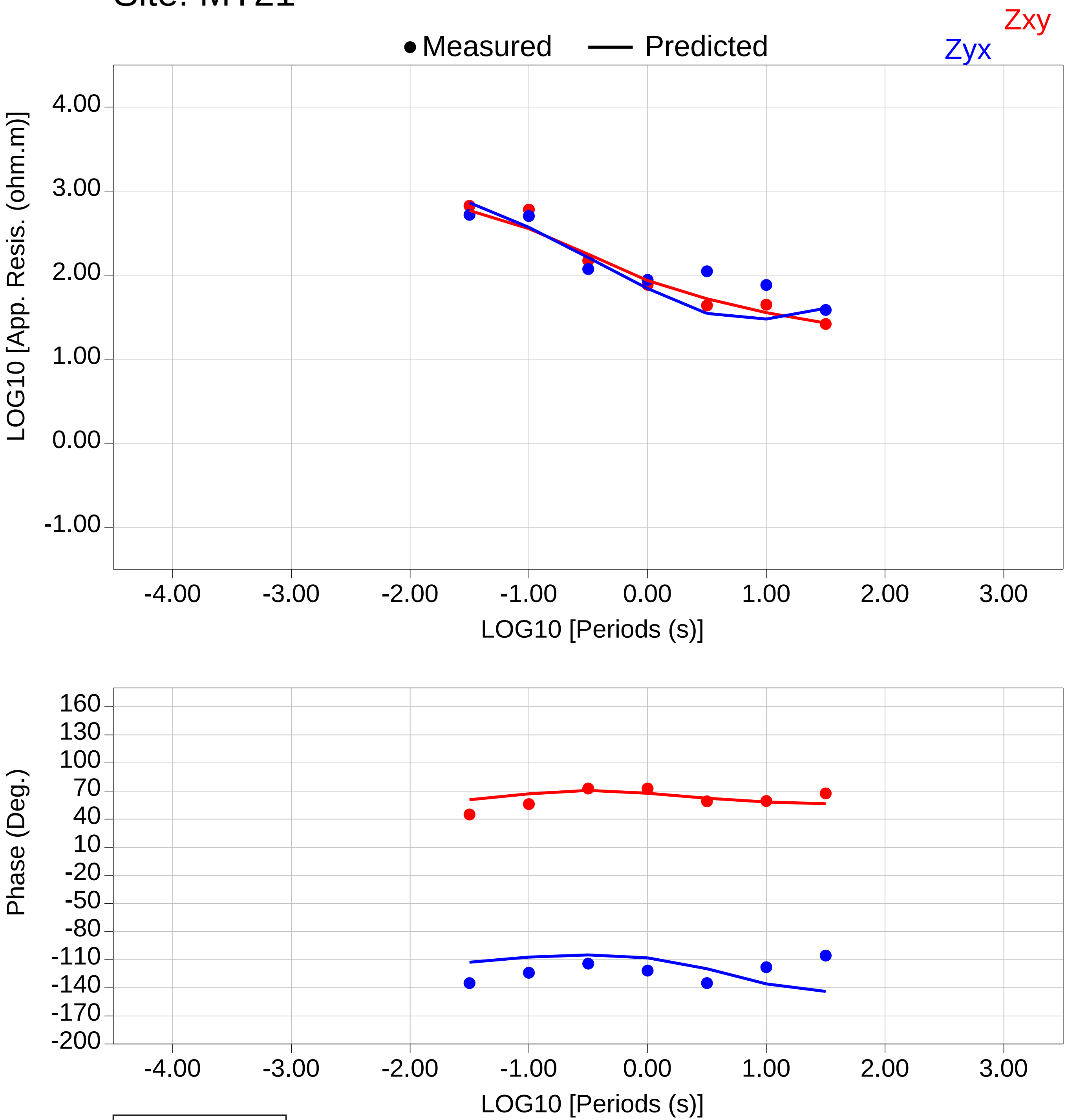

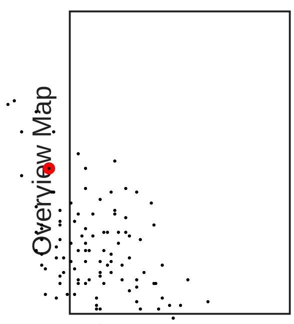

Total RMS = 17862.84

Zxy RMS = 18187.76
Zyx RMS = 17531.91

Site: X03

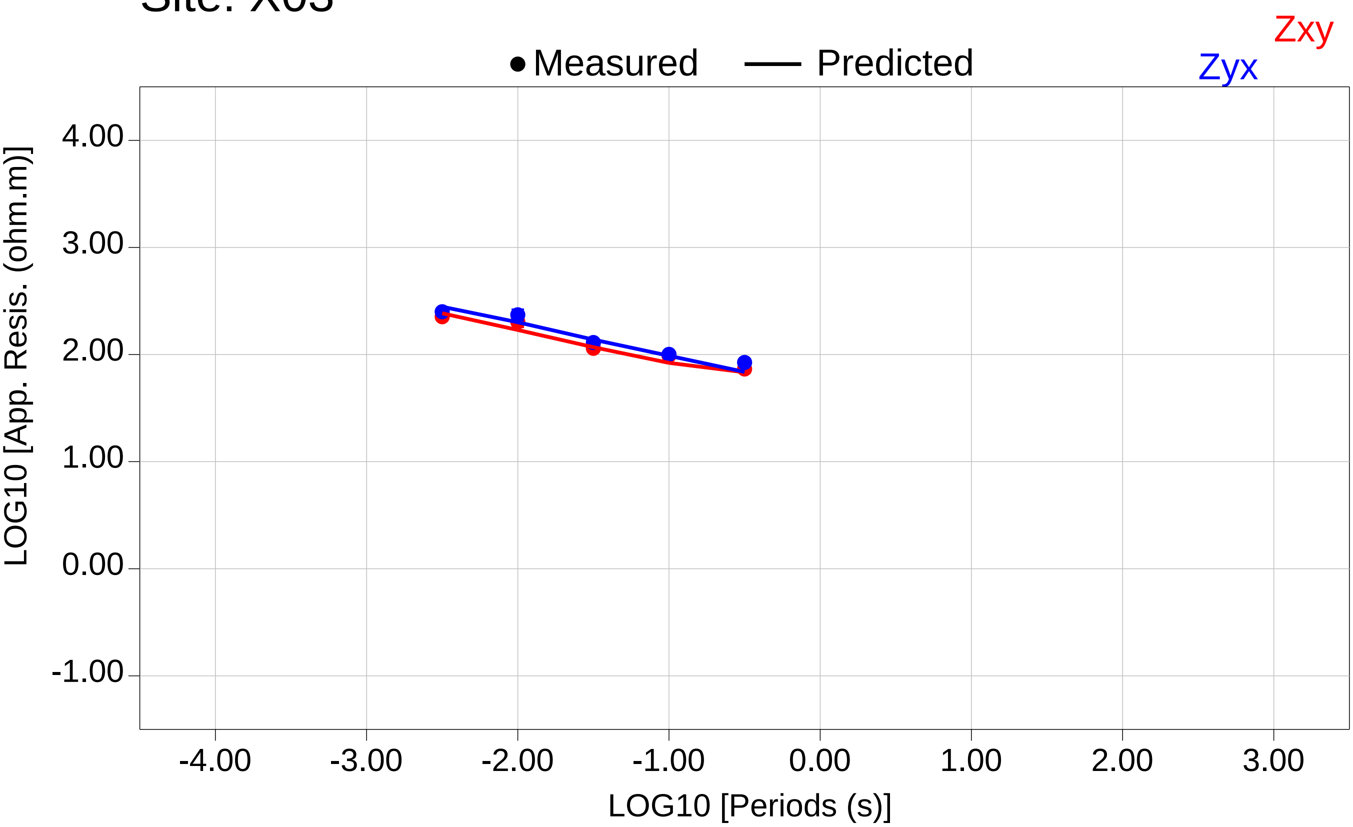

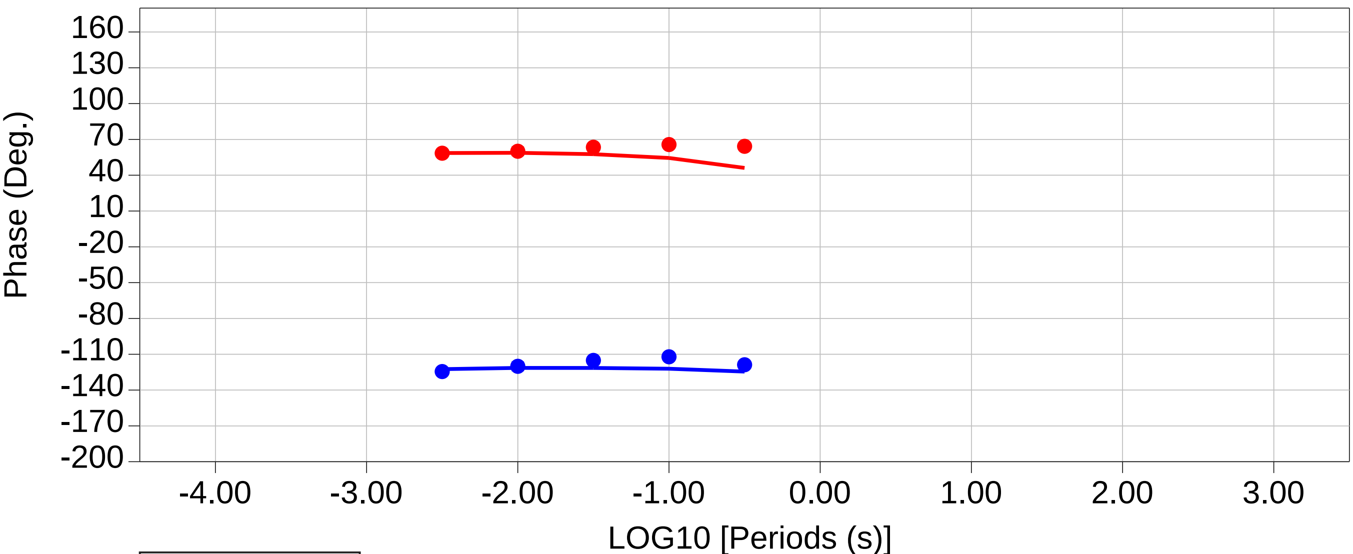

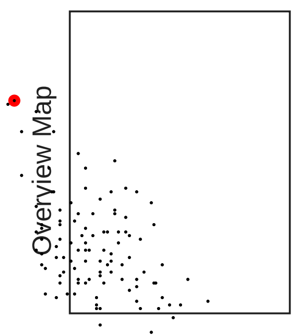

Total RMS = 15019.14

Zxy RMS = 14354.29
Zyx RMS = 15655.79

Site: X05

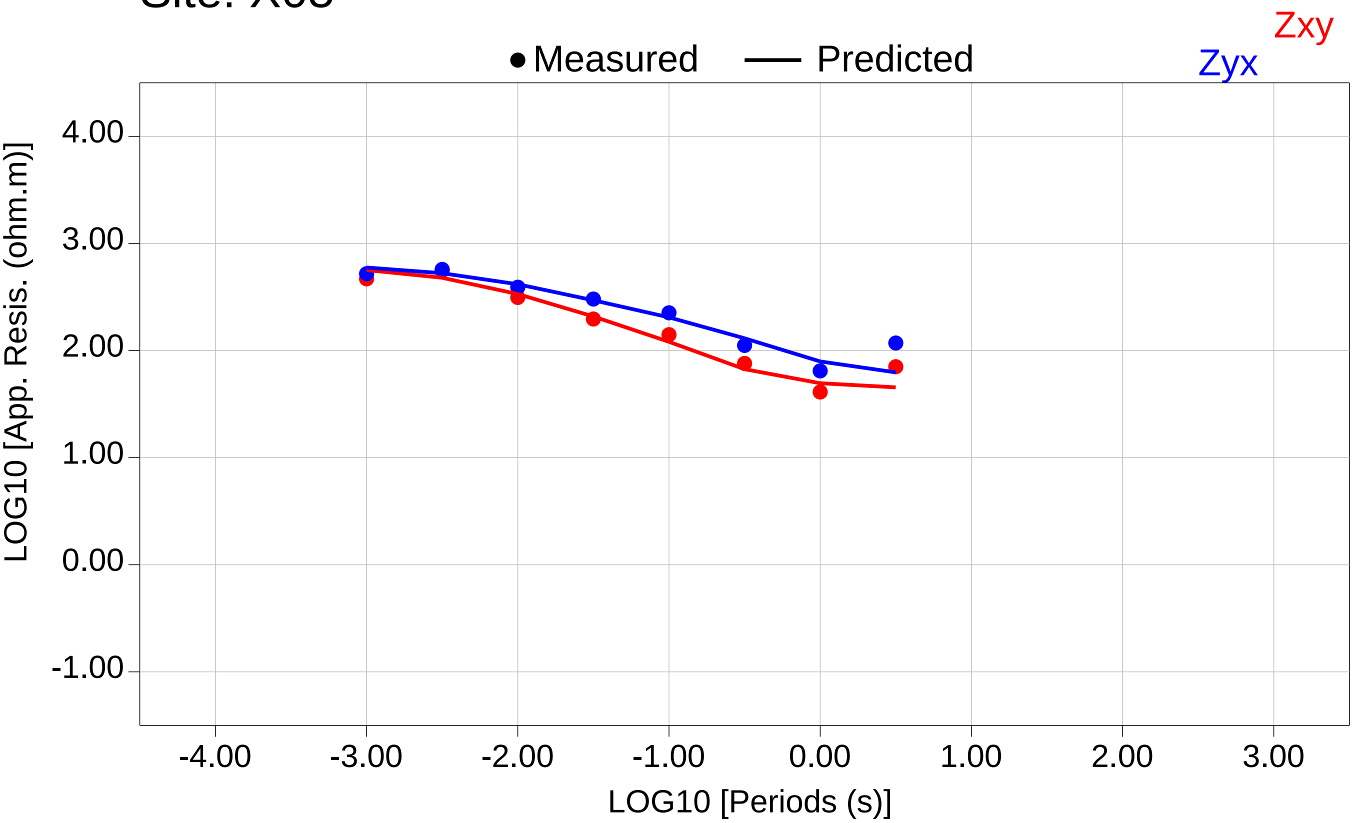

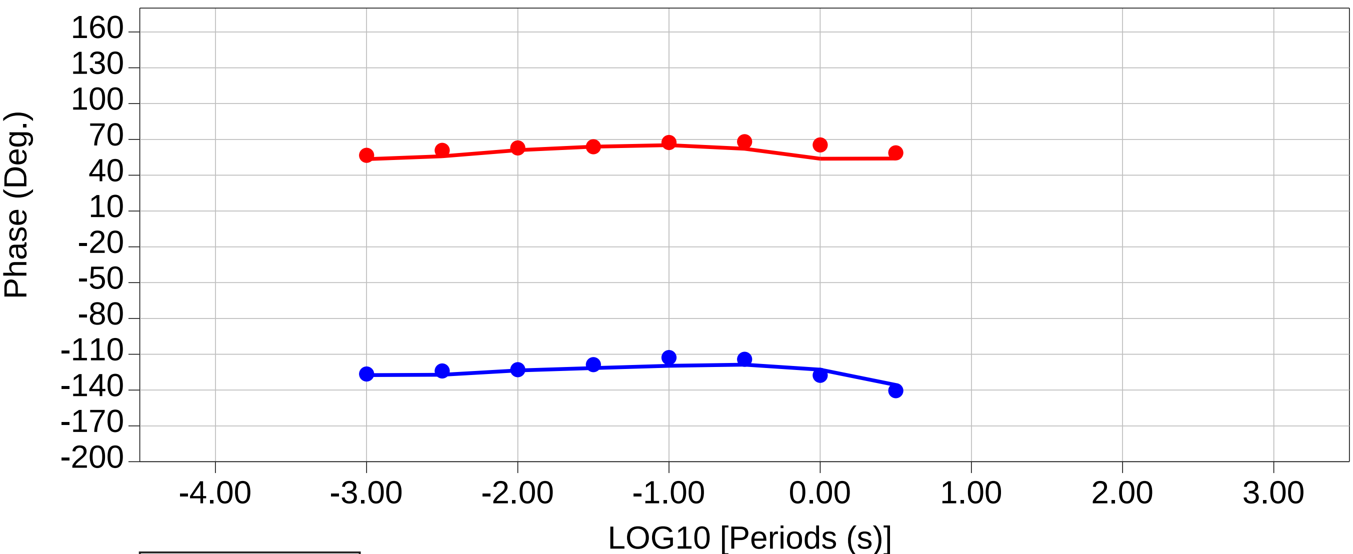

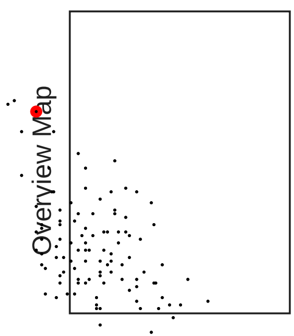

Total RMS = 17940.69

Zxy RMS = 16463.21

Zyx RMS = 19305.43

Site: X06

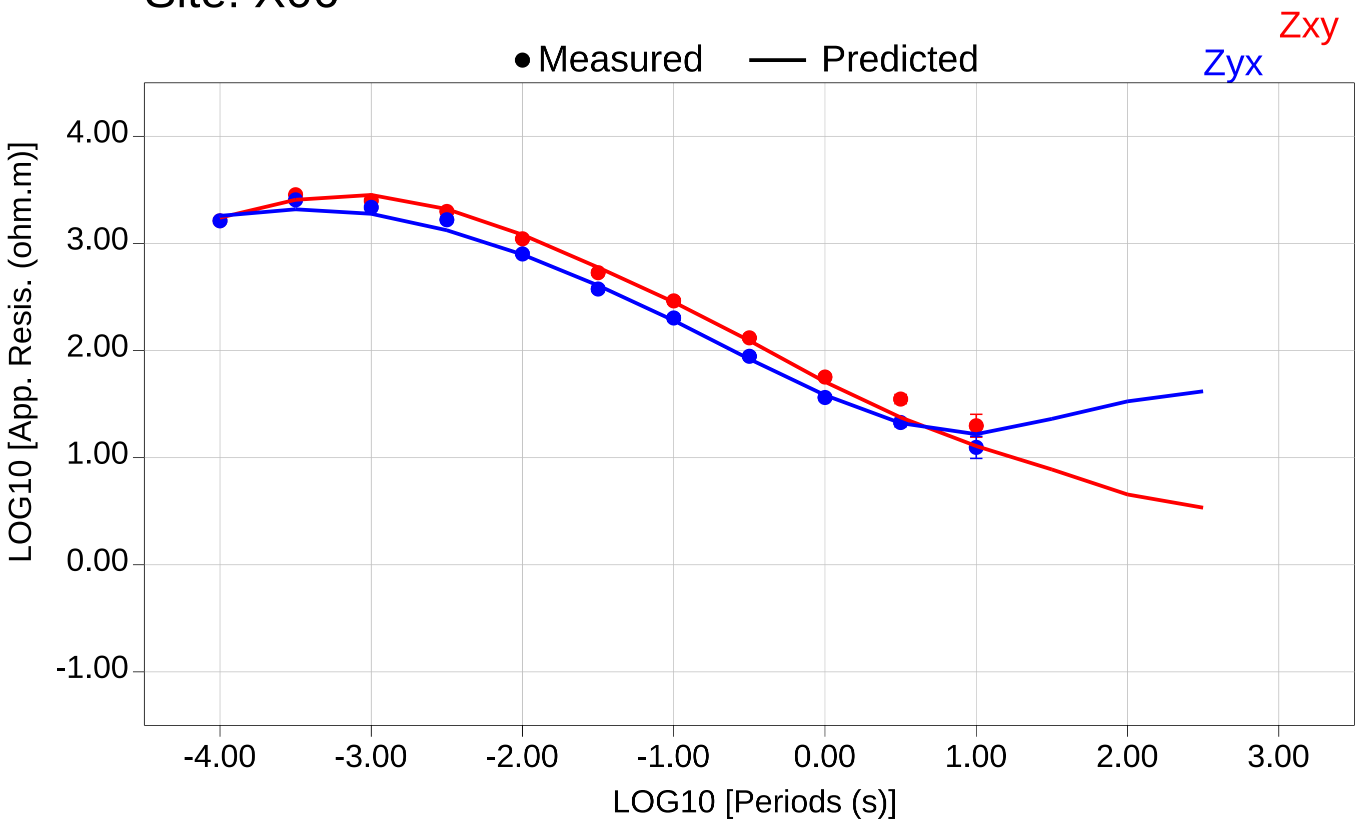

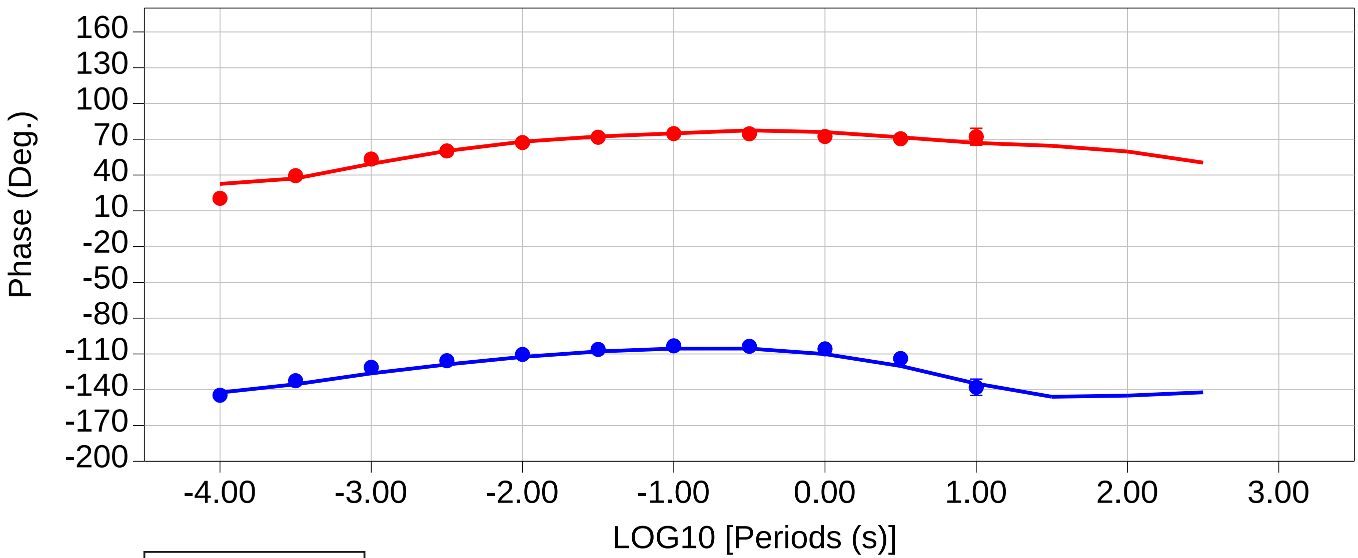

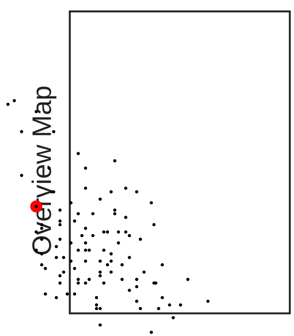

Total RMS = 18029.86

Zxy RMS = 19210.54
Zyx RMS = 16766.24

Site: X07

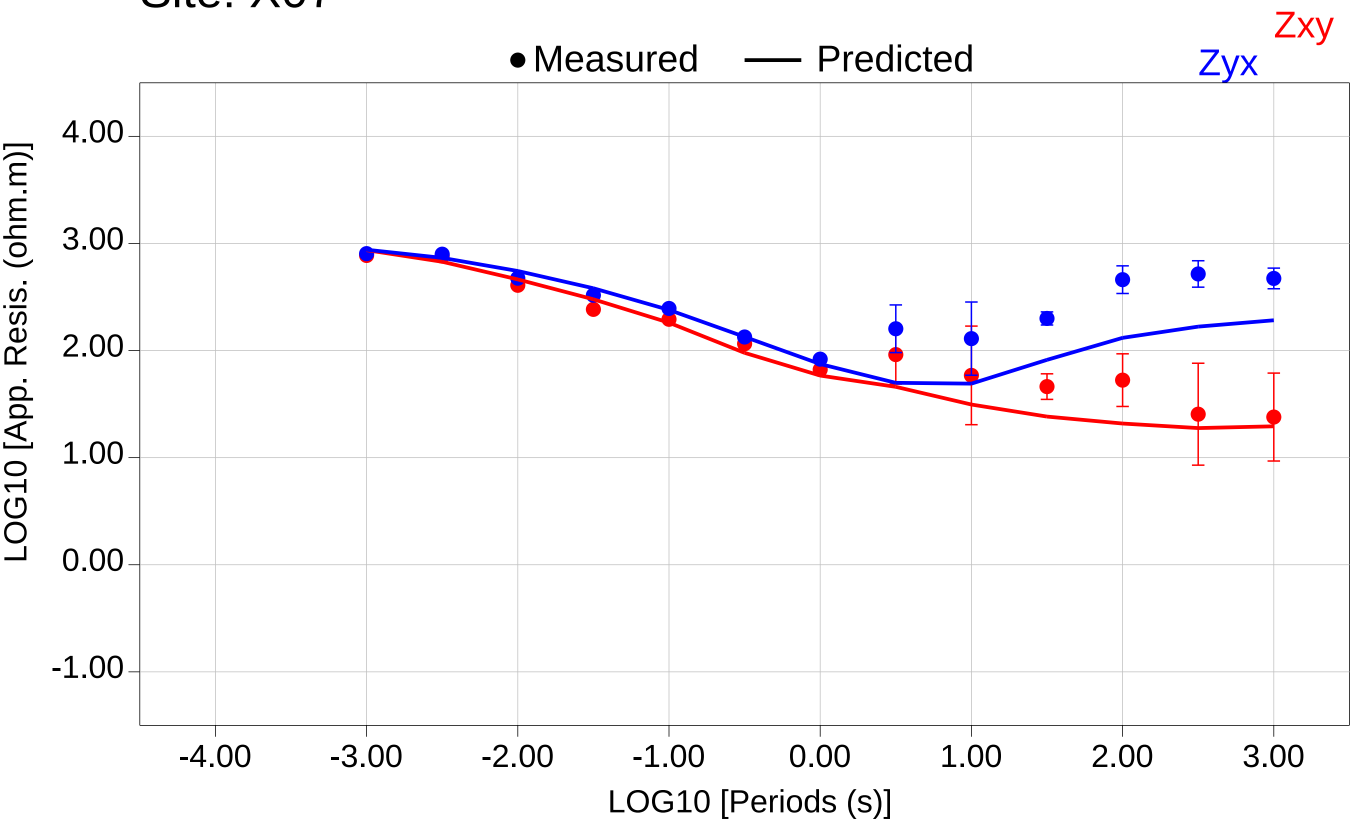

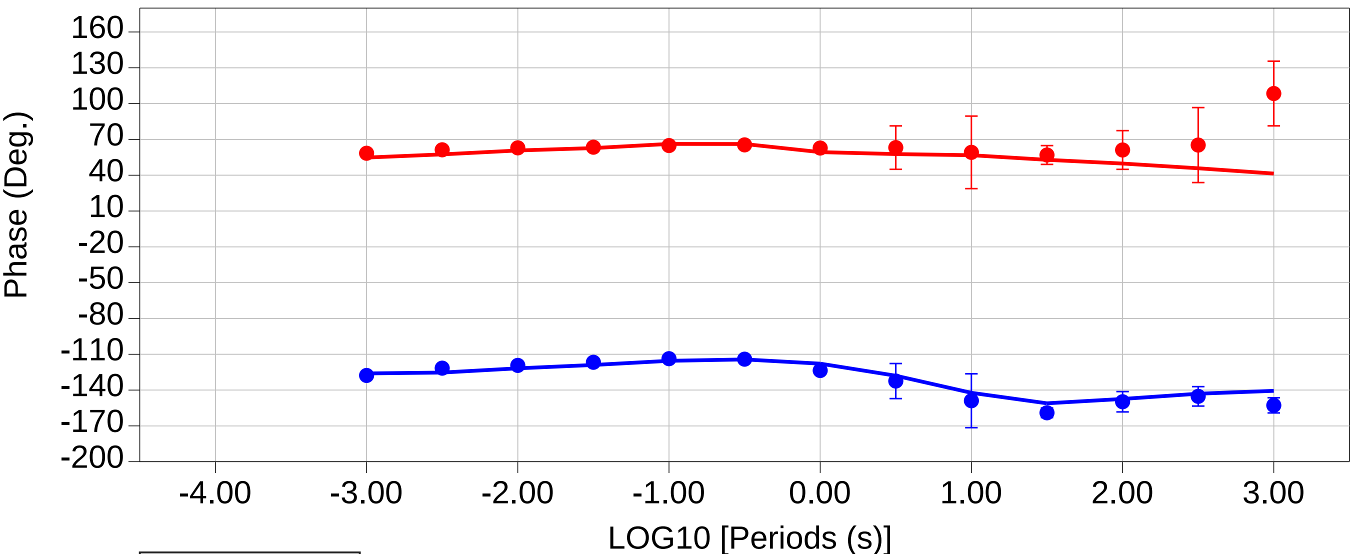

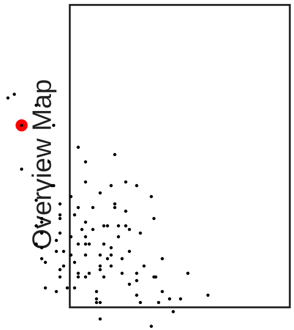

Total RMS = 13583.37

Zxy RMS = 12967.00
Zyx RMS = 14172.95

Site: X11

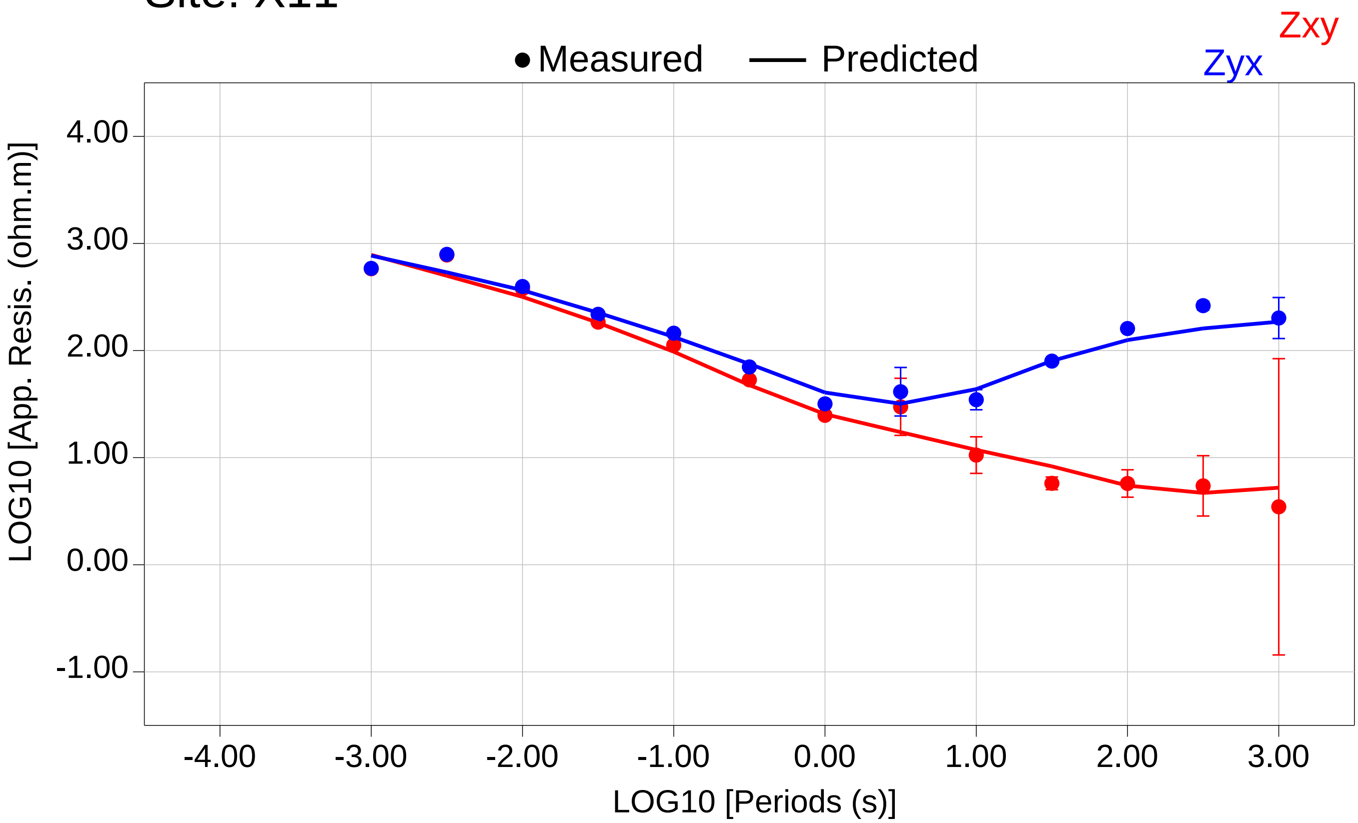

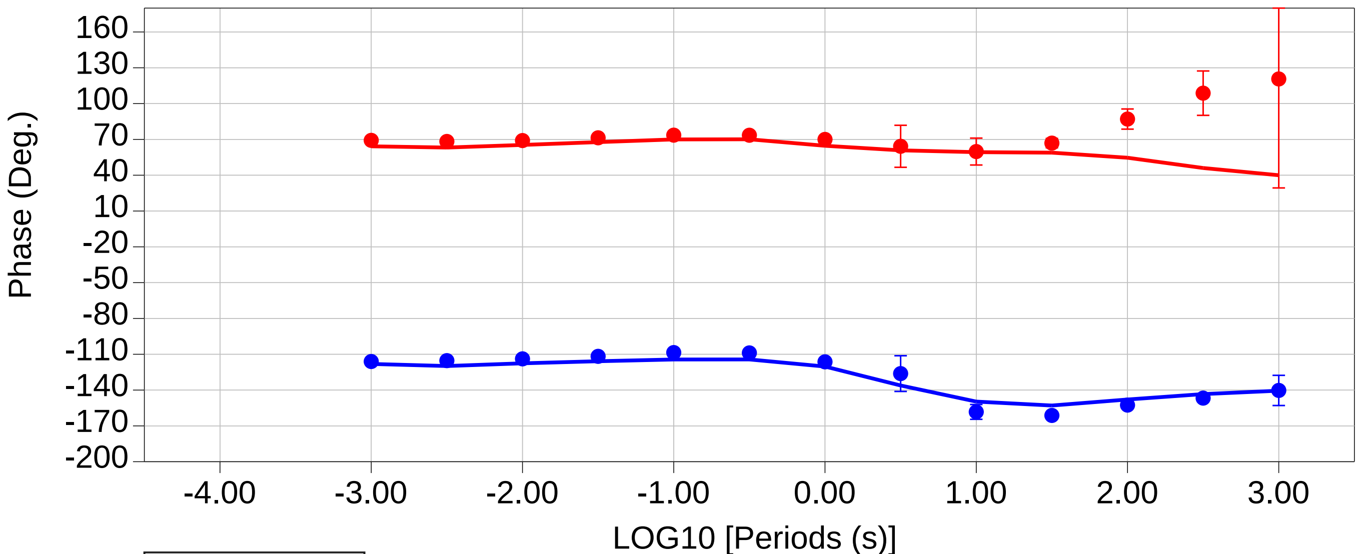

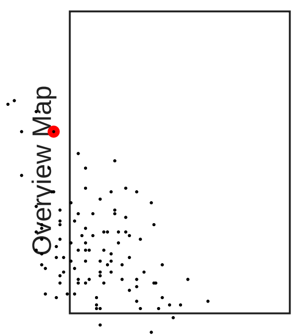

Total RMS = 15324.60

Zxy RMS = 13576.03

Zyx RMS = 16893.14

Site: X12

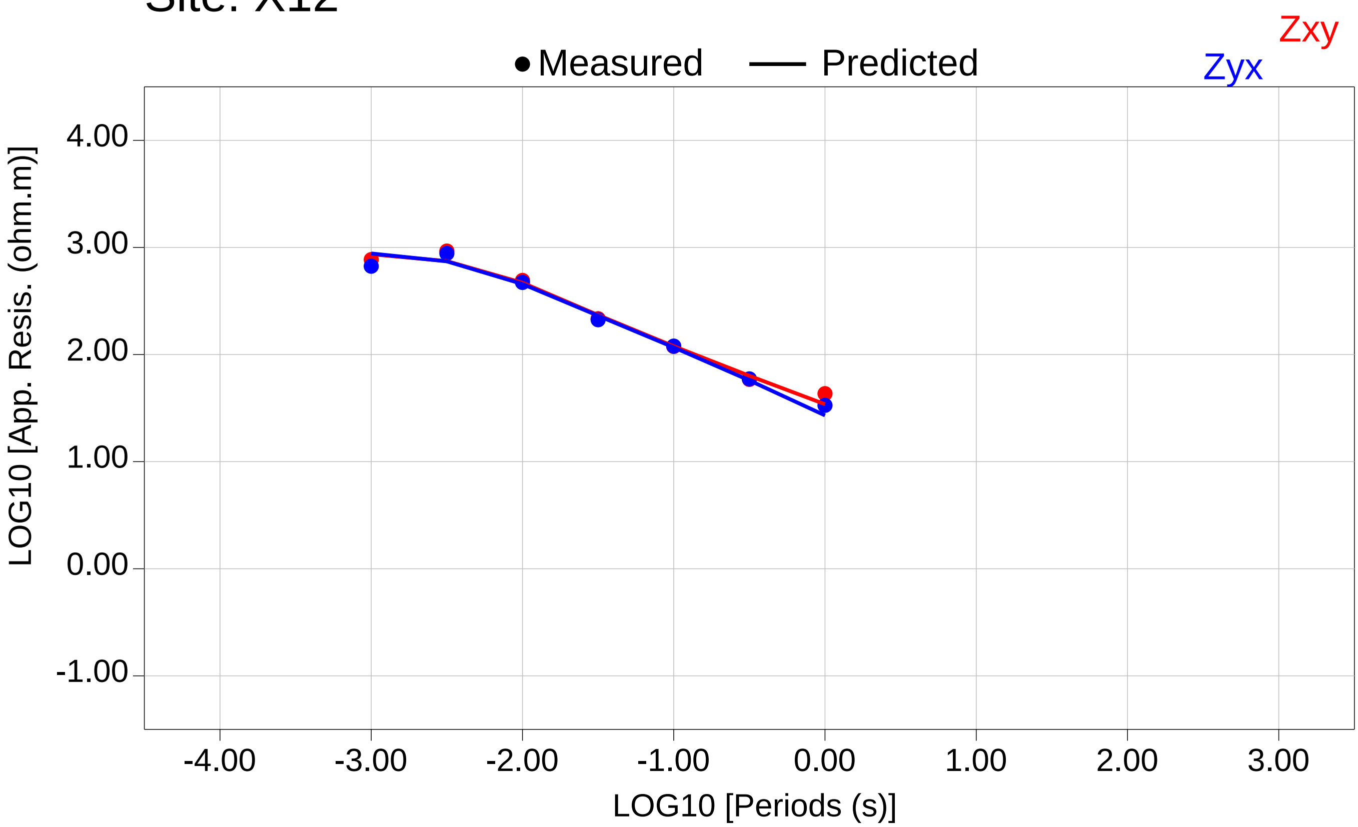

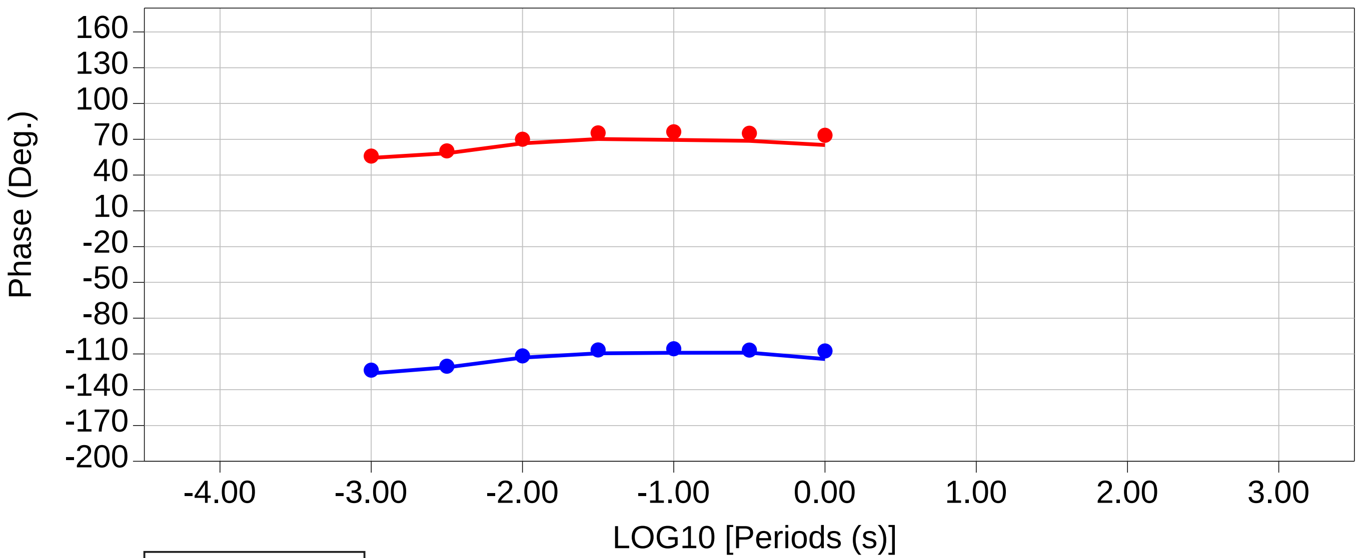

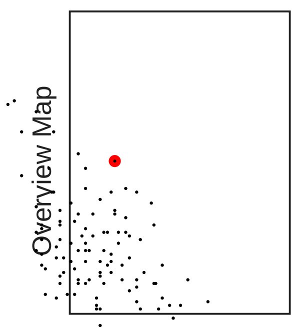

Total RMS = 19107.14

Zxy RMS = 19227.66
Zyx RMS = 18985.86

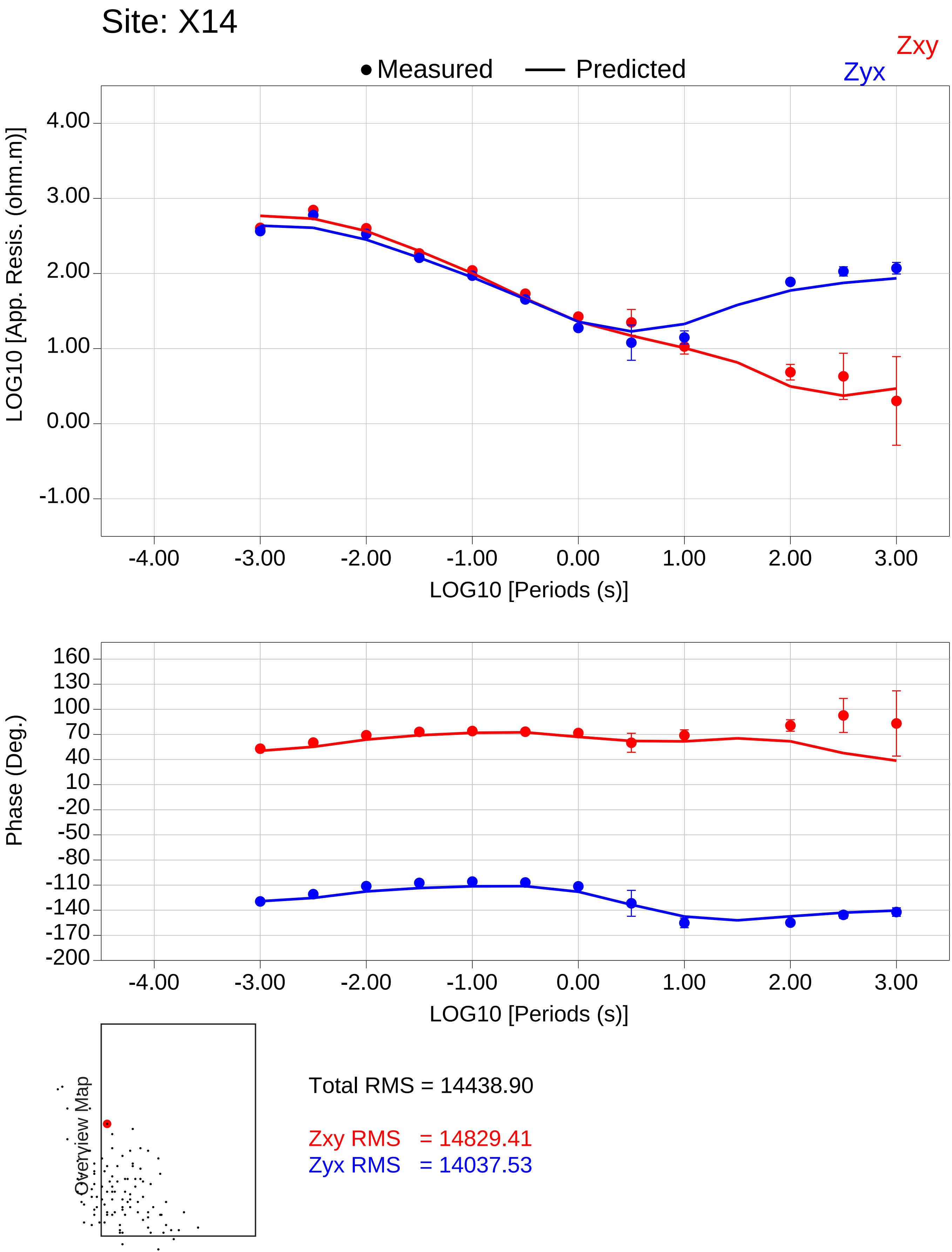

Total RMS = 14438.90

Zxy RMS = 14829.41
Zyx RMS = 14037.53

Site: X15

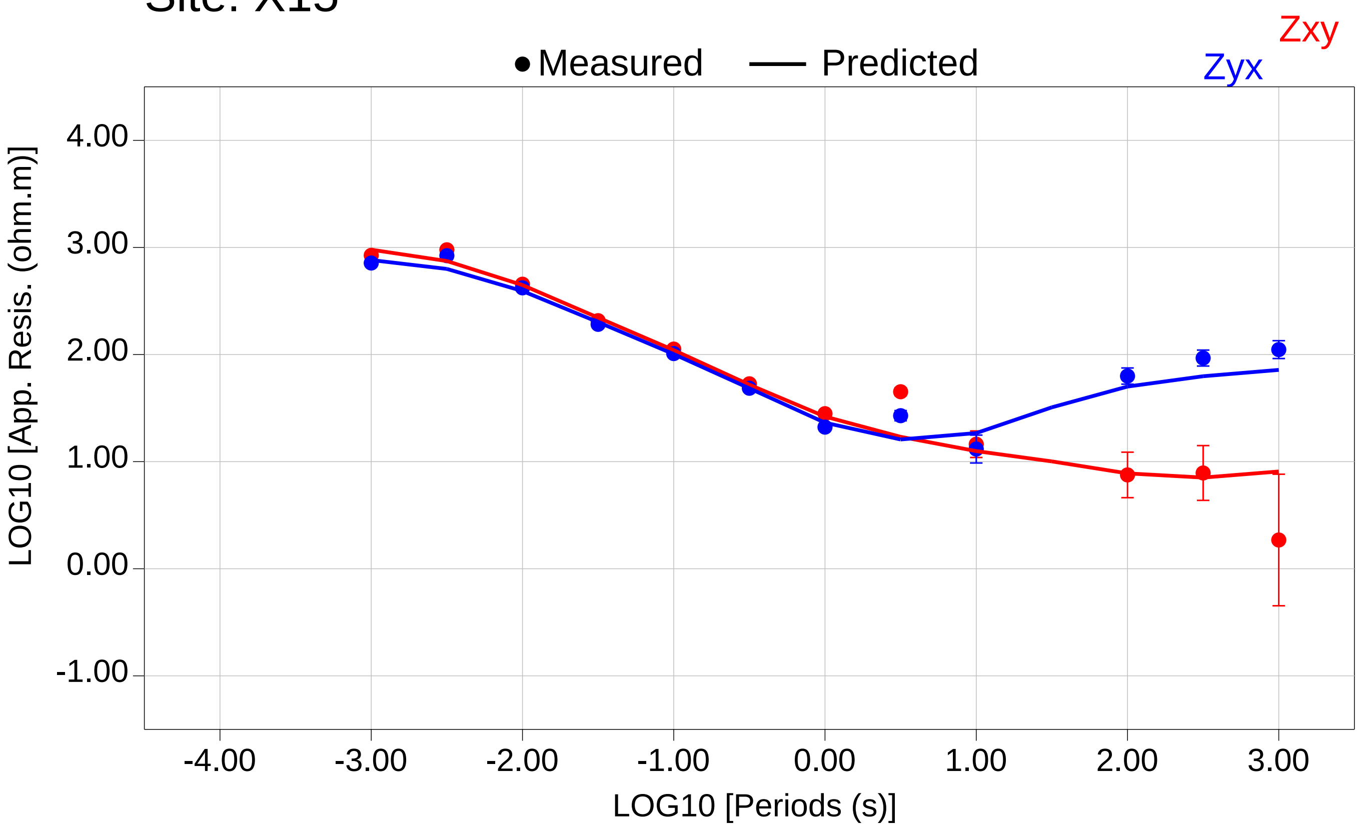

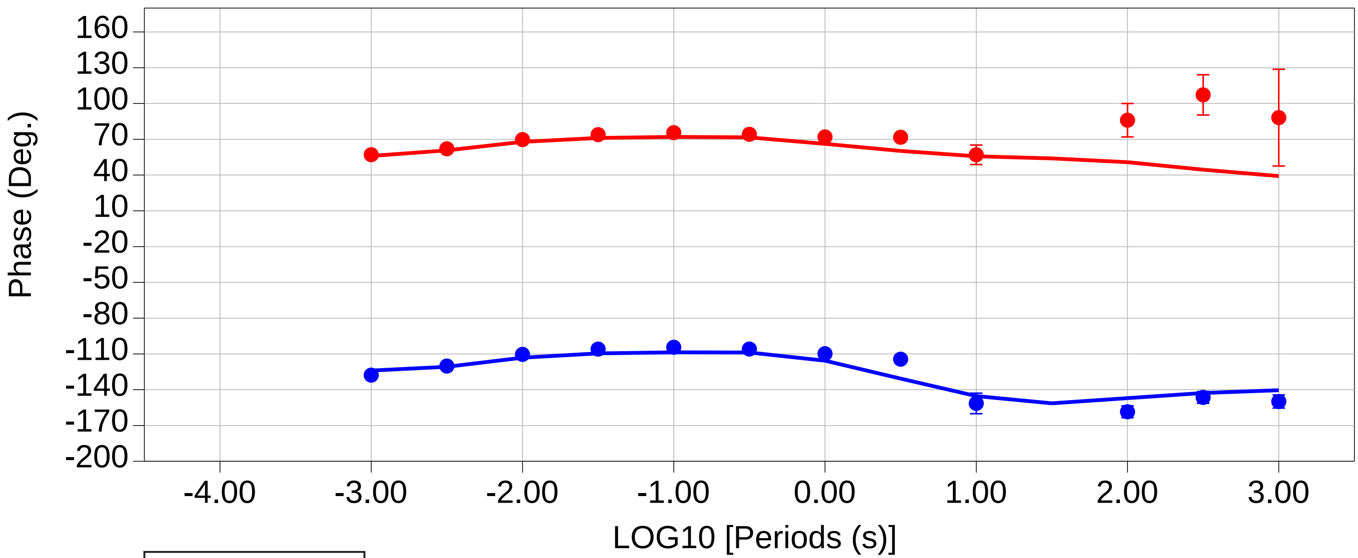

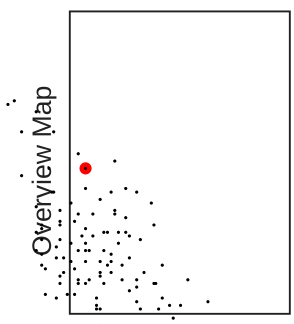

Total RMS = 15184.08

Zxy RMS = 15589.95
Zyx RMS = 14767.07

Site: X16

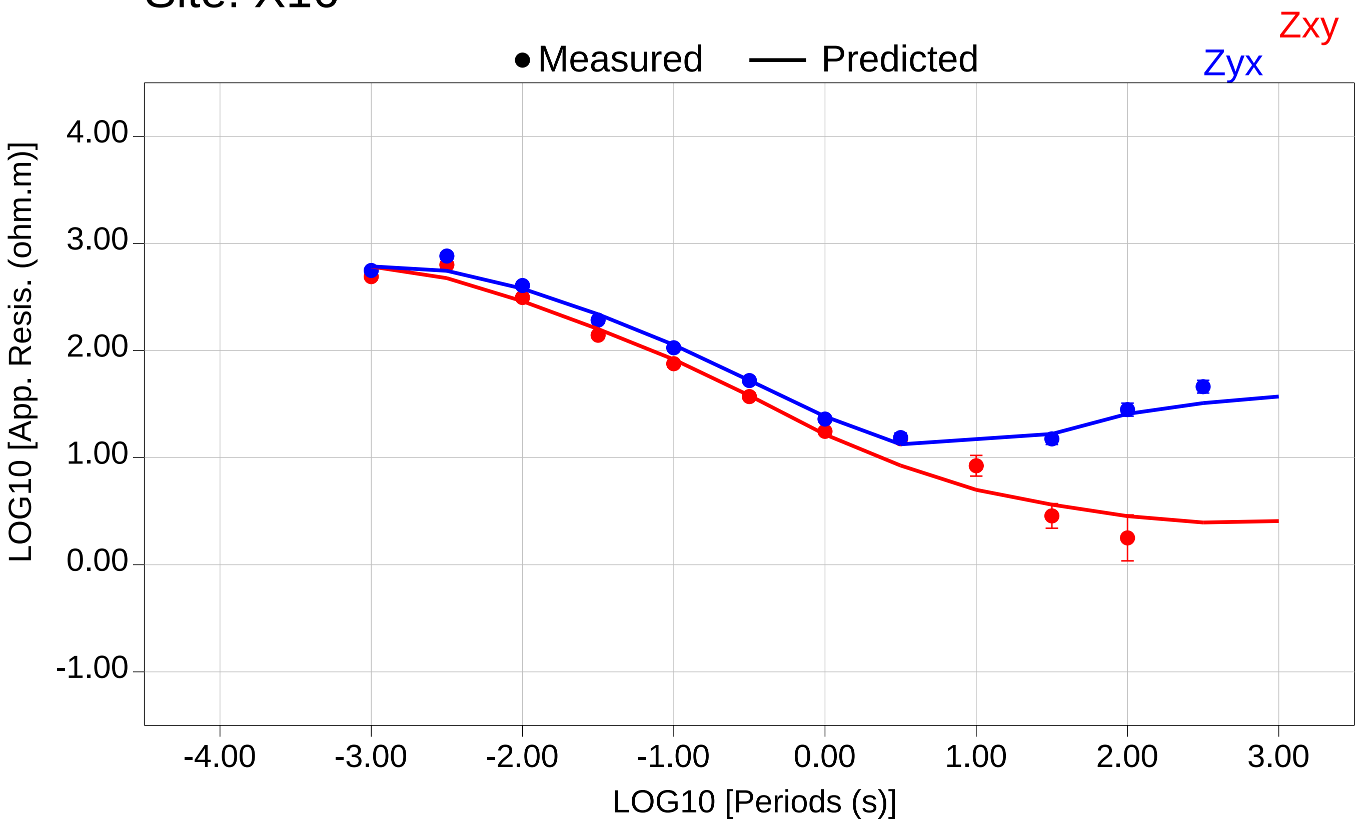

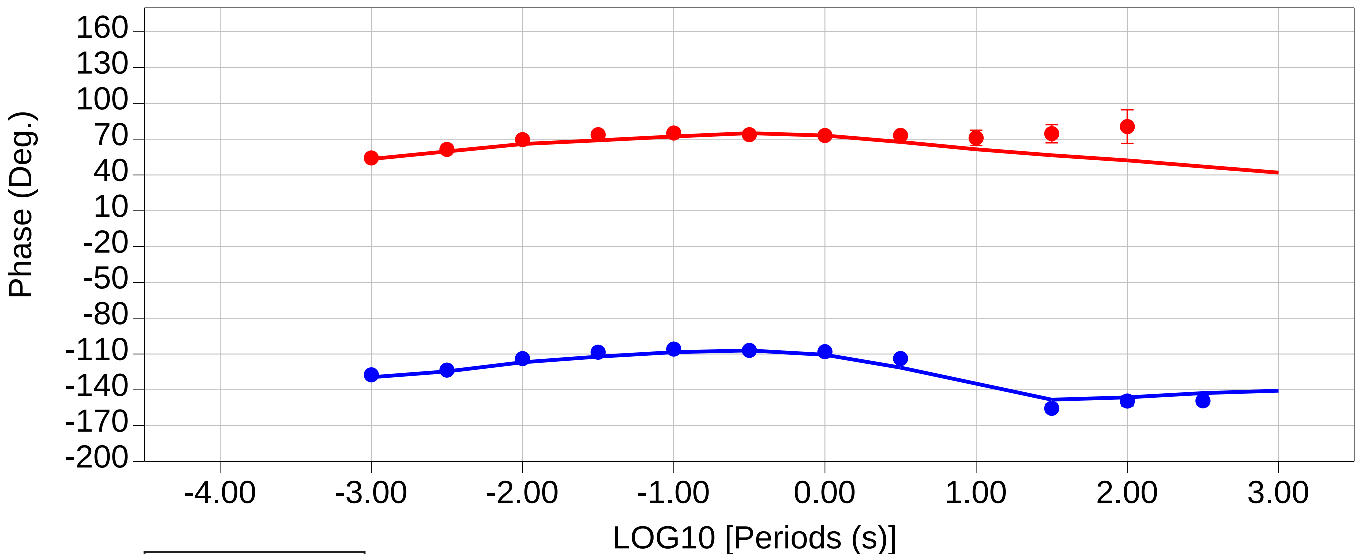

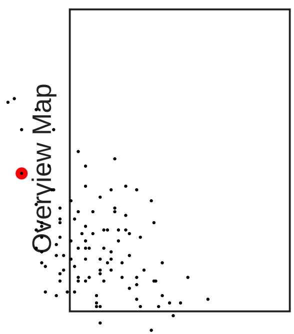

Total RMS = 16329.50

Zxy RMS = 15238.98

Zyx RMS = 17351.61

Site: X19

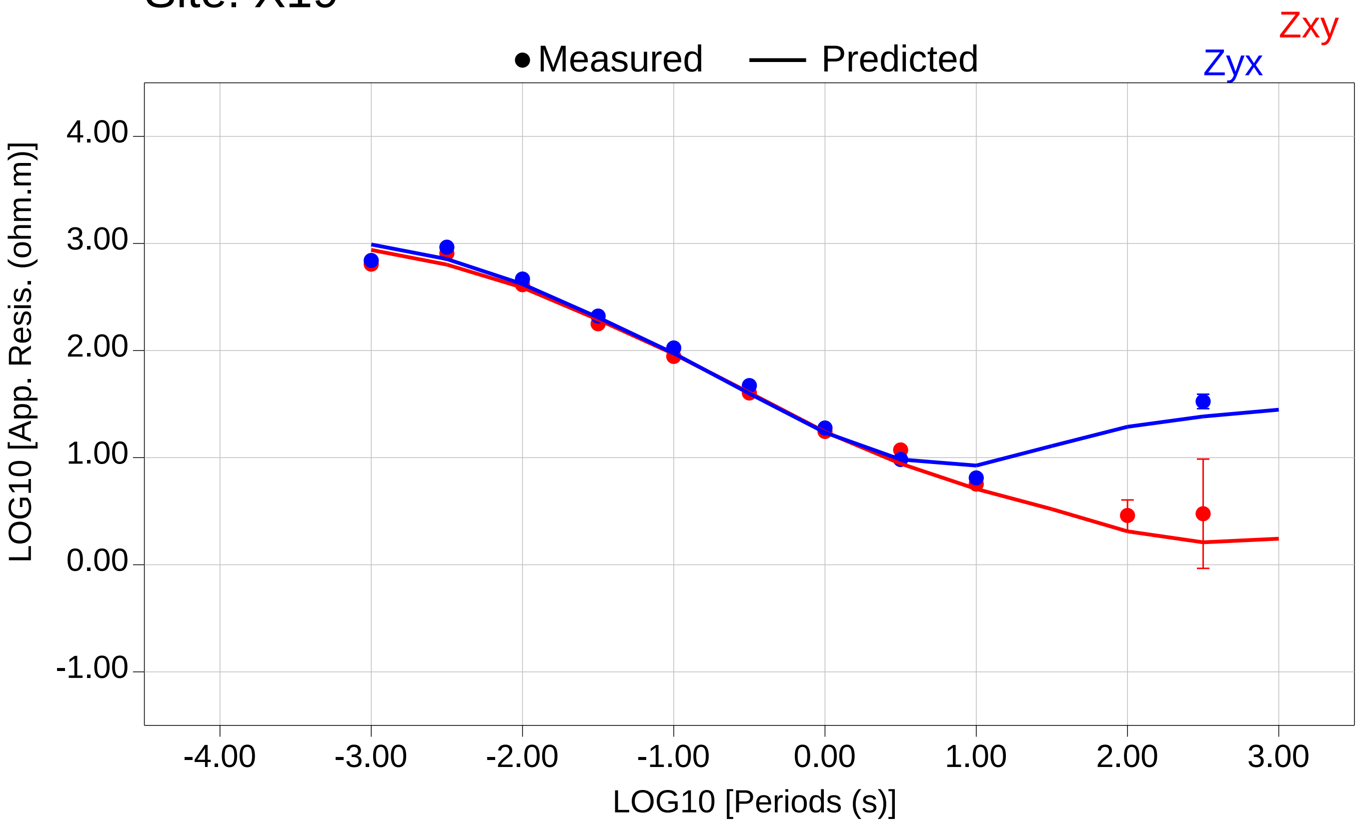

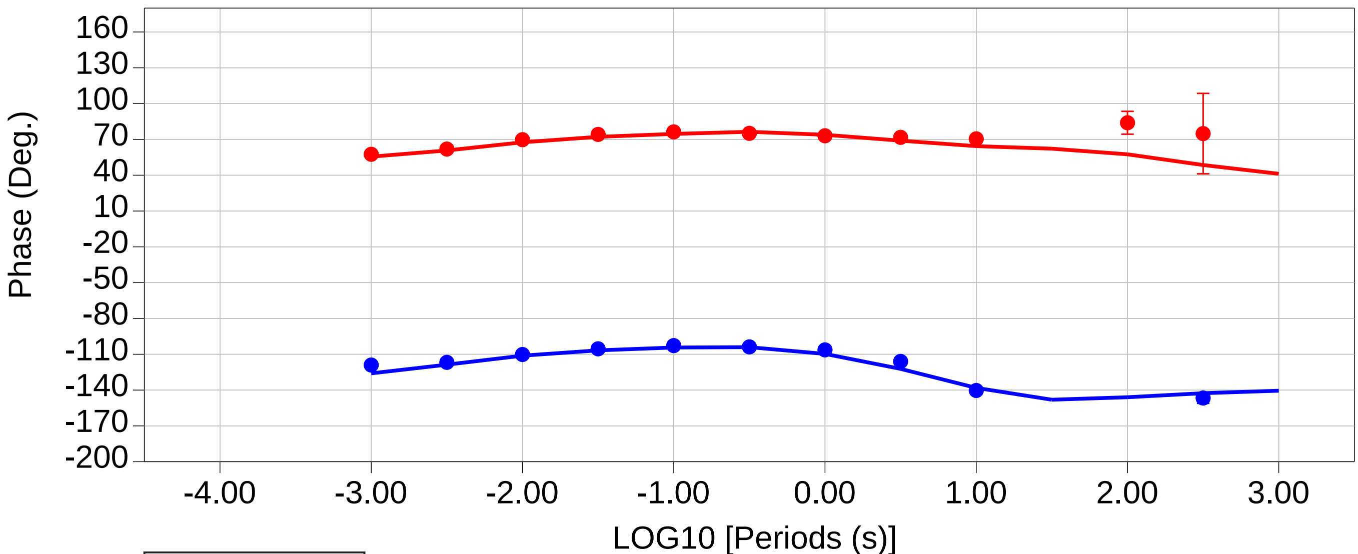

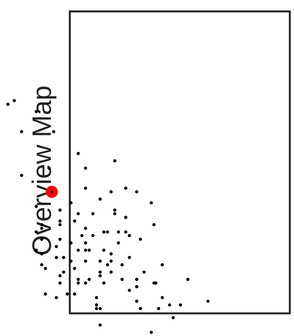

Total RMS = 18192.31

Zxy RMS = 17442.28

Zyx RMS = 18983.14

Site: X20

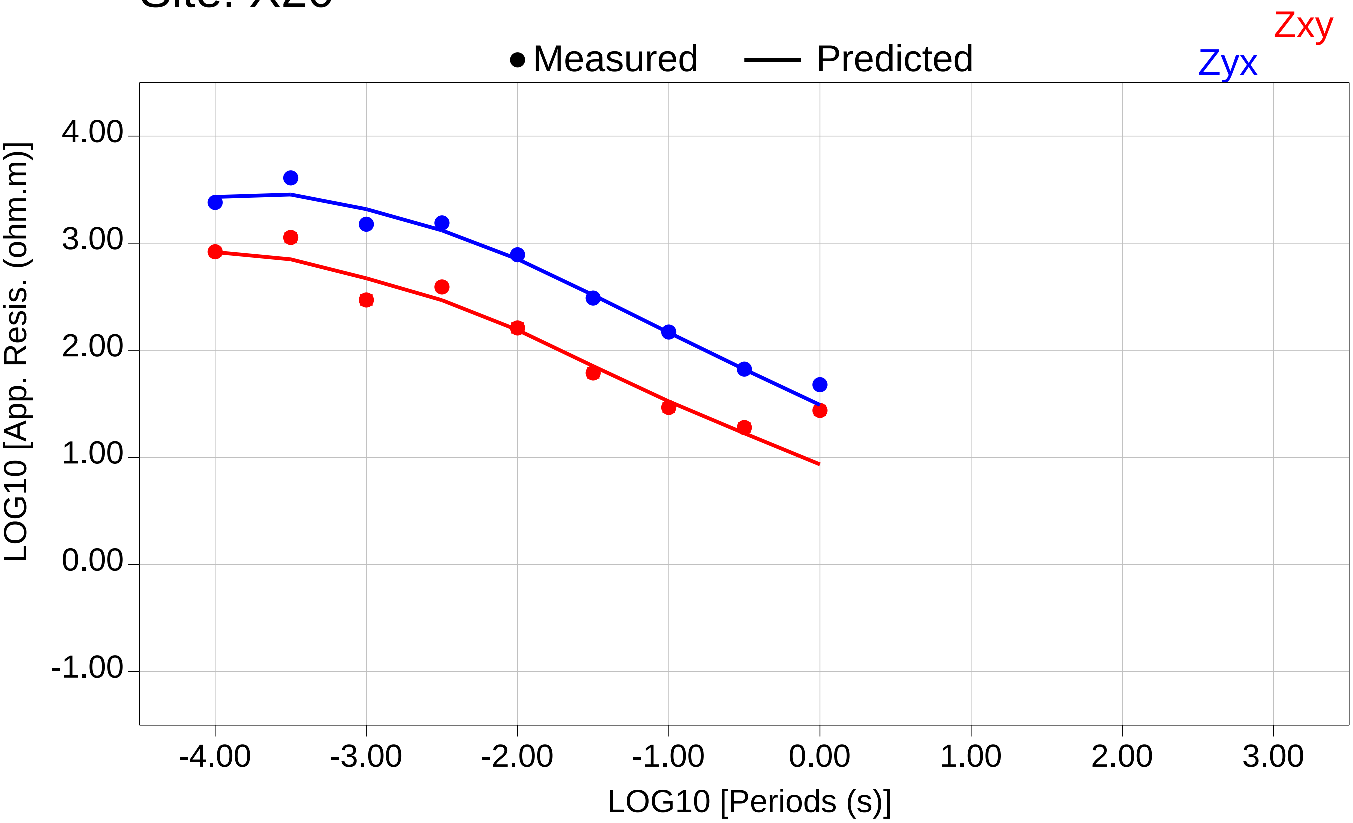

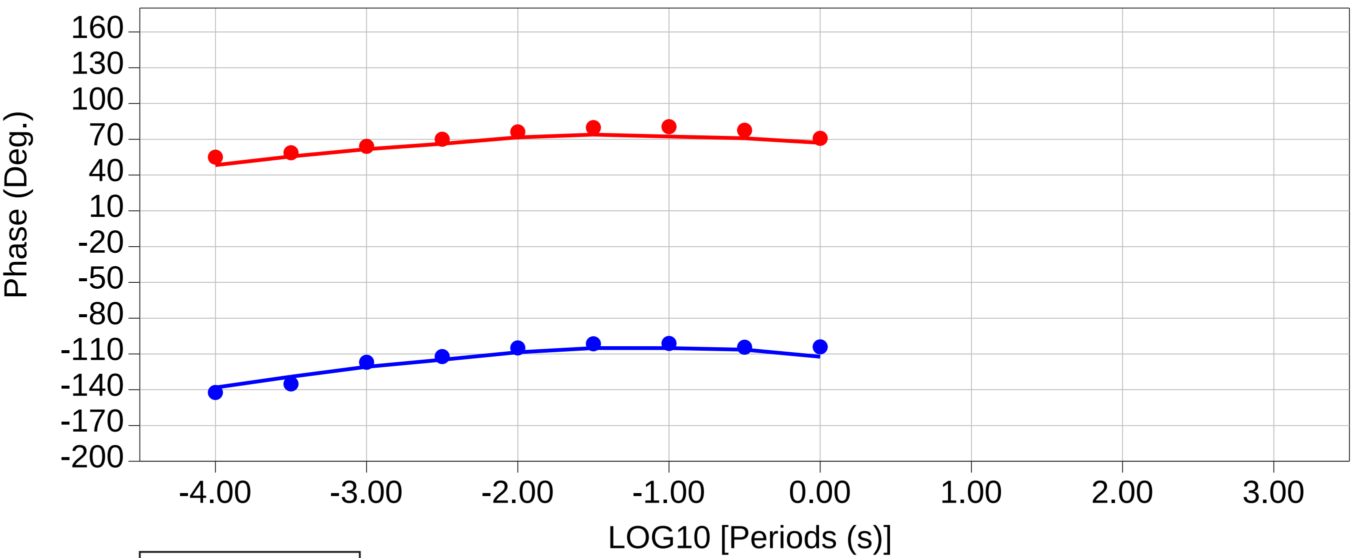

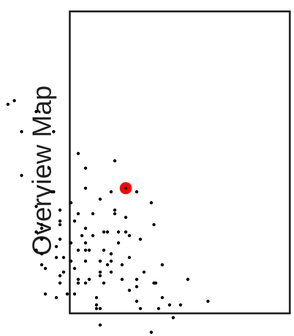

Total RMS = 21161.00

Zxy RMS = 13001.47
Zyx RMS = 26954.36

Site: X21

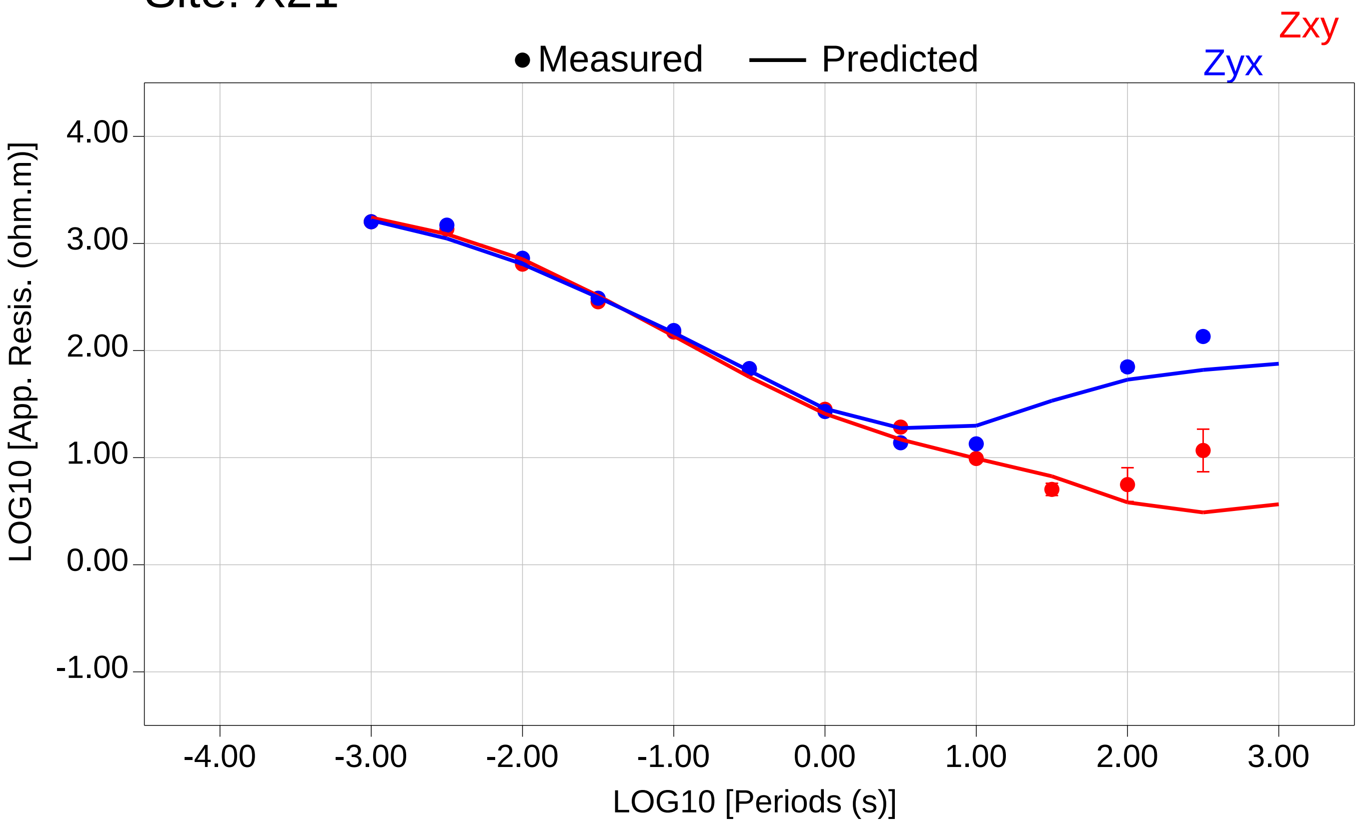

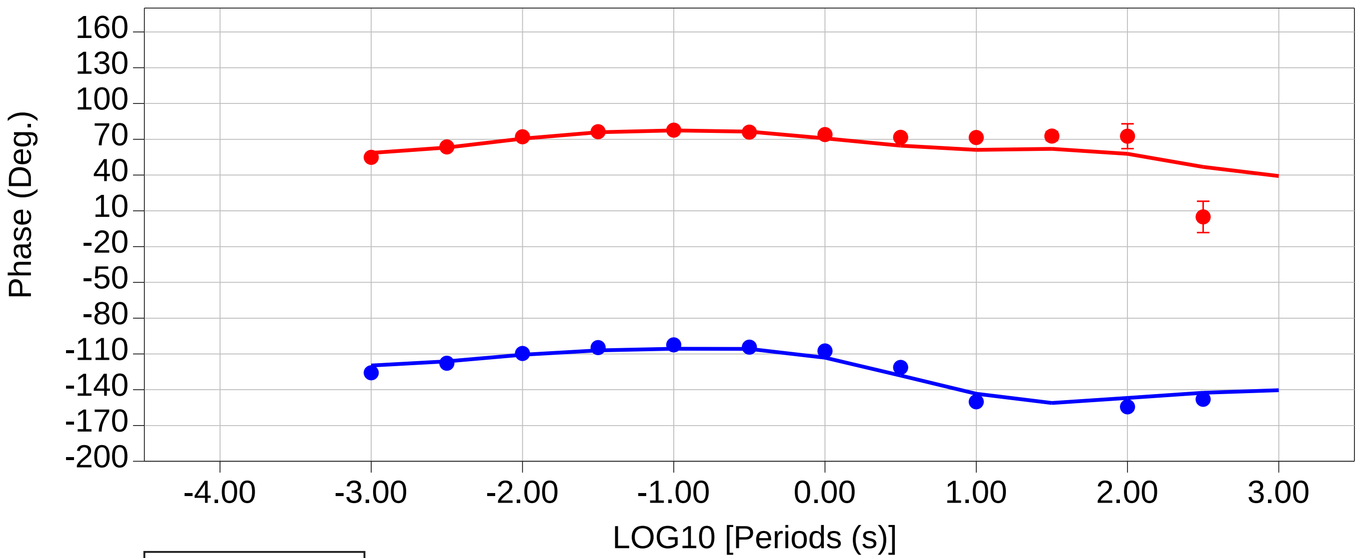

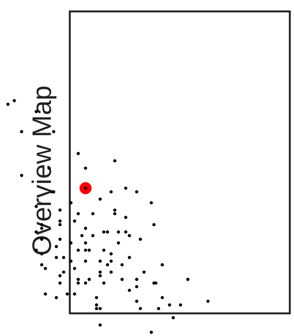

Total RMS = 18083.14

Zxy RMS = 17642.59
Zyx RMS = 18551.81

Site: X22

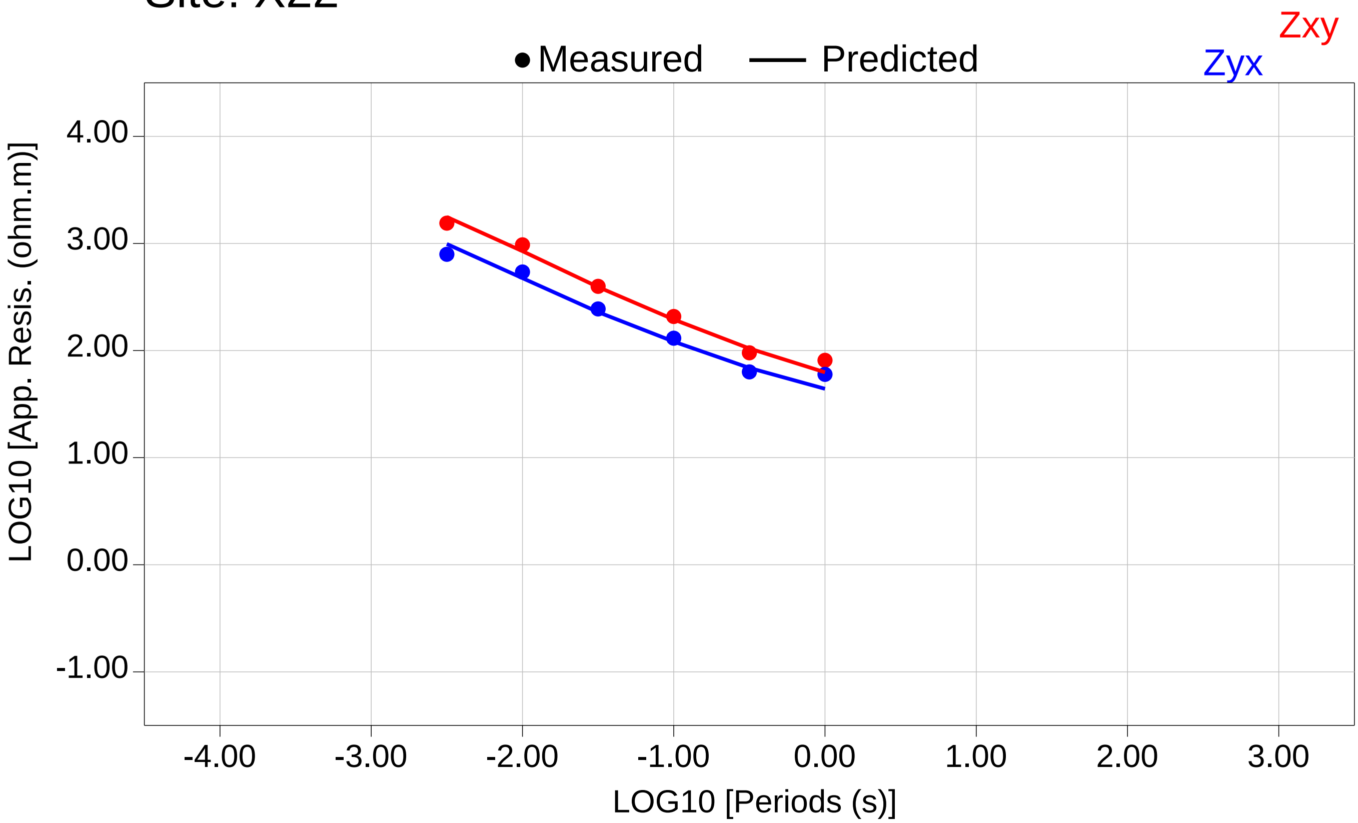

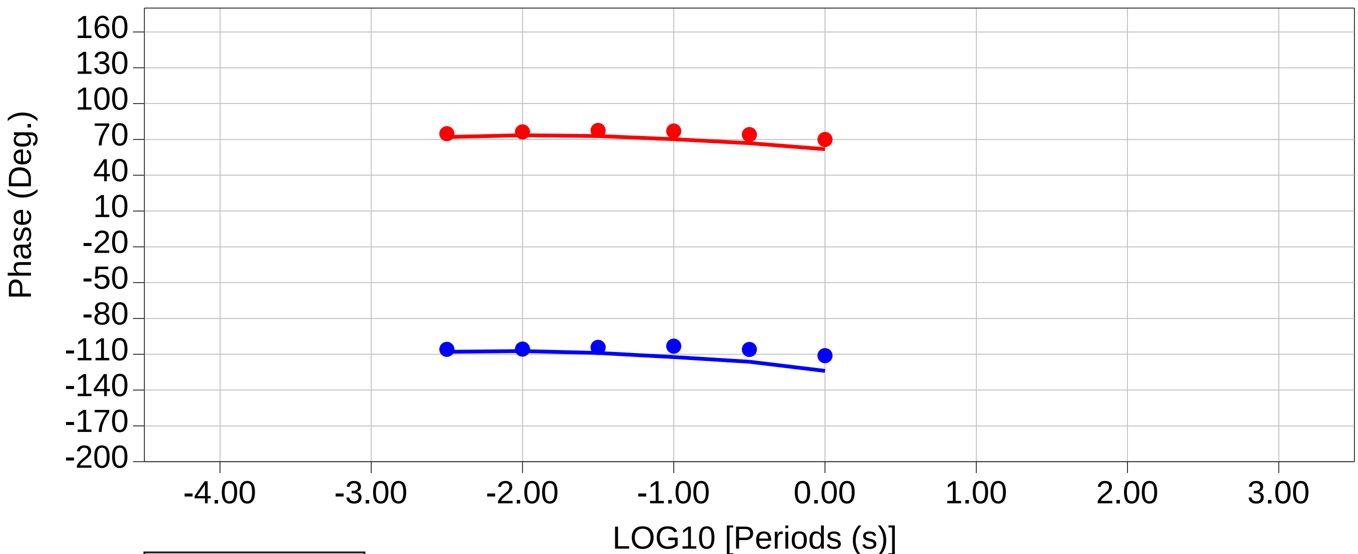

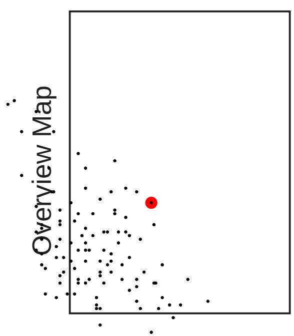

Total RMS = 18245.60

Zxy RMS = 20432.66
Zyx RMS = 15757.86

Site: X23

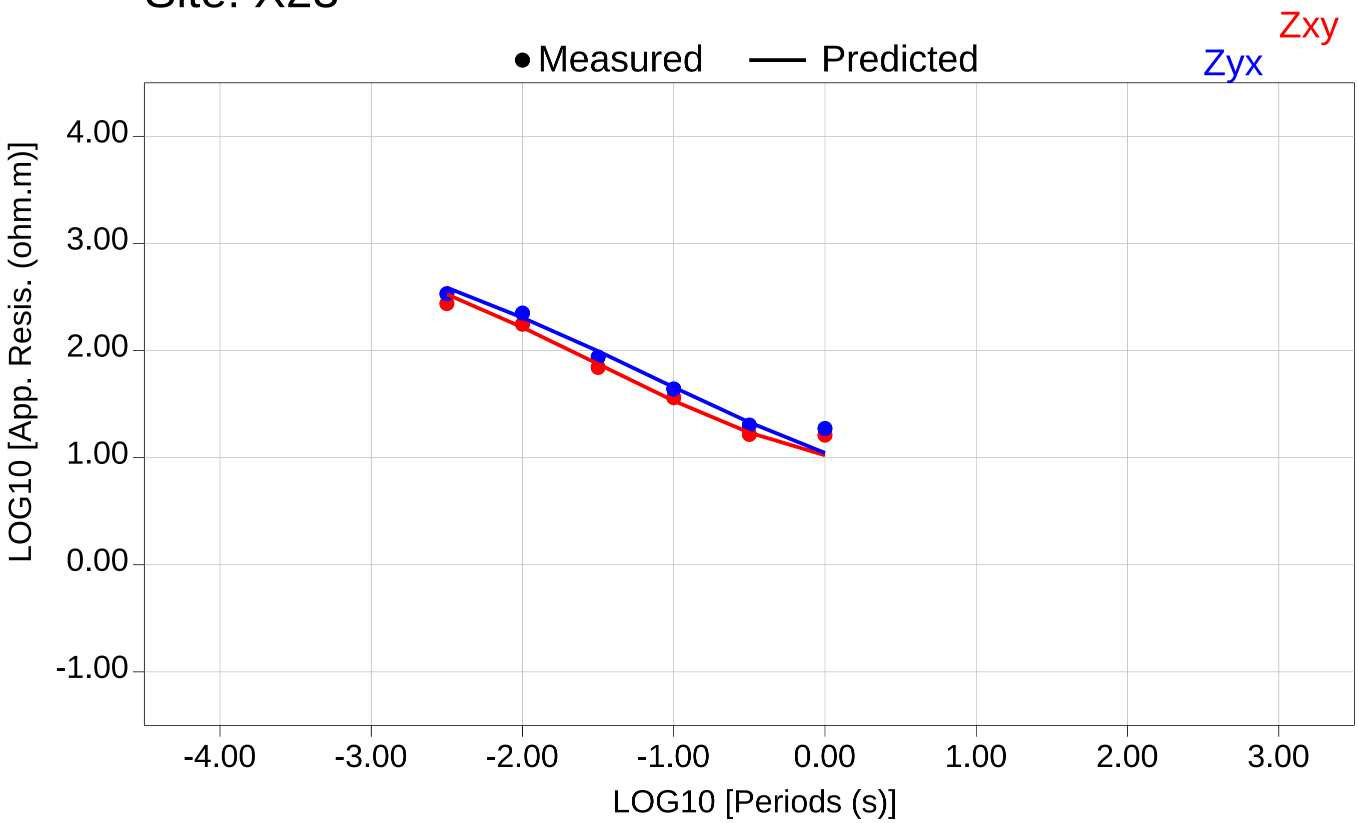

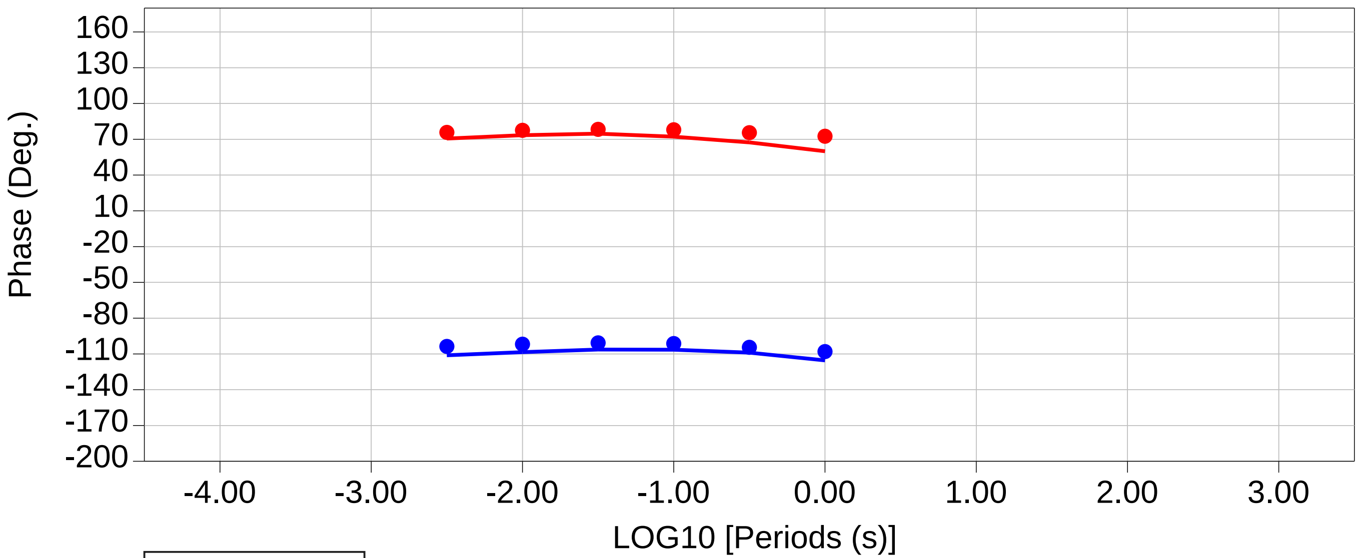

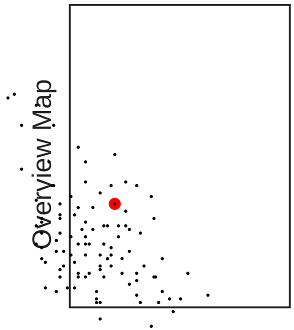

Total RMS = 18875.07

Zxy RMS = 17704.10
Zyx RMS = 19977.52

Site: X27

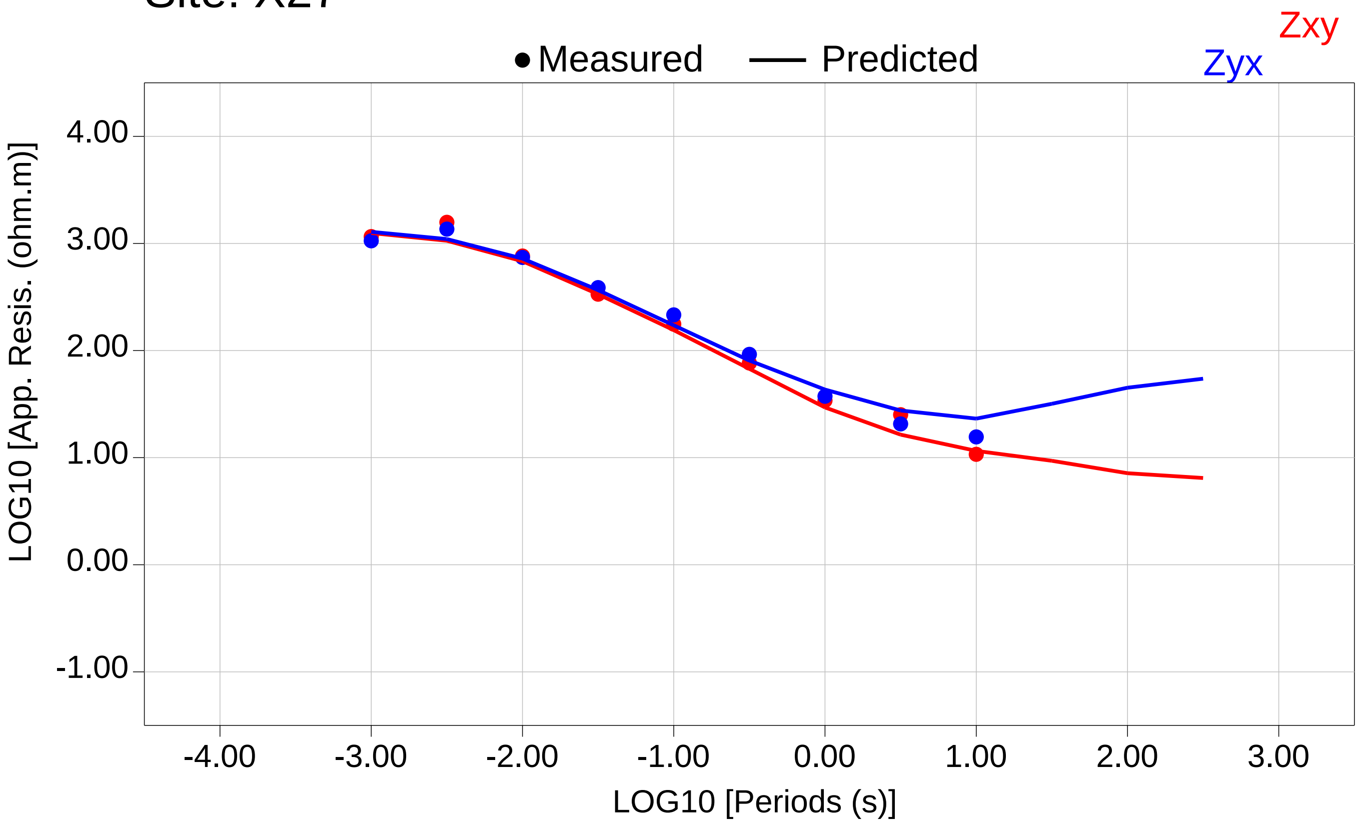

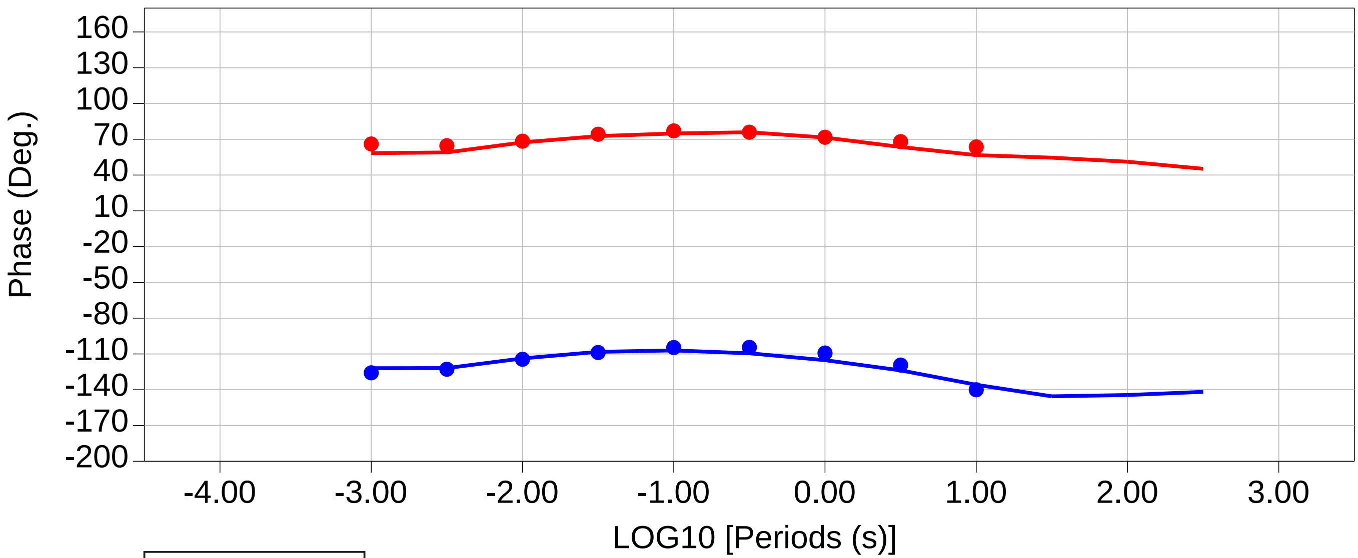

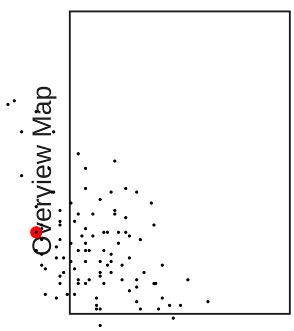

Total RMS = 18886.54

Zxy RMS = 18043.71
Zyx RMS = 19693.33

Site: X28

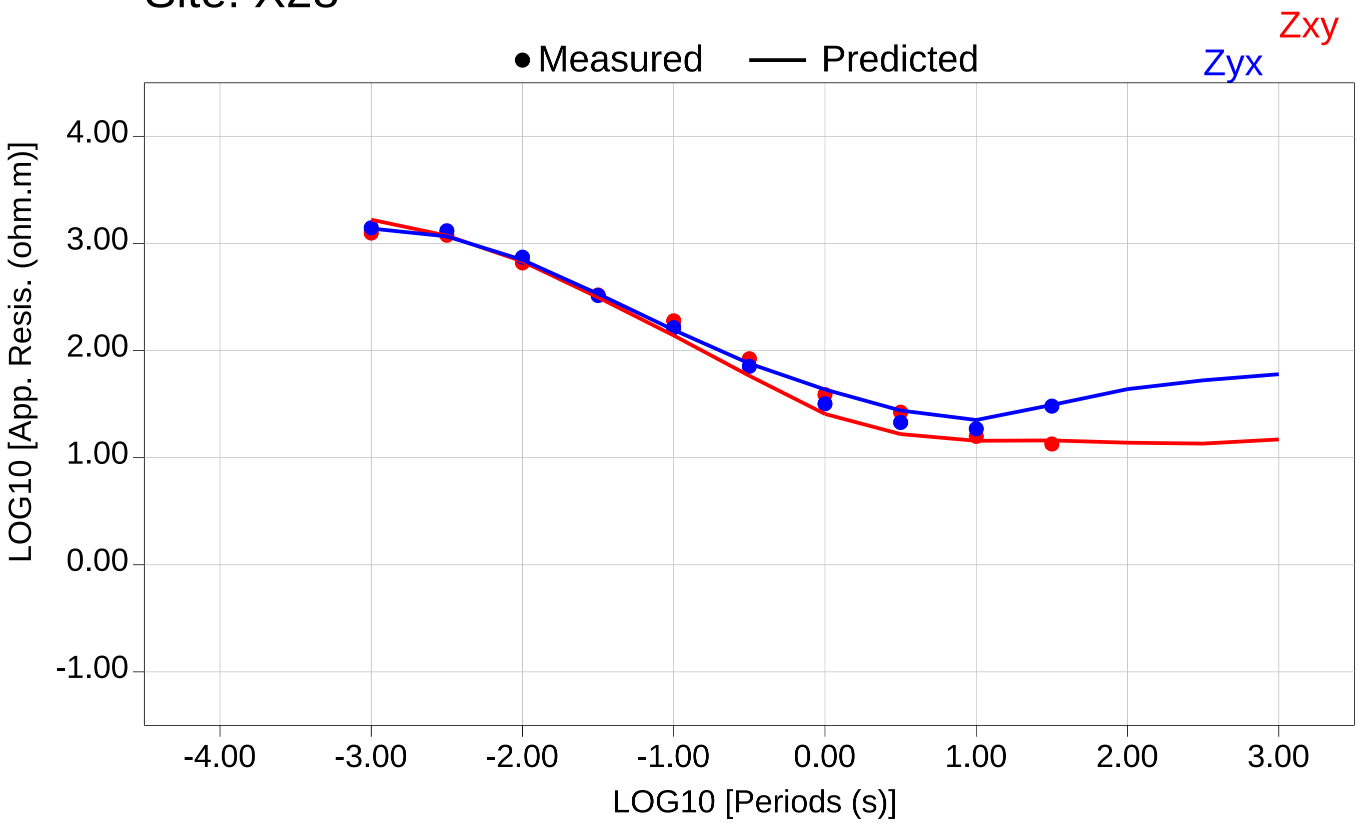

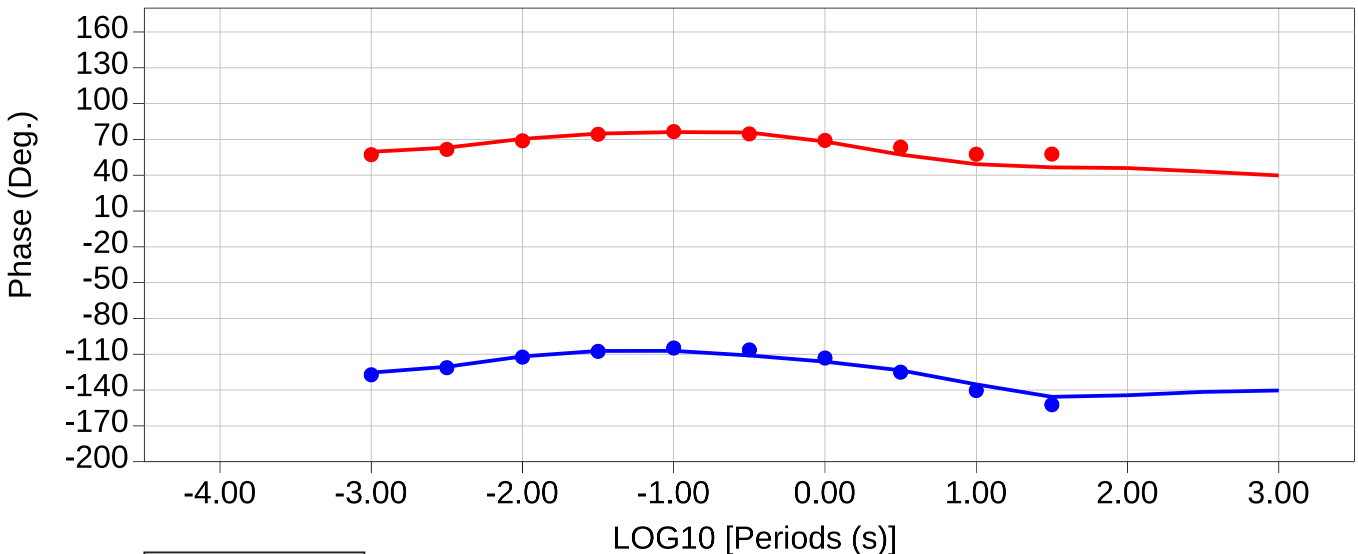

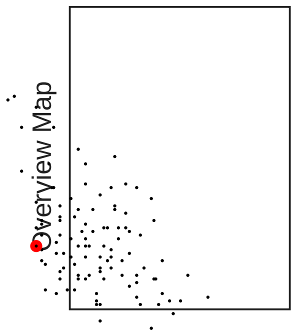

Total RMS = 19157.47

Zxy RMS = 18360.72
Zyx RMS = 19922.39

Site: X29

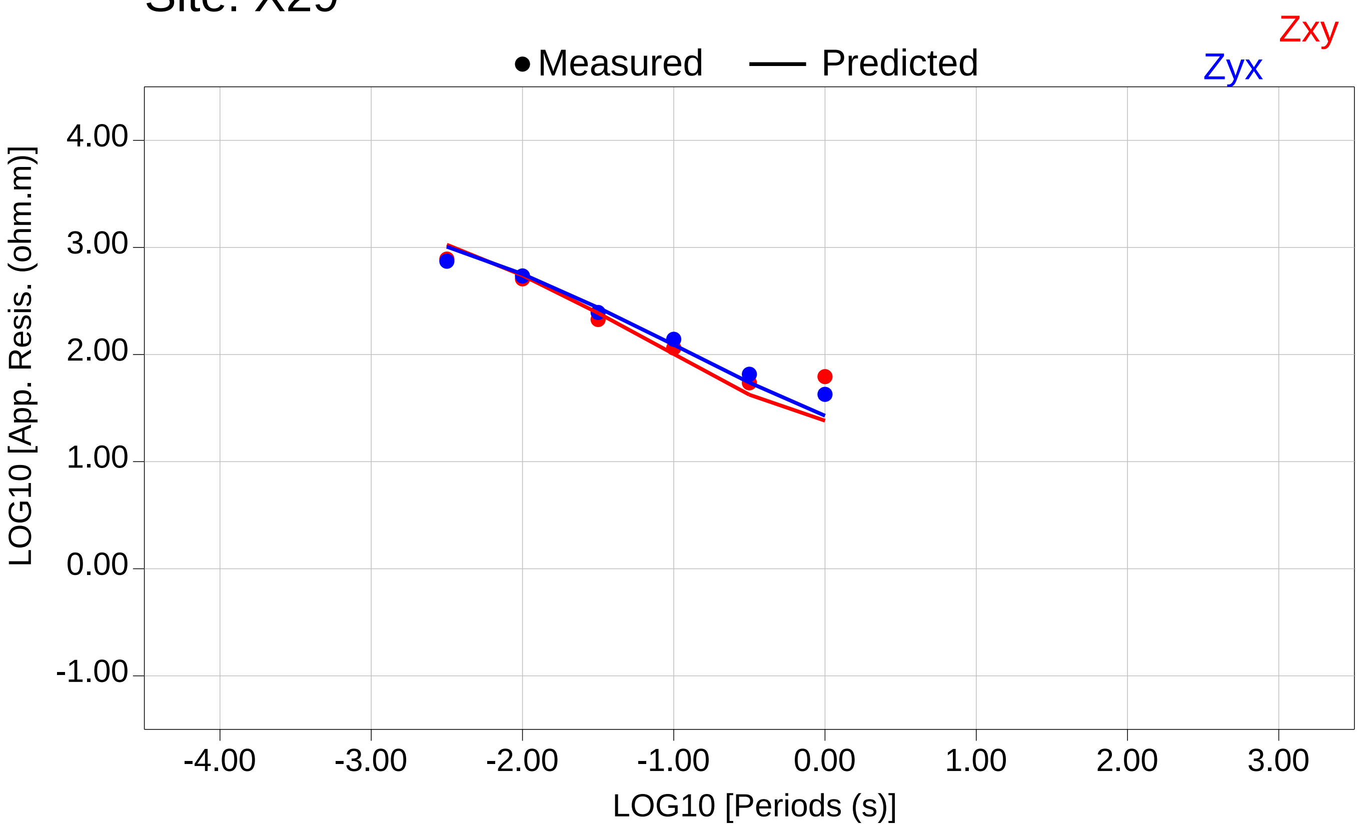

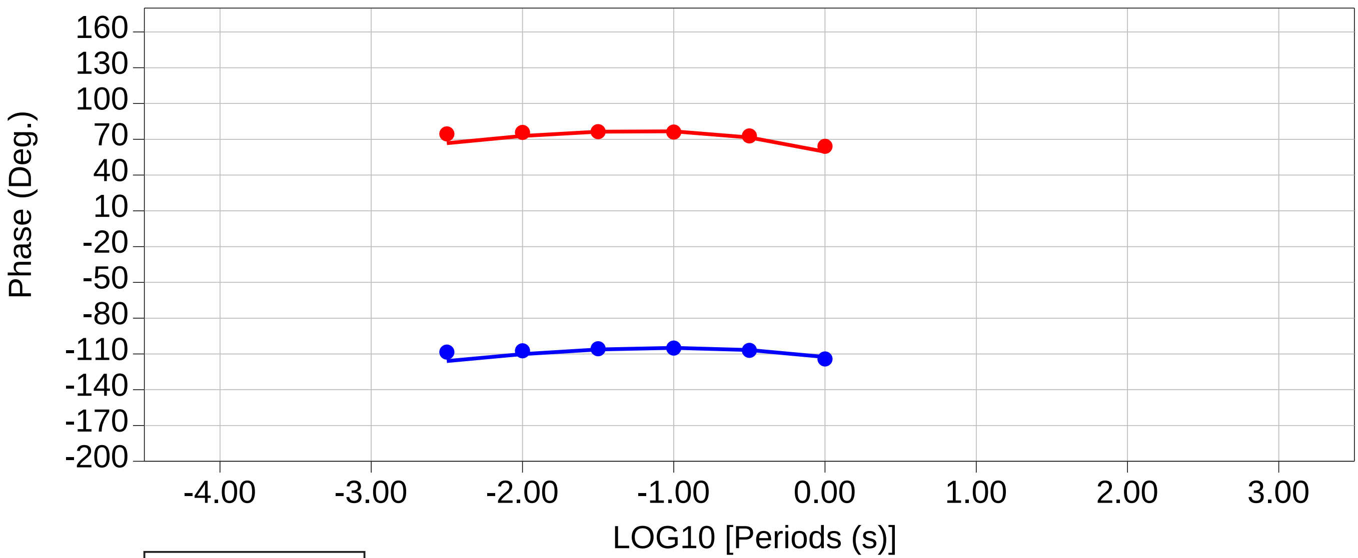

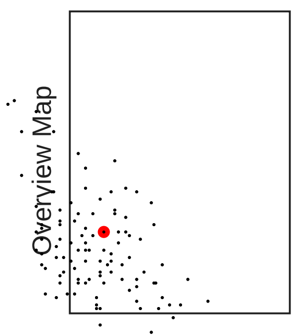

Total RMS = 18356.35

Zxy RMS = 17857.94
Zyx RMS = 18841.59

Site: X30

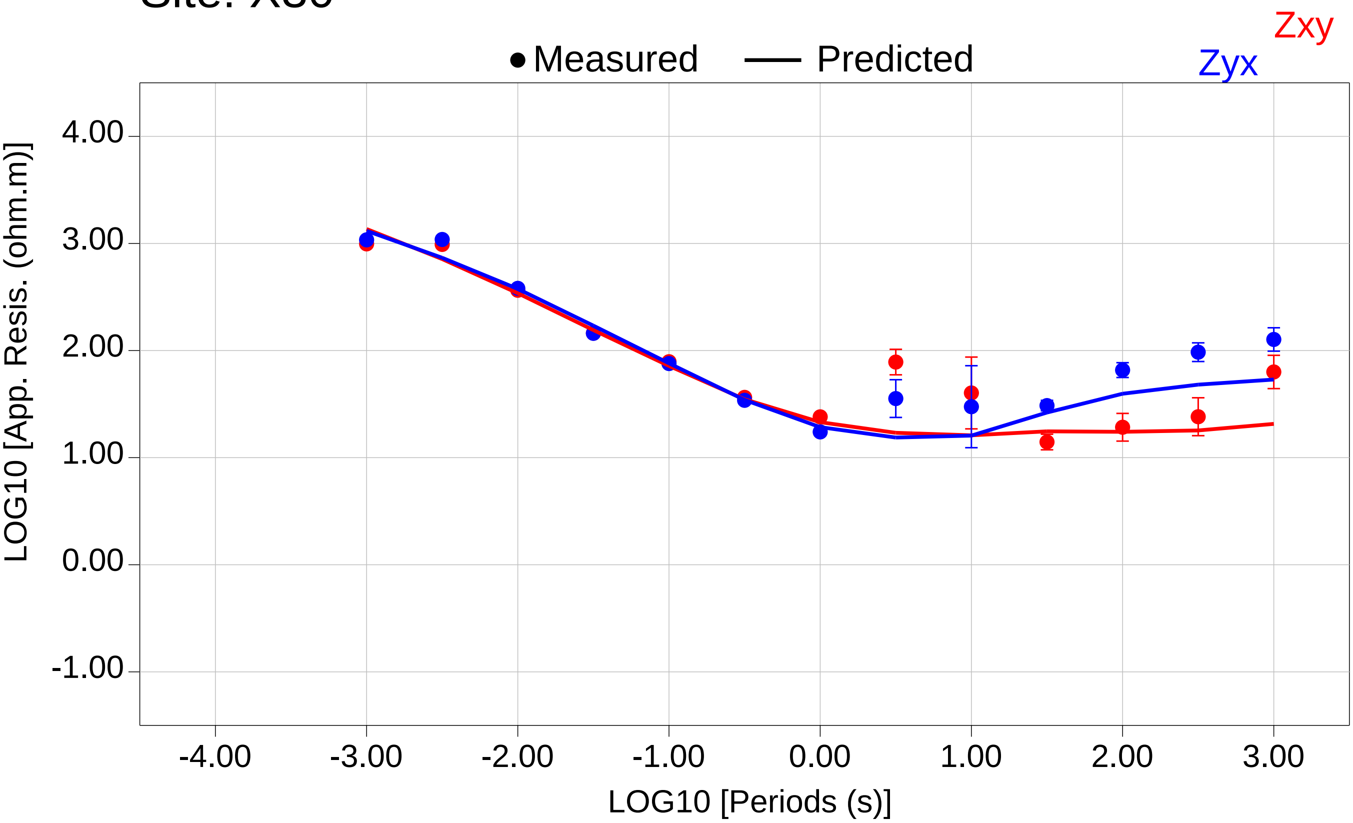

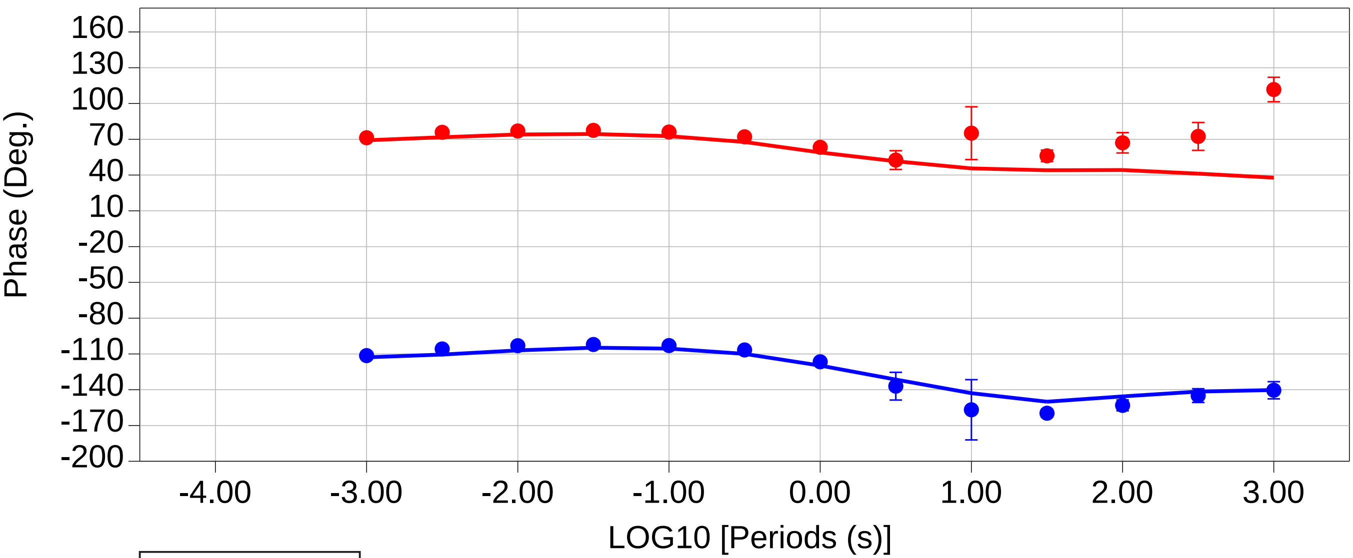

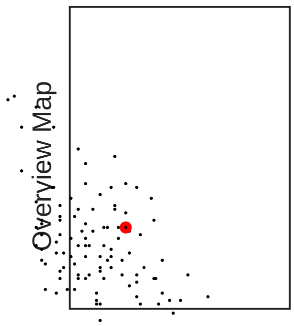

Total RMS = 15183.62

Zxy RMS = 15004.09
Zyx RMS = 15361.06

Site: X31

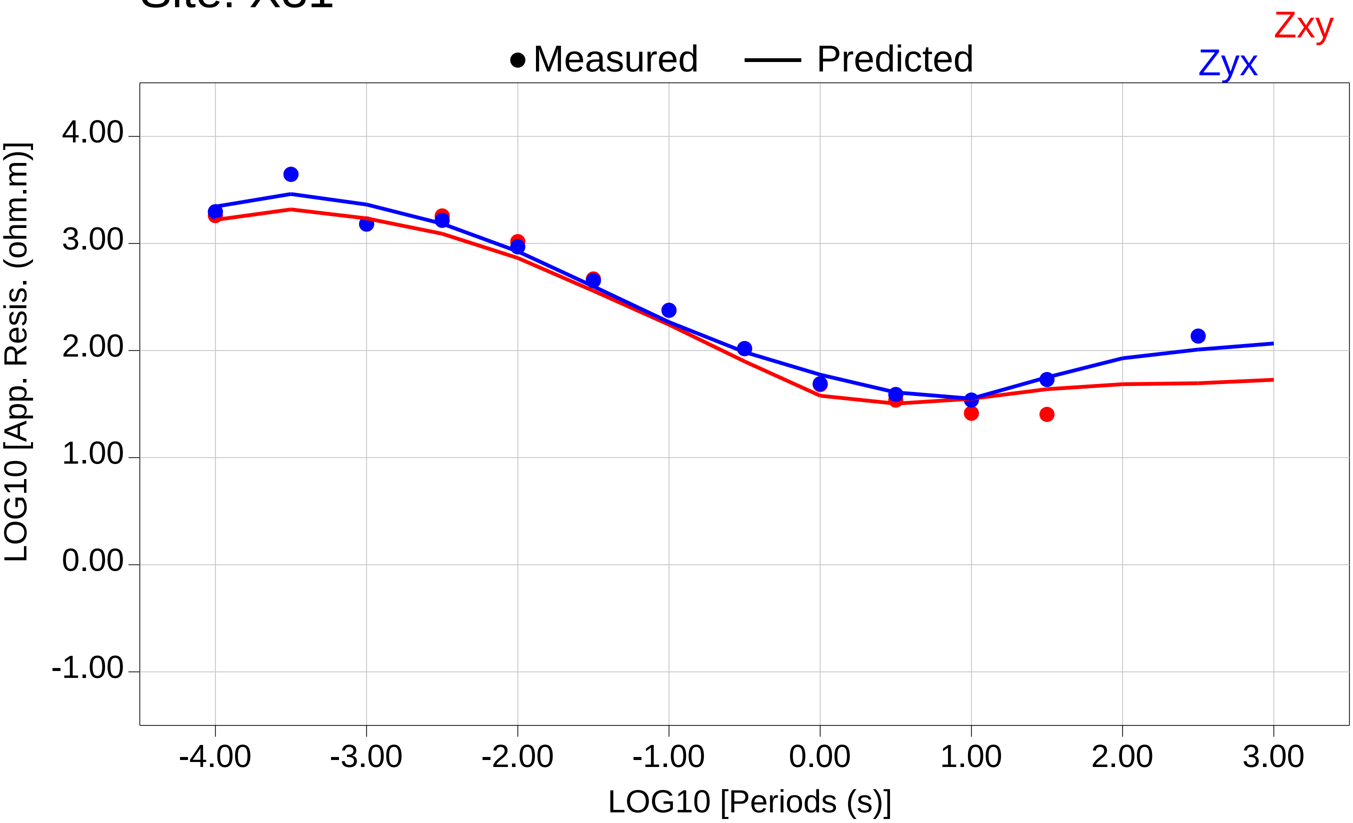

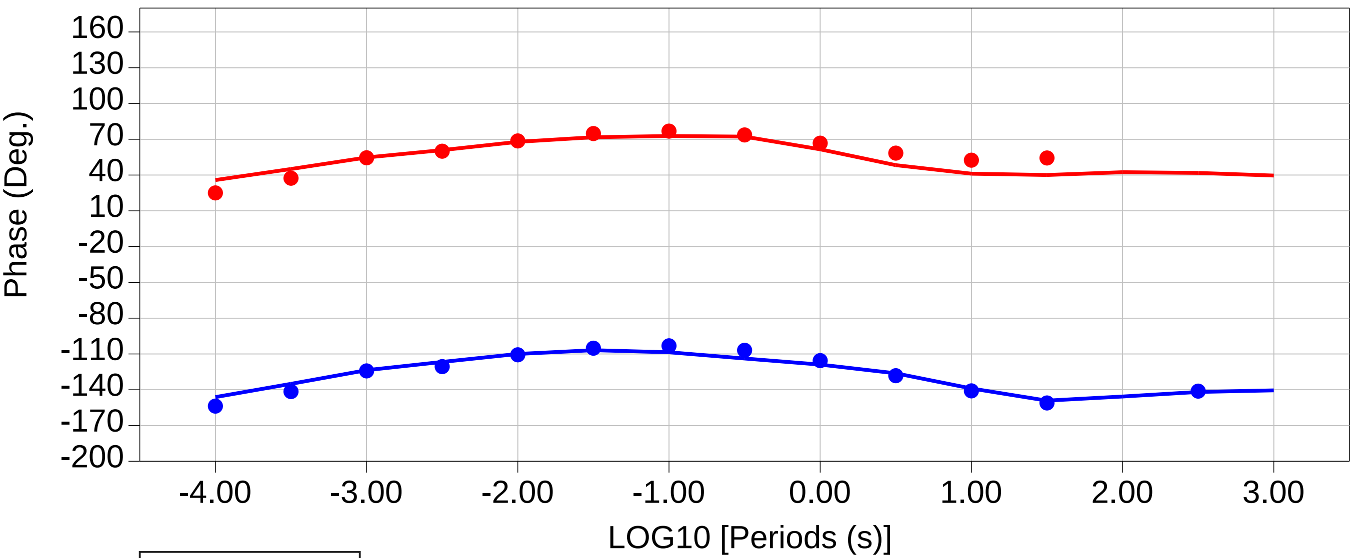

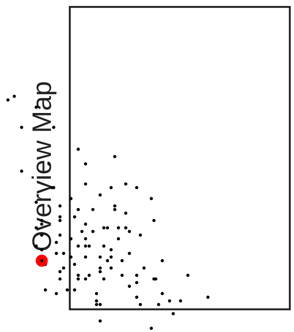

Total RMS = 17432.71

Zxy RMS = 16696.87
Zyx RMS = 18085.40

Site: X32

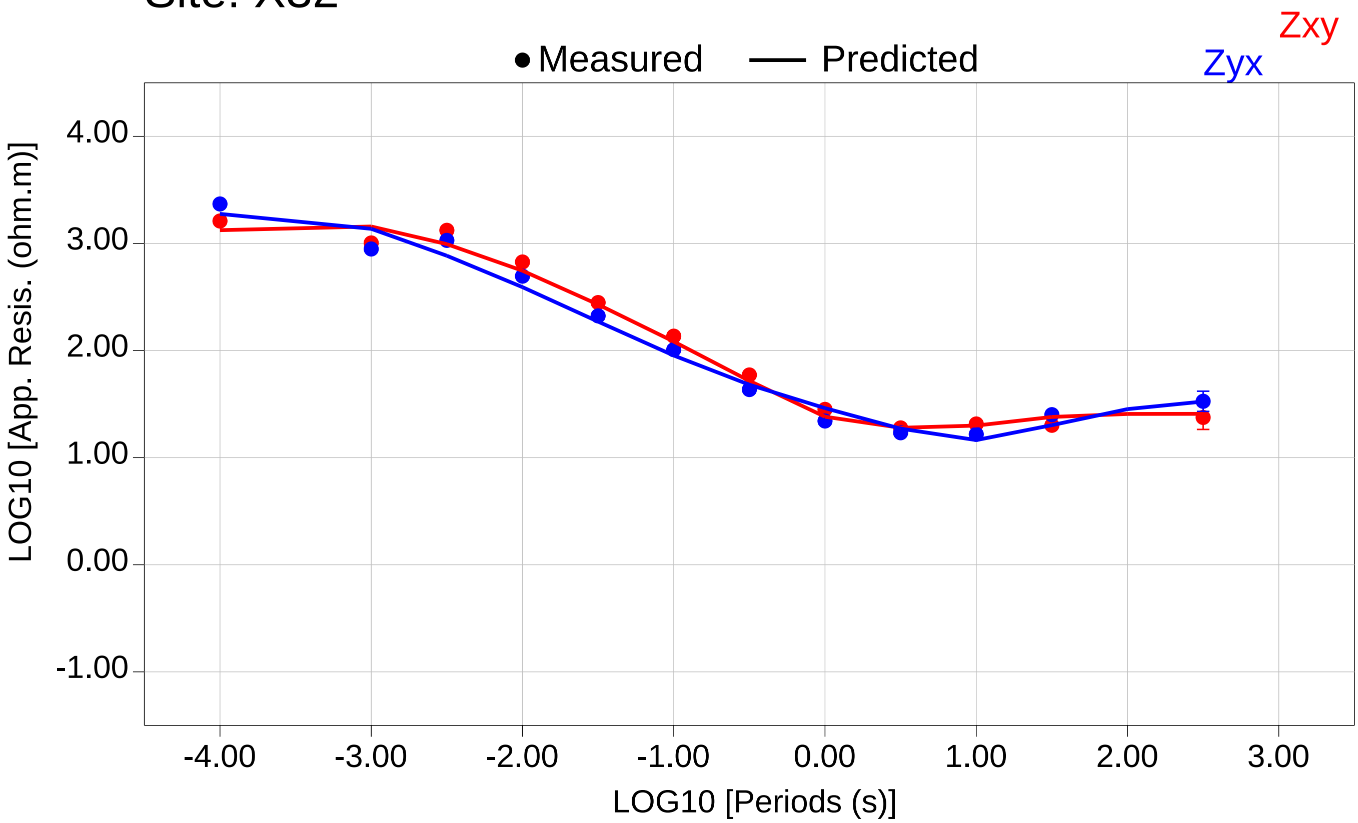

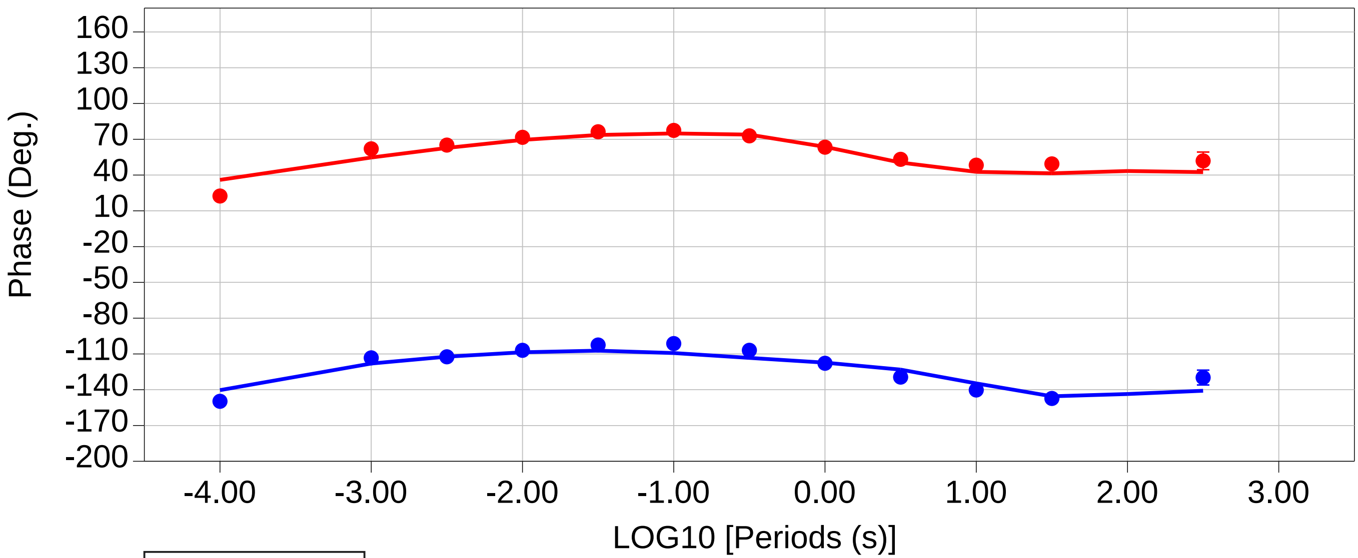

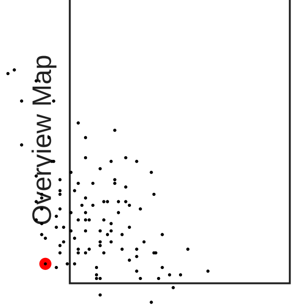

Total RMS = 17754.72

Zxy RMS = 18425.72

Zyx RMS = 17057.35

Site: X33

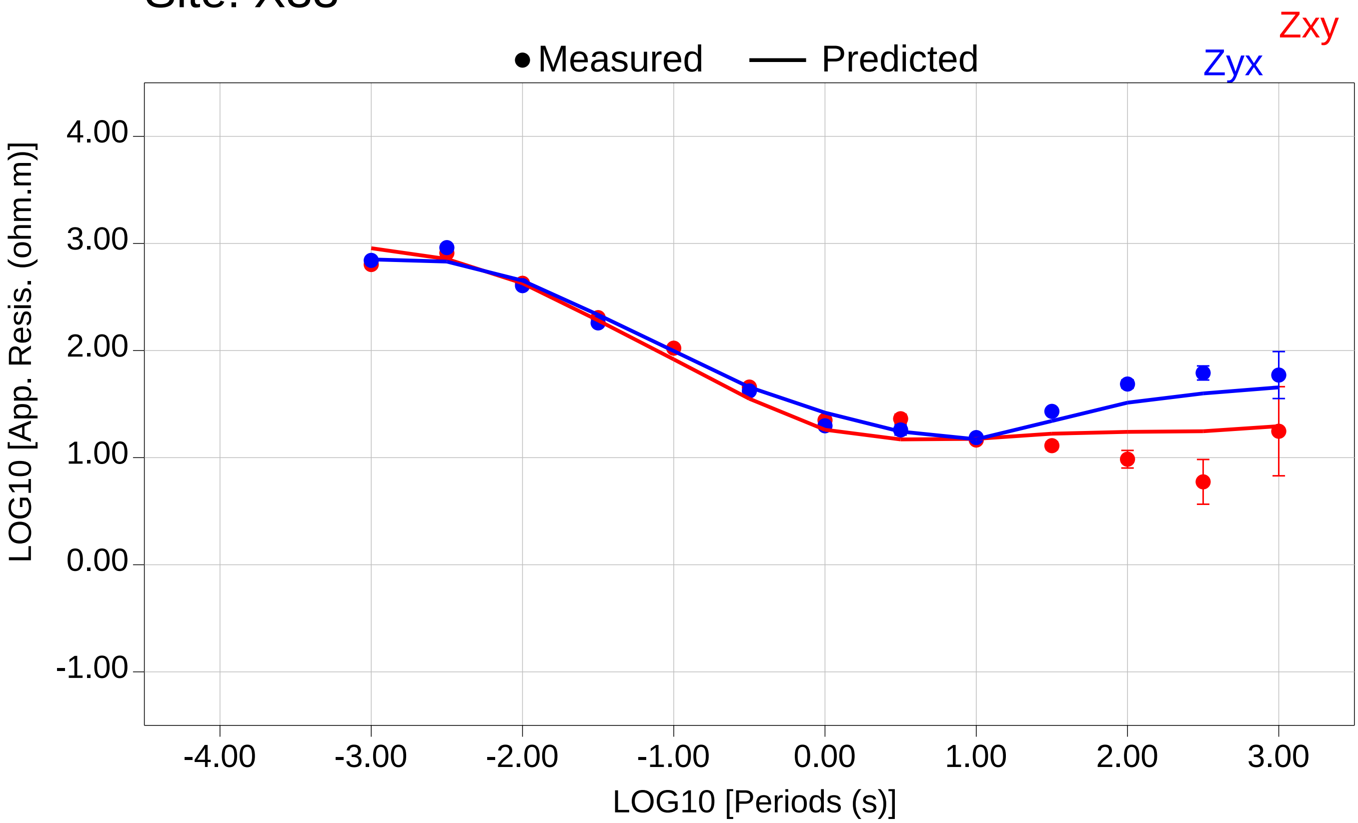

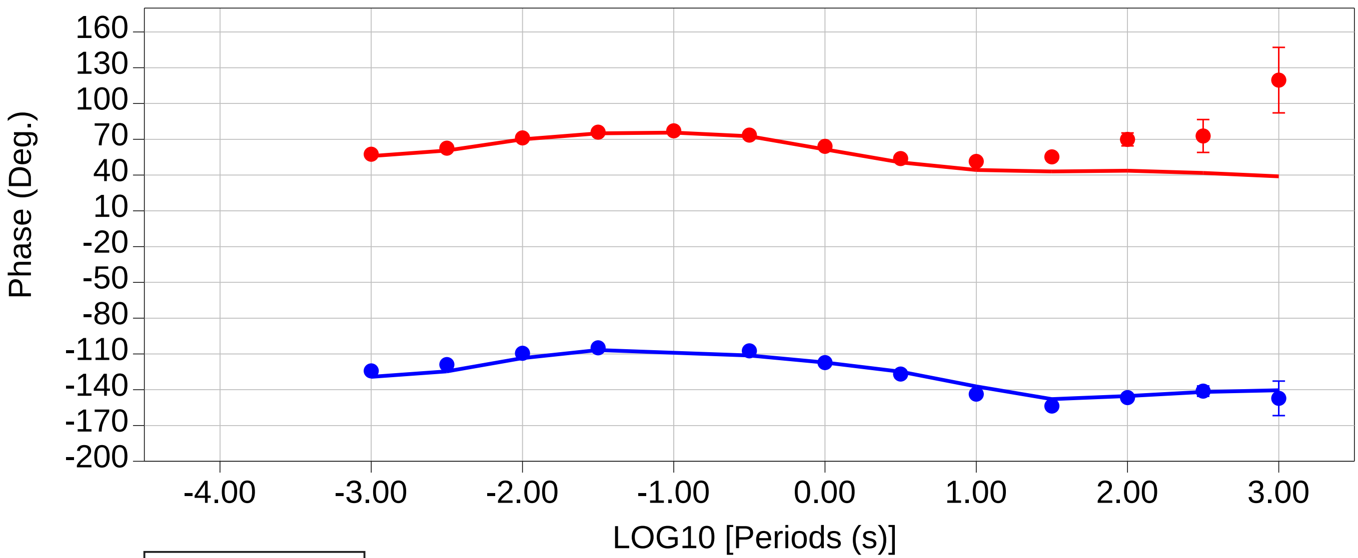

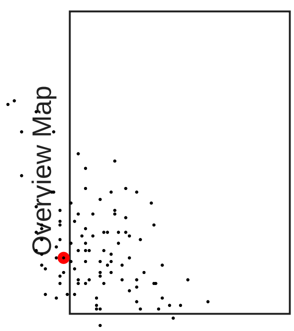

Total RMS = 15148.42

Zxy RMS = 15818.73

Zyx RMS = 14387.06

Site: X34

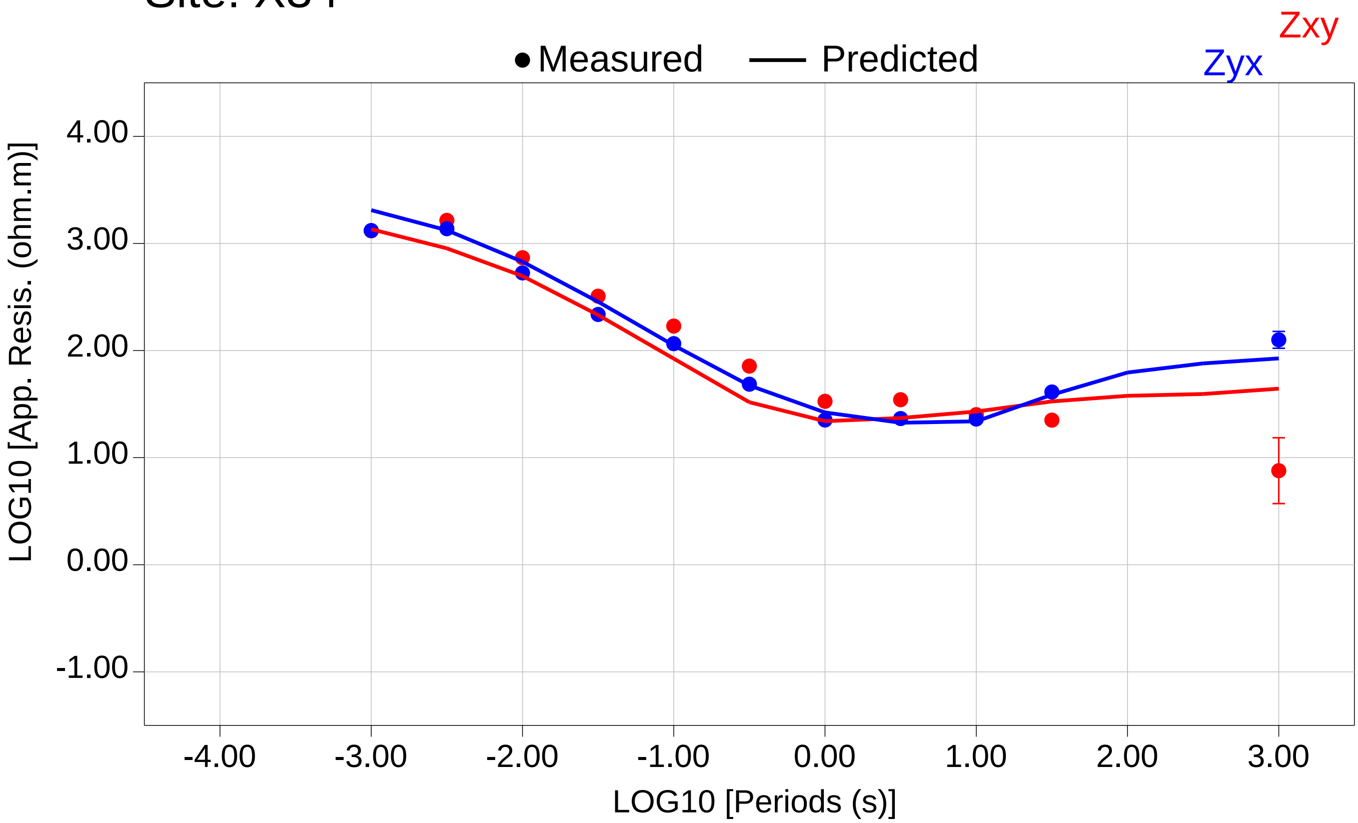

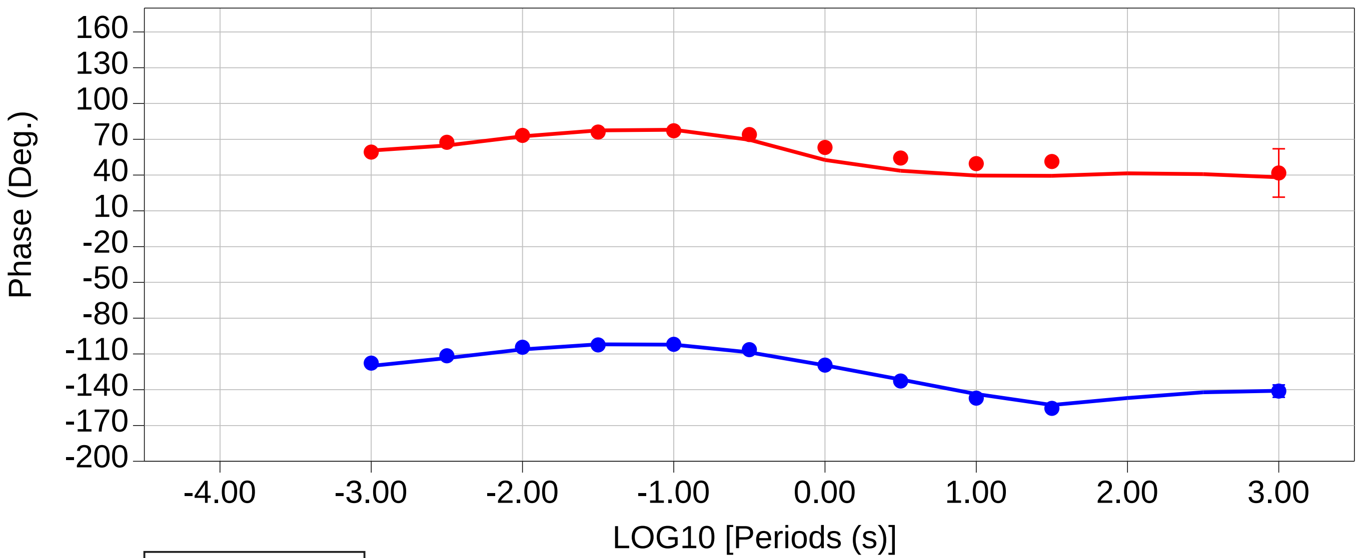

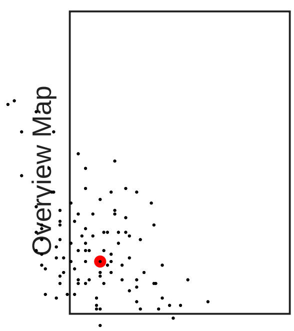

Total RMS = 17292.40

Zxy RMS = 16252.76
Zyx RMS = 18272.99

Site: X35

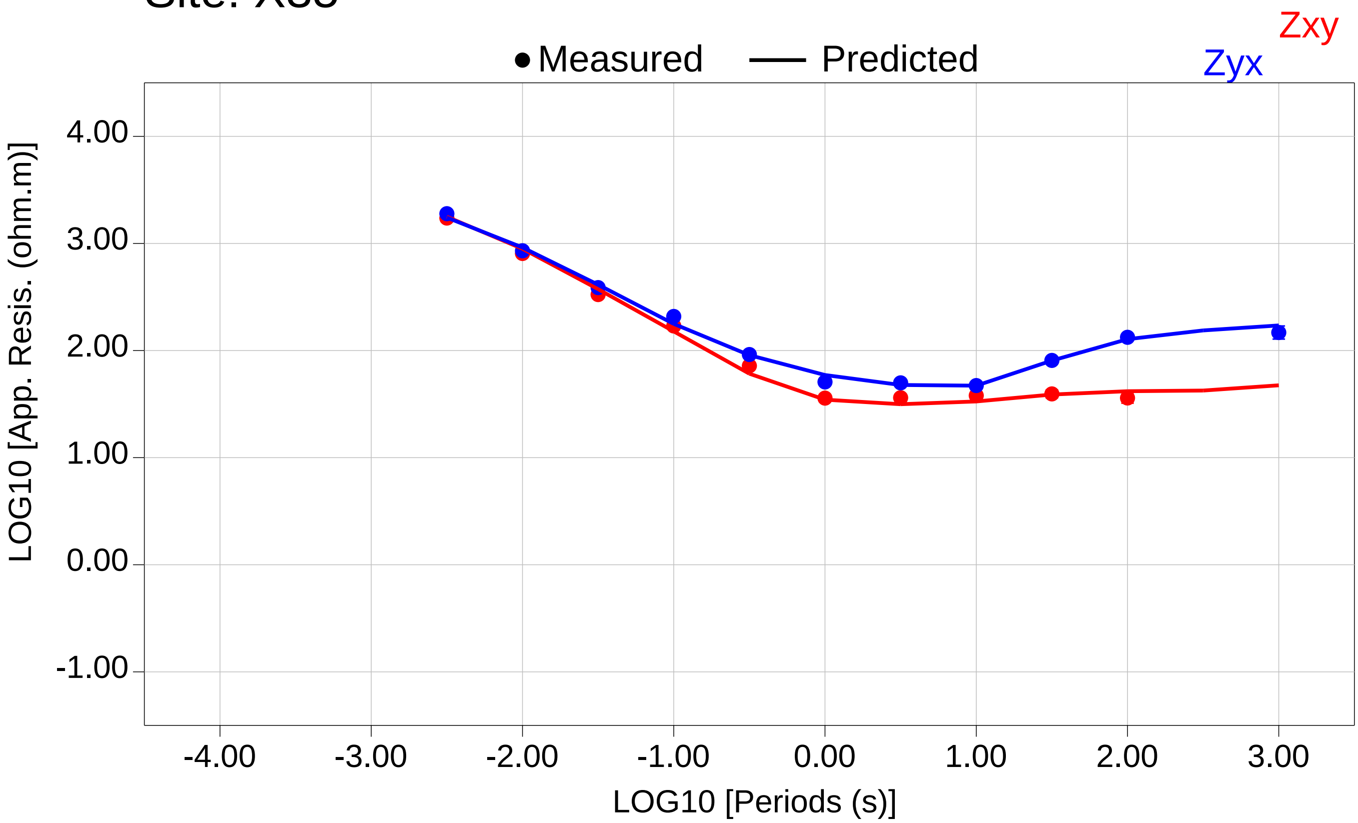

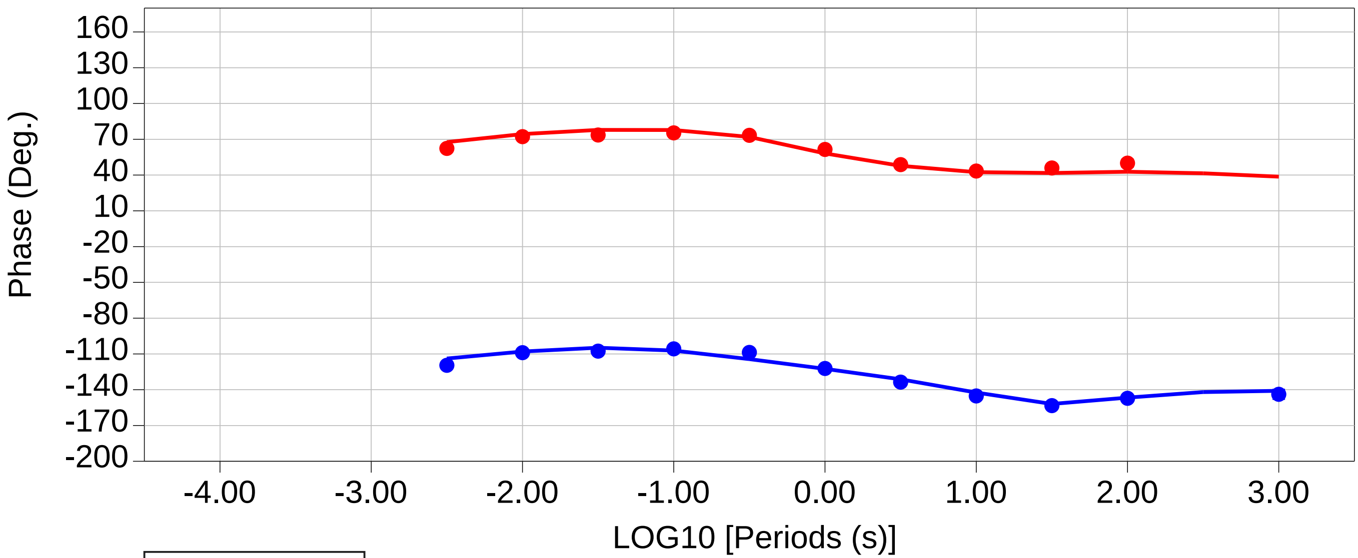

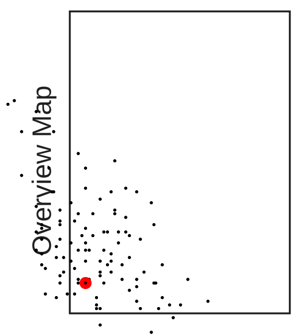

Total RMS = 17449.80

Zxy RMS = 16734.63

Zyx RMS = 18075.41

Site: X40

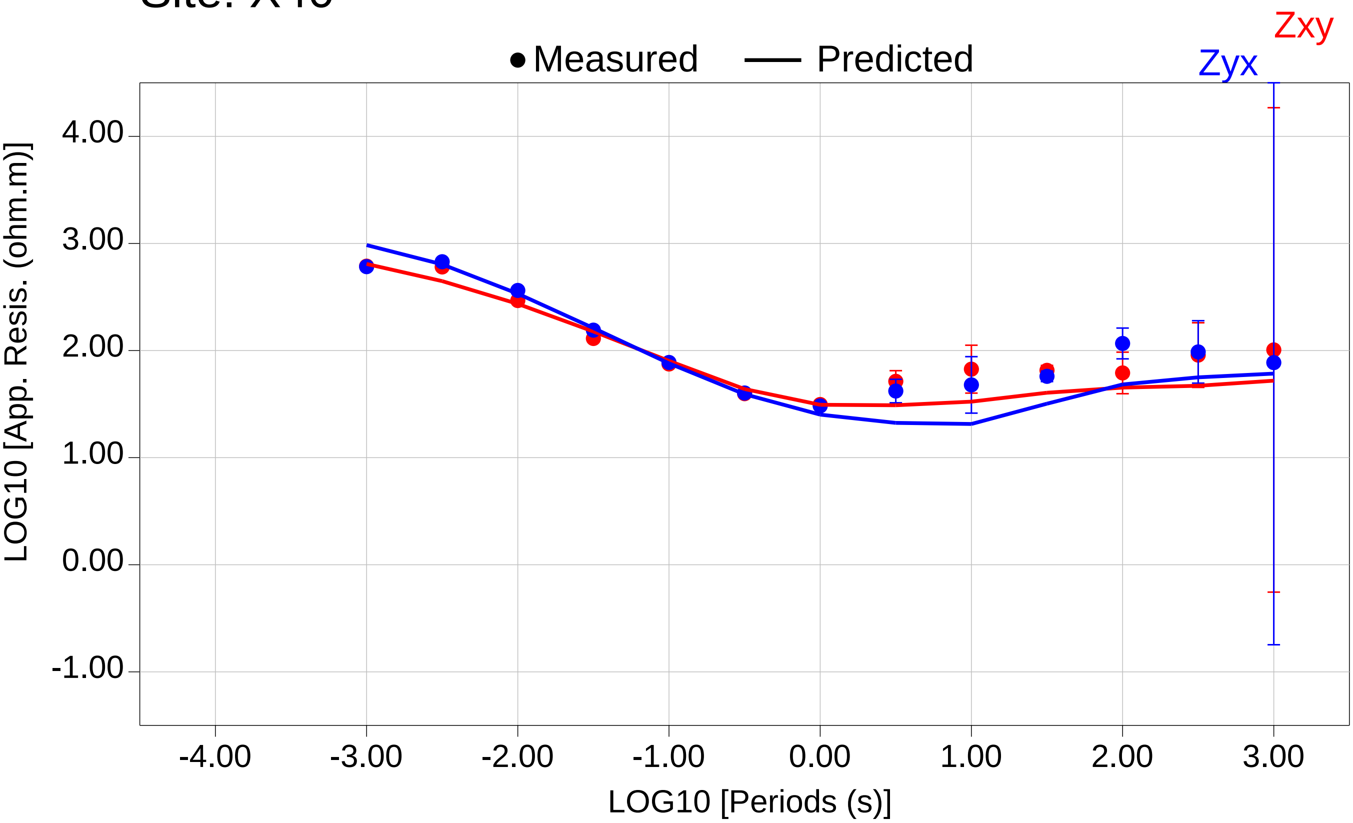

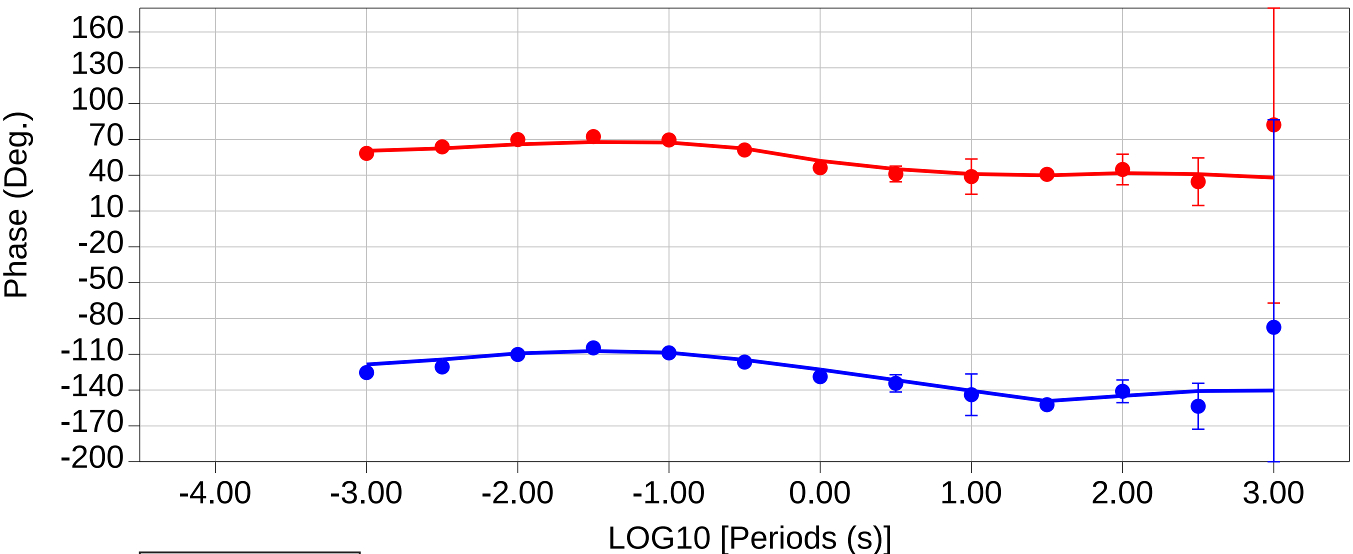

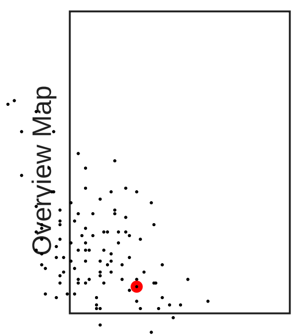

Total RMS = 14628.71

Zxy RMS = 14129.51
Zyx RMS = 15111.43

Site: X41

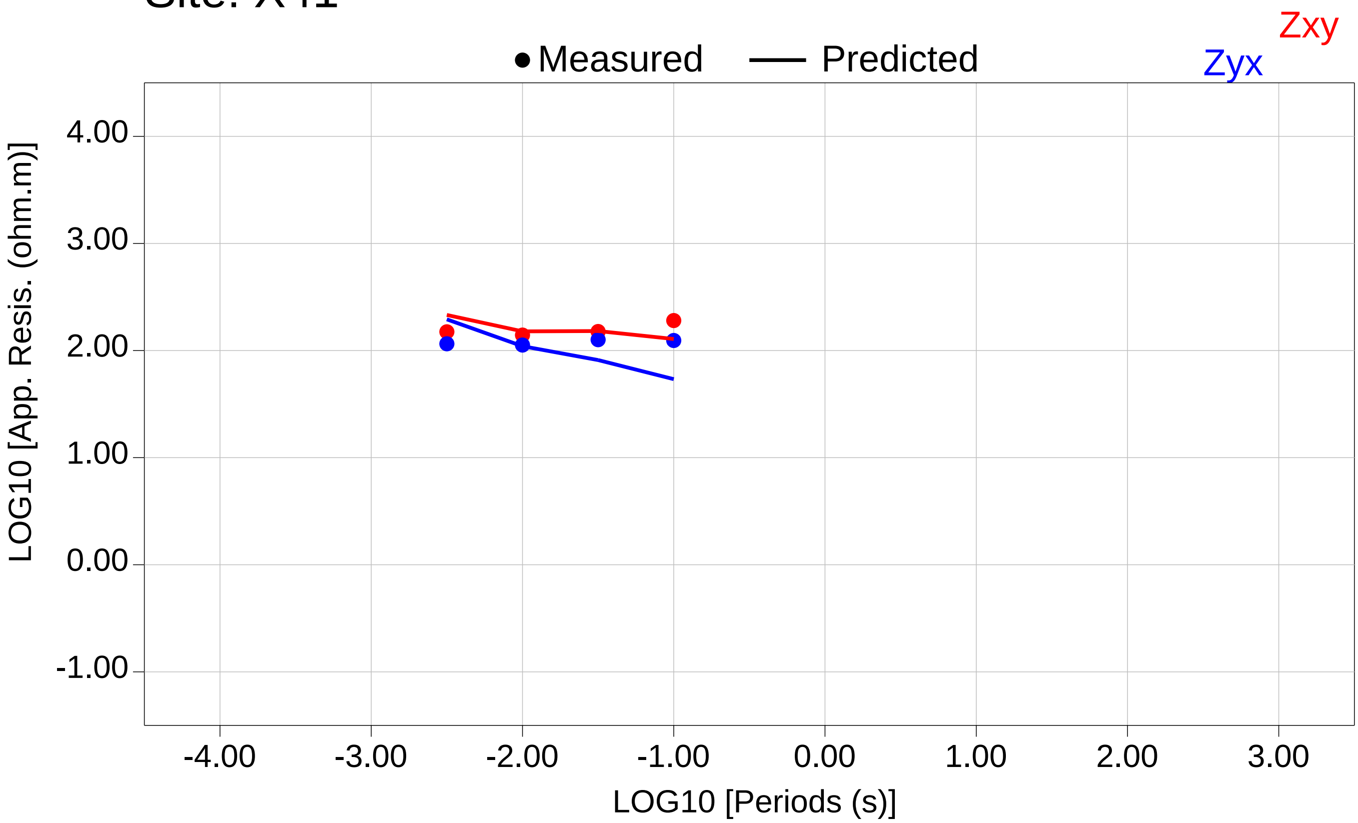

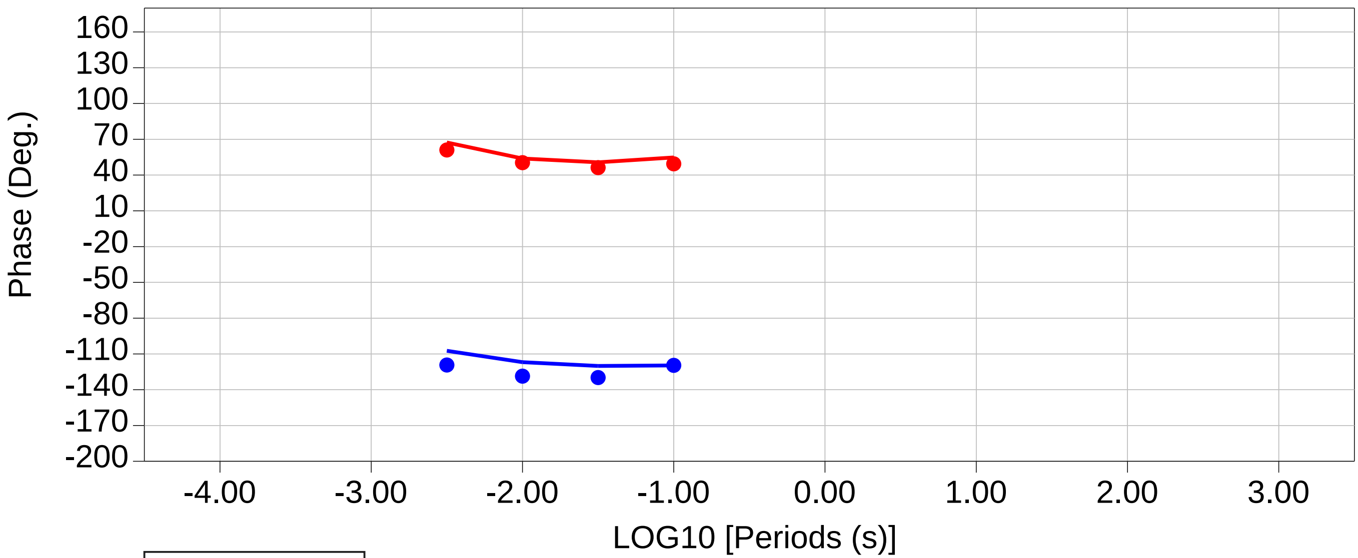

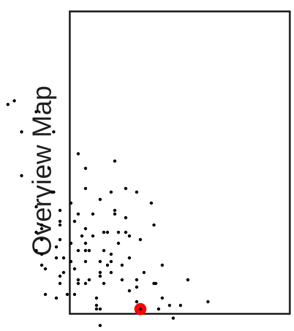

Total RMS = 12094.18

Zxy RMS = 13192.71

Zyx RMS = 10885.36

Site: X87

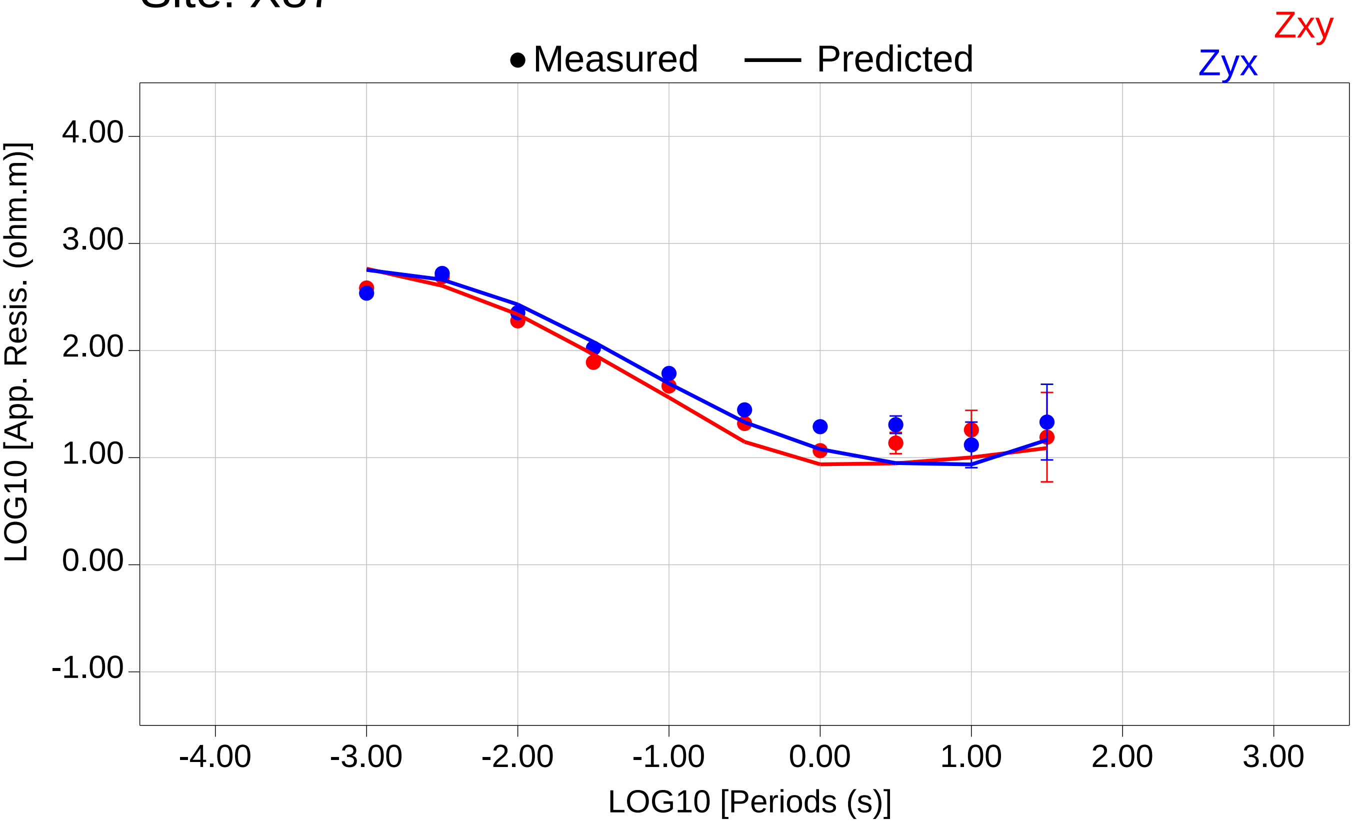

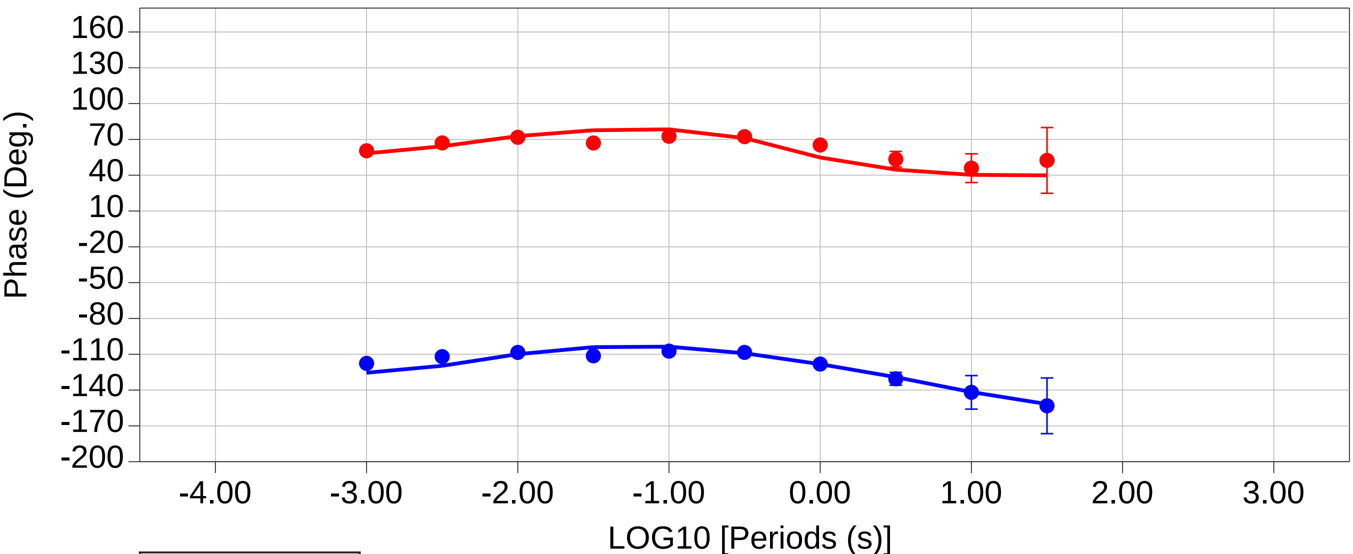

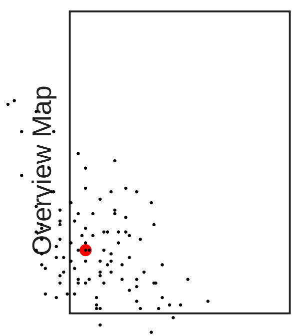

Total RMS = 16765.96

Zxy RMS = 15966.60
Zyx RMS = 17528.92